



Jayasekera, Geeshath (2020) *Unravelling the role of the left and right ventricles in pulmonary arterial hypertension: patient and small animal cardiac MRI studies*. PhD thesis.

<http://theses.gla.ac.uk/81612/>

Copyright and moral rights for this work are retained by the author

A copy can be downloaded for personal non-commercial research or study, without prior permission or charge

This work cannot be reproduced or quoted extensively from without first obtaining permission in writing from the author

The content must not be changed in any way or sold commercially in any format or medium without the formal permission of the author

When referring to this work, full bibliographic details including the author, title, awarding institution and date of the thesis must be given

Enlighten: Theses

<https://theses.gla.ac.uk/>  
[research-enlighten@glasgow.ac.uk](mailto:research-enlighten@glasgow.ac.uk)

**Unravelling the role of the left and  
right ventricles in pulmonary arterial  
hypertension: patient and small animal  
cardiac MRI studies**

*A thesis by*

*Dr. Geeshath Jayasekera  
MBChB (Hons), MRCP*

Conducted in the Scottish Pulmonary Vascular Unit  
and Institute of Cardiovascular and Medical Sciences,  
College of Medical, Veterinary and Life Sciences

Submitted for the degree of  
Doctor of Philosophy  
to  
The University of Glasgow 2020

# Author's Declaration

The experimental design of the works carried out in this thesis was that of myself and my supervisors Prof. Andrew Peacock, Dr. Aleksandra Radjenovic and Dr. David Welsh whom I collaborated with. The work reported in this thesis was carried out by myself, with the assistance of several colleagues acknowledged in the script. All of the final data interpretation and statistical analysis herein were carried out by myself. The manuscript was written solely by me.

This work has not previously been submitted for consideration of a higher degree. Much of this work has been published or submitted to journals for consideration of publication. A list of these published papers and other published abstracts relating to my work has been included.

Signed

Dr. Geeshath Jayasekera  
January 2020

# Acknowledgements

I would like to express my sincere thanks to my principal supervisors, Professor Andrew Peacock and Dr. Aleksandra Radjenovic. Professor Peacock provided me with the opportunity to work at the Scottish Pulmonary Vascular Unit and his enthusiasm and support made the SPVU a fantastic experience and made it possible for this thesis to come to fruition. Dr. Radjenovic provided me with valuable knowledge regarding cardiac MRI and her continuous encouragement and advice helped me to overcome a number of obstacles during my research.

I am also grateful to Dr. David Welsh for his invaluable contribution towards translational research and assistance with matters academic and thesis related. I would like to thank the consultant physicians at the SPVU Dr. Martin Johnson, Dr. Colin Church and Dr. Mel Brewis and my other colleagues in the unit. This work could not have been achieved without their assistance. I am also grateful to the staff of the cardiac MRI units at the University of Glasgow, Golden Jubilee National Hospital and the Glasgow Experimental MRI Centre for their patience and technical support.

Dr. Kat Wilson, Dr. William Holmes, Dr. Douglas Black, Chongmiao Yang, Alan MacDonald, Dick Sun Leow and Aysel Uckan collaborated with me in these projects and I am extremely thankful for their hard work and assistance.

Finally, I would like to thank the patients with pulmonary hypertension for their participation in the studies of this thesis. Their willingness to help, give up their time and travel across the country to attend hospital for CMR scans was hugely appreciated.

This thesis is dedicated to my parents Chandra and Vineetha.

## Table of Contents

<b>Author's Declaration</b> .....	<b>2</b>
<b>Acknowledgements</b> .....	<b>3</b>
<b>List of Tables</b> .....	<b>8</b>
<b>List of Figures</b> .....	<b>9</b>
<b>Appendix</b> .....	<b>11</b>
<b>Definitions / Abbreviations</b> .....	<b>12</b>
<b>Publications</b> .....	<b>16</b>
<b>Abstract</b> .....	<b>20</b>
<b>Chapter 1 Introduction</b> .....	<b>21</b>
<b>1.1 Definition and haemodynamic classification of pulmonary hypertension</b> .....	<b>22</b>
1.1.1 Right heart catheterisation .....	24
1.1.2 Upper limit of normal pulmonary artery pressure.....	24
1.1.3 Idiopathic pulmonary arterial hypertension .....	25
<b>1.2 Treatment</b> .....	<b>25</b>
<b>1.3 Non-invasive imaging in PH</b> .....	<b>27</b>
<b>1.4 Echocardiography</b> .....	<b>28</b>
1.4.1 Morphological assessment of the right heart and pulmonary circulation .....	28
1.4.2 Haemodynamic assessment of the right heart and the pulmonary circulation .....	28
1.4.3 Echocardiography definition of PH .....	29
1.4.4 Pulsatile pulmonary haemodynamics .....	29
1.4.5 Prognostic staging and follow up .....	30
1.4.6 Differential diagnosis .....	31
1.4.7 3D Echocardiography .....	31
<b>1.5 Chest radiography</b> .....	<b>31</b>
<b>1.6 Ventilation perfusion scintigraphy</b> .....	<b>33</b>
<b>1.7 Computed Tomography (CT)</b> .....	<b>34</b>
1.7.1 The main pulmonary artery (Main PA).....	35
1.7.2 Beyond the main pulmonary artery .....	36
1.7.3 Cardiac signs.....	37
1.7.4 Lung parenchyma.....	38
1.7.5 CT in chronic thromboembolic pulmonary hypertension .....	38
1.7.6 CT in pulmonary veno-occlusive disease .....	39
<b>1.8 Cardiac Magnetic Resonance imaging</b> .....	<b>40</b>
1.8.1 Ventricular volume, structure and function.....	40
1.8.2 Phase contrast CMR .....	43
1.8.3 Pulmonary artery stiffness and pulsatility .....	44
1.8.4 RV - PA coupling .....	44
<b>1.9 Non-invasive assessment of haemodynamics with CMR</b> .....	<b>45</b>
<b>1.10 Strain</b> .....	<b>45</b>
1.10.1 Cardiac deformation / strain by echocardiography.....	46
1.10.2 Speckle tracking echocardiography .....	46
1.10.3 RV strain and RV dyssynchrony in PH by echocardiography .....	46
1.10.4 CMR to assess myocardial deformation .....	48
1.10.5 RV strain by CMR imaging.....	50
1.10.6 Feature tracking CMR imaging.....	50

1.10.7	Left ventricular myocardium and strain .....	51
1.10.8	Torsion of the LV .....	53
<b>1.11</b>	<b>Myocardial tissue characterisation and myocardial perfusion by CMR .....</b>	<b>53</b>
1.11.1	Late gadolinium enhancement .....	54
1.11.2	T1 mapping techniques.....	55
1.11.3	T1 mapping methodology.....	55
1.11.4	T1 mapping in PH.....	58
1.11.5	Myocardial perfusion.....	59
<b>1.12</b>	<b>Positron emission tomography (PET) .....</b>	<b>59</b>
<b>1.13</b>	<b>Right and left ventricular Interaction .....</b>	<b>60</b>
<b>1.14</b>	<b>Left atrium.....</b>	<b>62</b>
1.14.1	Left atrial area / volume measurement by CMR in PH.....	62
1.14.2	Left atrial function .....	63
<b>1.15</b>	<b>Small animal CMR .....</b>	<b>63</b>
<b>1.16</b>	<b>Hypothesis and aims of the thesis.....</b>	<b>64</b>
<b>Chapter 2</b>	<b>Material and Methods.....</b>	<b>67</b>
<b>2.1</b>	<b>Scottish pulmonary vascular unit.....</b>	<b>68</b>
<b>2.2</b>	<b>WHO functional class .....</b>	<b>68</b>
<b>2.3</b>	<b>Patient recruitment and assessment.....</b>	<b>70</b>
<b>2.4</b>	<b>Non-invasive assessment .....</b>	<b>70</b>
<b>2.5</b>	<b>Right heart catheterisation.....</b>	<b>70</b>
<b>2.6</b>	<b>Cardiac Magnetic Resonance imaging .....</b>	<b>71</b>
2.6.1	Patient preparation and positioning .....	71
2.6.2	CMR image analysis.....	72
<b>2.7</b>	<b>Strain.....</b>	<b>73</b>
2.7.1	LV Strain .....	74
2.7.2	LV intra-ventricular dyssynchrony .....	76
<b>2.8</b>	<b>Left atrial strain.....</b>	<b>78</b>
<b>2.9</b>	<b>T1 mapping CMR.....</b>	<b>82</b>
2.9.1	Diagnosis, commencement of treatment and follow up .....	85
<b>2.10</b>	<b>CMR in a Sugden-hypoxia rat model of PH .....</b>	<b>85</b>
2.10.1	Small animal CMR imaging. ....	86
2.10.2	CMR imaging analysis .....	86
<b>2.11</b>	<b>In vivo hemodynamic measurements.....</b>	<b>87</b>
<b>2.12</b>	<b>RV hypertrophy and tissue harvest .....</b>	<b>87</b>
<b>2.13</b>	<b>Gross anatomy postpartum .....</b>	<b>87</b>
<b>2.14</b>	<b>Pulmonary vascular remodelling.....</b>	<b>88</b>
<b>2.15</b>	<b>Data Storage .....</b>	<b>88</b>
<b>2.16</b>	<b>Statistical analysis .....</b>	<b>88</b>
<b>Chapter 3</b>	<b>Left ventricular strain and intra-ventricular dyssynchrony by CMR in idiopathic pulmonary arterial hypertension .....</b>	<b>89</b>
<b>3.1</b>	<b>Introduction.....</b>	<b>90</b>
<b>3.2</b>	<b>Methods .....</b>	<b>94</b>
3.2.1	Patient recruitment.....	94
3.2.2	CMR imaging .....	94
3.2.3	Right heart catheterization .....	94
3.2.4	CMR image analysis.....	95
3.2.5	Strain analysis.....	95
3.2.6	Intra-ventricular dyssynchrony .....	96
3.2.7	Statistical analysis .....	98
<b>3.3</b>	<b>Results.....</b>	<b>99</b>
3.3.1	Demographics .....	99
3.3.2	CMR variables and baseline haemodynamic characteristics of IPAH patients.....	100

3.3.3	Inter-observer reproducibility.....	103
3.3.4	Healthy volunteer vs IPAH: strain, strain rate and dyssynchrony.....	104
3.3.4.1	Left ventricle .....	104
3.3.4.2	Right Ventricle .....	104
3.3.4.3	Severe vs mild / intermediate disease .....	104
3.3.5	Impaired LV ejection fraction in IPAH .....	108
3.3.6	Association with markers of disease severity .....	109
3.3.7	Baseline survival analysis .....	111
<b>3.4</b>	<b>Discussion.....</b>	<b>116</b>
<b>3.5</b>	<b>Conclusion .....</b>	<b>120</b>
<b>3.6</b>	<b>Limitations.....</b>	<b>120</b>
<b>Chapter 4 Left atrial strain by CMR imaging in idiopathic pulmonary arterial hypertension .....</b>		
<b>121</b>		
<b>4.1</b>	<b>Introduction.....</b>	<b>122</b>
<b>4.2</b>	<b>Methods .....</b>	<b>126</b>
4.2.1	Patient recruitment.....	126
4.2.2	CMR imaging .....	126
4.2.3	Right heart catheterization .....	126
4.2.4	CMR image analysis.....	127
4.2.5	Strain .....	127
4.2.6	Statistical Analysis .....	130
<b>4.3</b>	<b>Results.....</b>	<b>131</b>
4.3.1	Demographics .....	131
4.3.2	CMR variables and baseline haemodynamic characteristics of IPAH patients .....	132
4.3.3	Healthy volunteer vs IPAH: left atrial strain and strain rate .....	134
4.3.3.1	Left atrial strain.....	134
4.3.3.2	Left atrial strain rate .....	135
4.3.3.3	Severe vs Intermediate / Mild disease.....	135
4.3.4	Association with markers of disease severity .....	137
<b>4.4</b>	<b>Discussion.....</b>	<b>139</b>
<b>4.5</b>	<b>Conclusion .....</b>	<b>142</b>
<b>4.6</b>	<b>Limitations.....</b>	<b>142</b>
<b>Chapter 5 Non-invasive measurement of myocardial damage in pulmonary hypertension using Native T1 mapping from CMR: a novel segmentation technique and association with haemodynamic variables. ....</b>		
<b>143</b>		
<b>5.1</b>	<b>Introduction.....</b>	<b>144</b>
<b>5.2</b>	<b>Methods .....</b>	<b>149</b>
5.2.1	Patient recruitment.....	149
5.2.2	CMR imaging .....	151
5.2.3	Right heart catheterisation .....	153
5.2.4	CMR imaging analysis.....	153
5.2.5	T1 mapping analysis .....	153
5.2.6	Statistical analysis .....	155
<b>5.3</b>	<b>Results.....</b>	<b>156</b>
5.3.1	Treatment naive patient cohort - haemodynamics, ventricular volumes, mass and function .....	157
5.3.2	T1 analysis Inter-rater variability .....	159
5.3.3	Relationship between global T1 values, regions and segments .....	161
5.3.4	Global, regional and segmental T1 times.....	163
5.3.5	WHO groups of PH .....	167
5.3.6	Haemodynamics at right heart catheterisation and CMR findings .....	169
5.3.7	Subgroup analysis of IPAH.....	172
5.3.8	Multivariable linear regression .....	174
5.3.9	Validation cohort.....	175

5.4	Discussion.....	177
5.5	Conclusion.....	178
5.6	Limitations.....	179
Chapter 6 Longitudinal cardiac changes by CMR in a Sugen-hypoxia small animal model of pulmonary arterial hypertension..... 180		
6.1	Introduction.....	181
6.2	Method.....	183
6.2.1	Ethics.....	183
6.2.2	Study design.....	183
6.2.3	<i>In vivo</i> hemodynamic measurements.....	184
6.2.4	RV hypertrophy and tissue harvest.....	185
6.2.5	Gross anatomy postpartum.....	185
6.2.6	Pulmonary vascular remodelling.....	185
6.2.7	CMR imaging.....	185
6.2.8	CMR analysis.....	186
6.2.9	Statistical analysis.....	186
6.3	Results.....	187
6.3.1	Right heart catheterisation and RV hypertrophy.....	187
6.3.2	CMR.....	189
6.3.3	Inter-rater variability.....	191
6.3.4	Right ventricle.....	191
6.3.5	Left ventricle.....	193
6.3.6	LV eccentricity index (LVEI).....	193
6.3.7	Autopsy vs CMR in the measurement of RV hypertrophy.....	195
6.4	Discussion.....	197
6.4.1	The SuHx small animal model – PH.....	198
6.4.2	The SuHx small animal model – RV function.....	199
6.4.3	Adaptive vs maladaptive remodelling.....	199
6.4.4	Small animal model - LV function.....	200
6.5	Conclusion.....	200
6.6	Limitations.....	201
Chapter 7 General Discussion and Conclusions..... 202		
7.1	Left ventricular strain and intra-ventricular dyssynchrony by CMR in idiopathic pulmonary arterial hypertension.....	204
7.2	Left atrial strain by CMR in idiopathic pulmonary arterial hypertension.....	207
7.3	Non-invasive measurement of myocardial damage in pulmonary hypertension by CMR	209
7.4	Longitudinal cardiac changes by CMR in a sugen-hypoxia small animal model of pulmonary arterial hypertension.....	212
7.5	Future Directions.....	212
7.6	Limitations.....	213
7.7	Final comment.....	213

# List of Tables

Table 1.1 Clinical classification of pulmonary hypertension.....	23
Table 1.2 Cardiac Magnetic Resonance Imaging techniques of assessing myocardial deformation. .....	49
Table 2.1 WHO functional class classification of PH.....	69
Table 2.2 Definition of regions with the new myocardial segmentation using a modified AHA model.....	84
Table 3.1 Demographics of the study population.....	99
Table 3.2 The baseline CMR characteristics of the IPAH and healthy volunteer group .....	101
Table 3.3 The baseline characteristics of the IPAH group .....	102
Table 3.4 Reproducibility of the strain, strain rate and dyssynchrony variables.....	103
Table 3.5 Healthy volunteer vs IPAH LV strain, strain rate and dyssynchrony.....	105
Table 3.6 Healthy volunteer vs IPAH RV strain, strain rate and dyssynchrony.....	106
Table 3.7 Strain, dyssynchrony and strain rate measurements in IPAH patients with severe vs intermediate / mild disease.....	107
Table 3.8 Bivariate Cox proportional hazard regression analysis for survival in IPAH patients. ....	112
Table 3.9 Multivariate cox proportional hazard regression model for survival in IPAH patients...	113
Table 4.1 Demographics of the study population.....	131
Table 4.2 The baseline CMR characteristics of the IPAH and healthy volunteer group .....	132
Table 4.3 The baseline characteristics of the IPAH group .....	133
Table 4.4 Healthy volunteer vs IPAH Left atrial strain .....	134
Table 4.5 Healthy volunteer vs IPAH Left atrial strain rate.....	135
Table 4.6 Left atrial strain and strain rate measurements in IPAH patients with severe vs intermediate / mild disease.....	136
Table 4.7 Left atrial strain and association with markers of disease severity in IPAH patients .....	138
Table 5.1 Definition of regions with the new myocardial segmentation using a modified AHA model.....	155
Table 5.2 Demographics of the study population.....	156
Table 5.3 Haemodynamics during right heart catheterisation and biventricular volumes, mass and function determined by CMR for PH and for patients without PH.....	158
Table 5.4 Global, regional and segmental T1 values between PH and non PH patients .....	164
Table 5.5 Correlation between RV insertion region and global myocardial T1 values and haemodynamics during right heart catheterisation.....	171
Table 5.6 Correlation between RV insertion region and global myocardial T1 values and RV CMR variables.....	171
Table 5.7 Association between Insertion region T1 times, haemodynamics during right heart catheterisation and CMR variables in IPAH patients.....	174
Table 5.8 Multivariable linear regression analysis showing associations between haemodynamics during right heart catheterisation, RV structure and insertion region T1 times.....	175

# List of Figures

Figure 1-1 Evolution of current treatment options for patients with pulmonary arterial hypertension.	26
Figure 1-2 Myocardial deformation of the left ventricle	52
Figure 1-3 Normal and fibrotic myocardium pre and post gadolinium contrast injection	57
Figure 2-1 Feature tracking CMR 4-chamber image and a short axis image	75
Figure 2-2 Assessment of intra-ventricular dyssynchrony	77
Figure 2-3 LA myocardial feature tracking using a 2-chamber and 4-chamber view	79
Figure 2-4 Left atrial strain and strain rate profiles.	81
Figure 2-5 Cardiac Magnetic Resonance mid ventricular slice T1 map of a patient with pulmonary arterial hypertension	83
Figure 3-1 Left ventricular circumferential intra-ventricular synchrony in health and IPAH	97
Figure 3-2 IPAH patients with preserved LV ejection fraction vs impaired LV ejection fraction	108
Figure 3-3 Association of LV radial strain with RV ejection fraction (A) and RV end-systolic volume index (B) and association of RV average strain with RVEF (C) by CMR.	110
Figure 3-4 Kaplan Meir curves demonstrating survival of IPAH patients	115
Figure 4-1 Left atrial function compromises reservoir, conduit and contractile booster pump function.	129
Figure 5-1 The study design.	150
Figure 5-2 CMR mid ventricular T1 map of a patient with pulmonary arterial hypertension	152
Figure 5-3 Bland Altman plots for interobserver agreement for A) RV insertion region T1 times and B) global myocardial T1 values using the novel segmentation proposed in the thesis.	160
Figure 5-4 The association between a) anterior insertion segment and inferior insertion segment, b) RV insertion region and global myocardial T1 values of the LV.	162
Figure 5-5 Boxplots demonstrating a) Global myocardial T1 values between PH and no PH patients b) Insertion region T1 values between PH and non PH groups.	165
Figure 5-6 Boxplots of T1 values between PH and no PH groups grouped according to regional and segmental values.	166
Figure 5-7 Boxplots of global myocardial T1 values and insertion region T1 values between different WHO groups of pulmonary hypertension and symptomatic patients with no PH.	168
Figure 5-8 Associations between a) right ventricular end systolic volume index measured by CMR and b) mixed venous saturations obtained during right heart catheterisation and RV insertion region T1 values.	170
Figure 5-9 Correlation between a) RV insertion region T1 values and mixed venous saturations at right heart catheterisation and b) RV insertion region T1 values and RV end systolic volume index by CMR in IPAH patients.	173
Figure 5-10 a) ECV map demonstrating raised ECV values in the RV insertion regions, b) boxplot of the ECV values in the RV insertion regions in patients with established PAH.	176
Figure 6-1 Study design	184

- Figure 6-2 Right ventricular systolic pressure measured by right heart catheterization (A), RV/(LV + septum) by gross weight (B), the percentage of remodelled vessels in a lung section (C) and immunohistochemical analysis of  $\alpha$ -smooth muscle actin ( $\alpha$ -SMA) staining in the smooth muscle layer of small pulmonary arteries of the lungs (D - G). 188
- Figure 6-3 Cardiac MRI short axis image taken from a long axis (A) and a short axis cine stack (B – F) of a normoxic Sprague Dawley rat. 190
- Figure 6-4 RV end systolic volume index (RVESVI) (A), RV end diastolic volume index (RVEDVI) (B), RV mass index (C), RV ejection fraction (RVEF) (D), Ventricular mass index (VMI) (E) and Stroke volume index (SVI) (F). 193
- Figure 6-5 LV end systolic volume index (LVESVI) (A), LV end diastolic volume index (LVEDVI) (B), LV mass index (C), LV ejection fraction (LVEF) (D), LV eccentricity index (LVEI) in systole (E) and LV eccentricity index in diastole (F) 194
- Figure 6-6 Cardiac MR images (A – C) and light microscopy images (D and E) of short axis sections of rat hearts. 196
- Figure 7-1 The proposed mechanism of impaired LV mechanics in pulmonary arterial hypertension 206
- Figure 7-2 The proposed mechanism of impaired LA mechanics in pulmonary arterial hypertension 208
- Figure 7-3 The proposed mechanism of native T1 changes at the RV insertion regions in pulmonary arterial hypertension 211

# Appendix

Appendix 1 LV Strain variables and association with known markers of disease severity.	230
Appendix 2 RV strain variables and association with known markers of disease severity	231

# Definitions / Abbreviations

AcT	Time to peak flow
AHA	American Heart Association
BMI	Body mass index
BSA	Body surface area
CI	Cardiac index
CMR	Cardiac Magnetic Resonance imaging
CO	Cardiac output
CT	Computed Tomography
CTEPH	Chronic thromboembolic pulmonary hypertension
CTPA	CT pulmonary angiography
DLCO%	Diffusion capacity
dPAP	Diastolic pulmonary artery pressure
Ea	Arterial elastance
Ecc <sub>LV</sub>	LV circumferential strain
ECV	Extra cellular volume
Ees	End-systolic elastance
Ell <sub>LV</sub>	LV longitudinal strain
Err <sub>LV</sub>	LV radial strain
HCM	Hypertrophic cardiomyopathy
HFpEF	Heart failure with preserved ejection fraction
HLA	Horizontal long axis
IPAH	Idiopathic pulmonary arterial hypertension
IVC	Inferior vena cava
IVCT	Isovolumetric contraction time
IVRT	Isovolumetric relaxation time

IVS	Inter-ventricular septum
LA	Left atrium
LGE	Late gadolinium enhancement
LV	Left ventricle
LVEDV	Left ventricular end-diastolic volume
LVEDVI	Left ventricular end-diastolic volume Index
LVEF	Left ventricular ejection fraction
LVEI	Left ventricular eccentricity index
LVESV	Left ventricular end-systolic volume
LVESVI	Left ventricular end-systolic volume index
LVM	LV mass
LVSV	LV stroke volume (by CMR)
MDT	Multi-disciplinary team
mPAP	Mean pulmonary artery pressure
n	Number
NTproBNP	N-Terminal-pro B-type Natriuretic Peptide
PA	Pulmonary artery
PAH	Pulmonary arterial hypertension
PAWP	Pulmonary artery wedge pressure
PEA	Pulmonary endarterectomy
PET	Positron emission tomography
PH	Pulmonary hypertension
PTT	Pulmonary transit time
PVOD	Pulmonary veno-occlusive Disease
PVR	Pulmonary vascular resistance
Qp: Qs	Pulmonary artery: Aorta flow
r	Correlation coefficient (Pearson or Spearman)
RA	Right atrium
RAP	Right atrial pressure

RV	Right ventricle
RVEDV	Right ventricular end-diastolic volume
RVEDVI	Right ventricular end-diastolic volume index
RVEF	Right ventricular ejection fraction
RVESV	Right ventricular end-systolic volume
RVESVI	Right ventricular end-systolic volume index
RVET	Right ventricular ejection time
RVFAC	Right ventricular fractional area change
RVM	RV mass
RVSP	Right ventricular systolic pressure
RVSV	RV stroke volume (by CMR)
SA	Short axis
sPAP	Systolic pulmonary artery pressure
SPECT	Single-photon emission computed tomography
SPVU	Scottish Pulmonary Vascular Unit
SRa	Peak late negative strain rate
SRe	Peak early negative strain rate
SRs	Peak positive strain rate
SuHx	Sugen hypoxia
SV	Stroke volume
SVI	Stroke volume index
SvO2	Mixed venous saturation
TAPSE	Tricuspid annular plane systolic excursion
TR	Tricuspid regurgitation
TRPG	Tricuspid regurgitant pressure gradient
V/Q	Ventilation Perfusion scanning
VEGF	Vascular endothelial growth factor
VLA	Vertical long axis
VMI	Ventricular mass index

WHO FC	World Health Organisation functional class
WU	Wood units
$\epsilon_a$	Active strain
$\epsilon_e$	Passive strain
$\epsilon_s$	Total strain

# Publications

1. Jayasekera, G., Wilson, K. S., Buist, H., Woodward, R., Uckan, A., Hughes, C., ... Welsh, D. J. Understanding longitudinal biventricular structural and functional changes in a pulmonary hypertension Sugen-hypoxia rat model by cardiac magnetic resonance imaging. *Pulmonary Circulation*. 2020 doi.org/10.1177/2045894019897513
2. Jayasekera G, Crowe T, Peacock AJ. Non-invasive imaging of global and regional cardiac function in pulmonary hypertension. *Pulmonary Circulation*. 2018 doi: 10.1177/2045893217742000.
3. Jayasekera G, Johnson M, Hussey K, Church C. Pulmonary hypertension and severe right heart failure following lumbar spinal surgery. *SAGE Open Med Case Reports*. 2019 May 8. doi: 10.1177/2050313X19847805.
4. Brash L, Barnes GD, Brewis MJ, Church AC, Gibbs SJ, Howard LS, Jayasekera G, Johnson MK, McGlinchey N, Onorato J, Simpson J, Stirrat C, Thomson S, Watson G, Wilkins MR, Xu C, Welsh DJ, Newby DE, Peacock AJ. Short-Term Hemodynamic Effects of Apelin in Patients with Pulmonary Arterial Hypertension. *JACC Basic Transl Sci*. 2018 Mar 28;3(2):176-186. doi: 10.1016/j.jacbts.2018.01.013.
5. Pellino K, Kerridge S, Church C, Peacock AJ, Crowe T, Jayasekera G, Johnson MK, MacKenzie AM. Social deprivation and prognosis in Scottish patients with pulmonary arterial hypertension. *Eur Respir J*. 2018 Jan 31;51(2). pii: 1700444. doi: 10.1183/13993003.00444-2017.
6. Blyth KG, Bellofiore A, Jayasekera G, Foster JE, Steedman T, Chesler NC, Peacock AJ. Dobutamine stress MRI in pulmonary hypertension: relationships between stress pulmonary artery relative area change, RV performance, and 10-year survival. *Pulmonary Circulation*. 2017 Apr-Jun;7(2):465-475. doi: 10.1177/2045893217704838.
7. Panagiotou M, Vogiatzis I, Jayasekera G, Louvaris Z, Mackenzie A, McGlinchey N, Baker JS, Church AC, Peacock AJ, Johnson MK. Validation of

impedance cardiography in pulmonary arterial hypertension. *Clin Physiol Funct Imaging*. 2018 Mar;38(2):254-260. doi: 10.1111/cpf.12408. 28168802.

8. Panagiotou M, Vogiatzis I, Louvaris Z, Jayasekera G, McKenzie A, Mcglinchey N, Baker JS, Church AC, Peacock AJ, Johnson MK. Dynamic near-infrared spectroscopy assessment as an important tool to explore pulmonary arterial hypertension pathophysiology. *Eur Respir J*. 2017 Jan 4;49(1). pii: 1602161. doi: 10.1183/13993003.02161-2016.
9. Panagiotou M, Vogiatzis I, Louvaris Z, Jayasekera G, MacKenzie A, Mcglinchey N, Baker JS, Church AC, Peacock AJ, Johnson MK. Near infrared spectroscopy for the assessment of peripheral tissue oxygenation in pulmonary arterial hypertension. *Eur Respir J*. 2016 Oct;48(4):1224-1227. doi:10.1183/13993003.01022-2016.

## Book Chapters

1. Jayasekera G, Peacock AJ Advanced Imaging in Pulmonary Hypertension. Basic Science to Clinical Medicine DOI: 10.1007/978-3-319-23594-3\_12 January 2016
2. MacLean M, Church C, Mackenzie A, Jayasekera G, Mair K Pulmonary Hypertension. Textbook of Vascular Medicine DOI: 10.1007/978-3-030-16481-2\_41 August 2019

## Selected Abstract Presentations

1. Jayasekera G, Crowe T, Mackenzie A, Church A, Johnson M, Radjenovic A, Peacock A. Left Atrial Function by Cardiac MRI in Idiopathic Pulmonary Arterial Hypertension(IPAH) and Pulmonary Hypertension Due to Heart Failure with Preserved Ejection Fraction(PH-HFpEF). *American Journal of Respiratory and Critical Care Medicine* 2017;195:A6903 (Poster discussion)
2. Jayasekera G, Mangion K, Crowe T, Mackenzie A, McComb C, Johnson M, Church C, Berry C, Radjenovic A, Peacock A. Left ventricular strain and

- dyssynchrony by CMR Feature tracking in Idiopathic Pulmonary Arterial Hypertension. *European Respiratory Journal* 2017 50: OA1503; DOI: 10.1183/1393003.congress-2017.OA1503 (Oral presentation)
3. Jayasekera G, Church C, Johnson M, Peacock A, Radjenovic A. Right Ventricular free wall myocardial tissue characterisation by systolic Cardiac Magnetic Resonance T1 mapping in pulmonary hypertension. DOI: 10.1186/1532-429X-18-S1-P147 January 2016 *Journal of Cardiovascular Magnetic Resonance* 18(Suppl 1):P147 (Poster presentation)
  4. Jayasekera G, Johnson M, Church C, Peacock A. Vasoreactivity to inhaled nitric oxide does not predict long term survival in pulmonary arterial hypertension. DOI: 10.1183/13993003.congress-2016.PA1876 *European Respiratory Journal* 48(suppl 60):PA1876 (Poster discussion)
  5. Jayasekera G, Wilson K, Buist H, Liles J, Budas G, Fairfax S, Hughes C, Nilsen M, Church C, McLean M, Peacock A, Welsh D. Longitudinal cardiac changes in a SUGEN/Hypoxic Rat Model of Pulmonary Hypertension determined by Cardiac MRI. DOI: 10.1183/1393003.congress-2017.PA2383 September 2017 ERS International Congress 2017 abstracts (Poster presentation)
  6. Murphy G, Jayasekera G, Mullin J, Gallagher L, Dempsie Y, Welsh D. Macitentan treatment improves the dysfunctional right ventricle in a sugen/hypoxic rat model of pulmonary hypertension. DOI: 10.1183/13993003.congress-2019.PA5056 September 2019 ERS International Congress 2019 abstracts (Poster discussion)
  7. McGettrick M, Jayasekera G, Brewis M, Church C, Johnson M, Mackenzie A. The effect of exercise rehabilitation on cardiac function, measured by cardiac MRI, in patients with pre-capillary pulmonary hypertension. DOI: 10.1183/13993003.congress-2019.PA3946 September 2019 ERS International Congress 2019 abstracts (Poster presentation)
  8. Wilson K, Buist H, Jayasekera G, Liles J, Budas G, Fairfax S, Hughes C, Nilsen M, Church C, McLean M, Peacock A, Welsh D. Reversal of pulmonary

hypertension in a sugen/hypoxic rat model using an ASK1 inhibitor. DOI: 10.1183/1393003.congress-2017.OA4663 September 2017 ERS International Congress 2017 abstracts (Oral presentation)

9. Crowe T, Sonecki P, Jayasekera G, Mackenzie A, Church C, Johnson M, Peacock A. Late Diastolic dyssynchrony: A novel method to determine RV function in pulmonary hypertension? DOI: 10.1183/1393003.congress-2017.PA2445 September 2017 ERS International Congress 2017 abstracts (Poster presentation)
10. Mackenzie A, Jayasekera G, Crowe T, Church C, Peacock A, Johnson M. Haemodynamic effects of exercise therapy in stable, optimally treated pulmonary arterial hypertension. DOI: 10.1183/1393003.congress-2017.PA2395 September 2017 ERS International Congress 2017 abstracts (Poster presentation)
11. Crowe T, Sonecki P, Mackenzie A, Jayasekera G, Johnson M, Church C, Peacock A. 2-d segmental longitudinal strain rates correlate with prognostic indicators in idiopathic pulmonary arterial hypertension. DOI: 10.1136/thoraxjnl-2016-209333.116 Thorax 71(Suppl 3):A65.2-A66 (Poster discussion)

# Abstract

The definite hemodynamic diagnosis of pulmonary hypertension (PH) requires direct measurement of the pulmonary artery pressure by right heart catheterisation. As right heart catheterisation is an invasive test with a small risk of associated morbidity and mortality, diagnostic algorithms have been devised that combines clinical history and examination, cardio-respiratory assessment by non-imaging techniques and subsequently imaging techniques in patients suspected of having PH. The aim of these initial investigations is to establish a tentative diagnosis of PH, help identify the underlying aetiology and to provide information regarding disease severity and determine response to treatment.

Although PH is a disease of the pulmonary vasculature, it is the subsequent right ventricular (RV) failure that is the main cause of morbidity and mortality in PH patient. Thus, RV is the most widely studied of the chambers in PH, however focus has started to move to the left ventricle (LV). Although a disease of the pulmonary circulation and the RV, there is now evidence demonstrating LV abnormalities in PH. Further to this, the atrial chambers offer valuable information when measuring cardiac function as well as in identifying the aetiology of PH. Small animal (rodent) models are increasingly used to identify pathophysiology as well as therapies for PH with the intention of translating the findings to humans. Accurate monitoring of disease in rodents with emphasis on ventricular function and the ability to monitor the disease state without killing the animal is needed.

# Chapter 1 **Introduction**

## 1.1 Definition and haemodynamic classification of pulmonary hypertension.

Pulmonary hypertension (PH) is defined in guidelines as a resting mean pulmonary artery pressure (mPAP)  $\geq$  25mmHg measured at right heart catheterisation, resulting from a variety of conditions that can affect the pulmonary circulation (1). However, there are recent proposals to change the haemodynamic definition of PH and this will be discussed later in this chapter (2, 3). There is a progressive increase in pulmonary vascular resistance (PVR), which causes right ventricular (RV) failure and premature death. The term “primary pulmonary hypertension” was first reported in 1951 in a study of 39 patients with PH (4). However, the first description of the disease probably happened in 1891 by Ernst Von Romberg who described an autopsy as pulmonary arterial sclerosis (5). The 1<sup>st</sup> world symposium on PH organised by the World Health Organisation (WHO) in Geneva in 1973 was devoted to primary PH, few years after an outbreak related to the anorexigen Aminorex (6). In 1961, a report from the WHO expert committee on cor-pulmonale stated that mPAP does not normally exceed 15 mmHg in a healthy subject in supine position, however, in the World Symposium it was recognised the upper limit of normal mPAP was 25 mmHg. This was arbitrarily defined but this conservative cut-off value was used to discriminate patients with primary PH from severe PH due to other causes including lung diseases. This definition remained unchanged during the subsequent World Symposia from 1998 to 2013 at least in part to preclude potential over diagnosis and over treatment of PH (3).

In the first definition of the disease in 1973 in Geneva, the disease was classified as primary, secondary and associated PH (6). Since then subsequent world symposia have developed a more comprehensive clinical classification system based on 5 main groups of PH. Clinical classification as proposed at the 6<sup>th</sup> World Symposium on PH is summarised in Table 1.1 (3). The studies included in this thesis were conducted in patients with pulmonary arterial hypertension (PAH, Group 1 PH) unless otherwise stated.

**Table 1.1 Clinical classification of pulmonary hypertension**

<b>1 PAH</b>
1.1 Idiopathic PAH
1.2 Heritable PAH
1.3 Drug- and toxin-induced PAH
1.4 PAH associated with:
1.4.1 Connective tissue disease
1.4.2 HIV infection
1.4.3 Portal hypertension
1.4.4 Congenital heart disease
1.4.5 Schistosomiasis
1.5 PAH long-term responders to calcium channel blockers
1.6 PAH with overt features of venous/capillaries (PVOD/PCH) involvement
1.7 Persistent PH of the newborn syndrome
<b>2 PH due to left heart disease</b>
2.1 PH due to heart failure with preserved LVEF
2.2 PH due to heart failure with reduced LVEF
2.3 Valvular heart disease
2.4 Congenital/acquired cardiovascular conditions leading to post-capillary PH
<b>3 PH due to lung diseases and/or hypoxia</b>
3.1 Obstructive lung disease
3.2 Restrictive lung disease
3.3 Other lung disease with mixed restrictive/obstructive pattern
3.4 Hypoxia without lung disease
3.5 Developmental lung disorders
<b>4 PH due to pulmonary artery obstructions</b>
4.1 Chronic thromboembolic PH
4.2 Other pulmonary artery obstructions
<b>5 PH with unclear and/or multifactorial mechanisms</b>
5.1 Haematological disorders
5.2 Systemic and metabolic disorders
5.3 Others
5.4 Complex congenital heart disease

Modified from Simonneau et al (3). The clinical classification of PH is intended to categorise PH to 5 groups of clinical conditions according to clinical presentation, pathological findings, hemodynamic characteristics, and treatment strategy. 1 - pulmonary arterial hypertension, 2 - pulmonary hypertension due to left heart disease, 3 - pulmonary hypertension due to lung diseases and/or hypoxia, 4 - chronic thromboembolic pulmonary hypertension and other pulmonary artery obstructions, and 5 - pulmonary hypertension with unclear and/or multifactorial mechanisms.

### 1.1.1 Right heart catheterisation

Right heart catheterisation is the gold standard for diagnosis of PH. Apart from mPAP other haemodynamic measurements are taken during right heart catheterisation to characterise the pulmonary vasculature (7).

1. Cardiac output - cardiac output is usually measured by thermodilution or the estimated oxygen uptake Fick method.
2. Pulmonary Artery Wedge Pressure (PAWP) also known as pulmonary artery occlusion pressure and pulmonary capillary wedge pressure - this is measured by wedging the catheter in a branch of the pulmonary artery and inflating the balloon to a wedge position and reflects the pressure of the left atrium (LA). Elevated PAWP >15 mmHg is suggestive of left sided cardiac disease.
3. Pulmonary Vascular Resistance (PVR) - this is calculated by  $(\text{mPAP} - \text{PAWP}) / \text{CO}$

### 1.1.2 Upper limit of normal pulmonary artery pressure

As mentioned in chapter 1.1, the existing haemodynamic definition of PH had been based on a relatively arbitrary figure of mPAP  $\geq$  25 mmHg. However, in 2009 *Kovacs et al* analysed all available data obtained by right heart catheterisation in healthy individuals to determine the normal values of mPAP (8). In a large dataset of 1187 healthy subjects mPAP at rest was  $14.0 \pm 3.3$  mmHg; this value was independent of ethnicity and gender, and was not significantly affected by age and posture. Considering this value of 14 mmHg, two standard deviations would suggest mPAP > 20 mmHg as above the upper limit of normal. This haemodynamic definition is, therefore, no longer arbitrary, but based on a scientific approach. Thus, the most recent World Symposium of PH has proposed to reconsider the haemodynamic definition of PH to mPAP > 20mm Hg. However, they also recognised an isolated mPAP > 20 mmHg is not sufficient to define PH as this level of pressure rise could be due to an increase in cardiac output and PAWP. The task force has therefore proposed including a PVR  $\geq$  3 Wood Units (WU) into the definition of pre-capillary PH associated with mPAP > 20 mmHg, irrespective of aetiology (2, 3). However,

as most of the research included in our thesis predates this recent proposal, we have considered  $mPAP \geq 25$  mmHg as indicative of PH for the purpose of this thesis.

### **1.1.3 Idiopathic pulmonary arterial hypertension**

Idiopathic pulmonary arterial hypertension (IPAH) is a rare disease causing progressive pulmonary vasoconstriction, leading to RV failure and death. It is diagnosed after exclusion of other causes of PAH (group 1 PH) as shown in Table 1.1 (9). The annual incidence of IPAH has been estimated at 1-3.3 cases per million per year. Progressive shortness of breath is the common presentation and exertional chest pain, pre-syncope and syncope may occur. With further decline in RV function, leg swelling can occur. IPAH is often diagnosed at an advanced stage in terms of symptom burden as well as haemodynamic severity.

## **1.2 Treatment**

The treatment of PAH has significantly advanced in recent years. Five different classes of drugs are now available targeting 3 pathways i.e., Endothelin receptor antagonists, Phosphodiesterase 5 inhibitors, Soluble Guanylate Cyclase inhibitors, Prostacyclin analogues and Prostacyclin receptor antagonists. Studies have shown evidence that various combinations of these drugs to improve morbidity and survival in patients with PAH (10). In patients with left sided heart disease or lung disease causing PH (group 2 and group 3), the use of pulmonary vasodilator treatment has not shown to be safe or effective. For chronic thromboembolic PH (CTEPH) pulmonary endarterectomy (PEA) is the treatment of choice (11). In patients with inoperable CTEPH, Riociguat has proven efficacious (12). Other interventional options, including balloon pulmonary angioplasty has become a treatment option for these patients (13). Existing pharmaceutical treatment options for PH are shown in Figure 1.1.

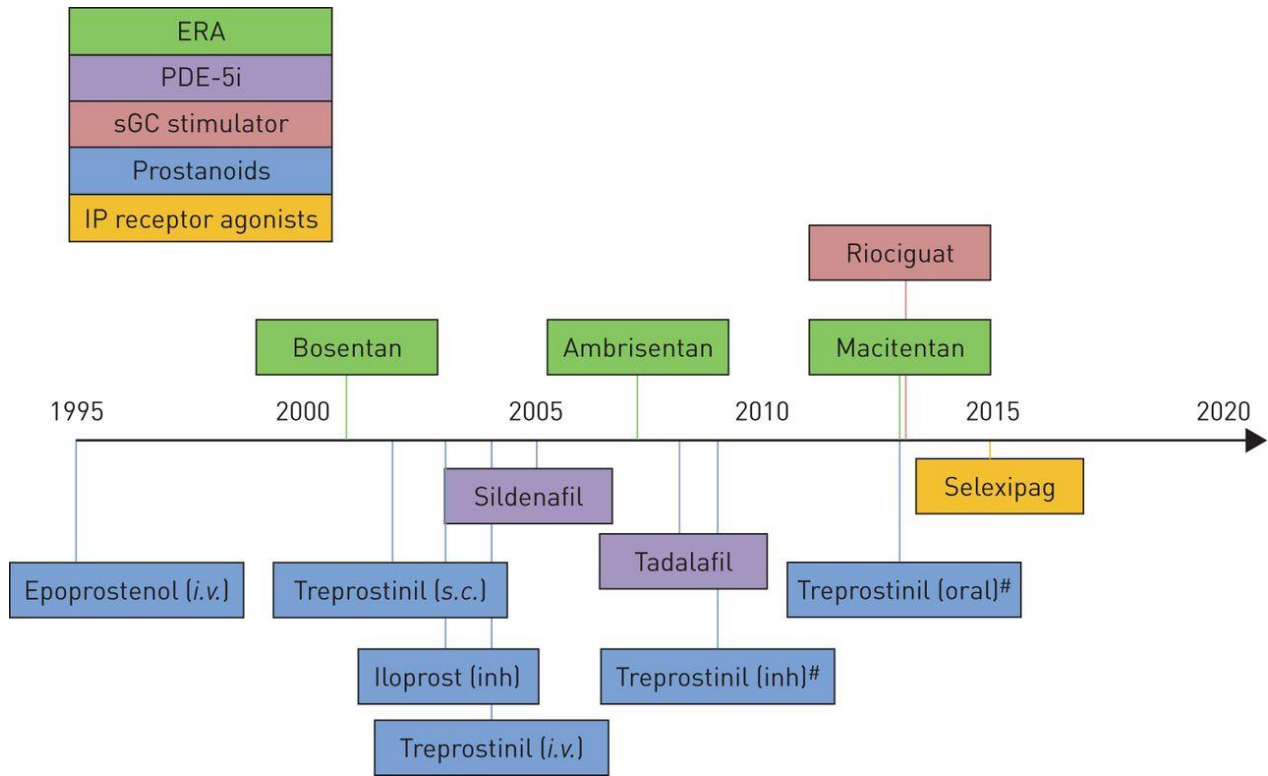


**Figure 1-1 Evolution of current treatment options for patients with pulmonary arterial hypertension.**

Modified from *Gaine et al* (10). Five different classes of drugs are now available i.e., Endothelin receptor antagonists, Phosphodiesterase 5 inhibitors, Soluble Guanylate Cyclase inhibitors, Prostacyclin analogues and Prostacyclin receptor antagonists. Studies have shown various combinations of these drugs to improve morbidity and survival in patients with PAH.

### 1.3 Non-invasive imaging in PH

The hemodynamic diagnosis of PH requires direct measurement of the pulmonary artery pressure by right heart catheterisation using a Swan-Ganz catheter. As right heart catheterisation is an invasive test with a small risk of associated morbidity and mortality, diagnostic algorithms have been devised that combines clinical history and examination, cardio-respiratory assessment by non-imaging techniques and subsequently imaging techniques in patients suspected of having PH (7, 14). The aim of these initial investigations is to establish a tentative diagnosis of PH. These imaging investigations also help to identify the underlying aetiology. Subsequently, guidelines recommend that the diagnosis of PH to be confirmed by right heart catheterisation. The initial tests will provide information regarding disease severity and will be used to monitor disease progression as well as response to treatment. Advanced imaging techniques may also help us to understand the cellular and molecular mechanisms responsible for the pathophysiology of PH in both the pulmonary circulation and the RV (15).

While it is noted that the RV is the most widely studied of the chambers in PH, focus has started to move to the left ventricle (LV). Although a disease of the pulmonary circulation and the RV, there is now evidence demonstrating LV abnormalities in PH (16, 17). Further to this, the atrial chambers offer valuable information when measuring cardiac function as well as in identifying the aetiology of PH (18). Small animal (rodent) models are increasingly used to identify pathophysiology as well as therapies for PH with the intention of translating the findings to humans (19). Accurate monitoring of disease in rodents with emphasis on ventricular function and the ability to monitor the disease state without killing the animal is needed.

The existing literature on imaging of the pulmonary circulation and the RV, particularly focusing on cardiac MRI (CMR) will be reviewed in the introduction of this thesis. Subsequently the rationale of the work undertaken in this thesis will be discussed. The introduction will also discuss the shifting of focus from the RV to the left heart and the importance of non-invasive imaging techniques in translational medicine. Finally, the aims and hypothesis of this thesis are introduced.

## 1.4 Echocardiography

### 1.4.1 Morphological assessment of the right heart and pulmonary circulation

Two-dimensional echocardiography using a subcostal or an apical 4-chamber view has been used to determine variables of RV morphology in patients with PH. Both RV end diastolic volume (RVEDV) and RV end diastolic volume indexed to body surface area (RVEDVI) have shown to correlate with mPAP (20, 21). However, RV volume calculation by two-dimensional echocardiography is extremely challenging due to the retrosternal location of the RV as well as its heavily trabeculated border. Measurements of RV free wall thickness and RV mass are also less practical due to the complex RV shape. The systolic and the diastolic positioning of the inter-ventricular septum (IVS) can be used to differentiate RV dilatation secondary to RV pressure overload from RV dilatation due to RV volume overload. In RV pressure overload the leftward IVS displacement is maximum at end-systole while RV volume overload due to increased RV preload resulted in predominantly end-diastolic IVS displacement (22). LV eccentricity index is the ratio of the length of two perpendicular minor axis diameters, which are obtained at both end-systole and end-diastole. One of these bisected and was perpendicular to the IVS. *Ryan et al* demonstrated that this index was 1.0 in normal subjects while it was greater than 1.0 in both end-systole and end-diastole in RV pressure overload. In RV volume overload the index was significantly increased at end-diastole, and approximately 1.0 at end-systole (23).

### 1.4.2 Haemodynamic assessment of the right heart and the pulmonary circulation

From the velocity of blood driving through a cardiac orifice, pressure is calculated using the modified Bernoulli equation (pressure gradient,  $\Delta P = 4V^2$  mmHg). From the apical 4-chamber view, tricuspid valve regurgitant jet velocity is used to calculate the tricuspid regurgitant pressure gradient (TRPG). From this, systolic pulmonary artery pressure (sPAP) can be calculated using the equation  $sPAP = TRPG + \text{right atrial pressure (RAP)}$  (24). RV systolic pressure (RVSP) is equivalent to sPAP assuming that there is no RV outflow tract stenosis. Right atrial pressure is required to calculate sPAP from TRPG. Inferior vena cava (IVC) diameter of

more than 1 cm and an IVC area of more than 2 cm<sup>2</sup> measured by echocardiography was a sensitive and a specific measure of raised RAP (8mm Hg) (25). *Kicher et al* suggested the percentage collapse of IVC during inspiration and expiration (caval index) as a predictor of RAP (caval index < 50% indicate RA pressure  $\geq$  10 mm Hg) (26).

### 1.4.3 Echocardiography definition of PH

Pulmonary hypertension has an invasive haemodynamic definition of mPAP of  $\geq$  25 mmHg during right heart catheterisation. Various attempts have been made to define PH based on non-invasive echocardiographic findings. Thus, these studies focused on finding the upper limit of normal sPAP or TRPG by echocardiography. In a study of 53 healthy people, TRPG ranged from 12.6 to 29.3 mmHg. The study authors concluded that TRPG of 30 mmHg should be considered the upper limit of normal (27). In a large database analysis of the Massachusetts General Hospital, among 3790 normal subjects, the estimated upper 95% limit for sPAP was 37.2 mmHg (RAP = 10mmHg). A sPAP > 40 mmHg was found in 6% of those >50 years old and 5% of those with a BMI > 30 kg/m<sup>2</sup> (28). *Syyed et al* demonstrated a relationship between sPAP measured by echocardiography and right heart catheterisation derived mPAP. This linear relationship ( $sPAP = 1.5 * mPAP + 0.46$ ) was maintained following changes in activity and posture (29).

The European Society of Cardiology and European Respiratory Society guidelines suggest grading the probability of PH based on tricuspid regurgitant velocity (and TRPG) and on the presence of additional echocardiographic variables. The probability of PH may be determined as high, intermediate or low probability and when interpreted in a clinical context can be used to decide on the need for right heart catheterisation(30).

### 1.4.4 Pulsatile pulmonary haemodynamics

Doppler techniques studying the flow velocity patterns of the RV outflow tract have been used to identify patients with PH. *Kitabake et al* identified characteristic abnormalities in the pulmonary valve motion in PH including rapid opening slope in systole and mid-systolic semi-closure of the pulmonary valve. In patients with PH, the flow velocity pattern demonstrated a rapid acceleration

reaching a peak level sooner than the normal cohort. Mid systolic notching due to a secondary slower rise during deceleration was also observed. They observed that the time to peak flow (AcT) and the ratio AcT/RVET (Right ventricular ejection time) decreased with rising pulmonary artery pressure (31). However ACT was also longer in patients with low cardiac index, congenital heart disease (32, 33) and shorter in patients with high body surface area and proximal pulmonary emboli (34, 35).

#### 1.4.5 Prognostic staging and follow up

Echocardiographic evidence of pericardial effusion, right atrial enlargement and septal displacement during diastole predicted adverse events in patients with PH and these are important in terms of prognosis in these patients (36). The Tei index or the myocardial performance index is a strong predictor of clinical status and survival in patients with PH. The Tei index is relatively unaffected by heart rate, RV pressure, RV dilatation or tricuspid regurgitation. The index is calculated using tissue Doppler recordings and is defined as  $(A-B)/B$  where A is the time interval between the end and onset of the trans-tricuspid flow and B is the right ventricular ejection time (RVET). The A interval includes the isovolumetric contraction time (IVCT), isovolumetric relaxation time (IVRT) and the RVET, thus the Tei index can also be expressed by the formula  $(IVCT + IVRT) / RVET$  (37). Using animal studies, *Cheung et al* demonstrated that the Tei index was significantly affected by changes in preload and afterload (38).

Tricuspid annular systolic plane excursion (TAPSE) is the most commonly used echocardiography derived prognostic indicator in PH. The RV contraction predominantly occurs on a longitudinal plane. Thus the displacement of the tricuspid annulus towards the RV apex is reflective of RV contraction, thus RV ejection fraction. TAPSE has shown to be highly reproducible and practical (39, 40). *Fofia et al* demonstrated that a TAPSE of less than 1.8 cm was associated with greater RV systolic dysfunction and right heart remodelling. A high TAPSE of 1.8 cm or more predicted survival with a 1 and 2-year survival rates of 94% and 88% compared to 60% and 50% in the low TAPSE group (41). In a study of 59 patients with IPAH, the group with  $TAPSE \leq 15$  mm and a left ventricular eccentricity index  $\geq 1.7$  had the highest adverse event rates (42). It is important to note that TAPSE

could be pseudo-normalised in significant volume loading as seen in left to right shunting or severe functional TR.

#### **1.4.6 Differential diagnosis**

Echocardiography may also aid in identifying the cause of PH including left heart disease, congenital cardiac diseases and valvular heart diseases. It may also help in identifying alternative causes of RV dilatation including RV arrhythmogenic dysplasia and RV infarction (43).

#### **1.4.7 3D Echocardiography**

RV measurements by 2-dimensional echocardiography are difficult due to its complex shape. 3-dimensional echocardiography (3D Echo) has been used frequently in the volumetry of the LV. *Grapsa et al* measured RVEDV and end-systolic volumes (RVESV), stroke volume and RV mass and compared these findings with CMR. Although CMR showed less inter-observer variability for some measures, RV volume and mass were similar for CMR and 3D echo in PH patients (44). In patients with dilated RV, 3D echocardiography has the disadvantage of suboptimal images, and the resulting exclusion of the RV free wall from the imaging has led to inaccurate volumes. As an alternative to this, *Bhave et al* suggested using a “knowledge-based reconstruction” method for 3D modelling of the RV endocardium from 2D images. This involved acquiring 2D images localised in 3D space by a magnetic field generator located under the patient and a magnetic field sensor, then using a reconstruction algorithm to construct a 3D model. This is based on identifying specific landmarks and a reconstructing algorithm using these landmarks to fit sub regions of the RV to hearts in a database of patients with similar pathology. These provided valuable and accurate RV volumes, which compared well with CMR, but larger studies are required (45).

### **1.5 Chest radiography**

Plain chest radiography (Chest X-ray) is inexpensive, widely available and in combination with echocardiography provide the first clue to the presence of PH. Enlargement of pulmonary arteries, cardiac enlargement, particularly the right sided chambers and rapid tapering of the pulmonary vessels as they extend to the periphery are all chest X-ray features of PH. There is also peripheral pruning

(reduction of the size of intrapulmonary vessels) (46). Transverse diameter of the proximal inter-lobar pulmonary artery on posterior-anterior chest radiograph that exceeds 16 mm in men and 15 mm in women is a useful measurement for enlargement of the central pulmonary arteries, likely to be due to PAH in the absence of a left-to-right shunt (47).

*Kanemoto et al* reviewed 59 chest radiographs in patients with “primary PH”. They compared five measured values between normal control and primary PH group.  $DPA / (T/2)$ , which is an indicator of the degree of protrusion of the main pulmonary artery, where DPA is the width of the main pulmonary artery from the midline and T is the thoracic diameter (divided by half thoracic diameter to eliminate differences) was significantly higher in the primary PH group. The average width of the descending branch of the right pulmonary artery (dPA) was more than twice that of the control group (12.1 to 25.1). The PL/T index (The point of union of the external border of the upper lobe artery with the pars interlobaris = point L, the sum of horizontal distances of the right and left L to the midline = pulmonary lobar diameter, PL) was increased in the “primary PH” population (48). Previously *Lupi et al* had suggested that the PL/T index as a radiological index suggesting PAH (49). The normal values for the width of the descending branch of the right pulmonary artery has been reported as 9-13 mm by *Schwedel et al* (50) 9-16 mm by *Simon et al* (51) and 9-16 mm for men and 9-15 mm for women by *Chang et al* (52).

In CTEPH apart from features of peripheral oligoemia there may be asymmetry of hilar vessels when thrombosis occurs in central pulmonary arteries. *Woodruff et al* reviewed 22 chest radiographs of patients with CTEPH (53). Cardiac enlargement was defined by a cardiothoracic ratio of more than 0.5 and RV enlargement was defined by a retrosternal cardiac silhouette height greater than one-third the distance between the anterior cardiophrenic sulcus and the angle of Louis. All the patients in both operative and non-operative groups had abnormal chest radiographs. Nineteen patients had cardiomegaly and 13 of these had predominantly RV enlargement. A value of 0.23 for the ratio of the diameter of the main PA to the diameter of the left hemithorax was considered normal in a previous study and all but one patient had a higher ratio in this study. Twelve patients had enlarged right descending pulmonary arteries (16 mm for men and 15

mm for women). Specific areas of diminished vascularity were found in about two third of the patients and these were confirmed by pulmonary angiography. Findings of an abnormal chest radiograph in this study and in a further study by *Tilkian et al* (54) were in contrast to previous studies by *Moser et al* (55) and *Benotti et al* (56) who concluded most patients with CTEPH have normal chest radiographs.

The aforementioned characteristic chest X-ray findings are only likely to be visible in severe disease limiting the use in diagnosing early or mild PH. Chest X-ray will also provide valuable information regarding the cause of PH during the diagnostic workup including parenchymal lung disease and left heart disease (24).

## 1.6 Ventilation perfusion scintigraphy

Ventilation Perfusion scintigraphy (V/Q scan) is recommended in the diagnostic workup of PH. Its main role is in distinguishing CTEPH from other types of PH (57, 58). Acute or chronic pulmonary embolism results in a characteristic wedge-shaped defect on the perfusion scan that corresponds to the thrombotic occlusion and the normal ventilation images produce the V/Q mismatch.

*Worsley et al* demonstrated that a high probability V/Q scan had sensitivity and specificity of 96 % and 94 % respectively in detecting CTEPH and when high and intermediate probability scans were combined the sensitivity was 100% at the expense of reduced specificity of 86%. None of the patients with a low probability scan had CTEPH (59). In a larger study of 227 patients by *Tunariu et al*, when only high probability scans were considered as suggestive of CTEPH the sensitivity was 96% with a specificity of 95%. When both high and intermediate probability scans were considered suggestive of CTEPH the specificity fell to 90% (57). These and a number of other studies demonstrate that V/Q scanning is a highly sensitive test for suspected CTEPH. Grouping intermediate probability results with low probability results provide a highly sensitive and specific investigation in the diagnosis of CTEPH. However mismatched defects at V/Q scanning maybe seen in patients with IPAH presumably due to thrombosis in situ (58). An abnormal perfusion scan similarly can be observed in large vessel vasculitis (60), fibrosing mediastinitis (61), pulmonary artery sarcoma (62) and pulmonary veno-occlusive disease (63).

Multi-detector CT pulmonary angiography (CTPA) has replaced V/Q scanning as the investigation of choice in the diagnosis of acute pulmonary embolism. However, the role of CTPA in detecting CTEPH is variable. *Pitton et al* showed multi-detector CTPA to have a sensitivity of 70.4% for segmental and 63.6% for sub-segmental branches when compared to pulmonary digital subtraction angiography (DSA) (64). The retrospective review by *Tunariu et al* confirmed that normal V/Q scintigraphy excluded CTEPH whereas normal CTPA did not (57). In the CTEPH group in this study, CTPA was reported as showing features suggestive of CTEPH in 40 of the 78 patients with a false negative report in 38 of the 78 (sensitivity 51%). A CTPA report was considered as suggestive of CTEPH, if it stated visualisation of the thrombus, calcified thrombus, recanalization, sudden change of vessel calibre, strictures, post-stenotic dilatation, webs or perfusion abnormalities. The presence of mosaicism was also noted but its presence alone without other features was not considered diagnostic of CTEPH.

On planar imaging, the detection of perfusion defects is dependent on camera position and the anatomical location of the defects, thus there is the potential that a defect can be masked if superimposed over normal lung. Single - photon emission computed tomography or SPECT scanning overcomes this by producing three-dimensional imaging data. *Soler et al* demonstrated higher sensitivity of SPECT scanning with minimal change to specificity in CTEPH patients (65).

## 1.7 Computed Tomography (CT)

There have been significant advances in CT scanning in recent years. There have been advances in contrast enhancement, post-processing power and sub millimetre thick slices. CT scanning is usually performed as part of the early diagnostic assessment in patients presenting with shortness of breath or atypical chest pain. CT scanning has the advantage of not just imaging the lung parenchyma but the heart, mediastinal structures and the pulmonary arteries in patients presenting with PH. CT scanning aids identifying parenchymal abnormalities that can occur sometimes in the presence of normal spirometry, CT pulmonary angiography will help assessing the pulmonary vasculature in PH patients. Other imaging biomarkers including RV to LV ratio, left atrial size and PA size are also derived from CT. CT will also aid in the classification of PH into

WHO groups (66). Due to repeated exposure to radiation, CT scanning is not routinely used in monitoring disease progression and response to treatment.

### 1.7.1 The main pulmonary artery (Main PA)

There have been various studies examining the reliability of the diameter of the main PA being a non-invasive surrogate of PH. The intra-pericardial main PA cannot be measured by plain chest radiography. However, it can be measured by CT. A diameter of the main PA of more than 28.6 mm predicted PH in an early study of 32 patients. The best estimate of PA pressure was given by the calculated cross sectional area of main and inter-lobar arteries normalised to body surface area (67).

*Ng et al* measured the main PA diameters at a defined level, where the right pulmonary artery is in continuity with the main PA and sweep across the midline. The ratio of the main PA to the ascending aorta as well as main PA alone were related to mPAP (68). In younger patients (<50), mPAP correlated more with the ratio than the diameter of the main PA alone. This is probably due to a gradual increase in the diameter of the aorta with advancing age. Another advantage of using the ratio of the main PA: aorta is the degree of internal normalisation with the lack of dependence on body surface area and gender, as both influence the pulmonary artery and aortic diameters to an equal degree. In another study where the main PA was measured at the widest portion of the main pulmonary artery within 3 cm from the bifurcation, PA diameter of  $\geq 29$  mm had a sensitivity of 87%, a specificity of 89% and a positive predictive value of 0.97 for predicting PH. *Mahammedi et al* attempted to establish the best method to measure the main PA by CT in suspected PH (69). The most reproducible method with the least inter-observer variability was the method in which the axial diameter of the main PA was measured along the line that originates from the centre of the adjacent aorta and passes perpendicular to the long axis of the main PA at the level of PA bifurcation. A main PA diameter of  $> 31.5$  mm demonstrated sensitivity and specificity 52% and 90% respectively. A main PA: aorta of  $> 1$  was 71% sensitive and 76% specific for PH. *Truong et al* used the transverse axial diameter of the main PA and the ascending aorta at the level of the bifurcation of the right PA. They established a 90<sup>th</sup> percentile sex-specific cut-off value for main PA for men of 29mm and women of 27mm and found an association with dyspnoea using the

aforementioned cut-off values. Interestingly they did not find an association with dyspnoea when using a 90<sup>th</sup> percentile cut off value of 0.9 or commonly used value of 1.0 for the pulmonary artery: aorta ratio (70).

As noted above, there is a large variation both in terms of the methodology and the reported cut-off diameter of the main PA on CT when determining dilatation.

### **1.7.2 Beyond the main pulmonary artery**

The studies that measures the calibre of right and left PA and the right inter-lobar artery did not appear to offer an advantage over main PA measurements on the strength of correlation with right heart catheter derived mPAP. In a study by *Tan et al*, they looked at CT determined measurements of main PA, right and left PA and the ratio between segmental arteries and their corresponding bronchi (ABR). An ABR of more than 1:1 in three of four lobes were higher in the PH population compared to the control group (65% vs 22 %). The apical segmental arteries and the bronchi of the upper lobes and the posterior basal segmental arteries and the bronchi of the lower lobes were chosen for this study (71). It is important to note that solitary segmental artery enlargement may be seen in normal subjects as well as patients with regional lung abnormalities such as pulmonary fibrosis. In this study the combination of a main PA diameter of or more than 29 mm and an ABR of more than 1:1 in three or four lobes was the most specific finding for the presence of PH (specificity 100%).

Hypertrophy of the bronchial arteries is a well-recognised radiological feature on conventional angiography and CT pulmonary angiography (CTPA) in patients with CTEPH. Although the mechanism of bronchial artery hypertrophy is not completely understood, their role is thought to be to maintain the viability of the lung parenchyma after pulmonary artery occlusion. Hypertrophied bronchial arteries are easily identified on CT and are usually not visualised in normal individuals. *Remi-Jardin et al* defined bronchial artery hypertrophy as a curvilinear mediastinal vessel of more than 1.5 mm diameter, which is seen along the course of the proximal bronchial tree. In an earlier study of patients with primary PH and CTEPH, they suggested that visualisation of bronchopulmonary collaterals and demonstration of bronchopulmonary collateral flow were a distinguishing feature of CTEPH from those with primary PH. However, more recent studies have

demonstrated bronchial artery hypertrophy to occur in patients with IPAH as well as Eisenmenger's syndrome (72).

A study by *Shimizu et al* showed that in CTEPH patients the cross-sectional area of bronchial arteries correlates to the extent of central pulmonary thrombus. When they grouped the CTEPH patients into main, lobar and segmental type based on the most proximal location of thrombi, they did not find any significant difference between the total area of bronchial arteries in segmental type CTEPH and PAH patients. The cross sectional area of bronchial arteries did not have a significant correlation with mPAP or PVR but their presence predicted a better post-surgical outcome (73).

### **1.7.3 Cardiac signs**

ECG gated CT can be used to obtain information regarding ventricular function and to detect congenital cardiac abnormalities. However, conventional CT provide information about the heart that can be used in the diagnostic workup in patients suspected of having PH. An axial RV to LV ratio of more than 1:1 at the mid ventricular level is indicative of RV enlargement. There may be paradoxical bulging of the IVS towards the LV, although this is better appreciated in cine review of ECG gated studies. When CT features of PH are associated with left sided cardiac chamber enlargement, pulmonary venous dilation and interlobular septal thickening, this is suggestive of pulmonary venous hypertension with a possible left heart cause. Thickening and calcification of the mitral valve leaflets with associated left atrial enlargement, which is suggestive of mitral valve disease and aortic valve calcification, and LV hypertrophy suggestive of aortic valve disease can be identified on conventional CT. Left atrial myxomas, by interfering with mitral valve function and pulmonary vein drainage can occasionally present with PH and can be identified as a well-defined intra-cavity mass with low attenuation (74-76).

The presence of contrast in the IVC or hepatic veins during first pass contrast enhanced chest CT is associated with tricuspid regurgitation. The extent of contrast reflux was associated with PA pressures measured at right heart catheterisation as well as the severity of tricuspid regurgitation by echocardiography (77). It is important to note that although this is a specific sign

of TR, the specificity decreases at higher contrast injection rates of greater than 3ml/sec (78).

Pericardial effusions are common in patients with severe PH and this was demonstrated in a multicentre trial of patients with severe PH on prostacyclin. The 1-year mortality in patients with small or moderate effusions was three times that of patients with trace or no effusions. The presence of an effusion also correlated with right atrial size, severity of tricuspid regurgitation and reduced 6-minute walk test (79). On CT pericardial effusions create an infilling of the space between the main pulmonary artery and ascending aorta which is known as the “bikini bottom sign”.

#### **1.7.4 Lung parenchyma**

Mosaicism of the lung parenchyma is characterised by sharply demarcated areas of heterogeneous attenuation that predominantly conform to the boundaries of the secondary pulmonary lobules. In the context of PH this is most commonly seen in patients with CTEPH. In CTEPH, mosaicism corresponds to V/Q mismatch. The darker areas represent hypoperfusion while the higher attenuation areas correspond to normal or hyperperfusion. However mosaicism is not specific for CTEPH and can be seen in patients with small airways diseases as well as infiltrative lung diseases (80). In small airways disease expiratory HRCT demonstrate air trapping which caused an increase in the conspicuity of the mosaic pattern. It was initially thought that this could be used to differentiate CTEPH from small airways disease but studies have reported air trapping as well as bronchial dilatation in patients with CTEPH (81, 82).

#### **1.7.5 CT in chronic thromboembolic pulmonary hypertension**

Contrary to the findings in acute pulmonary emboli, which result in a concavity within the contrast material on angiography, CTEPH may lead to a complete vessel cut off which appears as a convex margin of contrast material on CTPA. In a complete obstruction the distal vessel diameter will be decreased, and the pulmonary artery diameter may be increased at the site of the thrombus. In a partial obstruction CTPA findings include abrupt vessel narrowing, irregularity of the intimal surface contour and intravascular bands and webs. Bands are thin

structures attached to the vessel wall that can be up to 20 mm in length with a free mid portion. Webs are a descriptive term for a complex network of bands. These features seen in pulmonary angiography represent organising thrombi. Chronic organising thrombi can rarely be calcified (83). Pulmonary artery diameter may be increased with a raised main PA to ascending aorta ratio as described earlier in the section 1.6.1. The RV undergoes hypertrophy and subsequently dilates with RV failure. There may be displacement of the IVS towards the LV during systole. The reflux of contrast material to the inferior vena cava or hepatic veins maybe observed which would indicate tricuspid regurgitation. Bronchial artery hypertrophy as well as enlarged non-bronchial systemic arteries are more common in patients with CTEPH compared to other forms. The key parenchymal imaging feature of CTEPH is mosaic attenuation pattern of the lung parenchyma. Pulmonary infarcts may be visible especially at the lower parts of the lung as wedge shaped or linear, peripheral, irregular densities (84). They are due to occlusion of segmental and smaller pulmonary arteries and occur commonly in peripheral type CTEPH.

The morbidity and mortality from Pulmonary Endarterectomy (PEA) has fallen significantly over the last few years. Several studies have concentrated on imaging features that help predict surgical success in patients undergoing PEA. In a study by Bergin et al CTPA evidence of extensive central vessel disease and limited small vessel involvement predicted a favourable post-surgical outcome (85). In a study by *Shimizu et al* the total area of bronchial arteries correlated to the central extent of thrombi and also predicted the gas exchange improvement after PEA suggesting that these patients had a lower proportion of distal vascular disease (73). The presence of peripheral sub pleural densities, which reflect pulmonary infarcts commonly seen in peripheral type CTEPH demonstrated a positive correlation with postoperative PVR, which may lead to a poor postoperative outcome.

### **1.7.6 CT in pulmonary veno-occlusive disease**

Pulmonary veno-occlusive disease (PVOD) is a rare cause of PH where there is involvement of the post- capillary vasculature. It is difficult to make this diagnosis in vivo and a histopathological diagnosis using open surgical biopsy is usually contraindicated in these patients due to general frailty of this patient group. Two

studies that retrospectively identified fifteen and eight patients with PVOD, studied the radiological features that would assist non-invasive CT assessment in these patients (86, 87). The most common CT findings were septal lines, ground glass opacities particularly with a centrilobular distribution and lymphadenopathy. In the absence of other causes of PH; e.g.; CTEPH and left sided heart disease, adenopathy was highly specific for PVOD. Normal left sided cardiac chambers and normal PAWP allows distinction of PVOD from pulmonary venous hypertension.

## **1.8 Cardiac Magnetic Resonance imaging**

### **1.8.1 Ventricular volume, structure and function**

Although PAH is a disease of the pulmonary vasculature, it is the subsequent RV failure that is the main cause of morbidity and mortality in patients with PAH. Plain chest radiography and CT scanning do provide some information about RV structure; however, they do not give information regarding RV function. Although echocardiography is widely available RV volume and function calculation by two-dimensional echocardiography is extremely challenging due to the retrosternal location of the RV as well as the heavily trabeculated border (section 1.3).

Cardiac magnetic resonance imaging (CMR) is a non-invasive imaging tool and provides high-resolution 3D images of the heart (15). Short axis stacks are used to reconstruct a 3D image of the RV and LV and ventricular volumes and wall mass can be measured covering the entire cardiac cycle. Endocardial and epicardial contours are drawn at end-diastole and end-systole during post processing of images and ventricular volumes are calculated using the “Simpsons rule”, which takes the sum of individual slice volumes and the inter-slice gap into account. From the volume changes of the RV over time, systolic and diastolic function can be derived. New software solutions with semi-automatic analysis have resulted in decreased post processing times. The inter-study reproducibility and accuracy of CMR measurements using a semiautomatic analysis have been validated in several reports (88, 89). Velocity encoded cine CMR images are used to quantify PA flow. The aorta flow can be measured in the same plane and the ratio of pulmonary artery: aorta flow ( $Q_p: Q_s$ ) and vice versa can be used to assess intra-cardiac shunts. *Beerbaum et al* concluded that the calculation of  $Q_p: Q_s$  by CMR to be quick, safe and reliable in children with cardiac defects (90).

The ability to determine RV systolic function by conventional echocardiography based on volume calculations is limited. Although contrast-enhanced 3D echocardiography has become available recently and has shown to be useful in assessing RV mass and RV ejection fraction, CMR remains the gold standard(44). A large number of studies using CMR imaging in patients with PAH have been published. Many CMR measures have shown to be strongly predictive of mortality and survival thus offering potential for monitoring and assessing response to treatment.

Of these, Stroke volume (SV) is recognised as a key MR prognostic measure in PAH patients. *Van Wolferen et al* investigated the prognostic significance of a variety of LV and RV structural and functional measurements in patients with IPAH (91, 92). They showed that a low SV at baseline is a predictor of poor prognosis. They also showed that SV rather than cardiac index to have a stronger correlation with prognosis in these patients, possibly explained by the fact that there may be compensatory increase in heart rate which will flaw the relationship between cardiac output and prognosis. The results in this study also suggested that a decrease in SV during treatment to be an indicator of treatment failure. Although results were comparable when SV were measured by CMR or with the Fick method, CMR underestimated SV. This is probably explained by turbulent blood flow patterns observed in the main PA. This was evident both at baseline as well as follow up. In a large single centre cohort of patients with systemic sclerosis associated PH, stroke volume index (SVI) was a strong predictor of survival. There was two-fold increased risk of mortality in patients with a SVI of  $> 30\text{ml}/\text{m}^2$  (93). *Van Wolferen et al* evaluated 111 patients at baseline and at 1 year follow up to identify a minimally important difference in SV in patients with PH. They used both an anchor based method (using 6 minute walk distance as anchor) and a distribution-based method and showed a 10 ml change in stroke volume during follow up should be considered as clinically relevant (94).

Right ventricular ejection fraction (RVEF) is also an important prognostic factor in patients with PH and is poorly derived by conventional echocardiography. A study in a large group of WHO group 1 patients with PAH, RVEF measured at baseline was a better predictor of mortality compared to PVR (95). They showed, in patients who are on PAH targeted therapy that RV function can deteriorate despite

reduction in PVR, which occurred in 25% of the patients. They showed that the deterioration of RVEF was associated with poor outcome independent of any changes of PVR. They hypothesized that the deterioration in RVEF could be explained by pulmonary pressures and subsequently ventricular wall tension that was unaltered after medical treatment despite a fall in PVR. This study emphasized the importance of monitoring RV function during the course of the disease.

RV end diastolic volume is another predictor of prognosis in PAH. Kaplan-Meier survival analysis in a study by *Van Wolferen et al* demonstrated that patients with a RVEDVI of  $< 84\text{ml/m}^2$  at diagnosis had a significantly better survival compared to those with a RVEDVI of  $84\text{ ml/m}^2$  or more (91). A further study by *Yamada et al* showed that an increased RVEDVI predicted both hospitalisation and mortality in patients with IPAH but couldn't establish a significant difference between the aforementioned two groups in the previous study (96).

Swift et al identified patients with PAH undergoing MRI from the ASPIRE registry and determined the value of CMR metrics for mortality prediction in PAH (97). They confirmed the independent prognostic value of CMR measurements reflecting RV volume and proximal pulmonary vasculature in a large cohort of PAH patients. A model combining MRI measurements of RVESV and PA relative area change in combination with clinical data including age, sex, WHO functional class and the presence of underlying connective tissue disease improved the prognostication in PAH. In this study RVESV rather than RVEDV was independently prognostic in PAH patients and the authors suggested that loss of RV systolic function may explain the greater prognostic importance.

In a study by *Mauritz et al*, CMR defined geometric changes during the development of RV failure (98). They identified certain CMR derived geometric characteristics that defined non-survivors (survival less than 5 years) at the beginning of the study and at 1 year follow up. They identified that the RV longitudinal shortening (distance change between end-diastole and end-systole of the tricuspid annulus to apex distance) and transverse shortening (change between end-diastole and end-systole of the RV free wall to septal distance) are already reduced at baseline in non-survivors, that transverse shortening further declines over time while longitudinal shortening and RV free wall motion stay the

same. They demonstrated that the end stage decline in RV function is due to progressive leftward septal displacement rather than further changes in RV free wall transverse or longitudinal displacement. The authors concluded that although there is a parallel decline in longitudinal and transverse shortening during progressive RV failure, a floor effect is reached for longitudinal shortening. As transverse shortening incorporates both free wall and septal motion, it could be used as a variable of monitoring RV failure. They identified that the RV fractional area change (RVFAC) which combines the effect of both transverse and longitudinal shortening ( $RVFAC = 100 \times [(RVED \text{ area} - RVES \text{ area}) / RVED \text{ area}]$ ) to correlate well with RVEF. The study showed that a decline in RVFAC to be an accurate measure of RV failure in patients with severe PAH.

In a multicentre study prospectively assessing the use of CMR before and during PAH disease specific treatment, Peacock et al demonstrated the importance of including both right sided and left sided variables when determining cardiac function (99). In this EURO-MR study they highlighted that LV end-diastolic volume (LVEDV) to be more closely related to SV than RV end-diastolic volume. The authors suggested that poor LV output in PH patients was due to poor LV filling which was a consequence of prolonged RV contraction time. This contributed to a decreased stroke volume thus LVEDV reflected both the stroke volume and RV contraction time.

### 1.8.2 Phase contrast CMR

Blood flow of the main PA can be measured with phase contrast imaging using velocity encoded gradients. Various measurements such as average velocity, peak velocity, anterograde and retrograde flow can be determined. *Sanz et al* demonstrated that average velocity of the blood flow in the pulmonary artery to correlate with invasive pressure measurements (sPAP  $r = -0.76$ , mPAP  $r = -0.73$ ) and PVR index ( $r = -0.86$ ) (100). Average velocity with a cut off value of 11.7cm/sec was 92.9% sensitive and 82.4% specific to detect PH. *Mousseaux et al* demonstrated good correlations between right heart catheter measurements and CMR velocity encoded image derived flow measurements, enabling distinction of individuals with high PVR from normal PVR (101). Relative onset of time (ROT) of retrograde flow in the main PA (relative to cardiac cycle duration) were determined in a study by *Helderman et al*, consisting of 38 PAH patients (102). A

ROT of 0.25 distinguished PAH patients from non-PAH patients, demonstrating that early onset of retrograde flow to be characteristic of PAH.

### 1.8.3 Pulmonary artery stiffness and pulsatility

Pulmonary arterial elasticity is an important factor determining the relationship between the RV and the PA, RV - PA coupling. A study was conducted to evaluate pulmonary arterial stiffness in patients with PH, exercise induced PH and no PH. Various indices of PA stiffness were studied. These included 1. Relative change in lumen area during cardiac cycle (pulsatility), 2. Absolute change in lumen area for a given pressure (compliance), 3. Change in volume associated with a given pressure (capacitance), 4. Relative change in lumen area for a given pressure (distensibility), 5. Pressure change driving a relative increase in lumen area (elastic modulus) and 6. Slope of function between distending arterial pressure and arterial distension (stiffness index beta). Patients with exercise induced PH had lower median compliance and capacitance than patients with no PH. The aforementioned different measures of PA stiffness showed significant correlation with PA pressures ( $r^2 = 0.27$  to  $0.73$ ). They showed that reduced PA pulsatility of  $< 40\%$  to detect the presence of PH with a sensitivity of  $93\%$  and a specificity of  $63\%$ . The authors concluded that PA stiffness occur early in PH even when overt pressure elevations are not present at rest (103).

### 1.8.4 RV - PA coupling

The gold standard measure of RV systolic functional adaptation to changes in afterload is to measure end-systolic elastance ( $E_{es}$ ), which is derived by dividing end-systolic pressure (ESP) by end-systolic volume (ESV), corrected for arterial elastance ( $E_a$ ) (stroke volume/ ESP). This load independent measure of RV - PA coupling defines matching of RV contractility to afterload. Although this requires instantaneous measurements of RV pressure and volume which is not practical, this can be simplified for pressure and expressed either as a SV/ ESV ratio (the volume method) or simplified for volume and expressed as RV maximum pressure divided by mPAP minus 1 (the pressure method). In a study of 140 treatment naïve patients by *Brewis et al*, RV - PA coupling measurements by volume method

(SV/ESV) predicted outcome, however there were no added benefits of RV-PA coupling measurements by the pressure method (104).

An alternative descriptor of coupling has been analysed by echocardiography (105). In a study of 459 patients with heart failure, TAPSE/PASP ratio was used as a measure of RV and pulmonary arterial coupling. The group with the lowest ratio, that is low TAPSE with high PASP, had greater risk of adverse events and most impaired clinical function. Although the authors termed this study ventriculo-arterial coupling, their measurements did not calculate elastance within the ventricle or pulmonary vasculature.

## **1.9 Non-invasive assessment of haemodynamics with CMR**

As discussed in the Echocardiography section, the ability to non-invasively estimate pulmonary pressure is a key objective of imaging techniques. Systolic pulmonary artery pressure can be estimated with echocardiography using the tricuspid regurgitant jet velocity. Various CMR studies have assessed estimation of both mPAP and PVR with CMR metrics in PH(106, 107). In a study by Swift et al, mPAP was accurately estimated using a statistical model involving VMI and IVS angle.

### **1.10 Strain**

Myocardial strain measures the degree of deformation of a myocardial segment from its initial length. If the initial length is termed  $L_0$  and the maximum length  $L$ , strain can be determined by the following formula (108).  $\text{Strain} = (L - L_0) / L_0$

There are two main definitions of strain.

1. Lagrangian strain - the displacement is calculated at a fixed material point in the myocardium. The deforming myocardium is used as a reference.
2. Eulerian strain - tissue strain at a specific location in space, so spatial coordinates are fixed, but material points keep changing.

Strain imaging that is discussed in this thesis is based on the analysis of Lagrangian strain.

### **1.10.1 Cardiac deformation / strain by echocardiography**

In echocardiography strain has been assessed by Doppler imaging and speckle tracking. Doppler imaging requires identification of a “region of interest” in the myocardial wall and mapping changes in the velocity of this “region of interest” through the cardiac cycle. In recent years, this process has become superseded by the speckle tracking method. From strain, strain rate can be calculated by  $\Delta L/\Delta t$ . Whereas strain is a measurement from baseline, the rate can be measured continuously throughout the cardiac cycle. Peak systolic measurements of strain and strain rate are typically reported in studies looking at strain as a measure of cardiac function however, early and late diastolic peak values can be derived providing insight into diastolic function.

### **1.10.2 Speckle tracking echocardiography**

Speckle is the term given to the greyscale pixilation pattern created by the reflection of sound waves at an interface. The imperfection of a surface creates a unique reflection and therefore fingerprint of pixels at that region. This pixel fingerprint can subsequently be tracked across the cardiac cycle. By tracking many pixels across a “region of interest”, the deformation of the tracked structure can be measured, thus strain can be calculated along the entire “region of interest” (15). Unlike Doppler imaging, speckle tracking is not dependent on angle. Although measurement of deformation can be made in three planes, longitudinally, circumferentially and radially, imaging the latter two in the RV by two-dimensional imaging is challenging. Developments in 3D echocardiography assists with this limitation. Longitudinal strain of the RV free wall is the right ventricular measurement often reported in the literature.

### **1.10.3 RV strain and RV dyssynchrony in PH by echocardiography**

Strain analysis of the LV in post myocardial infarction hearts through speckle tracking has been reported since 2004 and LV strain analysis by echocardiography is well established (109, 110). The use of speckle tracking echocardiography to

analyse strain has been validated by sonomicrometry and MRI tagging (111, 112). *Rajdev et al* demonstrated reduced strain in RV and LV free walls and the IVS in PH using tissue Doppler imaging (113, 114). They did, however report inter-observer variabilities between 11.2% and 26.6% +/- 30.9, and intra-observer variability of 13.6 to 18.2% +/-13. In another study *Borges et al* demonstrated significant changes in RV strain pre-treatment and post-treatment in PH patients, using both Doppler imaging and speckle tracking(114). Both tissue Doppler measurements and speckle tracking showed significance between groups, although were not compared against each other.

Peak systolic longitudinal strain of the RV has become established as a measure of RV function in PH. *Filusch et al* used tissue Doppler imaging to measure peak systolic strain and strain rate of the RV free wall in controls and patients with IPAH. They demonstrated that RV strain and strain rate measurements to correlate with known markers of disease severity including PVR, cardiac output, TAPSE, Tei Index, NT-proBNP and 6 minute walk (115). Although, this implies that strain could be used as a continuous variable of cardiac function, in current guidelines, a value less than -20% (i.e. smaller measure of strain) is accepted as a cut-off measure of impairment (116). *Sachedev et al* studied a patient group with PAH and demonstrated impaired RV free wall peak systolic longitudinal strain and strain rates (average strain -15.5% and strain rate  $-0.80\text{ s}^{-1}$ ) (117). Comparing patients with a strain less than -12.5% compared to patients with a strain more than -20%, showed 4-year mortality of 93% versus 39% respectively. Regarding strain rate, a value less than  $-0.7\text{ s}^{-1}$  was associated with worsened disease progression and mortality. *Haeck et al* also looked at peak systolic longitudinal strain of the RV in a PH group (118). They found the group with a strain value less than -19% was associated with an impaired survival over a 5-year period of 55%. They also identified a higher WHO functional class, increased diuretic use, larger RV areas with reduced RVFAC and lower TAPSE in this group.

Global strain assessments of the RV, including measurement of the IVS and free wall, have also been studied (119-121). In a group of PH and control subjects, global peak systolic RV longitudinal strain was reduced in the PH group, -15.6% versus -23.8% (119). In another PAH group, a global peak RV longitudinal strain less than -15.5% was associated with reduced event free time and total survival

(121). In 2015 *Park and Kusunose* also looked at global RV longitudinal strain and isolated free wall strain pre and post treatment (120). They showed improvement in longitudinal strain measurements and moderate correlation with change in strain and mPAP. More recently a study looking at longitudinal RV free wall strain against other echocardiogram parameters and pulmonary pressures showed a strain value of -19.26% was diagnostic of mPAP  $\geq$  45mmHg with a sensitivity of 83.9% and a specificity of 73.4% (122).

Cardiac function assessment by strain recording across the cardiac cycle allows assessment of intra-ventricular dyssynchrony (123). Dyssynchrony is usually calculated by taking the standard deviation of time to peak strain measured across a chosen number of cardiac chamber segments. The higher the standard deviation, the greater the dyssynchrony. *Haeck et al* demonstrated worse RV intra-ventricular dyssynchrony to be associated with worse clinical function. They also suggested the presence of ventricular interdependence (124). *Badagliacca et al* also demonstrated the association of RV dyssynchrony with worse WHO functional class, six-minute walk distance, RV remodelling and impaired RV haemodynamics (125, 126).

#### **1.10.4 CMR to assess myocardial deformation**

Cardiac MRI is the gold standard for assessing biventricular structure and function. Recently there has been significant focus on using CMR to assess myocardial deformation. Various techniques have been used based on techniques that focus on image acquisition or techniques that focus on post processing methods. These techniques are summarised in the Table 1.2 below.

**Table 1.2 Cardiac Magnetic Resonance Imaging techniques of assessing myocardial deformation.**

CMR technique	Mechanism
Image acquisition method	
<ul style="list-style-type: none"> <li>• CMR tagging</li> </ul>	Tracks magnetization tags
<ul style="list-style-type: none"> <li>• PVM (Phase Velocity Mapping)</li> </ul>	Encodes myocardial velocity, in the three directions, in the phase of the signal
<ul style="list-style-type: none"> <li>• DENSE (Displacement Encoded with</li> </ul>	Encodes tissue displacement into the phase of an image
<ul style="list-style-type: none"> <li>• SENC (Strain Encoded Imaging)</li> </ul>	Uses magnetization tags parallel to the image plane combined with out-of-plane phase-encoding
Post-processing method	
<ul style="list-style-type: none"> <li>• CMR-FT (Feature tracking) or tissue tracking)</li> </ul>	Tracks features in the image and recognizes them in the successive image of the sequence

Various CMR techniques for the assessment of myocardial strain are summarised. Myocardial tagging, PVM, DENSE and SENC are image acquisition methods while CMR-FT focuses on post processing.

### 1.10.5 RV strain by CMR imaging

The application of tagging in the evaluation of RV had been limited by the relatively thin RV wall. To overcome this challenge *Shehata et al* developed a fast strain-encoded (SENC) imaging, to allow direct measurement of regional function by using a free-breathing single heart beat real time acquisition. They measured biventricular segmental peak systolic longitudinal strain as well as LV circumferential and RV tangential strains in patients with PAH and controls. Longitudinal contractility of the RV was reduced at the basal, mid and apical levels and tangential contractility was reduced at mid-ventricular level. Longitudinal contractility of the RV positively correlated with mPAP and PVR ( $r=0.62$  and  $r=0.77$  respectively). Interestingly in a subgroup of patients with normal RV function (measured by RVEF), significantly reduced RV strain was noted in septal as well as free wall regions (127).

### 1.10.6 Feature tracking CMR imaging

The advantage of feature tracking is that the post processing technique can be applied to routinely acquired CMR images without the need for additional imaging acquisition. The basis for CMR-FT is identifying certain features in an image and tracking these features in the successive images of the sequence. It is based on defining small square windows, centred around a feature, on a first image and searching the “as-much-as-possible similar” greyscale pattern on the following image (128). The endocardial and epicardial borders will be defined manually and CMR-FT software automatic border tracking will track these during the cardiac cycle. CMR-FT will estimate global longitudinal strain from two cine images while circumferential and radial strains are derived from the short-axis cine images.

The main limitation of CMR-FT is artefacts due to through-plane motion, as features moving out of plane cannot be tracked (128). CMR-FT was developed for two-dimensional images; however, this technology can be applied to track 3D regions. Furthermore, CMR-FT is based on the assumption that the deformation is derived from the myocardium and that the blood motion does not interfere with it. However, blood motion can affect the tracking close to the endocardial regions, where unrealistic results may be noticed. Finally, CMR-FT is limited by the pixel size; displacement of less than the pixel size may not be detected.

In a study by de Siqueira et al using CMR-FT, peak RV global longitudinal and circumferential strain and strain rates were quantified from standard CMR cine images. Patients were classified into three groups (no PH, PH with normal RVEF and PH with reduced RVEF). All RV strain and strain rate values were reduced in the PH group with reduced RVEF. After adjustment for six clinically meaningful covariates, RV global longitudinal strain ( $p = 0.026$ ), RV global longitudinal strain rate ( $p = 0.04$ ), and RV global circumferential strain rate ( $p = 0.01$ ) were associated with a poor outcome (death, lung transplantation, worsening functional class) (129).

### **1.10.7 Left ventricular myocardium and strain**

The LV myocardium is organized into three layers.

1. Subendocardial layer - fibres are orientated longitudinally from base to apex.
2. Midwall layer - fibres are orientated circumferentially.
3. Subepicardial layer - fibres are orientated longitudinally from apex to base.

Due to this complex architecture, LV deformation in systole is along different directions determining longitudinal shortening, circumferential shortening, radial thickening and torsion (128). Longitudinal strain represents the longitudinal shortening from base to apex and is expressed as a negative value. Circumferential strain represents myocardial shortening along the circular perimeter on a short axis view and is expressed as a negative value. Radial strain represents the radially directed myocardial fibres deformation towards the centre of the LV cavity and indicates LV thickening and thinning during the cardiac cycle. As there is thickening of the myocardium in this direction during systole, this is expressed as a positive value. LV torsion is created by the clockwise and counter-clockwise rotation of the ventricular base and apex respectively in relative to a stationary mid myocardial reference point. Strain rate (longitudinal, circumferential and radial) represent the rate at which myocardial deformation occur. The complex LV fibre architecture and LV deformation is shown in Figure 1-2.

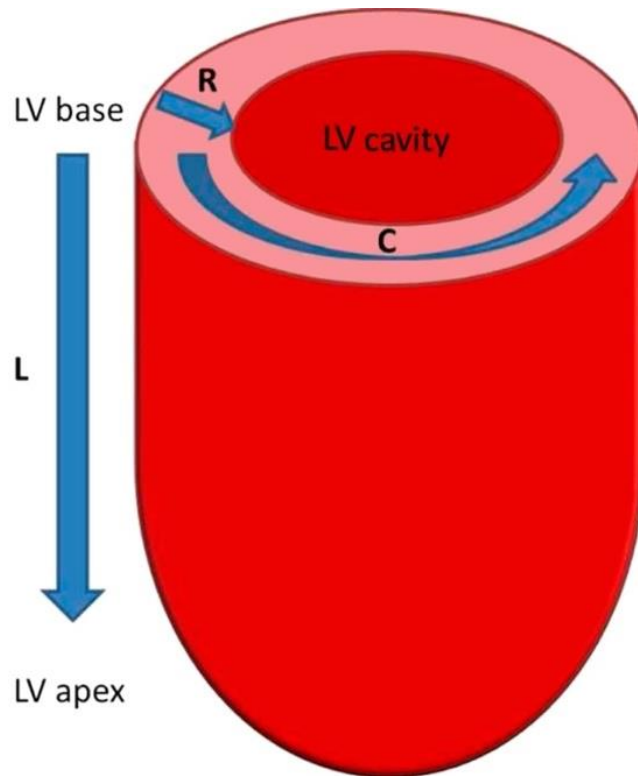


**Figure 1-2 Myocardial deformation of the left ventricle**

Modified from *Scetteia et al* (128) with permission. LV deformation in systole is along different directions determining longitudinal shortening (L), circumferential shortening (C), radial thickening (R) and torsion. This is due to the fact that the LV myocardium is organised into three layers. LV torsion is not shown but is created by the clockwise and counter-clockwise rotation of the ventricular base and apex respectively in relative to a stationary mid myocardial reference point.

### **1.10.8 Torsion of the LV**

During LV systole, when viewed from the apex, the apical segment rotates in an anti-clockwise direction, while the basal segment rotates clockwise, which is known as torsion of the LV. *Puwanant et al* demonstrated an impaired torsion in PH compared to controls,  $9.6^\circ$  vs.  $14.9^\circ$  but preserved untwisting rates (130). They suggested that raised RV pressure, causing septal flattening and bowing into the LV, impairs the ability of the LV to torque. While LV torsion continues to be studied in other conditions, there is limited additional data regarding echocardiography assessment of torsion in PH. The advent of 3D imaging should assist further in the analysis of torsion in this setting.

### **1.11 Myocardial tissue characterisation and myocardial perfusion by CMR**

The advantage of CMR is the ability to achieve high resolution imaging of the heart in multiple orientations without using radiation. Recently, there has been significant focus on non-invasive myocardial tissue characterisation. Longitudinal relaxation time (T1) and Transverse relaxation time (T2) are central properties of tissues and reflect their molecular make up (131, 132). Tissue T1 relaxation time is defined as the time when longitudinal proton magnetization recovers 63% of its equilibrium value. Late Gadolinium Enhancement (LGE, delayed cardiac enhancement, DCE) is the gold standard for determination of myocardial fibrosis. This is based on the difference in distribution of contrast between normal and fibrotic myocardium. The areas of fibrosis demonstrated a shorter T1 time than adjacent normal tissue. Conventionally this method is performed using inversion recovery gradient-echo sequences 10-15 minutes after gadolinium contrast injection. Retention of contrast within the extracellular space results in shortening of the inversion time (T1) and hyper-enhancement relative to normal myocardium (on T1 weighted MRI images) (Figure 1-3). Ischemic scar usually results in delayed enhancement in a sub-endocardial or transmural distribution consistent with the perfusion territories of epicardial coronary arteries, while non-ischemic fibrosis tends to be irregular and intramural or subepicardial in distribution. The main limiting factor when using LGE is that fibrotic process is

often a diffuse process thus lacking the normal non-fibrotic myocardium for reference. To ameliorate this issue, T1 mapping has been developed to quantify diffuse, non-ischemic myocardial fibrosis, as it does not rely on contrasting signal intensity.

### 1.11.1 Late gadolinium enhancement

*Blyth et al* used contrast enhanced CMR imaging to determine the presence of LGE in PH (133). They hypothesised that myocardial abnormalities may exist in patients with PH, that they could be identified by contrast enhanced CMR imaging and that the severity of the contrast enhancement would relate to the severity of PH. LGE was present in almost all patients with PH and the extent of contrast enhancement was associated with RV volumes, RV function as well as mPAP derived at right heart catheterisation. The authors also found LGE to be associated with IVS bowing and concluded that this may provide a novel marker for occult septal abnormalities directly relating to the haemodynamic stress experienced by these patients. McCann et al found similar results with the extent of LGE related to RV function and RV stroke volume. In two other patients who had post mortem histological analysis of the RV insertion points, fibrosis was present suggesting this may be the causal mechanism, however there was also evidence of interstitial space expansion and a small increase in fat which may have contributed to LGE. In a study by *Freed et al*, patients with RV insertion point LGE had larger RV volume index, lower RVEF and higher mPAP and LGE was a predictor for adverse outcomes ( $p=0.026$ ) in this population (134). In a study by *Swift et al*, LGE at the RV insertion points was suggestive of the presence of PH, however, after multivariable analysis, septal LGE was not associated with an increase in overall mortality(135).

In a study by *Shehata et al*, LGE at RV insertion points were observed in almost all patients with PH and LGE was associated with pulmonary haemodynamics, reduced RV function and reduced eccentricity index (127). Reduced longitudinal strain of the basal anterior septal insertion point was independently associated with LGE although the same was not observed for the posterior insertion point. The authors suggested that the two insertion regions may behave differently as they are part of anatomically and functionally distinct regions i.e. RV outflow and inflow tracts.

### 1.11.2 T1 mapping techniques

There have been numerous T1 based techniques for quantification of fibrosis. The modified Look Locker inversion recovery (MOLLI) technique was designed to overcome the limitations caused by motion and prolonged acquisition time (136). Specifics included an ability to acquire data within one breath-hold at a designated time within the cardiac cycle and the capability of merging images from multiple Look Locker experiments at different consecutive inversion times into one data set. MOLLI sequencing employs a balanced steady-state free precession (SSFP) readout to achieve a higher signal to noise ratio with a narrow image acquisition period of less than 200 ms in end-diastole to minimize motion artefact. In a later study *Messroghli et al* demonstrated high reproducibility of this technique (137). *Piechnik et al* introduced a shortened MOLLI sequence (ShMOLLI) that generated immediate, high-resolution myocardial T1-maps in a short breath-hold with high precision. Other prototype vendor specific sequences are in development including a modified Look-Locker FIESTA technique using saturation-recovery imaging, saturation-recovery single shot acquisition (SASHA), and saturation pulse prepared heart-rate-independent inversion recovery, which consists of a combination of saturation and inversion pulses (131).

### 1.11.3 T1 mapping methodology

Typically, a series of short axis images are acquired pre contrast and approximately 12 minutes' post gadolinium contrast with between 6 and 12 consecutively longer inversion times depending on the protocol. Image acquisition is usually performed with ECG gating with breath holding at end-inspiration. During post processing, standard basal, mid-ventricular and/or apical slices are selected and can be further divided into conventional myocardial segments (or discrete regions of interest) and blood-pool for analysis if desired. A curve fitting technique is employed to reconstruct the consecutively acquired images into one data set from which a T1 map of voxels is generated.

The signal intensity of each voxel directly represents the T1 relaxation time of the corresponding myocardial tissue. An exponential recovery curve of signal intensities at the different inversion times is then created for each designated region of interest (slice or segment) to determine the myocardial T1 relaxation

time. These can be averaged to extrapolate T1 as an index of diffuse fibrosis, where shorter T1 time and higher signal intensity correspond to increased gadolinium contrast accumulation within the extracellular matrix. Standardization of myocardial T1 values to non-myocardial tissue (blood) assists in minimizing the dynamic features of gadolinium contrast. The ratio of myocardial to blood post-contrast T1 values is expressed as the partition coefficient. By preceding post-contrast T1 mapping with pre-contrast T1 mapping, myocardial extra-cellular volume (ECV) can similarly be derived. This pseudo-equilibrium technique employs the reciprocals of myocardial and blood T1 values pre- and post-contrast and then adjusts for haematocrit to correct for the blood contrast volume of distribution. This ECV is expressed as a percentage of the total myocardial extracellular space. Gadolinium equilibrium between blood and myocardium must be achieved prior to image acquisition to enable accurate estimation of ECV. Typically, this occurs from 8.5 minutes' post contrast injection, after which ECV differences between time-points are minimal. A larger ECV represents increased contrast accumulation in an expanded extra cellular matrix (131).

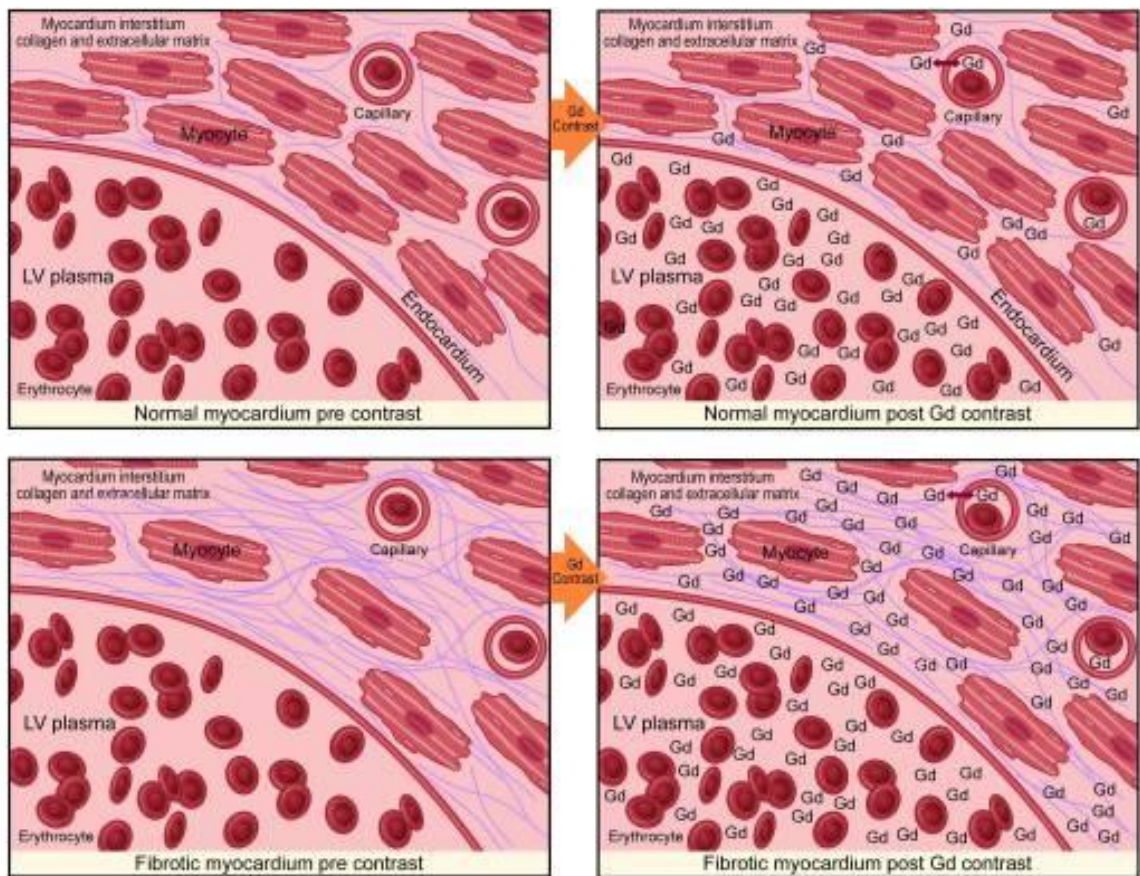


**Figure 1-3 Normal and fibrotic myocardium pre and post gadolinium contrast injection**

From *Jellis et al (131)* with permission. Normal myocardium (top) and fibrotic myocardium (bottom) pre and post injection of Gadolinium contrast. By preceding post-contrast T1 mapping with pre-contrast T1 mapping, myocardial extra-cellular volume (ECV) can be derived. This pseudo-equilibrium technique employs the reciprocals of myocardial and blood T1 values pre- and post-contrast and then adjusts for haematocrit to correct for the blood contrast volume of distribution. This ECV is expressed as a percentage of the total myocardial extracellular space.

### 1.11.4 T1 mapping in PH

*Sprujit et al* used CMR T1 mapping for myocardial tissue characterisation in IPAH, connective tissue disease associated PH and CTEPH (138). They used regions of interest in the RV and LV free wall, interventricular septum and the RV insertion points. In PH patients, native T1-values of the RV insertion regions were significantly higher than the native T1-values of the RV free wall, LV free wall and interventricular septum. They showed that the T1 values at the RV insertion regions were significantly related to disease severity. *Saunders et al* also used regions of interest in the IVS, LV free wall and RV insertion points during T1 mapping assessment. Elevated myocardial native T1 was found to a similar extent in PH patient subgroups and was independently associated with IVS angle. The authors did not find an additive value of native T1 mapping in the diagnostic and prognostic evaluation of PH patients (139). In another study by *Reiter et al* using CMR imaging, LV global, segmental and ventricular insertion point T1 times were evaluated manually and corrected for blood T1. AHA segmentation was used to segment the LV myocardium including RV insertion points. Septal, lateral and global T1 times were significantly higher in PH than in non PH subjects (132).

Although identification of raised native T1 times has been used to identify myocardial histological changes this has been limited due to

1. The need for visual assessment of the insertion points (*Sprujit et al*, *Saunders et al*) or,
2. The existing AHA segmentation of the LV fails to isolate the regions of RV insertion for analysis (*Reiter et al*)

*Ana García-Álvarez et al* used an experimental pig model of PH to assess the association between native myocardial T1 values and ECV with haemodynamics and RV performance (140). Native T1 values and ECV values were higher at RV insertion points in the experimental model animals compared to controls and also showed significant correlations with haemodynamics and RV-PA coupling. Interestingly ECV values were increased before overt RV dysfunction, which may offer a potential for early detection of PH. In another study, *Homsí et al* used mapping techniques and strain imaging to explore the mechanism of myocardial

changes in PH (141). They demonstrated higher T1 and ECV values in PAH and also showed impairment of LV longitudinal strain. However, there was no change in LV ejection fraction (LVEF). They hypothesised that due to longstanding LV under-filling, there may be LV myocardial fibrosis and LV atrophy despite preserved LVEF.

### **1.11.5 Myocardial perfusion**

Myocardial perfusion imaging using CMR enables monitoring passage of contrast through the lung. This is dependent on pulmonary pressures, PVR and cardiac output. Pulmonary transit time (PTT) describes the transit time of contrast between RV and LV while LV full width at half maximum (FWHM) and LV time to peak (TTP) contains information regarding bolus dispersion in the left ventricle. *Skrok et al* demonstrated PH patients to have a longer PTT, FWHM and TTP compared to healthy controls (142). These myocardial perfusion variables associated with mPAP and cardiac index. There is increased RV workload and RV hypertrophy in PH due to increased RV afterload. This demands increased RV myocardial perfusion. However, there may be a reduction in systolic flow in the right coronary artery in PAH. Therefore, reduced myocardial perfusion reserve may contribute to further RV dysfunction and RV failure. In a study by *Vogel-Claussen et al*, who evaluated biventricular myocardial perfusion with biventricular function and pulmonary haemodynamics in PH patients by adenosine stress perfusion MR imaging showed that, myocardial perfusion reserve indices were lower in PH compared to non PH controls (143). Myocardial perfusion indices inversely correlated with RV workload and RVEF, concluding that reduced myocardial perfusion reserve may contribute to RV dysfunction.

## **1.12 Positron emission tomography (PET)**

There is evidence that inflammation and immune dysregulation may play a role in IPAH. Elevated levels of pro-inflammatory cytokines have been found in the serum of IPAH patients.  $^{18}\text{F}$ -FDG PET have been extensively used in oncology to identify primary and metastatic tumour cells and a similar increased glycolytic metabolism has been seen in endothelial cells derived from IPAH-transplant patients. *Hagan et al* demonstrated higher FDG uptake in the lung parenchyma and the RV in IPAH patients compared to patients with CTEPH and controls (144). They suggested

using FDG uptake as a surrogate marker of cellular metabolism and immune activation as underlying mechanism of the disease. Another study by *Can et al* demonstrated that increased FDG uptake in RV myocardium was associated with elevated systolic PAP (145). The myocardial FDG uptake also correlated with pre-existing prognostic markers including elevated BNP and reduced exercise capacity.

In another study *Wang et al* evaluated gated  $^{18}\text{F}$ -FDG PET for the assessment of right ventricular volume and function in patients with PH and compared it to Cardiac MR and Cardiac CT data (146). Right ventricular end-diastolic and end-systolic volumes and RV ejection fraction were calculated. They determined  $^{18}\text{F}$ -FDG uptake as RV corrected standardized uptake value (SUV) and the ratio of RV to LV corrected standardized uptake value (corrected SUV R/L). Their study demonstrated that gated PET correlated well with CMR in assessing RV volume and function, however gated PET underestimated RVESV and RVEDV while overestimating RVEF when compared to CMR. They also found statistically significant negative correlation between RV SUV and RVEF by CMR as well as corrected SUV R/L. This study demonstrated that  $^{18}\text{F}$ -FDG gated PET could be used in the simultaneous assessment of RV function as well as RV metabolism. Previously *Bokhari et al* had suggested that perfusion and metabolic PET imaging using N-NH(3) and  $^{18}\text{F}$ -FDG respectively to be a feasible modality to quantify RV blood flow and metabolism. The RV free wall myocardial glucose uptake correlated well with mPAP suggesting the possibility that this could be used as a novel early biomarker in patients with PAH (147).

### **1.13 Right and left ventricular Interaction**

Although PAH is a disease of the pulmonary vasculature, it is the subsequent RV failure that is the main cause of morbidity and mortality in patients with PAH. Thus, CMR studies measuring myocardial deformation and myocardial tissue characterisation in patients with PH have been focused on the RV.

Frank Starling mechanism or the Starling's Law of the heart explains the ability of the heart to change its force of contraction and therefore stroke volume in response to changes in venous return (148). An increase in venous return increases the end-diastolic volume (ventricular filling) and therefore ventricular preload. This causes the initial stretching of cardiac myocytes prior to contraction. Myocyte

stretch causes an increase in sarcomere length, which causes an increase in myocyte force generation. This enables the heart to eject the additional volume of venous return causing an increase in stroke volume. In mechanical terms, increasing preload increases the active tension developed by the muscle fibre and increases the velocity of fibre shortening at a given afterload and inotropic state. Although other mechanisms may be involved, increasing the sarcomere length increases Troponin C calcium sensitivity, which increases the rate of cross bridge attachment and detachment and the amount of tension developed by the muscle fibre, increasing contractile force. This is termed length dependent activation.

Under normal conditions the impact of the RV on LV function is negligible. However ventricular interdependency plays an important role when the RV is pressure loaded as in PH. Ventricular interdependency can be affected both by parallel and series interaction (149). Leftward septal bowing hampers filling of the LV due to parallel interaction. Lowered RV stroke volume causes a decrease in LV filling due to series interaction. There is also the anatomical consideration that both these chambers are enclosed within a space limited pericardium. The primary reason for the leftward paradoxical motion of the IVS is due to the prolonged RV contraction time compared to the LV contraction time. Doppler echocardiography studies had demonstrated that the post systolic isovolumetric time is prolonged in severe PAH (149, 150). This hampers early diastolic LV filling. (RV contraction continues while the LV is already in diastole).

Because of the ventricular interdependency, measures of ventricular interaction are clinically useful to measure disease state as they contain information on the stroke volume as well as wall tension. As mentioned in the chapter earlier, several large studies have demonstrated that LV volume parameters to have important prognostic information in addition to RV function and volumes (99). Parameters that incorporate post systolic isovolumetric time such as the myocardial performance index have also shown to be of clinical relevance (37). Under filling of the LV may also bring the LV myocytes into an atrophic state. This is of importance as unloading the RV and improving LV preload might induce LV failure. Re-setting ventricular interdependency by means of pacing has also been explored in small cohorts of patients (151, 152). The importance of the LV in PH is

underlined by the fact that SV is closely related to LV but not RV end diastolic volume (16).

## 1.14 Left atrium

Left atrial function is increasingly studied and is known to have a significant role in the prognosis and risk stratification in different cardiac diseases. The principal role of the LA is to modulate left ventricular filling by three basic functions (153).

1. Reservoir function - collection of pulmonary venous return during LV systole
2. Conduit function - passage of blood to the LV during early ventricular diastole
3. Booster pump function - during late diastole augmentation of LV filling.

When assessing atrial function, it is important to recognise that there is significant interplay that exist between atrial function and ventricular performance during the cardiac cycle (153). This is discussed in detail in chapter 2.

LA function is most often assessed by echocardiography using volumetric analysis, spectral Doppler analysis or by tissue Doppler analysis. Subsequently *Kowallick et al* demonstrate CMR-FT to be reliable quantifier of LA longitudinal strain and strain rate from standard SSFP cine images. They also demonstrated that CMR- FT to discriminate between patients with impaired LV relaxation and healthy controls (154).

### 1.14.1 Left atrial area / volume measurement by CMR in PH

Pulmonary hypertension due to heart failure with preserved ejection fraction (HFpEF) is venous in origin and causes dilatation of the left atrium. Thus, determination of the LA size is primary used to exclude PH due to left sided cardiac dysfunction (group 2 PH) in the diagnostic workup of PH. In a study by *Crawley et al*, they determined LA size using a standard 2 and 4 chamber CMR views using the biplane area - length method. Left atrial volume was significantly lower in patients with IPAH compared to patients with HFpEF. Using an LA volume

threshold of 43 ml/m<sup>2</sup> as the cutoff, they could distinguish IPAH from HFpEF with 97% sensitivity and 100% specificity (18).

### **1.14.2 Left atrial function**

Abnormal LA function in patients with left heart disease is relatively well explored. In the above study by *Kowallick et al*, they demonstrated significantly decreased passive strain in patients with HFpEF and hypertrophic cardiomyopathy (HCM) corresponding to reduced conduit function (154). As atrial conduit function is closely related to LV compliance the authors suggested that this represented impaired LV relaxation. In the same study, total strain and peak positive strain rate which correspond to atrial reservoir function were decreased in HCM and HFpEF which might indicate impaired atrial compliance. They also showed increased active strain and peak late negative strain rate corresponding to booster pump function in HCM while decreased in HFpEF. They hypothesised that this may represent an initial increase in LA booster pump at early stages of impairment of LV relaxation followed by progressive decompensation of global LA performance. This was also demonstrated in a study by *Murata et al* using 3D echocardiography to study LA function (155).

Although PAH is defined, in-part by normal LV filling pressures, aforementioned series and parallel interactions from the RV to the LV affect LV performance. Thus, due to the direct interplay between LV and LA, study of LA function is of interest to further explore the ventricular interdependence in PAH.

### **1.15 Small animal CMR**

Small animal (rodent) models are increasingly used to identify pathophysiology as well as therapies for PAH with the intention of translating the findings to humans (19). Accurate monitoring of disease in rodents with emphasis on ventricular function and with the ability to monitor the disease state without killing the animal is needed. This is particularly important as some models are expensive to create.

Various rodent models to recapitulate human PAH have been produced. *Taraseviciene-Stewart et al* described the Sugden-hypoxia (SuHx) rat model in 2001

(156). Based on the fact that vascular endothelial growth factor (VEGF) is an important maintenance and differentiating factor for vascular endothelial cells, they designed an experiment to inhibit VEGF signalling in rats exposed to chronic hypoxia and normoxia. They showed that a selective VEGF receptor-2 (VEGFR-2) inhibitor, SU5416 (Sugen) to cause mild PH and pulmonary vascular remodelling in rats exposed to normoxia. However, in rats exposed to chronic hypoxia, Sugden caused severe PH associated with pulmonary arterial endothelial cell proliferation. The VEGFR-2 blockade caused endothelial cell apoptosis, which under chronic hypoxic conditions triggered luminal obliterative endothelial cell proliferation in the pulmonary circulation. In 2010, *Abe et al* showed that SuHx rats demonstrated evidence of severe pulmonary arteriopathy including concentric neo-intimal and complex plexiform-like lesions which closely resemble plexiform lesions seen in humans (157). Subsequently, other groups have attempted to characterize hemodynamics in a SuHx model beyond right heart catheterization alone (158-161).

Our group has a proven track record using CMR imaging to evaluate RV function in humans with PAH (99, 104, 133). The same non-invasive and repeatable measurements would be of great advantage for the study of rodent models to allow a detailed understanding of bi-ventricular structural and functional changes that occur, to enhance efficacy in translational medicine.

## **1.16 Hypothesis and aims of the thesis**

Although right heart catheterisation is the gold standard in the diagnosis of pulmonary hypertension, imaging methods play an important role in the diagnostic process, in measuring response to treatment and determining prognosis. These non-invasive investigations provide more information about RV function than acquired from right heart catheterisation. At present there are few imaging methods, which assist in the understanding of the molecular and cellular processes occurring in the RV and pulmonary circulation in patients with PH. However, advances in imaging techniques such as PET imaging will provide insight into the basic pathobiology of pulmonary vascular remodelling and RV dysfunction.

In the past, the RV has been the most widely studied of the cardiac chambers in PH, but now the focus has started to move towards the left ventricle (LV) (section

1.11). Although a disease of the pulmonary circulation and the RV, there is now evidence demonstrating LV abnormalities in PH. Furthermore, the atrial chambers offer valuable information when measuring cardiac function as well as in identifying the aetiology of PH (section 1.12). Small animal (rodent) models are increasingly used to identify pathophysiology as well as therapies for PAH with the intention of translating the findings to humans. Accurate monitoring of disease in rodents with emphasis on ventricular function and with the ability to monitor the disease state without killing the animal is needed (section 1.13).

The overall aim of the thesis was to determine if CMR could be used to address contemporary issues in the assessment of patients with PAH.

1. To explore LV mechanics including longitudinal, circumferential and radial myocardial deformation and LV intra-ventricular synchrony in patients with PAH and to identify the importance of LV mechanics in the disease progression, prognostication and survival in patients with PAH. (chapter 3)
2. To explore LA strain in PAH and to identify whether LA function assessment beyond LA volume will provide additional / incremental information about disease severity in patients with PAH. (chapter 4)
3. To identify a novel segmentation of the LV that isolate RV insertion regions of the IVS during native T1 mapping that will provide additional prognostic information about the LV myocardial changes in PAH. The existing AHA segmentation of the LV fails to isolate the RV insertion region for analysis. (chapter 5)

Small animal (rodent) models are increasingly used to identify pathophysiology as well as therapies for PAH with the intention of translating the findings to humans. The intention is to translate the findings from animal studies to humans. However, monitoring of the disease in small animals is done by cardiac catheterisation. Accurate monitoring of disease in small animals with emphasis on ventricular function and with the ability to monitor the disease state without killing the animal is needed.

4. To explore the feasibility of CMR to study longitudinal cardiac changes in a small animal model of PH and to discuss the suitability of a small animal model for translational studies of the mechanisms of RV dysfunction in PAH. (chapter 6)

## Chapter 2 **Material and Methods**

## **2.1 Scottish pulmonary vascular unit**

All patients recruited for the studies in this thesis were attending the Scottish pulmonary vascular unit (SPVU). The SPVU was founded in 1990 and is the tertiary referral centre for patients suspected of PH in Scotland (162). Apart from diagnosis, SPVU is the tertiary centre in Scotland for the ongoing management of all adult patients with PAH. Scotland has a population of 5.4 million (2018) of whom approximately 4.5 million are adults of age 16 years or over and therefore served by the SPVU (163). The National Audit of PH gathers data from all 8 specialised PH centres in the United Kingdom, seven of which treat adult patients and one paediatric centre. The most recent data from this audit from 2018 shows that the SPVU managed 474 patients with PH in the preceding year (164).

## **2.2 WHO functional class**

WHO functional class (WHO-FC) has been used since 1998 and is well established in the functional assessment of PH patients (165). It was modified from the New York Heart Association classification which describes the functional impact of heart failure. WHO FC classification is summarised in table 2.1.

**Table 2.1 WHO functional class classification of PH.**

Class I	Patients with pulmonary hypertension but without resulting limitation of physical activity. Ordinary physical activity does not cause undue dyspnoea or fatigue, chest pain or near syncope.
Class II	Patients with pulmonary hypertension resulting in a slight limitation of physical activity. They are comfortable at rest. Ordinary physical activity causes undue dyspnoea or fatigue, chest pain or near syncope.
Class III	Patients with pulmonary hypertension resulting in marked limitation of physical activity. They are comfortable at rest. Less than ordinary activity causes undue dyspnoea or fatigue, chest pain or near syncope.
Class IV	Patients with pulmonary hypertension with inability to carry out any physical activity without symptoms. These patients manifest signs of right heart failure. Dyspnoea and/or fatigue may even be present at rest. Discomfort is increased by any physical activity.

---

From *Barst et al* (165). WHO functional class has been used in the functional assessment of PH patients describing the impact of PH on limitation of physical activity.

## **2.3 Patient recruitment and assessment**

We retrospectively identified all patients who were referred to the SPVU between 2010 to 2017 for investigations of PH and underwent right heart catheterisation and CMR. Patients underwent multidisciplinary evaluation including non-invasive diagnostic tests and right heart catheterisation during a four to five-day diagnostic admission. Patients underwent non-invasive measurements and CMR within 72 hours from right heart catheterisation and gave informed written consent to undergo these procedures. An additional group of healthy volunteers with no known history of arrhythmias, ischaemic heart disease and lung disease were used as controls in the LV / LA strain studies. The study protocols were approved by the local research ethics committee. All patients had either been assessed first in an out-patient pulmonary vascular clinic and offered diagnostic admission for further assessment or admitted directly for assessment following faxed or telephone referral from other hospitals within Scotland.

## **2.4 Non-invasive assessment**

During the diagnostic admission, all patients underwent a series of investigations as part of the diagnostic algorithm for PH. These included blood investigations including autoantibodies and blood borne virus testing, arterial blood gas analysis, NT pro BNP level, pulmonary function testing, cardio pulmonary exercise testing, 6-minute walk test, transthoracic echocardiography, chest radiography, CTPA, High resolution CT of thorax and V/Q scanning. These investigations were performed at the Golden Jubilee National Hospital unless they had been performed recently at a referring hospital. Patients also had their WHO FC assessed in accordance to current guidelines (30).

## **2.5 Right heart catheterisation**

Right heart catheterisation was performed at the cardiac catheterisation lab at the Golden Jubilee National Hospital during the diagnostic admission. This was done during free breathing in the supine position with a 7 F quadruple lumen, flow directed balloon tipped Swan-Ganz catheter using the internal jugular approach. To facilitate this, an 8F introducer sheath was inserted in the internal jugular vein under ultrasound guidance. Pre-medication or sedation was not routinely used.

The external pressure transducer was zeroed at mid-thoracic line with the patient in the supine position, halfway between the anterior sternum and the bed surface, representing the level of the LA. Measurements were recorded in this supine position and were determined at the end of normal expiration. Right atrial pressure, mPAP, sPAP and diastolic pulmonary artery pressures (dPAP), PAWP were obtained. PAWP was obtained by catheter in the wedge position and the balloon inflated, reflecting the pressure of the LA. Cardiac output (CO) by thermodilution and PVR was determined by the following [ $PVR = (mPAP - PAWP) / CO$ ]. Mixed venous Saturations ( $SvO_2$ , pulmonary artery oxygen saturations) were measured during right heart catheterisation. Systemic blood pressure, heart rate and oxygen saturations were monitored during right heart catheterisation.

If the initial non-invasive tests and the right heart catheterisation results were suggestive of IPAH, pulmonary vasoreactivity testing was performed. This was performed by inhalation of Nitric Oxide (40 ppm) for 5 mins. A positive vasoreactivity was defined as a reduction in mPAP  $\geq 10$  mmHg to absolute value of  $< 40$  mmHg without a drop in cardiac output measured by thermodilution. If the non-invasive imaging (CTPA and V/Q scanning) was suggestive of chronic thromboembolic disease, conventional pulmonary angiography was also performed.

## **2.6 Cardiac Magnetic Resonance imaging**

### **2.6.1 Patient preparation and positioning**

Cardiac MRI scanning was done prior to right heart catheterisation during the diagnostic assessment in these patients. CMR imaging was performed in the supine position on a 1.5T MRI scanner (Avanto, Siemens, Erlangen, Germany). Patients signed a safety questionnaire prior to entering the scanning room. This was to ensure there was no contraindication to performing CMR. Patients were asked to lie supine on a CMR examination table. Patients had continuous ECG monitoring via monitoring pads. The phased array chest coil was placed on the patient's chest and this was secured with a Velcro strap. Patients were also supplied with an emergency buzzer. The centre of the chest coil, approximating the position of the heart, was defined by a laser pointer attached to the magnet's inner circumference at the 12 o'clock position. This reference point was obtained to

allow the patient to be moved within the bore of the magnet, to the point where their heart was at the centre of the main magnetic field. Once the patient was moved inside the bore of the magnet the scanning door was closed. Image acquisition was commenced with direct communication between the CMR radiographer and patient.

Steady State precession sequences (True FISP) were used to generate the initial axial scout images in the coronal, transverse and sagittal planes which helped localising the heart within the thoracic cavity. They were used for planning the subsequent cine images. Vertical long axis (VLA) and Horizontal long axis (HLA) cine were acquired based on the initial scout images. The HLA cine was then used to plan a series of short axis (SA) cine images, intersecting the atrioventricular valve roots. Images were acquired during end-expiratory breath holds. The SA imaging plane was then propagated towards the cardiac apex, covering both ventricles with 6-mm SA imaging slices, separated by a 2-mm inter-slice gap.

Imaging parameters, which were standardised for all subjects, included: TR (repetition time)/ TE (echo time) 3.2-3.9/0.6-2 ms, flip angle 45-90°, slice thickness 6 mm, temporal resolution 33-45 ms, spatial resolution 1.5-2 mm.

### **2.6.2 CMR image analysis**

All CMR images were analysed by the author using the Medis suite analysis software (Medis medical imaging systems, Leiden, Netherlands). Individual scans were anonymised and analysed by the author who was blinded to the identity and haemodynamic results of any given subject at the time of analysis. RV and LV volumes [RVEDV, RVESV, LV end-diastolic volume (LVEDV), and LV end-systolic volume (LVESV)] were determined by manual planimetry of selected short axis images, as described previously. Particular methodological points of note included the deliberate inclusion of trabeculations and papillary muscles in all analyses, as discussed by previous authors (166, 167). Right and left ventricular stroke volume (RVSV and LVSV), ejection fraction (RVEF and LVEF), and mass (RVM and LVM) were determined as previously described. RV mass was determined as RV free wall mass, the IVS was considered part of the LV. Ventricular Mass index (VMI) was determined as RV Mass: LV Mass. For analyses, RV and LV variables were index to body surface area (BSA).

## 2.7 Strain

The concept of strain as a measure of myocardial deformation was introduced in section 1.8. The LV myocardium is organized into three layers.

1. Sub-endocardial layer - fibres are orientated longitudinally from base to apex.
2. Mid-wall layer - fibres are orientated circumferentially.
3. Sub-epicardial layer - fibres are orientated longitudinally from apex to base.

Due to this complex architecture, LV deformation in systole is along different directions: longitudinal shortening, circumferential shortening, radial thickening and torsion. Myocardial strain measures the degree of deformation of a myocardial segment from its initial length. If the initial length is termed  $L_0$  and the maximum length  $L$ , strain can be determined by the following formula.

$$\text{Strain} = L - L_0 / L_0$$

There are two main definitions of strain.

1. Lagrangian strain - the displacements calculated at a fixed material point in the myocardium using the deforming myocardium as a reference.
2. Eulerian strain - tissue strain at a specific location in space, so spatial coordinates are fixed, but material points keep changing.

The cardiac imaging that is discussed in this thesis is based on the analysis of Lagrangian strain. As mentioned above, due to the different directions of the myocardium deformation, longitudinal, circumferential and radial strain and strain rate can be calculated.

### 2.7.1 LV Strain

Feature tracking CMR was performed using dedicated software (QStrain, Medis medical imaging Systems, Netherlands). The 4-chamber view was used to calculate LV longitudinal strain ( $E_{ll_{LV}}$ ). LV short axis circumferential ( $E_{cc_{LV}}$ ) and radial strains ( $E_{rr_{LV}}$ ) were derived from a mid-ventricular short axis view containing both papillary muscles. The horizontal long-axis SSFP cine series was used to identify the slice closest to the true mid cavity at end diastole (equidistant between apex and ring). The RV upper septal insertion of the LV was manually defined to allow accurate segmentation according to AHA segmentation template. Endocardial values were calculated for longitudinal and circumferential strain. (Figure 2-1) Global as well as segmental peak systolic longitudinal, radial and circumferential strain and strain rates were derived. To minimize variability, user adjustments after the first attempt at tracking were kept to a minimum. However, as with any deformation technique, inaccuracies can arise, because the boundary between the trabecular and compact portions of the wall may shift as the blood spaces between the trabeculae close during systole. This can result in an artefactual, apparent inward motion of the endocardial contour. If this was deemed to be a significant problem, the cine series was re-tracked with manual contouring using an end-systolic frame. Tracking was repeated for three times.

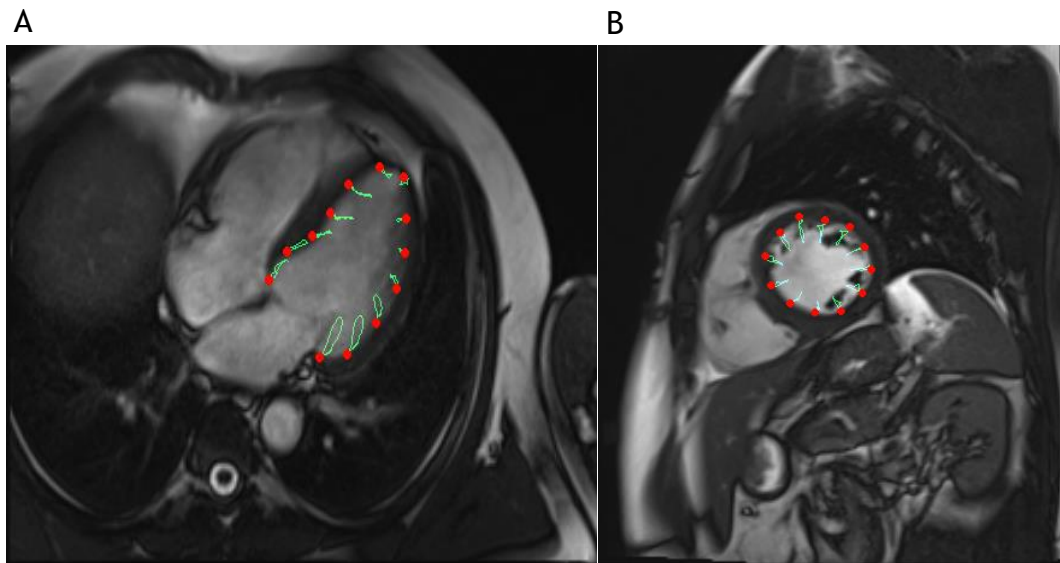


**Figure 2-1 Feature tracking CMR 4-chamber image and a short axis image**

CMR feature tracking was performed using dedicated software (Qstrain, Medis medical imaging systems, Leiden, Netherlands). Four chamber long axis view (A) was used to calculate LV longitudinal strain ( $E_{ll_{LV}}$ ). A mid-ventricular short axis slice (B) was used to calculate LV circumferential strain ( $E_{cc_{LV}}$ ). Radial strain ( $E_{cc_{LV}}$ ) was also calculated from the mid-ventricle short axis slice. The horizontal long-axis SSFP cine series was used to identify the slice closest to the true mid cavity at end diastole (equidistant between apex and ring). (Author's own image)

### 2.7.2 LV intra-ventricular dyssynchrony

The strain software tracks 48 tissue segments throughout the cardiac cycle in radial, circumferential and longitudinal directions. The following dyssynchrony indices were calculated. 1) **Radial dyssynchrony** - Standard deviation of the time to peak (TTP-SD6) radial strain of six mid ventricular myocardial segments given as a percentage of the length of the cardiac cycle. 2) **Circumferential dyssynchrony** - Standard deviation of the time to peak circumferential strain of six mid ventricular myocardial segments given as a percentage of the length of the cardiac cycle. 3) **Longitudinal dyssynchrony** - Standard deviation of the time to peak of seven (TTP-SD7) longitudinal myocardial segments given as a percentage of the length of the cardiac cycle (168). (Figure 2-2)



**Figure 2-2 Assessment of intra-ventricular dyssynchrony**

Dyssynchrony was calculated from the standard deviation of the time to peak of six (radial/circumferential) or seven (longitudinal) myocardial segments and was given as a percentage of the length of the cardiac cycle. The figure demonstrates the circumferential strain curves (yellow arrow) of six myocardial segments. (Author's own image)

## 2.8 Left atrial strain

Left atrial myocardial feature tracking was performed using dedicated software (Qstrain, Medis medical imaging systems, Leiden, Netherlands). LA endocardial borders were manually traced using the 2-chamber and 4-chamber views using a point and click approach when the LA was at its minimum volume after atrial contraction. The atrial endocardial border surface was manually delineated, and the automated tracking algorithm was applied. Subsequently this was visually reviewed to ensure accurate tracking of the atrium. In case of insufficient automated border tracking, manual adjustments were made to the initial contour and the algorithm was reapplied. If the tracking quality was not sufficient, e.g. due to the presence of pulmonary veins or left atrial appendage, the corresponding segment was excluded from the analysis. Tracking was repeated for three times in both the 2 and 4-chamber view. LA longitudinal strain and SR results were averaged across all three repetitions in both views.

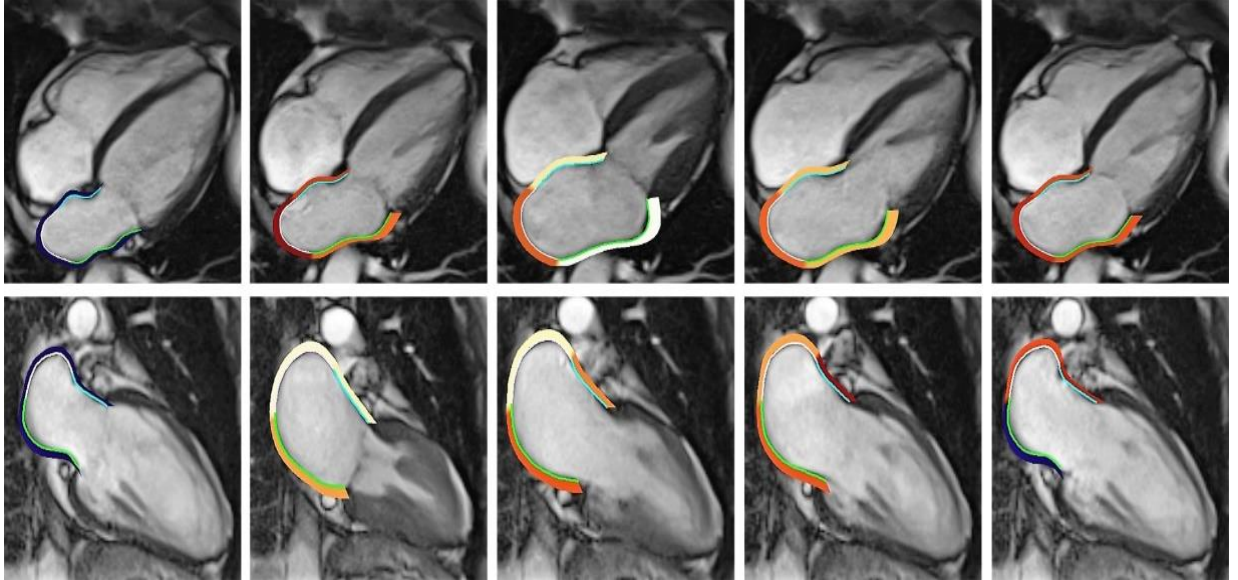


**Figure 2-3 LA myocardial feature tracking using a 2-chamber and 4-chamber view**

Left atrial endocardial borders were manually traced using the 4-chamber (top row) and 2-chamber (bottom row) views using a point and click approach when the LA was at its minimum volume after atrial contraction. The atrial endocardial border surface was manually delineated and the automated tracking algorithm was applied. Subsequently this was visually reviewed to ensure accurate tracking of the atrium. (Image provided by Chongmiao Yang)

Three aspects of atrial function were analysed:

1. Total strain, the sum of passive and active strain ( $\epsilon_s$ , corresponding to atrial reservoir function).
2. Passive strain ( $\epsilon_e$ , corresponding to atrial conduit function)
3. Active strain ( $\epsilon_a$ , corresponding to atrial contractile booster pump function)

Accordingly, three strain rate parameters were evaluated:

1. Peak positive strain rate (SRs, corresponding to atrial reservoir function),
2. Peak early negative strain rate (SRe, corresponding to atrial conduit function)
3. Peak late negative strain rate (Sra, corresponding to atrial contractile booster pump function)

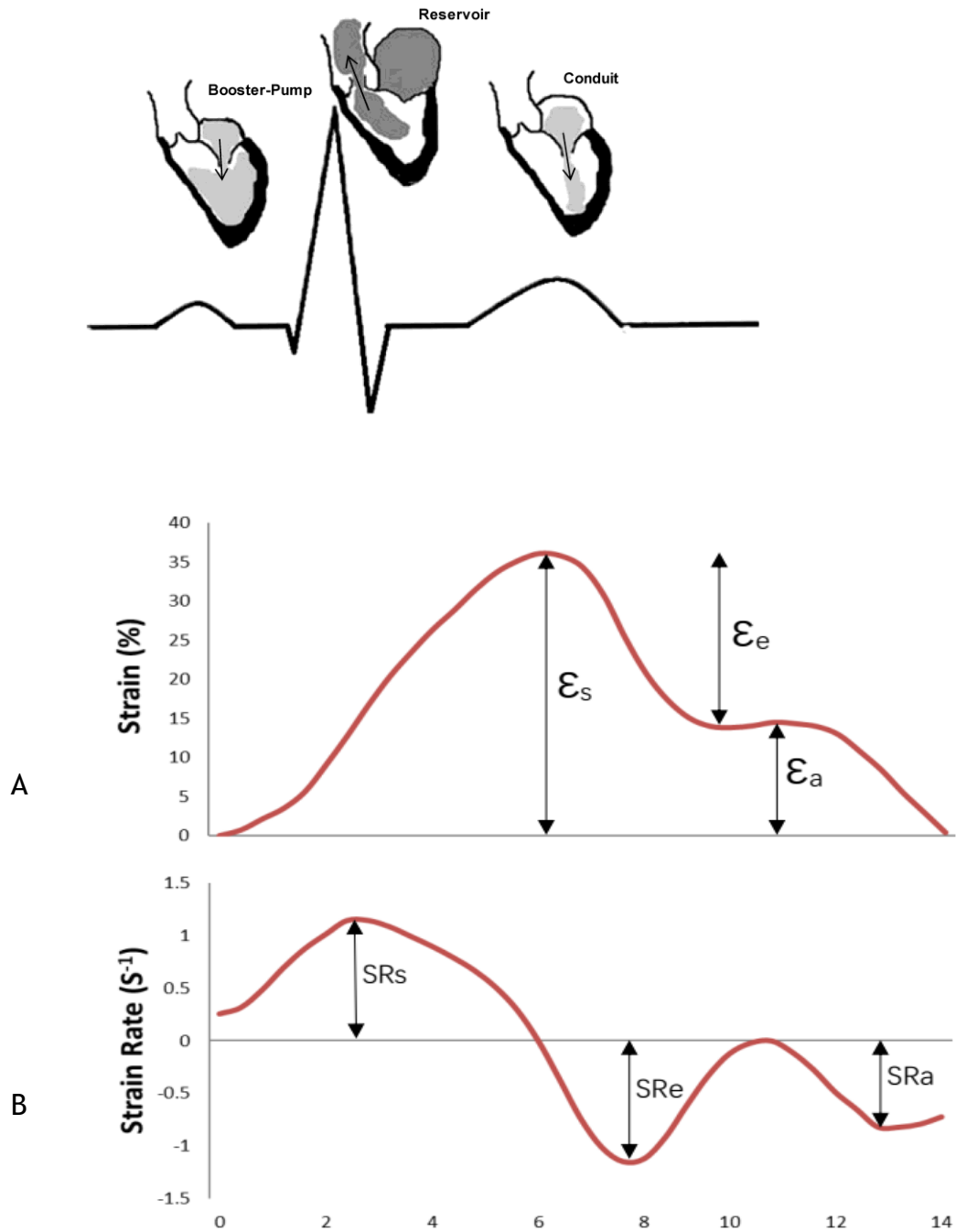


**Figure 2-4 Left atrial strain and strain rate profiles.**

Left atrial function comprises reservoir, conduit and contractile booster pump function. Total strain ( $\epsilon_s$ ) and peak positive strain rate ( $SR_s$ ) correspond to reservoir function. Passive strain ( $\epsilon_e$ ) and peak early negative strain rate ( $SRe$ ) correspond to conduit function. Active strain ( $\epsilon_a$ ) and peak late negative strain rate ( $SRa$ ) correspond to contractile booster pump function. Profile A demonstrates strain, while profile B demonstrates corresponding strain rate. (Image provided by Chongmiao Yang)

## 2.9 T1 mapping CMR

T1 maps were acquired using a MOLLI (Modified Look-Locker Inversion Recovery) sequence on a mid-ventricular short axis plane with a trigger delay to coincide with systole. T1 maps were generated from the individual motion corrected T1 relaxation images using dedicated software (Qmap, Medis medical imaging systems, Leiden, Netherlands). The LV was segmented using our modified AHA segmentation carefully excluding blood pool, papillary muscles and trabeculae. Segment 6 was drawn with the inferior RV insertion point at its centre. Segment 4 and Segment 6 were defined as anterior and inferior RV insertion segments respectively. These two segments were combined to form the RV insertion region. Segments 1, 2 and 3 represented the LV lateral wall. Segment 5 was defined as the septal segment. (Figure 2-5) Definition of regions with the new myocardial segmentation using a modified AHA model is summarised in Table 2.2.

In the validation cohort, subjects underwent native and post contrast T1 mapping. ECV values were calculated from T1 maps acquired pre and post contrast calibrated by blood haematocrit. ECV value was calculated as  $ECV = (1 - \text{hematocrit}) \left( \frac{1}{T1 \text{ myocardium post contrast}} - \frac{1}{T1 \text{ myocardium pre contrast}} \right) \left( \frac{1}{T1 \text{ blood post contrast}} - \frac{1}{T1 \text{ blood pre contrast}} \right)^{-1}$  (169).

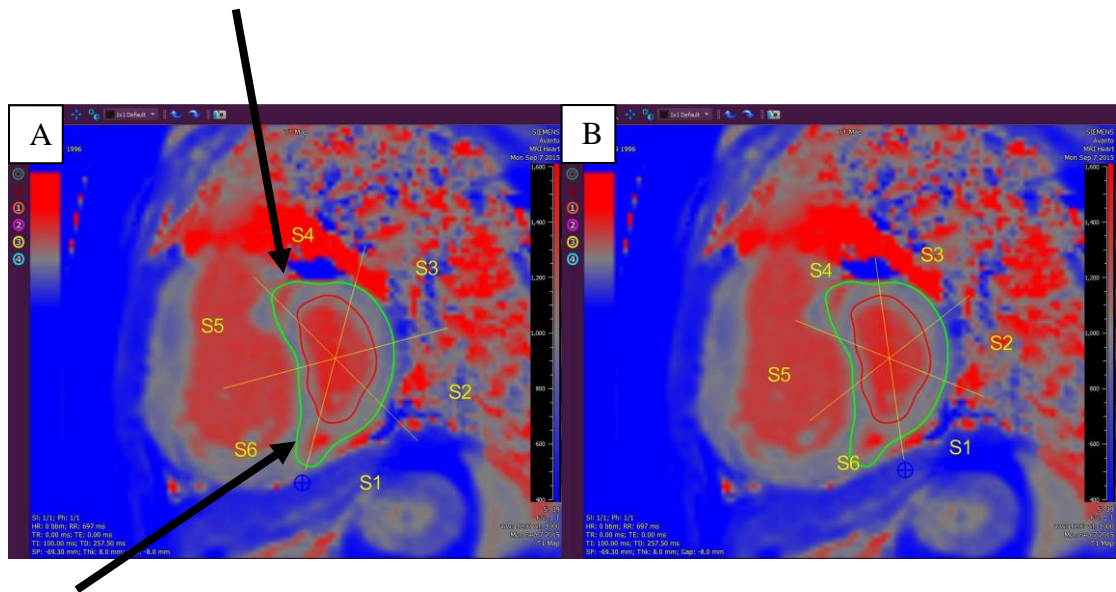


**Figure 2-5 Cardiac Magnetic Resonance mid ventricular slice T1 map of a patient with pulmonary arterial hypertension**

Cardiac MR native T1 map of the PAH patient demonstrating raised native T1 at right ventricular insertion points (arrows). The image A) uses traditional AHA segmentation and image B) demonstrates the novel segmentation proposed which encompasses the two insertion points into segments S4 and S6. T1 maps were generated from the individual motion corrected T1 relaxation images. The LV was segmented using our modified AHA technique carefully excluding blood pool, papillary muscles and trabeculae. Segment 6 was drawn with the inferior RV insertion point at its centre. Segment 4 and Segment 6 were defined as anterior and inferior RV insertion segments respectively. These two segments were combined to form the RV insertion region. Segments 1, 2 and 3 represented the LV lateral wall. Segment 5 was defined as the septal segment. (Author's own image)

**Table 2.2 Definition of regions with the new myocardial segmentation using a modified AHA model.**

Segments	Definition
4 and 6	Right ventricular insertion region (anterior and inferior segment respectively)
1, 2 and 3	LV lateral wall
5	Septal segment

The LV was segmented using our modified AHA segmentation carefully excluding blood pool, papillary muscles and trabeculae. Segment 6 was drawn with the inferior RV insertion point at its centre. Segment 4 and Segment 6 were defined as anterior and inferior RV insertion segments respectively. These two segments were combined to form the RV insertion region of the interventricular septum. Segments 1, 2 and 3 represented the LV lateral wall. Segment 5 was defined as the septal segment.

### **2.9.1 Diagnosis, commencement of treatment and follow up**

A multidisciplinary team (MDT) meeting is held at the end of the diagnostic admission. The MDT is attended by the pulmonary vascular consultants, consultant radiologists, pulmonary vascular research fellows, clinical nurse specialists and clinical trials nurses. For each patient undergoing assessment the relevant clinical history, examination findings, imaging, non-invasive investigations and pulmonary haemodynamics were reviewed. A diagnosis was then made in accordance with current PH guidelines and agreed by the MDT (30). If a diagnosis of PAH or CTEPH was made, then the patient was offered PAH specific treatment in accordance with the current clinical guidelines. If disease-targeted therapy was commenced following the diagnostic admission, then the patient was reviewed in an out-patient clinic after approximately 3-4 months, 6 months, 9 months and 12 months of treatment. Assessment at out-patient follow-up clinics involved history taking and examination, documentation of WHO FC, and a repeat 6-minute walk test was performed. Routine blood investigations and NT-ProBNP was performed at each visit.

## **2.10 CMR in a Sugen-hypoxia rat model of PH**

All experimental procedures were carried out in accordance with the United Kingdom Animal Procedures Act (1986) and with the US NIH publication No. 85-23, revised 1996, and ethical approval was also granted by the University of Glasgow Ethics Committee. Rodents were housed in a 12-hour light dark cycle with access to food and water ad libitum. Male Sprague Dawley rats (three weeks) (n=32) were divided into two groups (n=16 in each group). Group 1) *Sugen-hypoxia* - a single dose of subcutaneous Sugen-5416 (Sigma, UK) suspended in vehicle (20mg/kg)), before being placed in a hypobaric chamber (atmospheric pressure 550 mbar) for 2 weeks and then placed in normal room pressure (1013 mbar) for 3 weeks whilst PH developed. Group 2) *Normoxia* maintained at normal room pressure for 5 weeks. In each group (n=16) half the animals entered the CMR arm of the study (n=8) while the other half underwent right heart catheterization for hemodynamic

assessment (n=8). Animals were assessed at five weeks and eight weeks from the beginning of the study (170). A detailed study design is discussed in chapter 6.

### **2.10.1 Small animal CMR imaging.**

CMR imaging was performed in a Bruker Biospec 7-T/30-cm (Bruker Biospin, Ettlingen, Germany) system with a gradient coil insert (400 mT/m). Using a 72mm transmit birdcage resonator and 4 channel phased array rat cardiac receiver coil. Anesthesia was induced with gas flow at 2-3 l/min, and the isoflurane delivered via a vaporizer (Vetamac, Rossville, IN) at 3-4%. The exhaust was connected to the Omnicon F/Air device (AM Bickford). After induction, animals were maintained at 2% (v/v) isoflurane supplemented with a constant flow of 5% (v/v) oxygen. An external water jacket was used to maintain a core temperature of 37°C. During all procedures, body temperature, ECG, and respiration were monitored (Echo: Indus Instruments, Houston, TX; MRI: SA Instruments, Stony Brook, NY; Cath: Powerlab, Ad instruments, Colorado Springs, CO). Long and short axis scout images were acquired so that short axis images could be planned using a segmented, cardiac - triggered FLASH sequence. The images were acquired with a slice thickness of 1.5mm ensuring the entire biventricular length is covered. The CMR parameters were as follows. Slice thickness-1.50mm, field of View-30.00mm x 30.00mm, image matrix-192 x 192 pixels, image resolution-156µm x 156µm, Flip angle-15 degrees, Echo time-2.50ms, Rep. time-7.02ms, number of frames-25, number of averages-6, software version-Paravision 5.1.

### **2.10.2 CMR imaging analysis**

Scans were coded by number and analysed in batches by the author who was blinded to the identity and haemodynamic results at the time of analysis. Trabeculations and papillary muscles were considered as part of the blood pool. The epicardial and endocardial borders were manually outlined in end-diastolic and end-systolic frames using Qmass (Medis medical imaging systems, Leiden, Netherlands). Stroke volume was determined from LVEDV and LVESV. Ejection fraction  $[(SV/EDV)*100\%]$  was also determined. RV and LV masses were determined by manual planimetry at diastole. VMI was defined as the ratio between RV to LV mass, with the IVS considered part of the LV. LV eccentricity index (LVEI) was defined as the ratio between maximum anterior-posterior to septal lateral

diameters of the LV and was measured at both systole and diastole. All ventricular volumes and mass measurements were indexed to body surface area (171).

## **2.11 In vivo hemodynamic measurements**

In the small animal CMR study, the in vivo haemodynamic measurements, RV hypertrophy and tissue harvest, gross anatomy and pulmonary vascular remodelling assessment was performed with the assistance of colleagues Dr. David Welsh and Dr. Kat Wilson at the University of Glasgow.

Animals were anaesthetically induced with 3% (v/v) isoflurane and then maintained at 2% (v/v) isoflurane supplemented with a constant flow of 5% (v/v) oxygen. Hemodynamic measurements were taken using an ultra-miniature Polyimide Nylon catheter capable of measuring ventricular pressure continuously (AD instruments spr-869NR, Millar). The catheter was used as per the manufacturer's instructions with the PowerLab 35 Series data acquisition system with LabChart Pro and the pressure volume (PV) Loop analysis module. For right heart pressure analysis, the catheter was inserted into the jugular vein and guided into the RV to measure RVSP.

## **2.12 RV hypertrophy and tissue harvest**

Following hemodynamic assessment, animals were culled and hearts flushed with PBS using a blunt needle to clear peripheral blood cells. Euthanasia consisted of an overdose of anaesthetic followed by a schedule 1 kill (cervical dislocation). The heart was isolated, atria removed and tissue fixed with 10% (v/v) neutral buffered formalin (NBF) for 48 hours before paraffin processing for histological analysis by immunohistochemistry. Tissue was sectioned by microtome at width of 5µm and stained by Gomori's Trichrome staining kit (Atom Scientific, Manchester, UK) as per manufacturer's instructions.

## **2.13 Gross anatomy postpartum**

After the heart was isolated and atria removed, the RV and LV weights were obtained to determine RV hypertrophy. Interventricular septum was considered part of the LV.

## **2.14 Pulmonary vascular remodelling**

Vascular thickening was determined by smooth muscle actin antibody (ab5694, Abcam, Cambridge, UK) staining, thickening was characterized by an increase in the vessel wall diameter of more than 50% of the arterial wall or complete occlusion. The number of remodelled vessels over the total number of vessels present in a lung section was determined. Sections were analysed in a blinded manner.

## **2.15 Data Storage**

In all the aforementioned studies, on completion of each CMR scan, the images were saved to the hard-drive of the scanner and backed up onto an encrypted portable device. All scans were coded by number and stored in a locked office until data analysis.

## **2.16 Statistical analysis**

In survival analysis, survival was recorded from the date of diagnostic right heart catheterisation and endpoint was date of either death, lung transplantation or censoring. All-cause mortality was used for survival analysis and patients were censored if they were lost to follow-up or alive at last day of study. Survival predictors were determined using a bivariate Cox proportional hazard regression analysis with age. Results were presented as hazard ratios with 95% confidence intervals. Variables that were significant were considered for multivariate analysis. Survival of patients were compared by a long rank test. A p-value of greater than 0.05 indicated a lack of statistical significance. Statistical analysis was performed using SPSS (IBM SPSS Statistics, USA) and Graphpad Prism (Graphpad Software inc, USA). Additional statistical methodology pertaining to each study in this thesis is described separately, within the relevant chapters.

**Chapter 3 Left ventricular strain  
and intra-ventricular  
dyssynchrony by CMR in  
idiopathic pulmonary arterial  
hypertension**

### 3.1 Introduction

A review of the existing literature on cardiac and pulmonary imaging was presented in chapter 1. CMR is the gold standard imaging investigation of biventricular structure and function (172). As described in chapter 1, many CMR measures have shown to be strongly predictive of mortality and survival in IPAH thus offering potential for monitoring and determining disease response to treatment (15). Stroke volume, RVEF, RVEDVI are recognised as the key CMR prognostic measures in PAH patients. In a multicentre study prospectively using CMR before and during PAH disease specific treatment, Peacock et al demonstrated the importance of measuring both right sided and left sided variables when determining cardiac function (99). The concept of ventricular interdependency was also discussed, although in normal conditions the impact of the RV on LV function is negligible, in a pressure loaded RV, LV performance may be affected. Chapter 1 also discussed that measurements of myocardial deformation and synchrony may provide additional and incremental information regarding ventricular function beyond conventional volume and ejection fraction assessment.

The LV myocardium is organised into three layers (128). The sub-endocardial layer where fibres are orientated longitudinally from base to apex, the mid-wall layer where the fibres are orientated circumferentially and the sub-epicardial layer where fibres are orientated longitudinally from apex to base. Due to this complex architecture, LV deformation in systole is along different directions determining longitudinal shortening, circumferential shortening, radial thickening and torsion.

Myocardial strain measures the degree of deformation of a myocardial segment from its initial length (108). If the initial length is termed  $L_0$  and the maximum length  $L$ , strain can be determined by the following formula.  $\text{Strain} = (L - L_0) / L_0$ . As mentioned above, due to the different directions of the myocardial deformation longitudinal, circumferential and radial strain can be calculated. Longitudinal strain represents the longitudinal shortening from base to apex and is expressed as a negative value. Circumferential strain represents myocardial shortening along the circular perimeter on a short axis view and is expressed as a negative value. Radial strain represents the radially directed myocardial fibres deformation towards the centre of the LV cavity and indicates LV thickening and

thinning during the cardiac cycle. As during systole there is thickening of the myocardium in this direction, this is expressed as a positive value. Strain rate (longitudinal, circumferential and radial) represent the rate at which myocardial deformation occur.

Ventricular dyssynchrony can be observed at different levels (173). Inter-ventricular dyssynchrony is the delayed activation of one ventricle with respect to the other. Intra-ventricular dyssynchrony refers to the late activation of different regions of a single ventricle compared to other regions of the same ventricle. This chapter will focus on intra-ventricular dyssynchrony assessment.

Both echocardiography and CMR imaging are capable of measuring myocardial strain. Echocardiographic methods of strain imaging including speckle tracking are limited by noise interference, angle dependency and image quality. CMR derived myocardial strain measurement was first achieved by CMR tagging in the 1980s (174). However, CMR tagging requires prospective image acquisition and time consuming protocols. CMR-FT is based on optical flow technology (175). In CMR-FT anatomic elements that are different along the cavity (blood pool) and myocardial tissue boundary are found by methods of maximum likelihood in 2 regions of interest between 2 frames. This is initiated by manually tracing the endocardium or epicardium or both usually at end-diastole. The feature tracking proceeds by tracking each feature along the contour, based on a hierarchical algorithm and combining one-dimensional tracking with two-dimensional tracking (176). It is important to note there may be differences in strain between different CMR-FT solutions (177). All two-dimensional strain techniques can be affected by through plane motion. CMR-FT has been validated against myocardial tagging for strain analysis and also against RV speckle tracking imaging for RV longitudinal strain evaluation (178, 179). In practical terms, CMR-FT derived strain offers incremental clinical information beyond measurements of LV volumes and ejection fraction in patients with left heart disease. There are a large number of studies looking at CMR-FT derived LV strain in myocardial ischaemia and viability detection (180, 181), dilated cardiomyopathy (182) and arrhythmogenic RV cardiomyopathy (183).

Assessment of intra-ventricular dyssynchrony is well established by both tissue Doppler and speckle tracking echocardiography. *Cho et al* assessed patients with

congestive heart failure with a normal QRS duration and concluded that mechanical dyssynchrony assessed by tissue Doppler imaging to be a significant predictor of mortality (184). In another study of 132 patients who had undergone cardiac resynchronisation therapy, patients who lacked both radial and transverse dyssynchrony had unfavourable clinical outcomes (185).

RV strain has been studied by CMR-FT in PH patients. In a study by *de Siqueira et al* 116 patients who were referred for PH assessment were evaluated using CMR-FT of the RV. They concluded that CMR-FT of the RV was feasible in a majority of patients, and RV longitudinal and circumferential strain variables correlated with disease severity and were associated with poor outcomes in PH (129).

IPAH is a disease of the pulmonary vasculature and the RV. Conceptually the LV function should be normal. However as mentioned in chapter 1, the RV and LV do not function in isolation. In PH, RV pressure overload causes paradoxical motion of the IVS towards the LV disturbing LV geometry and filling. LV preload is reduced due to decreased cardiac output from the RV. These series and parallel interactions from the RV to the LV affect LV performance. There is also the anatomical consideration of RV dilatation in a contained pericardial sac affecting LV geometry (149). In a study using echocardiography, *Hardegree et al* studied RV and LV function in patients with PAH (186). They demonstrated that despite normal LV size and normal conventional measures of LV systolic function (end-diastolic dimension, ejection fraction, cardiac index by echo), patients had reduced LV free wall systolic strain. Reduced LV strain was associated with increased mortality in this study. They highlighted the significance of inter-ventricular dependence in PAH. However, they did not study LV radial strain in this study and had not assessed intra-ventricular dyssynchrony.

We conducted a comprehensive retrospective study of LV strain and intra-ventricular dyssynchrony in patients with IPAH using CMR-FT. To the best of our knowledge, the significance of myocardial strain and dyssynchrony of the LV using quantitative analysis of CMR-FT in IPAH has not been investigated. The aims of the study were: 1) Assessment of feasibility of performing LV longitudinal, circumferential and radial strain and LV intra-ventricular dyssynchrony in IPAH. 2) Characterise the pattern of LV strain abnormalities and intra-ventricular

dyssynchrony. 3) Investigate the significance of these abnormalities on disease severity, prognostication and survival in IPAH.

## **3.2 Methods**

### **3.2.1 Patient recruitment**

We retrospectively identified all patients who were referred to a tertiary referral centre between 2010 to 2017 for investigations of PH and underwent right heart catheterisation and CMR. From these, we identified 76 treatment-naïve patients who were diagnosed of IPAH after a multidisciplinary evaluation including blood investigations (autoantibodies, HIV testing and NTProBNP), right heart catheterization, echocardiography (including TAPSE), pulmonary function testing, 6-minute walk distance and CT scan of thorax (CTPA and High Resolution CT thorax). After exclusion of six patients due to inadequate image quality, presence of arrhythmia and a history of myocardial infarction, 70 patients with IPAH were included in the present analysis. All patients underwent invasive haemodynamic measurements and CMR within 72 hours from catheterisation, and gave informed written consent to undergo these procedures. An additional group of 40 healthy volunteers with no known history of arrhythmias, ischaemic heart disease and lung disease were used as controls. A composite end point of all-cause mortality and lung transplantation was recorded. The study protocol was approved by the local research ethics committee.

### **3.2.2 CMR imaging**

CMR imaging was performed in the supine position on a 1.5T MRI scanner (Avanto, Siemens, Erlangen, Germany). Images were acquired during end-expiratory breath holds. Long axis 4-chamber cine images and contiguous short axis cine images covering both ventricles from base to apex were acquired with cine SSFP imaging with following parameters: TR (repetition time)/ TE (echo time) 3.2-3.9/0.6-2 ms, flip angle 45-90°, slice thickness 6 mm, temporal resolution 33-45 ms, spatial resolution 1.5-2 mm.

### **3.2.3 Right heart catheterization**

Right heart catheterisation was performed during free breathing in the supine position with a 7 F quadruple lumen, flow directed balloon tipped Swan - Ganz

catheter using the internal jugular approach. Pressure measurements including RAP, mPAP, dPAP, sPAP and PAWP were obtained. Cardiac output was obtained by thermodilution and PVR data were obtained. Mixed venous saturations were also obtained during right heart catheterisation. Systemic blood pressures, heart rate and oxygen saturations were measured during right heart catheterisation. The method of right heart catheterisation is described in detail in section 2.5.

### **3.2.4 CMR image analysis**

All CMR images were analysed by the author using the Medis suite analysis software (Medis medical imaging systems, Leiden, Netherlands). A second observer (AM) analysed 20 scans for inter-observer agreement analysis. Individual scans were anonymised and analysed by the author who was blinded to the identity and haemodynamic results of any given subject at the time of analysis. RV and LV volumes (RVEDV, RVESV, LVEDV, LVESV) were determined by manual planimetry of selected short axis images, as described previously. Particular methodological points of note included the deliberate inclusion of trabeculations and papillary muscles in all analyses, as discussed by previous authors(166, 167). Right and left ventricular stroke volume (RVSV and LVSV), ejection fraction (RVEF and LVEF), and mass (RVM and LVM) were determined as previously described. RV mass was determined as RV free wall mass, the IVS was considered part of the LV. Ventricular Mass index was determined as RV Mass: LV Mass. For correlation analyses, RV and LV variables were index to body surface area (BSA). Cardiac MR image analysis is described in detail in chapter 2.6.2.

### **3.2.5 Strain analysis**

CMR feature tracking was performed using dedicated software (Qstrain, Medis medical imaging systems, Leiden, Netherlands). The 4-chamber view was used to calculate LV longitudinal strain ( $E_{LLV}$ ). LV short axis circumferential ( $E_{CCLV}$ ) and radial strains ( $E_{rLV}$ ) were derived from a mid-ventricular short axis view containing both papillary muscles. The horizontal long-axis SSFP cine series was used to identify the slice closest to the true mid cavity at end diastole (equidistant between apex and ring). The RV upper septal insertion of the left ventricle was manually defined to allow accurate segmentation according to AHA segmentation template. Endocardial values were calculated for longitudinal and circumferential

strain. Global as well as segmental peak systolic longitudinal, radial and circumferential strain and strain rates were derived. To minimize variability, user adjustments after the first attempt at tracking were kept to a minimum. RV longitudinal strain from the 4-chamber cine images were also derived. RV endocardium was divided in to the RV free wall and RV septum and average RV longitudinal strain was also calculated.

### **3.2.6 Intra-ventricular dyssynchrony**

The strain software tracks 48 tissue segments throughout the cardiac cycle in radial, circumferential and longitudinal directions. The following dyssynchrony indices were calculated. 1) **Radial dyssynchrony** - Standard deviation of the time to peak (TTP-SD6) radial strain of six mid ventricular myocardial segments given as a percentage of the length of the cardiac cycle. 2) **Circumferential dyssynchrony** - Standard deviation of the time to peak circumferential strain of six mid ventricular myocardial segments given as a percentage of the length of the cardiac cycle. 3) **Longitudinal dyssynchrony** - Standard deviation of the time to peak of seven (TTP-SD7) longitudinal myocardial segments given as a percentage of the length of the cardiac cycle (168). Figure 3-1 demonstrates a healthy volunteer and a patient with IPAH short axis CMR assessment of circumferential synchrony.

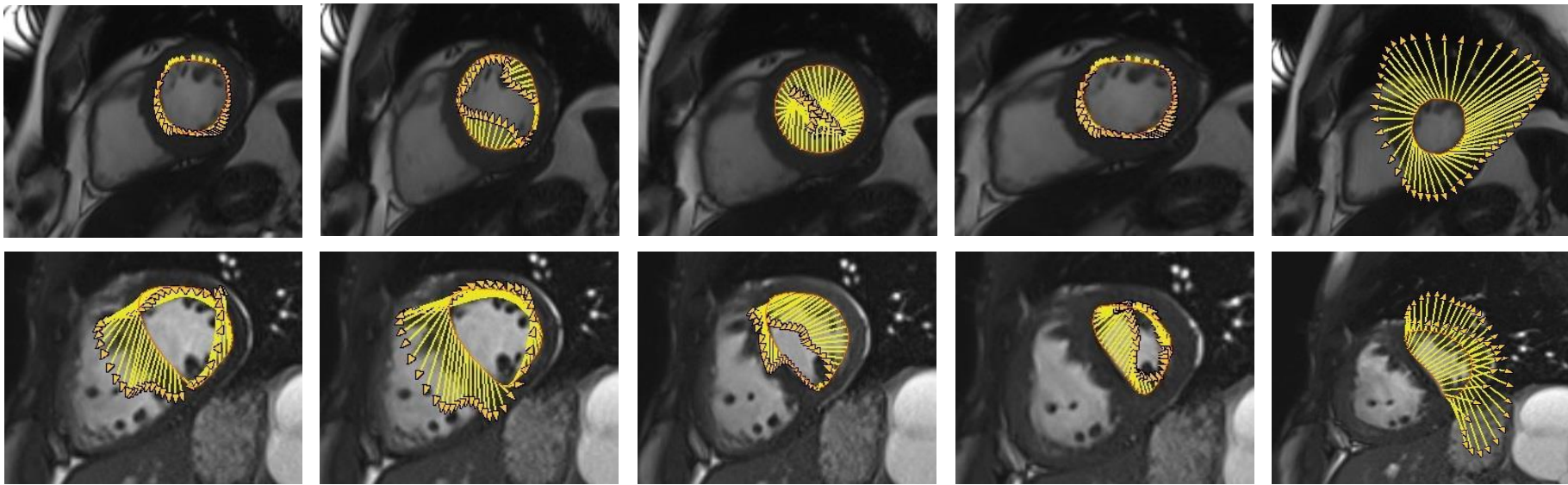


**Figure 3-1 Left ventricular circumferential intra-ventricular synchrony in health and IPAH**

The top row represents a healthy volunteer demonstrating a short axis showing synchronous contraction and relaxation of the left ventricle. The bottom row demonstrates a patient with idiopathic pulmonary arterial hypertension demonstrating LV intra-ventricular dyssynchrony. (Author's own image)

### 3.2.7 Statistical analysis

Continuous variables are summarised as mean  $\pm$  SD, median (interquartile range) depending on their distribution. Categorical variables are summarised as n (%). Normality of groups was assessed using a Shapiro-Wilk test. IPAH and healthy volunteer groups were compared using student t-tests, Mann-Whitney U tests and Fisher's exact tests, where appropriate. Spearman correlation coefficients are used to assess association between continuous variables. To test for inter-observer variability in strain measurements intra-class correlation coefficient with a 2-way random model of absolute agreement was used. Survival was recorded from the date of diagnostic right heart catheterisation and endpoint was date of either death, lung transplantation or censoring. All-cause mortality was used for survival analysis and patients were censored if they were lost to follow-up or alive at the last day of study. Survival predictors were determined using a bivariate Cox proportional hazard regression analysis with age. Results were presented as hazard ratios with 95% confidence intervals. Variables that were significant were considered for multivariate analysis. Survival of patients were compared by a long rank test. A p-value of greater than 0.05 indicated a lack of statistical significance. Statistical analysis was performed using SPSS (IBM SPSS Statistics) and Graphpad Prism (Graphpad Software inc).

### 3.3 Results

#### 3.3.1 Demographics

70 patients with IPAH and 40 healthy volunteers were included in the study. There was no significant difference between the IPAH and the healthy volunteer groups in terms of gender, age, BSA or weight. Demographics of the study population are given in table 3.1.

**Table 3.1 Demographics of the study population.**

	All	IPAH	Healthy volunteer	P value
n	110	70	40	
Gender (Female)	75	45	23	0.5429
Age	58 (45,67)	61(46,70)	53.5(42,63)	0.0605
Height	1.65 +/-0.9	1.63 +/- 0.8	1.68 +/- 0.9	0.0015
Weight	78.2 +/-15.5	78.6 +/- 15.8	77.5+/- 15.1	0.7220
BSA	1.9 +/- 0.2	1.9 +/-0.2	1.9 +/- 0.2	0.6587

IPAH and the healthy volunteer groups in terms of gender, age, height, weight and BSA are shown. There was no significant difference between the IPAH and the healthy volunteer groups in terms of gender, age, BSA or weight. Continuous variables are summarised as mean  $\pm$  SD, median (interquartile range) depending on their distribution. Categorical variables are summarised as n (%). IPAH and healthy volunteer groups were compared using student t-tests, Mann-Whitney U tests and Fisher's exact tests, where appropriate. Normality of groups was assessed using a Shapiro-Wilk test. A p-value of greater than 0.05 indicated a lack of statistical significance. IPAH – idiopathic pulmonary arterial hypertension, BSA – body surface area

### **3.3.2 CMR variables and baseline haemodynamic characteristics of IPAH patients**

There were no significant differences between the patient group and healthy volunteers in terms of LV function measured by LV ejection fraction (LVEF) (66.1% vs 64.2%  $p=0.6672$ ). The RV function measured by RV ejection fraction (RVEF) was lower in the IPAH group as expected (34% vs 58.8%  $p<0.0001$ ). There were significant differences in not only the right sided volume variables and VMI but also in the left sided volume variables (all  $p<0.0001$ ). The baseline CMR characteristics of the IPAH and healthy volunteer groups are summarised in table 3.2.

**Table 3.2 The baseline CMR characteristics of the IPAH and healthy volunteer group**

	ALL	IPAH	Healthy	p value
n	110	70	40	
LVEF	65.2(60.3,71.2)	66.1(57.4,71.9)	64.2(61.3,67.9)	0.6672
RVEF	44.6(30.3,57.2)	34.0(24.9,44.1)	58.8(54.6,64.3)	<0.0001
LVEDVI	62.5 (48.7,78.6)	50.6(43.7,62.4)	79.2(76.0,90.7)	<0.0001
LVESVI	22.4(14.9,28.2)	18.3(12.5,23.6)	27.7(24.7,34.2)	<0.0001
RVEDVI	97.9(85.8,118.7)	113.5(92.0,130.6)	86.3(75.8,95.8)	<0.0001
RVESVI	52.9(37.6,78.1)	73.2(53.0,93.5)	34.7(28.9,44.2)	<0.0001
LV Mass index	49.0(42.9,57.3)	46.6(41.4,55.6)	52.7(46.4,61.0)	<0.05
RV Mass index	23.1(14.3,31.3)	30.6(24.2,35.3)	12.7(10.9,14.9)	<0.0001
VMI	0.5(0.3,0.7)	0.6(0.5,0.8)	0.2(0.2,0.3)	<0.0001

IPAH and the healthy volunteer groups in terms of biventricular function, volume and mass are shown. There were no significant differences between the patient group and healthy volunteers in terms of LV function measured by LVEF. The RV function measured by RVEF was lower in the IPAH group as expected. There were significant differences in not only the right sided volume variables and VMI but also in the left sided volume variables. Continuous variables are summarised as median (interquartile range) due to their distribution. IPAH and healthy volunteer groups were compared using Mann-Whitney U tests. Normality of groups was assessed using a Shapiro-Wilk test. A p-value of greater than 0.05 indicated a lack of statistical significance. LVEDVI – LV end-diastolic volume index, LVESVI – LV end-systolic volume index, RVEDVI – RV end-diastolic volume index, RVESVI – RV end-systolic volume index, VMI – ventricular mass index

The baseline characteristics of the IPAH group are summarised in Table 3.3. The patients had a mPAP range of 25-79 mmHg. Of note is the normal PAWP in the patient group indicating normal LV filling pressures (median PAWP 8 mmHg, range 0 - 14 mmHg).

**Table 3.3 The baseline characteristics of the IPAH group**

Variable	Median (interquartile range)
Log NT pro BNP	3.2 (2.7,3.6)
DLCO (%)	45 (26,62)
6-minute walk distance	250 (161,388)
TAPSE	1.5 (1.2,1.9)
Right atrial pressure	8 (4,13)
Mean pulmonary artery pressure	50 (44,59)
Pulmonary artery wedge pressure	8 (5,10)
Cardiac output	3.6 (2.8,4.2)
Cardiac index	1.9 (1.6,2.3)
Stroke volume index	26.6 (19.8,30.9)
Pulmonary vascular resistance	12.3 (8.5,16.1)
Mixed venous saturations	63.2 (53.7,68.8)
Heart rate	77 (68,88)
Systolic blood pressure	127 (112,147)

The IPAH patients had a mean pulmonary artery pressure range of 25-79 mmHg. Pulmonary artery wedge pressure was low indicating low LV filling pressures 8(5,10) mmHg. Continuous variables are summarised as median (interquartile range) due to their distribution. Normality of groups was assessed using a Shapiro-Wilk test. LOG NT pro BNP- N Terminal pro Brain Natriuretic Peptide, DLCO% - diffusion capacity, TAPSE – Tricuspid Annular Plane Systolic Excursion by echocardiography.

### 3.3.3 Inter-observer reproducibility

Among the variables measured radial dyssynchrony demonstrated the best reproducibility (ICC = 0.9 95% CI 0.765 to 0.960). All the other variables demonstrated good to very good reproducibility. The results are summarised in table 3.4.

**Table 3.4 Reproducibility of the strain, strain rate and dyssynchrony variables**

Variable	Intraclass correlation coefficient	95% CI lower bound	95% CI upper bound
Ecc <sub>LV</sub>	.832	.630	.928
Ell <sub>LV</sub>	.863	.622	.948
Err <sub>LV</sub>	.703	.385	.873
LV Circ. dyssynchrony	.814	.581	.922
LV Long. dyssynchrony	.853	.663	.939
LV Radial dyssynchrony	.900	.765	.960
LV Circ. strain rate	.899	.764	.959
LV Long. strain rate	.794	.517	.916

Among the variables measured radial dyssynchrony demonstrated the best reproducibility (ICC = 0.900 95%CI 0.765 – 0.960). All the other variables demonstrated good to very good reproducibility. To test for inter-observer variability in strain measurements, intra-class correlation coefficient with a 2-way random model of absolute agreement was used. Ecc<sub>LV</sub> – LV circumferential strain, Ell<sub>LV</sub> – LV longitudinal strain, Err<sub>LV</sub> – LV radial strain.

### **3.3.4 Healthy volunteer vs IPAH: strain, strain rate and dyssynchrony**

#### **3.3.4.1 Left ventricle**

There were no significant differences between the two groups in  $Err_{LV}$  (65.3 vs 70.7  $p=0.1729$ ). However,  $Ecc_{LV}$  (-29.1 vs -32.1  $p=0.0323$ ) and  $Ell_{LV}$  (-16.6 vs -23.7  $p<0.0001$ ) were significantly lower in the IPAH group compared to healthy volunteers. LV synchrony (SD-6 and SD-7 indices) was impaired in radial (0.59 vs 0.25  $p<0.0001$ ), circumferential (0.93 vs 0.49  $p<0.0001$ ) and longitudinal (1.45 vs 0.89  $p<0.0001$ ) directions in the IPAH group. LV Strain rate (radial, circumferential and longitudinal) were not significantly different between the two groups. (Table 3.5)

#### **3.3.4.2 Right Ventricle**

In the RV, free wall (-14.1 vs -27.9  $p<0.0001$ ), septum (-8.6 vs -16.6  $p<0.0001$ ) and average strain (-10 vs -21.5  $p<0.0001$ ) as well as strain rates were impaired in the IPAH group compared to the healthy volunteer group. (Table 3.6)

#### **3.3.4.3 Severe vs mild / intermediate disease**

Although there was no significant difference between the patient group and healthy volunteer group in terms of LV radial function, patients with more severe disease (classified according to cardiac index  $<2$  at right heart catheterisation) demonstrated impairment of  $Err_{LV}$  compared to patients with less severe disease (50.9 vs 87.5  $P<0.0001$ ). In the same analysis,  $Ecc_{LV}$  (-27.2 vs -32.1  $p=0.0403$ ) and  $Ell_{LV}$  (-14.9 vs -19.3  $p=0.0021$ ) were also different between the severe and mild disease groups. LV radial dyssynchrony was higher in patients with more severe disease (0.89 vs 0.39  $p=0.0043$ ). Table 3.7. shows the LV and RV strain and dyssynchrony variables between patients with severe disease (cardiac index  $<2$ ) and patients with less severe (intermediate and mild disease - cardiac index  $>2$ ).

**Table 3.5 Healthy volunteer vs IPAH LV strain, strain rate and dyssynchrony.**

Strain parameter	IPAH	Healthy volunteer	p value
Err <sub>LV</sub>	65.3 (41.3,92.2)	70.7 (61.4,83.9)	0.1729
Ecc <sub>LV</sub>	-29.1 (-35.1,-23.7)	-32.1 (-34.0,-29.7)	0.0323
Ell <sub>LV</sub>	-16.6(-21.4,-12.0)	-23.7(-25.2,-21.0)	<0.0001
LV Radial dyssynchrony	0.59 (0.22,0.97)	0.25 (0.18,0.3)	<0.0001
LV Circ. dyssynchrony	0.93 (0.62,1.34)	0.49 (0.21,0.8)	<0.0001
LV Long. dyssynchrony	1.45 (1.02,2)	0.89 (0.71,1.42)	<0.0001
LV Radial strain rate	2.1(1.7,2.8)	2.4(2,2.7)	0.2576
LV Circ. strain rate	-1.8(-2.2,-1.4)	-1.7(-1.9,-1.5)	0.5353
LV Long. strain rate	-1.1(-1.4,-0.8)	-1.1(-1.3,-0.9)	0.6090

There were no significant differences between the two groups in Err<sub>LV</sub> (65.3 vs 70.7 p = 0.1729). However, Ecc<sub>LV</sub> (-29.1 vs -32.1 p = 0.0323) and Ell<sub>LV</sub> (-16.6 vs -23.7 p <0.0001) were significantly lower in the IPAH group compared to healthy volunteers. LV was dyssynchronous in radial (0.59 vs 0.25 p<0.0001), circumferential (0.93 vs 0.49 p<0.0001) and longitudinal (1.45 vs 0.89 p<0.0001) directions in the IPAH group. LV Strain rates were not significantly different between the two groups. Results are shown as mean (interquartile range). The IPAH group and healthy volunteer cohort were compared using Mann Whitney U test. Normality of groups was assessed using a Shapiro-Wilk test. A p-value of greater than 0.05 indicated a lack of statistical significance. Ecc<sub>LV</sub> – LV circumferential strain, Ell<sub>LV</sub> – LV longitudinal strain, Err<sub>LV</sub> – LV radial strain.

**Table 3.6 Healthy volunteer vs IPAH RV strain, strain rate and dyssynchrony.**

Strain parameter	IPAH	Healthy volunteer	p value
RV Free wall strain	-14.1(-19.2,-9.6)	-27.9(-31.9,-24.6)	<0.0001
RV Septum strain	-8.6(-12.3,-5.8)	-16.6(-20.3,-13.4)	<0.0001
RV Average strain	-10.0(-14.1,-7.4)	-21.5(-24.4,-19.4)	<0.0001
RV Free wall strain rate	-0.8(-1.1,-0.6)	-1.5(-1.6,-1.3)	<0.0001
RV Septum strain rate	-0.7(-0.8,-0.5)	-0.8(-1.1,-0.7)	0.0031
RV Average strain rate	-0.6(-0.8,-0.4)	-1.1(-1.2,-1)	<0.0001

In the RV, free wall (-14.1 vs -27.9  $p<0.0001$ ), septum (-8.6 vs -16.6  $p<0.0001$ ) and average strain (-10 vs -21.5  $p<0.0001$ ) as well as strain rates were impaired in the IPAH group compared to the healthy volunteer group. Results are shown as mean (interquartile range). The IPAH group and healthy volunteer cohort were compared using Mann Whitney U test. A p-value of greater than 0.05 indicated a lack of statistical significance.

**Table 3.7 Strain, dyssynchrony and strain rate measurements in IPAH patients with severe vs intermediate / mild disease.**

Strain parameter	Severe disease	Intermediate and mild disease	
Err <sub>LV</sub>	50.9 +/- 25.0	87.5 +/- 33.4	<0.0001
Ecc <sub>LV</sub>	-27.2 +/- 9.5	-32.1 +/- 9.6	0.0403
Ell <sub>LV</sub>	-14.9 +/- 5.1	-19.3 +/- 6.4	0.0021
LV Radial dyssynchrony	0.89 (0.30,1.17)	0.39 (0.17,0.67)	0.0043
LV Circ. dyssynchrony	1.05 (0.74,1.29)	0.83 (0.53,1.73)	0.5970
LV Long. dyssynchrony	1.52 (1.30,2.25)	1.33 (0.92,1.89)	0.0570
LV Radial strain rate	2.0 +/- 0.7	2.6 +/- 0.7	0.0004
LV Circ. strain rate	-1.7 (-2.1, -1.3)	-1.9 (-2.5,-1.5)	0.1610
LV Long. strain rate	-1.1 (-1.2,-0.8)	-1.4 (-1.5,-0.8)	0.1577
RV free wall strain	-11.0 +/- 4.1	-17.9 +/- 6.0	<0.0001
RV septum strain	-7.4 +/- 3.3	-11.3 +/- 5.5	0.0006
RV Average strain	-8.0 +/- 2.9	-14.0 +/-5.2	<0.0001
RV free wall strain rate	-0.65 (-0.8, -0.5)	-1.1 (-1.3,-0.8)	<0.0001
RV septum strain rate	-0.65 (-0.8, -0.5)	-0.7 (-0.9, -0.6)	0.3561
RV average strain rate	-0.5 (-0.6,-0.3)	-0.8 (-0.9,-0.6)	<0.0001

Although there was no significant difference between the patient group and healthy volunteer group in terms of LV radial function, patients with more severe disease (classified according to cardiac index <2) demonstrated impairment of Err<sub>LV</sub> compared to patients with less severe disease (50.9 vs 87.5 p<0.0001). Ecc<sub>LV</sub> (-27.2 vs -32.1 p=0.0403) and Ell<sub>LV</sub> (-14.9 vs -19.3 p=0.0021) were also different between the severe and mild disease groups. LV radial dyssynchrony was higher in patients with more severe disease (0.89 vs 0.39 p=0.0043). Disease severity was classified by cardiac index derived from right heart catheterisation (cardiac index < 2). Results are shown as mean +/- SD or median (interquartile range) as appropriate. The two groups were compared using T test or Mann Whitney U test as appropriate. A p value greater than 0.05 demonstrated a lack of statistical significance. Ecc<sub>LV</sub> – LV circumferential strain, Ell<sub>LV</sub> – LV longitudinal strain, Err<sub>LV</sub> – LV radial strain.

### 3.3.5 Impaired LV ejection fraction in IPAH

A small group of patients with impaired LV ejection fraction was studied to understand the mechanisms of LV impairment in IPAH patients. In the subgroup of patients with impaired LVEF (LVEF < 55%),  $E_{ll_{LV}}$  (-9.9 vs -31.93  $p < 0.0001$ ) and  $E_{rr_{LV}}$  (32.21 vs 76.2  $p < 0.0001$ ) were significantly lower than patients with preserved LVEF. However,  $E_{cc_{LV}}$  (-18.82 vs -18.82  $p = 0.8905$ ) was similar in the two groups. The results are summarised in figure 3-2.

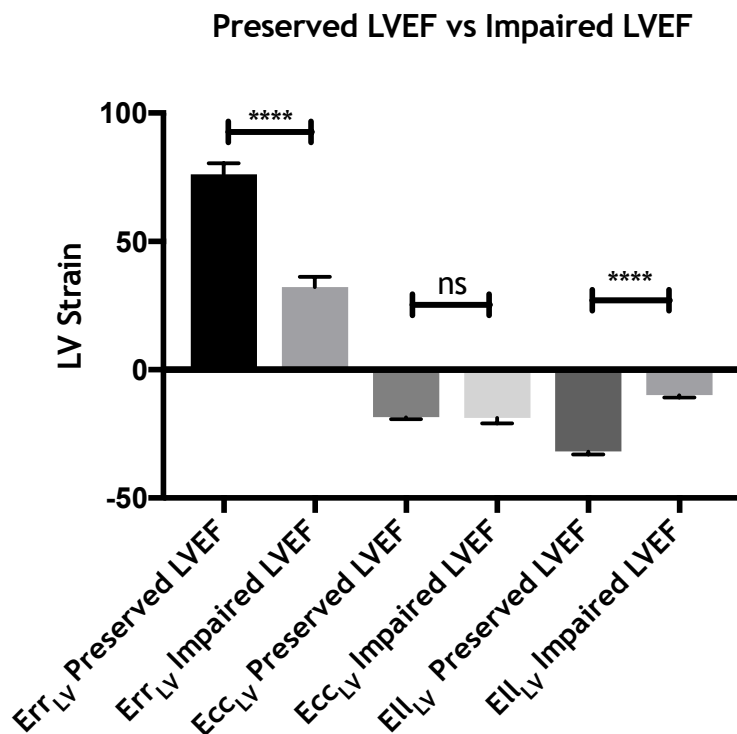


**Figure 3-2 IPAH patients with preserved LV ejection fraction vs impaired LV ejection fraction**  
 In the subgroup of patients with impaired LVEF (LVEF < 55%) (n=12),  $E_{ll_{LV}}$  (-9.9 vs -31.93  $p < 0.0001$ ) and  $E_{rr_{LV}}$  (32.21 vs 76.2  $p < 0.0001$ ) were significantly lower than patients with preserved LVEF (n=58). However,  $E_{cc_{LV}}$  was similar in the two groups. The two groups were compared for each variable by a t test. A p value greater than 0.05 demonstrated a lack of statistical significance. LVEF – LV ejection fraction,  $E_{cc_{LV}}$  – LV circumferential strain,  $E_{ll_{LV}}$  – LV longitudinal strain,  $E_{rr_{LV}}$  – LV radial strain.

### 3.3.6 Association with markers of disease severity

LV radial strain was significantly associated with known markers of disease severity including RVEF ( $r=0.66$ ), RVESVI ( $r=-0.59$ ), PVR ( $r=0.51$ ) and SVI ( $r=0.44$ ). (Figure 3-3) The association of longitudinal and circumferential strain with markers of disease severity was significant, however with a weaker strength. Among the LV dyssynchrony indices, radial dyssynchrony demonstrated the strongest association with known markers of disease severity ( $r$  values RVEF = -0.44, RVESVI=0.46 respectively). The association of strain rate measurements were consistent with the aforementioned LV strain values. Considering the RV strain variables, RV average strain (average of septal and free wall strain) demonstrated strong association with RVEF ( $r=-0.7$ ), RVESVI ( $r=0.63$ ) and SVI ( $r=-0.63$ ). The LV and RV strain variables and association with markers of disease severity are summarised in appendix 1 and 2.

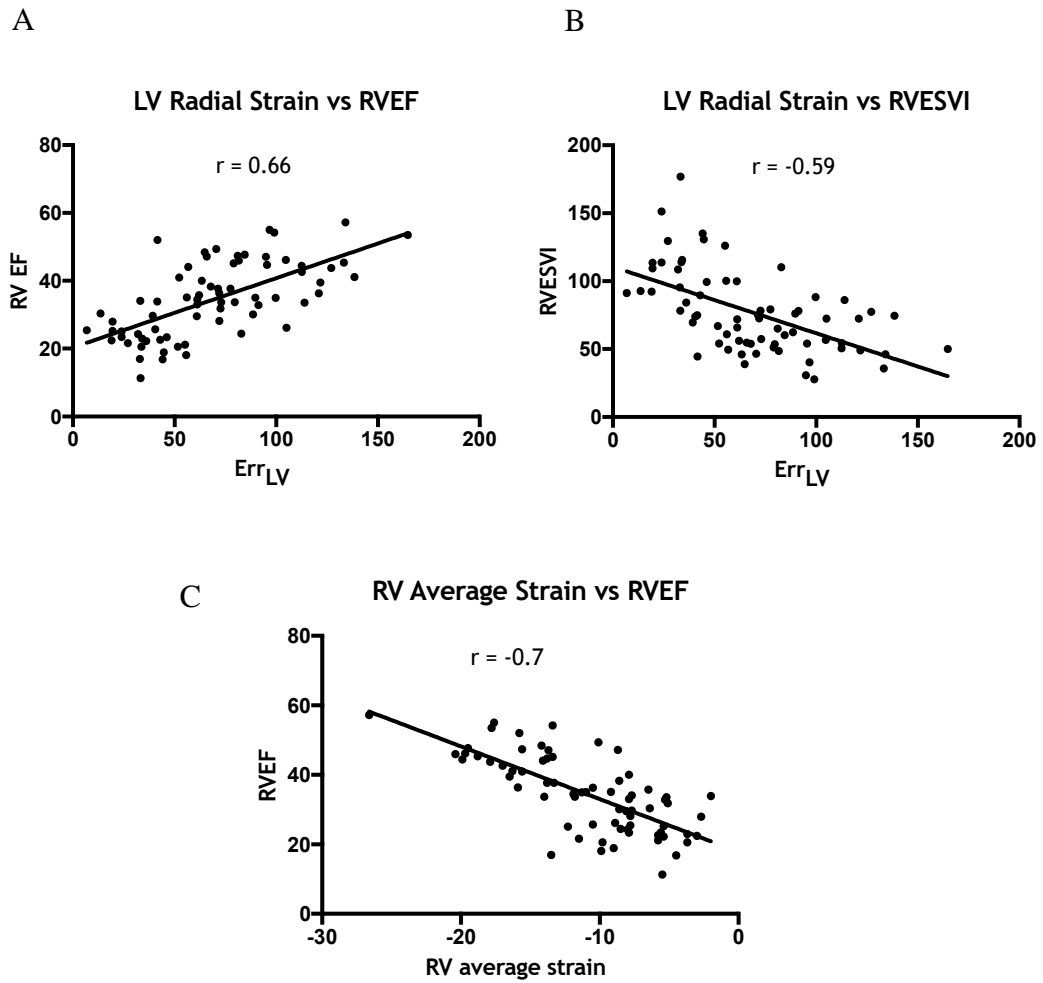


**Figure 3-3 Association of LV radial strain with RV ejection fraction (A) and RV end-systolic volume index (B) and association of RV average strain with RVEF (C) by CMR.**

LV radial strain was significantly associated with known markers of disease severity including RV ejection fraction ( $r=0.66$   $p < 0.0001$ ) and RV end-systolic volume index ( $r=-0.59$   $p < 0.0001$ ). RV average strain (average of septal and free wall strain) demonstrated strong association with RVEF ( $r=-0.7$   $p < 0.0001$ ). Spearman correlations were used to assess association between continuous variables as appropriate. Err<sub>LV</sub> – LV radial strain, RVEF – RV ejection fraction, RVESVI – RV end-systolic volume index.

### 3.3.7 Baseline survival analysis

In the cohort of 70 patients with IPAH, 25 deaths occurred during the follow up period. Median survival was 6.19 years. RVEF by CMR, cardiac index (right heart catheterisation), stroke volume index (right heart catheterisation), TAPSE by echocardiography, and CMR derived  $Err_{LV}$ , radial strain rate and radial dyssynchrony were predictive of death on bivariate cox proportional hazards regression with age. Right heart catheter derived mPAP was not a predictor of death in this model. The results are summarised in table 3.8.

**Table 3.8 Bivariate Cox proportional hazard regression analysis for survival in IPAH patients.**

Variable	HR	95% CI	P value
LVEF	0.975	(0.937 - 1.015)	0.222
RVEF	0.911	(0.866-0.959)	<0.001
RAP	1.002	(0.935-1.073)	0.956
mPAP	0.997	(0.956-1.041)	0.900
Cardiac index	0.397	(0.164-0.961)	0.041
PVR	1.083	(0.997-1.176)	0.060
SVI	0.936	(0.885-0.991)	0.023
TAPSE	0.363	(0.145-0.908)	0.030
Err <sub>LV</sub>	0.967	(0.949-0.985)	<0.001
Ecc <sub>LV</sub>	1.001	(0.963-1.041)	0.952
Ell <sub>LV</sub>	1.001	(0.945-1.061)	0.971
LV Radial dyssynchrony	3.329	(1.688-6.566)	<0.001
LV Circ. dyssynchrony	0.696	(0.453-1.070)	0.099
LV Long. dyssynchrony	0.777	(0.453-1.331)	0.358
LV Radial strain rate	0.396	(0.190-0.825)	0.013
LV Circumferential strain rate	0.921	(0.605-1.402)	0.701
LV Longitudinal strain rate	0.608	(0.216-1.715)	0.347
RV free wall strain	1.070	(0.997-1.148)	0.059
RV septal strain	1.013	(0.936-1.096)	0.754
RV average strain	1.068	(0.982-1.161)	0.125
RV free wall strain rate	1.446	(0.410-5.103)	0.567
RV septal strain rate	0.399	(0.090-1.768)	0.226
RV average strain rate	1.061	(0.211-5.348)	0.943

In the cohort of 70 patients with IPAH, RVEF, cardiac index, stroke volume index, Err<sub>LV</sub>, radial strain rate and radial dyssynchrony were predictive of death on bivariate cox proportional hazards regression with age. Data are shown as Hazard ratio with 95% confidence interval. All variables are analysed with age. A p value greater than 0.05 demonstrated a lack of statistical significance. LVEF – LV ejection Fraction, RVEF – RV ejection Fraction, RAP – right atrial pressure, mPAP – mean pulmonary artery pressure, PVR – pulmonary vascular resistance, SVI – stroke volume index, TAPSE – tricuspid annular systolic plane excursion, Ecc<sub>LV</sub> – LV circumferential strain, Ell<sub>LV</sub> – LV longitudinal strain, Err<sub>LV</sub> – LV radial strain.

In a multivariate model with age, SVI and PVR, Err<sub>LV</sub> (HR 0.970 CI 0.952 - 0.989 p=0.002) and radial dyssynchrony (HR 3.759 CI 1.745-8.097 p<0.0001) independently predicted survival. In the same multivariate model RVEF independently predicted survival (HR 0.902 CI 0.839-0.969 p=0.005), however TAPSE by echocardiography did not (HR 0.622 CI 0.205-1.887 p 0.402). These are shown in table 3.9.

**Table 3.9 Multivariate cox proportional hazard regression model for survival in IPAH patients**

a)

	<b>Hazard Ratio</b>	<b>95% Confidence Interval</b>	<b>p value</b>
Age	1.098	(1.052-1.146)	<0.001
SVI	0.955	(0.881-1.035)	0.259
PVR	0.973	(0.858-1.103)	0.665
Err <sub>LV</sub>	0.970	(0.952-0.989)	0.002

b)

	<b>Hazard Ratio</b>	<b>95% Confidence Interval</b>	<b>p value</b>
Age	1.019	(1.047-1.136)	<0.001
SVI	0.919	(0.841-1.004)	0.062
PVR	0.970	(0.852-1.103)	0.639
Radial dyssynchrony	3.759	(1.745-8.097)	<0.0001

Multivariate Cox proportional hazard regression model for survival in IPAH patients including a) radial strain as a prognostic variable b) radial dyssynchrony as prognostic variable. In a multivariate model with age, SVI and PVR, Err<sub>LV</sub> (HR=0.970 p=0.002) and radial dyssynchrony (HR=3.759 p<0.0001) independently predicted survival. In the same multivariate model RVEF independently predicted survival however, TAPSE by echocardiography did not. A p value greater than 0.05 demonstrated a lack of statistical significance. SVI – stroke volume index, PVR – pulmonary vascular resistance, Err<sub>LV</sub> – LV radial strain.

The Kaplan-Meier survival curves according to median value for  $Err_{LV}$ , RVEF and PVR are shown in Figure 3-4. Survival was worse in IPAH patients with LV radial strain  $< 65.3$  (Logrank  $p=0.05$ ), however low RVEF and low PVR at right heart catheterisation was not statistically significant.

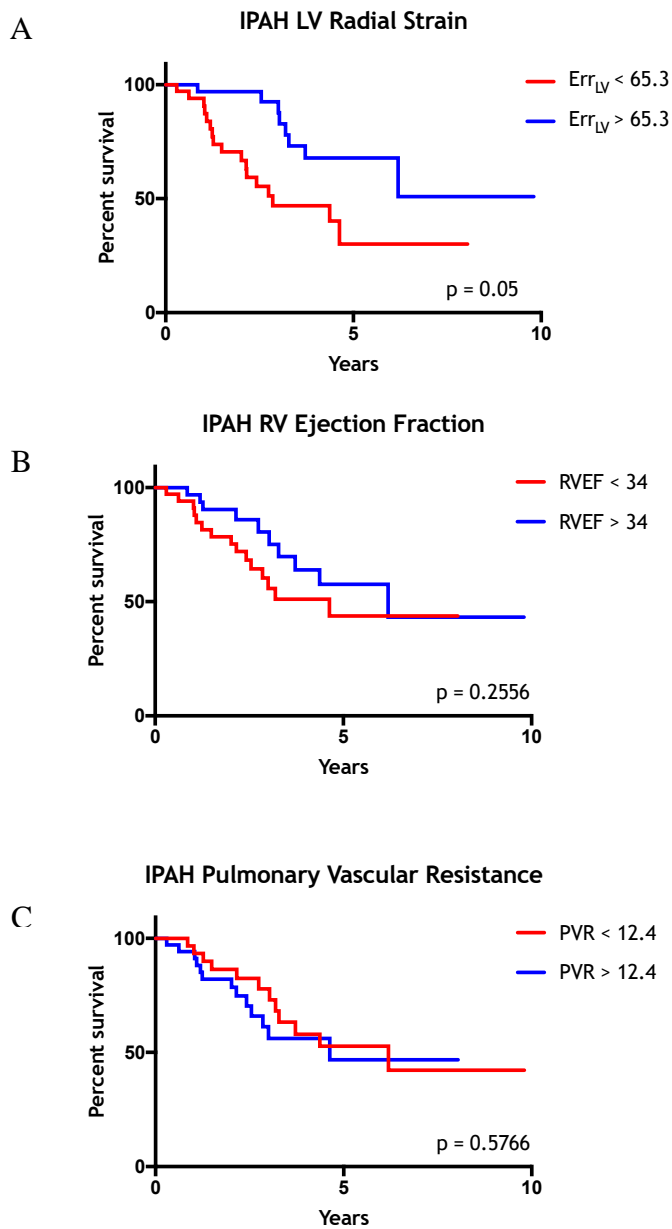


**Figure 3-4 Kaplan Meir curves demonstrating survival of IPAH patients**

Kaplan Meir curves demonstrating survival of IPAH patient with a) LV radial strain and b) RVEF and c) Pulmonary vascular resistance. Survival was worse in IPAH patients with low  $Err_{LV}$ , however low RVEF or high PVR was not statistically significant. The Kaplan-Meier survival curves were determined by median values. A p value greater than 0.05 demonstrated a lack of statistical significance.  $Err_{LV}$  – LV radial strain, RVEF – RV ejection fraction. PVR – pulmonary vascular resistance.

### 3.4 Discussion

The major findings of our study are as follows:

- 1) Evaluation of LV strain in radial, circumferential and longitudinal directions is feasible in IPAH patients by CMR-FT.
- 2) LV longitudinal strain and (LV circumferential strain to a lesser extent) is impaired in patients with IPAH compared to age matched healthy controls, and LV is dyssynchronous in radial, circumferential and longitudinal directions in IPAH.
- 3) In more severe disease, LV radial strain is impaired compared to patients with less severe disease.
- 4) LV strain variables especially radial strain and radial dyssynchrony indices are associated with markers of disease severity in IPAH
- 5) LV radial dysfunction is associated with poor outcome in patients with IPAH and may provide incremental value to known CMR derived RV variables in IPAH.

In IPAH there is progressive pulmonary vasoconstriction resulting in an increased afterload to the RV. Right ventricle initially adapts by increasing muscle thickness and contractility which is termed coupling. With advancing disease, the hypertrophy process will be halted and subsequently stroke volume will decrease. The RV dilates and the heart rate will increase to maintain RV cardiac output. Finally, RV uncoupling will occur with falling stroke volume. As uncoupling occur at a severe stage of the disease, the mechanisms of adaptations of the RV to prevent uncoupling/ maintain coupling become important in determination of survival of patients with PAH. Thus, traditionally measures of RV stroke volume, RV end diastolic and RV end systolic volume as well as RVEF and SV/ RVESV have been variables monitored during follow up of patients with PAH and have shown to be of high prognostic value (149).

Although it is well established that RV function, especially that relating to the dynamic function of the right heart is associated with outcome in PAH patients, some left heart variables are known to have better correlations with cardiac function in IPAH patients. LVEDV is more closely related to RV stroke volume than RVEDV in PH patients (16). Echocardiography studies had also demonstrated that LV eccentricity index but not RVEDV to be closely associated with outcome in PAH (36). Previous studies have also demonstrated that poor LV output in PH is related to poor LV filling and prolonged contraction time of the RV. These studies have therefore highlighted the importance of LVEDV as it reflected both reduced RV output and prolonged RV contraction time (187, 188).

The LV myocardium is organized into three distinctive layers; the sub-endocardial layer formed by fibres orientated longitudinally from base to apex, the sub-epicardial layer with fibres orientated from apex to base and the mid wall layer with fibres orientated along the circumferential axis. Due to this architecture the normal LV deforms along several different directions: longitudinal and circumferential shortening, radial thickening and torsion (128). After myocardial infarction it is known that both LV longitudinal and circumferential function are independent predictors of outcome, and circumferential function was predictive of LV remodelling, suggesting that the circumferential function serves to restrain ventricular enlargement after MI (189). Although myocardial strain is most extensively studied in ischaemic heart disease, LV myocardial strain is also impaired in non-ischaemic heart diseases including dilated cardiomyopathy, hypertrophic cardiomyopathy and acute myocarditis providing prognostic information as well as pathophysiological insights in patients with left heart disease (190, 191).

The impact of the RV on LV function is minimal under normal conditions. However, this does change when it comes to a pressure loaded RV. There are both parallel and series interactions of the RV on the LV. In PH, the direct effect of the paradoxical motion and the bowing of the interventricular septum impairs early diastolic filling of the LV. This is due to the prolonged isovolumetric contraction of the RV (150). The main mechanism appears to be increased RV wall tension; RV contraction continues while the LV is already in its diastolic phase. LV filling is also affected by the low RV cardiac output. There is also the anatomical

consideration of RV dilatation with a geometrically restricted pericardial sac. Thus, measures of ventricular interaction and interdependency are extremely useful to assess disease severity as this not only contains information regarding stroke volume but also increasing RV wall tension. As mentioned in the introduction, several large studies in the past have shown the prognostic value of LV volume variables in PAH patients (99).

LV strain measurements, especially LV radial and circumferential strain as well as LV intra-ventricular dyssynchrony, reflect the effects of parallel effect of RV septal bowing and the series effect of low RV cardiac output. Thus, it is not surprising that some of these measurements are coming out as superior prognostic markers compared to RV function/ volume. As discussed in the introduction, because of the ventricular interdependency, measures of ventricular interaction are clinically useful to measure disease state as they contain information on the stroke volume as well as wall tension. Parameters that incorporate post systolic isovolumetric time such as the myocardial performance index have also shown to be of clinical relevance (37).

A small group of IPAH patients who had impaired LV ejection fraction (LVEF < 55% by CMR) were also studied to understand the mechanisms of LV impairment in this patient group. The LV longitudinal and radial function were significantly impaired, and LV circumferential function was preserved in IPAH patients who had impaired LVEF. We can hypothesise that LV maintains its ejection function initially by radial and circumferential contraction (in the setting of reduced longitudinal function) and subsequently LV radial function is impaired too as the disease progress.

The alternative explanation for impaired LV mechanics in this study is the possible presence of intrinsic left heart disease in this population. All subjects included in this study met the conventional classification of group 1 with a mPAP of  $\geq 25$  mm Hg and a PAWP  $\leq 15$  mm Hg. Patients with raised PAWP were excluded and the patient population had a median PAWP of 8 mmHg. It is also important to note the diagnosis of IPAH was based on multiple imaging modalities discussed at a multi-disciplinary meeting, including the absence of other features pointing to left heart disease, such as the presence of a dilated left atrium, pleural effusions, septal

lines etc. However, it is difficult to exclude that patients may have had elevations in left atrial pressure in the past.

This study demonstrated that LV strain is significantly impaired in patients with IPAH compared to healthy volunteers. This is despite the conventional measure of LV function i.e. LVEF being preserved in a majority of the patients. In patients with more severe disease the LV strain impairment is more significant. LV lacks intra-ventricular synchrony in radial, circumferential and longitudinal directions in patients with IPAH compared to healthy volunteers. These abnormalities in strain and synchrony are associated with known markers of disease severity including haemodynamic markers, CMR markers and echocardiography derived TAPSE. Interestingly, both LV radial strain and dyssynchrony was superior to conventional markers of disease prognosis including stroke volume index derived at right heart catheterisation and RV ejection fraction measured by CMR in predicting survival.

In the pan European EURO-MR study (99), patients with PH who were on disease targeted therapy demonstrated significant improvements not only in RV variables but in LVEF and LVEDV. Increases in 6-minute walk distance correlated with LVEDV. These results indicate that LV CMR-FT appear to be sensitive to the degree of disease severity than LVEDV, thus potentially providing a novel, sensitive marker of monitoring treatment response and disease progression in PAH patients.

Previous studies had shown that under filling of the LV may also bring the LV myocytes into an atrophic state (17). *Manders et al* demonstrated substantially reduced contractile function in cardiomyocytes in a study of PAH patients using CMR and myocardial biopsy. Left ventricular dysfunction is also recognised as a post-operative complication in IPAH patients who have undergone lung transplantation (192). This is of importance as unloading the RV and improving LV preload might induce LV failure. Thus, the impact of pharmaceutical as well as mechanical interventions in PAH patients on the LV mechanics is of extremely importance and need to be explored in detail in a future study.

### 3.5 Conclusion

Patients with IPAH had significant differences in LV strain and synchrony when compared to healthy volunteers despite the conventional measures of LV systolic function (LV ejection fraction) being normal in a majority. Furthermore, IPAH patients with more severe disease demonstrated worse LV strain and LV intra-ventricular dyssynchrony when compared to patients with less severe disease. LV strain and intra-ventricular dyssynchrony, especially LV radial function, were associated with known markers of disease severity and predicted survival in patients with IPAH. These LV variables will provide incremental value to known RV CMR variables in terms of their ability to reflect disease severity and predict survival.

### 3.6 Limitations

There are several limitations to our study. This was a single centre retrospective observational study. There were patients who were diagnosed with IPAH who were not included in the study if they did not undergo cardiac MR imaging. This may exclude patients with severe breathlessness who probably did not manage CMR (breath holding difficulties) and may also exclude patients with mild disease who may not be diagnosed till they show significant symptoms. Survival analysis was done with a relatively small number of events (n= 25 deaths). A large-scale multicentre study is required to validate the findings of this study. Secondly, CMR feature tracking can be affected by through plane motion artefacts and also is limited by pixel size (175, 193). Previous feature tracking strain studies have demonstrated significant variability of strain values, mainly due to the lack of standardization in signal acquisition and image processing (177). In this study the interrater reproducibility of the variables was good to very good, however radial strain reproducibility demonstrated a wide confidence interval (Table 3.4). This study didn't examine LV torsion and previous literature had proposed decreased LV torsion with delayed diastolic untwisting as a mechanism of LV diastolic dysfunction in PAH patients (130).

**Chapter 4 Left atrial strain by  
CMR imaging in idiopathic  
pulmonary arterial  
hypertension**

## 4.1 Introduction

In the previous chapter, the study demonstrated impaired LV mechanics in patients with IPAH despite the conventional measures of LV function being normal. These LV variables were probably superior to known RV CMR variables in terms of their ability to reflect disease severity and predict survival in IPAH patients.

In patients with PH, left atrial assessment has been limited to measuring the volume or area of the LA. PH due to heart failure with preserved ejection fraction (HFpEF) occurs as a result of impaired LV distensibility and relaxation. Distinguishing PH due to HFpEF (group 2 PH) from PAH is extremely important, as there is currently no evidence for using pulmonary vasodilators in the treatment of patients with group 2 PH. At present, right heart catheterisation is the definite investigation to confirm the diagnosis, a raised PAWP indicating group 2 disease. However, assessment of LA volume by CMR has been used to distinguish PAH from PH due to HFpEF. *Crawley et al* showed that left atrial volume of 43 ml/m<sup>2</sup> to be a useful mean of distinguishing between PAH and group 2 PH, avoiding the need for invasive right heart catheterisation (18).

Left atrial function is increasingly used to have a significant role in the prognosis and risk stratification in different cardiac diseases. The principal role of the LA is to modulate LV filling by three basic functions. They are reservoir function (collection of pulmonary venous return during LV systole), conduit function (passage of blood to the LV during early ventricular diastole) and booster pump function (during late diastole augmentation of LV filling) (153).

When assessing LA function, it is important to recognise that there is significant interplay that exist between LA and LV performance during the cardiac cycle. Reservoir function is defined by atrial compliance during ventricular systole, however this is influenced by LV end-systolic volume. Conduit function is dependent on atrial compliance during ventricular diastole; however, is closely related to LV relaxation and stiffness and is reciprocally related to atrial reservoir function. Atrial booster function is dependent on the degree of venous return (atrial preload), magnitude and timing of atrial contractility and also on LV end-diastolic pressure (atrial afterload) (153, 194).

Although LA volume has shown to correlate with cardiovascular outcomes there is an increasing amount of evidence suggesting that LA functional measurements will provide incremental and stronger evidence than LA volume alone. In a study using speckle tracking echocardiography by *Mondillo et al*, LA deformation mechanics were impaired in patients with systemic hypertension and diabetes with normal LA size (195). In another study by *Kojima et al*, where velocity encoded echocardiogram was used to assess LA function in patients with paroxysmal AF, LA functional impairment was observed before enlargement of LA (196).

LA function is assessed by echocardiography using volumetric analysis, spectral Doppler analysis or by tissue Doppler analysis. Volumetric assessment of the LA is obtained by measuring LA volumes at their maximum (at end-systole before the opening of the mitral valve) and at their minimum (at end-diastole as the mitral valve closes) and immediately before the atrial systole (before the p wave on ECG). From these volumes, total ejection fraction, passive ejection fraction and active ejection fraction can be calculated. Spectral Doppler analysis uses trans-mitral, pulmonary venous and left atrial appendage flows. Tissue velocities during ventricular systole (S') and early diastole (E') correspond to the atrial reservoir and atrial conduit function (194).

There are a large number of studies using echocardiography derived LA function analysis in determining prognosis and risk stratification in different cardiac diseases. In the Dallas heart study of 1802 patients, LA emptying fraction but not the LA volume index was independently associated with mortality. It added incremental power to the Framingham risk score (197). In a community-based cohort, LA emptying fraction was a predictor of cardiovascular events and its predictive ability was stronger than for LA volumes suggesting that LA dysfunction may represent a more advanced state of LA remodelling than LA enlargement (198).

Echocardiography derived LA strain analysis has also been extensively studied in patients with left heart diseases. In patients HCM, echocardiography derived LA booster function was augmented while they observed impaired reservoir and conduit function. *Kobayashi et al* also observed that LA function was impaired even in patients with minimally symptomatic non obstructive HCM (199). In patients who have suffered an acute coronary syndrome, LA function determined

by tissue Doppler imaging predicted adverse cardiac outcomes adding to prognostication of these patients (200).

As mentioned in previous chapters' CMR-FT is a new post-processing technique allowing the quantification of myocardial strain and strain rate using standard SSFP cine images. *Kowallick et al* demonstrated that CMR-FT to reliably quantify LA longitudinal strain and strain rate from standard SSFP cine images discriminating between patients with impaired LV relaxation and healthy controls (154). In the above study by *Kowallick et al*, they demonstrated significantly decreased passive strain in patients with HFpEF and HCM corresponding to impaired conduit function. As atrial conduit function is closely related to LV compliance, the authors suggested that this represented impaired LV relaxation. In the same study, total strain and peak positive SR which correspond to atrial reservoir function were decreased in HCM and HFpEF that might indicate impaired atrial compliance. They also showed increased active strain and peak late negative strain rate corresponding to booster pump function in HCM while decreased in HFpEF. They hypothesised that this may represent an initial increase in LA booster pump at early stages of impairment of LV relaxation followed by progressive decompensation of global LA performance. This was also demonstrated in a study by *Murata et al* using 3D echocardiography to study atrial function (155).

Although PAH is partly defined by normal LV filling pressures, LV function/performance can be affected. RV pressure overload causes paradoxical motion of the inter-ventricular septum towards the LV disturbing LV geometry and filling. LV preload is reduced due to decreased cardiac output from the RV. These parallel and series interactions from the RV to the LV affect LV performance. There is also the anatomical consideration of RV dilatation in a contained pericardial sac (149). Considering the significant interplay that exist between LA and LV performance during the cardiac cycle, studying LA function may provide additional/ incremental information regarding cardiovascular performance in PAH patients.

A comprehensive retrospective study of LA strain in patients with IPAH was conducted. To the best of our knowledge, the significance of LA strain has not been studied in patients with IPAH. The aims of the study were a) Determining the feasibility of performing LA strain in IPAH 2) To characterise the pattern of LA

strain abnormalities in IPAH 3) Investigate the significance of these abnormalities on disease severity in IPAH.

## **4.2 Methods**

### **4.2.1 Patient recruitment**

We retrospectively identified all patients who were referred between 2010 to 2017 for investigations of PH and underwent right heart catheterisation and CMR. From these, we identified treatment-naïve patients who were diagnosed of IPAH after a multidisciplinary evaluation including blood investigations (autoantibodies, HIV testing), right heart catheterization, echocardiography, pulmonary function testing and CT scan of thorax (CT pulmonary angiogram and High Resolution CT thorax). After exclusion of patients due to inadequate image quality, presence of arrhythmia and a history of myocardial infarction, 56 patients with IPAH were included in the present analysis. A majority of these patients as well as healthy volunteers were also included in the study described in chapter 3. All patients underwent invasive haemodynamic measurements and CMR within 72 hours from catheterisation and gave informed written consent to undergo these procedures. An additional group of 30 healthy volunteers with no known history of arrhythmias, ischaemic heart disease and lung disease were used as controls. The study protocol was approved by the local research ethics committee.

### **4.2.2 CMR imaging**

CMR imaging was performed in the supine position on a 1.5T MRI scanner (Avanto, Siemens, Erlangen, Germany). Images were acquired during end-expiratory breath holds. Long axis 4 chamber cine images and contiguous short axis cine images covering both ventricles from base to apex were acquired with cine SSFP imaging with following parameters: TR (repetition time)/ TE (echo time) 3.2-3.9/0.6-2 ms, flip angle 45-90°, slice thickness 6 mm, temporal resolution 33-45 ms, spatial resolution 1.5-2 mm.

### **4.2.3 Right heart catheterization**

Right heart catheterisation was performed during free breathing in the supine position with a 7 F quadruple lumen, flow directed balloon tipped Swan - Ganz catheter using the internal jugular approach. Pressure measurements including

RAP, mPAP, dPAP, sPAP and PAWP were obtained. Cardiac output was obtained by thermodilution and PVR data were obtained. Mixed venous saturations were also obtained during right heart catheterisation. Systemic blood pressures, heart rate and oxygen saturations were measured during right heart catheterisation. The method of right heart catheterisation is described in detail in chapter 2.5.

#### **4.2.4 CMR image analysis**

All MR images were analysed by the author using the Medis suite analysis software (Medis medical imaging systems, Leiden, Netherlands). Individual scans were anonymised and analysed by the author who was blinded to the identity and haemodynamic results of any given subject at the time of analysis. RV and LV volumes, mass and function were determined by manual planimetry as described in the methodology chapter 2.6.2.

#### **4.2.5 Strain**

LA myocardial feature tracking was performed using dedicated software (Qstrain, Medis medical imaging systems, Leiden, Netherlands). LA endocardial borders were manually traced using the 2-chamber and 4-chamber views using a point and click approach when the LA was at its minimum volume after atrial contraction. The atrial endocardial border surface was manually delineated and the automated tracking algorithm was applied. Subsequently this was visually reviewed to ensure accurate tracking of the LA. (Figure 2-3 and Figure 2-4) In case of insufficient automated border tracking, manual adjustments were made to the initial contour and the algorithm was reapplied. If the tracking quality was not sufficient, e.g. due to the presence of pulmonary veins or left atrial appendage, the corresponding segment was excluded from the analysis. Tracking was repeated for three times in both the 2- and 4-chamber view. LA longitudinal strain and SR results were averaged across all three repetitions in both views. Three aspects of atrial function / strain were analysed.

1.  $\epsilon_s$ , Reservoir function. (Total strain)
2.  $\epsilon_e$ , Conduit function (Passive strain)
3.  $\epsilon_a$ , Booster pump function (Active strain)

Accordingly, three strain rate parameters were evaluated.

1. Peak positive strain rate (SRs, corresponding to atrial reservoir function),
2. Peak early negative strain rate (SRe, corresponding to atrial conduit function)
3. Peak late negative strain rate (SRa, corresponding to atrial contractile booster pump function)

These strain rate and strain rate measurements are shown in figure 4-1.

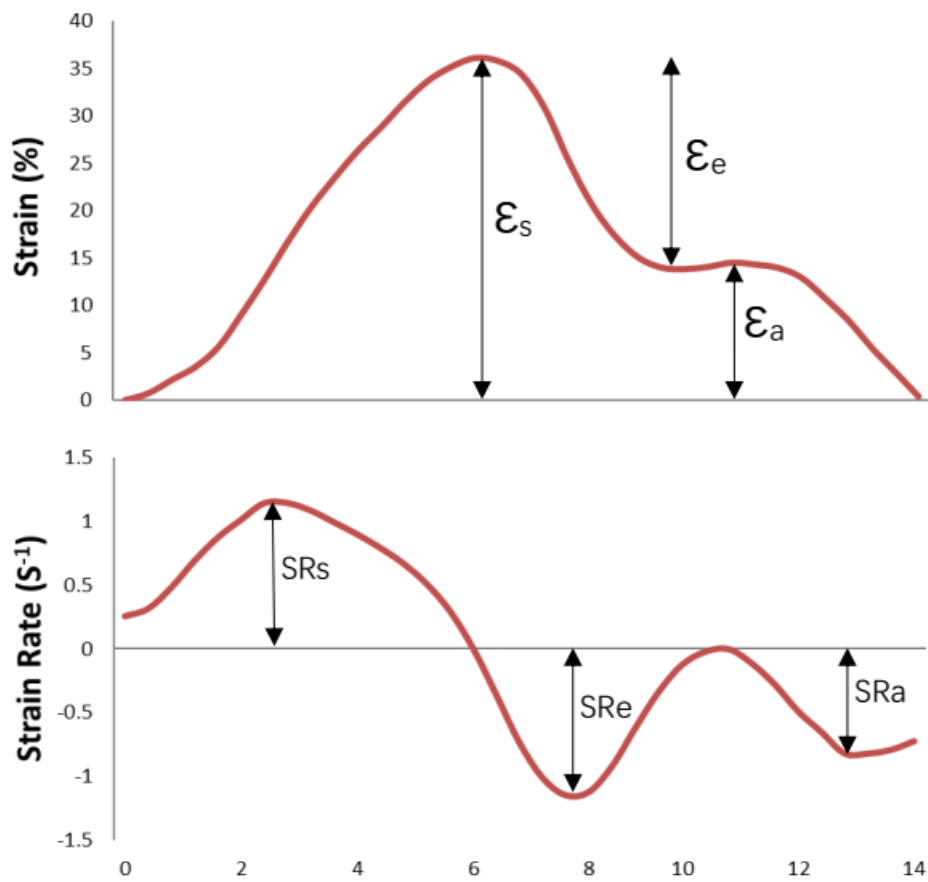


**Figure 4-1 Left atrial function comprises reservoir, conduit and contractile booster pump function.**

Total strain ( $\epsilon_s$ ) and peak positive strain rate ( $SR_s$ ) correspond to reservoir function. Passive strain ( $\epsilon_e$ ) and peak early negative strain rate ( $SRe$ ) correspond to conduit function. Active strain ( $\epsilon_a$ ) and peak late negative strain rate ( $SR_a$ ) correspond to contractile booster pump function.

#### **4.2.6 Statistical Analysis**

Continuous variables are summarised as mean  $\pm$  SD, median (interquartile range) depending on their distribution. Categorical variables are summarised as n (%). Normality of groups was assessed using a Shapiro-Wilk test. IPAH and healthy volunteer groups were compared using student t-tests, Mann-Whitney U tests and Fisher's exact tests, where appropriate. Spearman correlation coefficients are used to assess association between continuous variables. A p-value of greater than 0.05 indicated a lack of statistical significance. Statistical analysis was performed using SPSS (IBM SPSS Statistics) and Graphpad Prism (Graphpad Software inc).

## 4.3 Results

### 4.3.1 Demographics

Eighty-six patients were included in the analysis which included 56 patients with IPAH and 30 healthy volunteers. There was no significant difference between the IPAH and the healthy volunteer groups in terms of gender, age, or weight. Demographics of the study population are given in table 4.1.

**Table 4.1 Demographics of the study population**

	All	IPAH	Healthy volunteer	p value
n	86	56	30	
Gender (Female)	46	31	15	0.5429
Age	58 (46,70)	62 (47,70)	50 (43,62)	0.0658
BSA	1.65 +/-0.9	1.63 +/- 0.8	1.69 +/- 0.9	0.0007

There was no significant difference between the IPAH and the healthy volunteer groups in terms of gender, age, or weight. Continuous variables are summarised as mean  $\pm$  SD, median (interquartile range) depending on their distribution. Categorical variables are summarised as n (%). Normality of groups was assessed using a Shapiro-wilk test. PH and healthy volunteer groups were compared using student T tests, Mann-Whitney U tests and Fisher's exact tests, where appropriate. A p-value of greater than 0.05 indicated a lack of statistical significance.

### 4.3.2 CMR variables and baseline haemodynamic characteristics of IPAH patients

There were no significant differences between the patient group and healthy volunteers in terms of LV function measured by LV ejection fraction (LVEF) (67.0% vs 63.8% p= 0.3890). The RV function measured by RV ejection fraction (RVEF) was lower in the IPAH group as expected (34.7% vs 63.8% p<0.0001). There were significant differences in not only the right sided volume variables and VMI but also in the left sided volume variables (all p<0.0001). The baseline CMR characteristics of the IPAH and healthy volunteer groups are summarised in table 4.2.

**Table 4.2 The baseline CMR characteristics of the IPAH and healthy volunteer group**

	ALL	IPAH	Healthy	p value
LVEF	66.1(60.4,71.5)	67.0(59.7,72.3)	63.8(61.3,67.5)	0.3890
RVEF	45.0(32.8,56.1)	34.7(28.0,45.1)	63.8(61.3,67.5)	<0.0001
LVEDVI	63.6 (48.9,77.5)	50.8(46.7,64.0)	78.4(75.0,90.6)	<0.0001
LVESVI	22.4(14.8,28.2)	18.2(12.4,23.3)	27.8(24.8,33.8)	<0.0001
RVEDVI	97.4(86.5,116.4)	106.5(90.1,129.7)	88.2(77.2,96.9)	<0.0001
RVESVI	50.4(38.1,75.1)	70.2(50.1,89.3)	37.4(31.5,44.5)	<0.0001
LV Mass index	50.0(43.0,58.1)	49.4(42.4,56.2)	55.0(45.6,61.3)	0.1022
RV Mass index	23.1(13.7,31.3)	30.6(23.4,35.2)	12.7(11.1,14.8)	<0.0001
VMI	0.5(0.3,0.6)	0.6(0.5,0.7)	0.3(0.2,0.3)	<0.0001

There were no significant differences between the patient group and healthy volunteers in terms of LV function measured by LV ejection fraction (LVEF) (67 vs 63.8 p=0.3890). The RV function measured by RV ejection fraction (RVEF) was lower in the IPAH group (34.7 vs 63.8 p<0.0001). Results are shown as median (interquartile range). IPAH and healthy volunteer groups were compared using Mann-Whitney U test. A p-value of greater than 0.05 indicated a lack of statistical significance. LVEDVI – LV end-diastolic volume index, LVESVI – LV end-systolic volume index, RVEDVI – RV end-diastolic volume index, RVESVI – RV end-systolic volume index, VMI – ventricular mass index

The baseline characteristics of the IPAH group are summarised in Table 4.3. The patients had a mPAP of 51 (43,59) mmHg. As mentioned in the previous chapter of note again is the low PAWP of 8 (3,9) mmHg in the patient group ensuring that patients with intrinsic left heart disease are excluded.

**Table 4.3 The baseline characteristics of the IPAH group**

<b>Variable</b>	<b>Median (interquartile range)</b>
LogNTproBNP	3.1 (2.7,3.5)
DLCO (%)	35 (26,57)
6-minute walk distance	245 (140,365)
TAPSE	1.3 (1.45,1.88)
Right atrial pressure	7 (4,10)
Mean pulmonary artery pressure	51 (43,59)
Pulmonary artery wedge pressure	8 (3,9)
Cardiac output	3.7 (3,4.3)
Cardiac index	2 (1.5,2.4)
Stroke volume index	27.6 (20.5,30.9)
Pulmonary vascular resistance	12.1 (8.3,16.5)
Mixed venous saturations	64 (56,69)
Heart rate	75 (66,85)
Systolic blood pressure	129 (113,148)

The patients had a mPAP of 51 (43,59) mmHg and low PAWP 8 (3,9) mmHg. Continuous variables are summarised as median (interquartile range) due to their distribution. LogNTproBNP- N Terminal pro Brain Natriuretic Peptide, DLCO% - diffusion capacity, TAPSE – Tricuspid Annular Plane Systolic Extraction by Echocardiography.

### 4.3.3 Healthy volunteer vs IPAH: left atrial strain and strain rate

#### 4.3.3.1 Left atrial strain

Left atrial strain indices of  $\epsilon_s$  (23.6 vs 32.8  $p < 0.0001$ ) and  $\epsilon_e$  (6.1 vs 18.2  $p < 0.0001$ ) corresponding to atrial reservoir function and conduit function respectively were impaired in IPAH patients compared to healthy volunteers. There was no significant difference in LA  $\epsilon_a$  corresponding to booster pump function, however active strain was higher in IPAH patients compared to healthy volunteers (17.3 vs 13.9). The results are summarised in table 4.4.

**Table 4.4 Healthy volunteer vs IPAH Left atrial strain**

Strain parameter	IPAH	Healthy volunteer	p value
$\epsilon_s$	23.6 (16.3,29.5)	32.8 (28.8,42.6)	<0.0001
$\epsilon_e$	6.1 (3.4, 10.4)	18.2(14.9,24.9)	<0.0001
$\epsilon_a$	17.3 (11.7, 21.2)	13.9 (12.1,19.1)	0.4692

Left atrial  $\epsilon_s$  corresponding to reservoir function (23.6 vs 32.8  $p < 0.0001$ ) and  $\epsilon_e$  corresponding to conduit function (6.1 vs 18.2  $p < 0.0001$ ) was significantly lower in IPAH patients. Although  $\epsilon_a$  wasn't different between the two groups, was higher in IPAH patients (17.3 vs 13.9  $p = 0.4692$ ). Results are shown as median (interquartile range). IPAH and healthy volunteer groups were compared using Mann-Whitney U test. A p-value of greater than 0.05 indicated a lack of statistical significance.  $\epsilon_s$  = total strain corresponding to reservoir function,  $\epsilon_e$  = passive strain corresponding to conduit function and  $\epsilon_a$  = active strain corresponding to booster pump function of the left atrium.

#### 4.3.3.2 Left atrial strain rate

SRe (corresponding to conduit function) was significantly lower in IPAH patients compared to healthy volunteers (-0.39 vs -1.0  $p < 0.0001$ ). However, there were no significant differences between the IPAH and healthy volunteer group in SRs or SRa. Results are summarised in table 4.5.

**Table 4.5 Healthy volunteer vs IPAH Left atrial strain rate**

Strain rate	IPAH	Healthy volunteer	p value
SRs	0.99 (0.75,1.31)	1.05 (0.94,1.21)	0.4918
SRe	-0.39 (-0.57,-0.25)	-1.0 (-1.2,-0.79)	<0.0001
SRa	-1.08 (-1.38,-0.72)	-0.97 (-1.24,-0.69)	0.3539

SRe or peak early negative strain rate (corresponding to conduit function) was significantly lower in IPAH patients compared to healthy volunteers (-0.39 vs -1.0  $p < 0.0001$ ). Results are shown as median (interquartile range). IPAH and healthy volunteer groups were compared using Mann-Whitney U test. A p-value of greater than 0.05 indicated a lack of statistical significance. SRs = peak positive strain rate corresponding to reservoir function, SRe = peak early negative strain rate corresponding to conduit function and SRa = peak late negative strain rate corresponding to booster pump function of the left atrium.

#### 4.3.3.3 Severe vs Intermediate / Mild disease

Patients were categorised based on cardiac index derived by right heart catheterisation. Patients with more severe disease (cardiac index  $< 2$ ) demonstrated impairment of  $\epsilon$ e (5.4 vs 7.6  $P=0.0473$ ) and SRe (-0.3 vs -0.47  $p=0.024$ ) compared to patients with less severe disease. Patients with severe disease had augmented SRa (-1.3 vs -1.00  $p=0.0459$ ). Results are summarised in table 4.6.

**Table 4.6 Left atrial strain and strain rate measurements in IPAH patients with severe vs intermediate / mild disease.**

Strain parameter	Severe disease	Intermediate and mild disease	p value
$\epsilon_s$	23.6 (15.8,29.6)	23.3 (17.1,28.4)	0.7701
$\epsilon_e$	5.4 (2.2,7.8)	7.6 (4.5,11.7)	0.0473
$\epsilon_a$	19.6 (12.0,23.5)	14.6 (11.2,20.1)	0.1371
SRs	1.1 (0.75,1.50)	0.93 (0.73,1.22)	0.2131
SRe	-0.3 (-0.50,-0.17)	-0.47 (-0.67,-0.32)	0.0240
SRa	-1.3 (-1.54,-0.80)	-1.00 (-1.24,-0.65)	0.0459

Patients with more severe disease demonstrated impairment of  $\epsilon_e$  (5.4 vs 7.6 P=0.0473) and SRe (-0.3 vs -0.47 p=0.0240) compared to patients with less severe disease. Patients with severe disease had augmented SRa (-1.3 vs -1.00 p=0.0459). Disease severity was classified by cardiac index derived from right heart catheterisation (cardiac index < 2). Results are shown as mean median (interquartile range). The two groups were compared using Mann Whitney U test. A p value greater than 0.05 demonstrated a lack of statistical significance.  $\epsilon_s$  = total strain,  $\epsilon_e$  = passive strain and  $\epsilon_a$  = active strain, SRs = peak positive strain rate, SRe = peak early negative strain rate, SRa = peak late negative strain rate.

#### 4.3.4 Association with markers of disease severity

Left atrial  $\epsilon_e$  demonstrated strongest correlations with known markers of disease severity including, RVEF ( $r=0.41$   $p=0.0017$ ) and logNTproBNP ( $r=0.38$   $p=0.0071$ ) and significant but weaker correlations with right heart catheter derived stroke volume index. Similarly, SRe demonstrated significant correlations with LogNTproBNP ( $r=0.54$   $p<0.0001$ ), CO ( $r=-0.41$   $p<0.002$ ) and RVEF ( $r=0.35$   $p<0.008$ ). There were no significant correlations with  $\epsilon_s$  or  $\epsilon_a$  with known markers of disease severity. The results are shown in Table 4.7.

**Table 4.7 Left atrial strain and association with markers of disease severity in IPAH patients**

	$\epsilon_s$	$\epsilon_e$	$\epsilon_a$	SRs	SRe	SRa
LVEF	0.14	0.02	0.11	-0.05	-0.04	-0.2
RVEF	0.2	0.41**	-0.04	-0.1	-0.35**	0.15
LVEDVI	0.01	0.28*	-0.17	-0.14	-0.19	0.31*
LVESVI	-0.07	0.14	-0.14	-0.04	-0.07	0.28
RVEDVI	-0.25	-0.21	-0.13	-0.1	0.28*	0.08
RVESVI	-0.24	-0.31*	-0.06	0.01	0.32*	-0.03
mPAP	-0.28	-0.06	-0.27*	-0.18	-0.04	0.03
CO	-0.02	0.26	-0.2	-0.01	-0.41**	0.24
SVI	0.06	0.37**	-0.16	-0.18	-0.26	0.23
LogNTproBNP	-0.09	0.38**	0.09	-0.02	0.54***	-0.15

Left atrial  $\epsilon_e$  demonstrated strongest correlations with RVEF ( $r=0.64$   $p<0.0001$ ), LVEDVI ( $r=0.41$   $p=0.0017$ ) and logNTproBNP ( $r=0.38$   $p=0.0071$ ) and significant but weaker correlations with right heart catheter derived stroke volume index. Similarly, SRe demonstrated significant correlations with LogNTproBNP ( $r=0.54$   $p<0.0001$ ), CO ( $r=-0.41$   $p<0.002$ ) and RVEF ( $r=0.35$   $p<0.008$ ). There were no significant correlations with  $\epsilon_s$  or  $\epsilon_a$  with known markers of disease severity. Spearman correlations were used to assess association between continuous variables as appropriate. LVEF – LV ejection fraction, RVEF – RV ejection fraction, LVEDVI - LV End-diastolic volume index, LVESVI – LV End-systolic volume index, RVESVI – RV end-systolic volume index, mPAP – mean pulmonary artery pressure, CO – Cardiac output, SVI – Stroke volume index.

## 4.4 Discussion

To best of our knowledge this is the first CMR study of LA function in patients with pulmonary arterial hypertension.

This study demonstrates that the LA function is impaired in patients with PAH compared to healthy volunteers. Among the strain indices, conduit function was the most affected. Conduit function is the passage of blood to the LV during early diastole and is dependent on atrial compliance and related to atrial reservoir function but is also affected by LV relaxation. We also noted that in patients with more severe disease LV conduit function (and corresponding peak early negative strain rate) was affected compared to IPAH patients with less severe disease.

To explain these findings, it is important to reiterate the significant interplay that exist between the LA and the LV and also the direct and series interaction of the RV to LV. Under normal conditions the impact of the RV on LV function is negligible. However ventricular independency plays an important role in the pressure loaded RV in PH. Ventricular interdependency can be affected both by parallel and series interaction. Leftward septal bowing hampers filling of the LV due to parallel interaction. Lowered RV stroke volume causes a decrease in LV filling due to series interaction (149).

Evidence that inter-ventricular dyssynchrony might play a role in PAH is known. This is evidenced on an Electrocardiogram showing a complete or incomplete Right Bundle Branch Block (RBBB) pattern. *Stojnic et al* demonstrated a reduction in early diastolic filling of the LV in PH secondary to congenital cardiac disease (201). They also demonstrated a prolonged pressure decline in the RV compared to the LV. They concluded that early diastolic LV filling impairment is mediated by the deformation of the IVS towards the LV cavity in early LV diastole. The significantly reduced LA conduit function is likely to be related to impaired early LV relaxation. This study also demonstrated, albeit to a lesser extent, impaired LA reservoir function in IPAH patients compared to healthy volunteers. This is likely to reflect the increased RV afterload and the resultant reduced RV stroke volume. On further assessment of patients with severe disease vs intermediate or mild disease, LA conduit function was significantly different between the two groups, while LA reservoir function was not. Strain rate indices followed a similar pattern

demonstrating LA peak early negative strain rate, relating to LA conduit function to be the most significantly impaired.

Interestingly although not statistically significant, LA booster pump function was augmented in IPAH patients. As LVEF is preserved, LV filling is maintained by increased LA booster pump function in these patients. As discussed earlier in this chapter patients with HCM demonstrated a similar increase in LA booster pump function and a reduced reservoir and conduit function. The authors in that study hypothesised that this may be a compensatory change that is likely to be followed by a progressive decrease in global LA performance.

In PAH patients, series and parallel interaction occur concomitantly causing impairment of LV - LA mechanics. Although similar to previous studies focusing on LV, our results cannot confirm the dominant mechanism between these two, however from the results of our study we can conclude and hypothesise the following.

1. This study demonstrates that the most significantly affected LA index is LA conduit function. LA conduit function is related to atrial compliance, however significantly affected by early LV relaxation / LV compliance. Considering atrial compliance is unlikely to be affected in the absence of left heart disease, impaired LA conduit function is likely related to LV relaxation. Early LV relaxation is affected by paradoxical septal motion of the RV during systole and prolonged RV contraction.
2. LA conduit function, representing passive movement of blood during early diastole and not the LA reservoir function had the significant association with known markers of disease severity. LA conduit function was also the index that was significantly affected in the severe disease population compared to mild disease.
3. The lack of early LV filling is to a degree compensated by LA booster pump function which is augmented in IPAH patients compared to healthy volunteers although did not reach a statistical significance. Whether this compensatory change is likely to be followed by a progressive decrease in global LA performance with disease progression is unknown.

Both pharmaceutical agents and mechanical resynchronisation therapy may improve inter-ventricular dyssynchrony. Whether these interventions that will improve left heart mechanics will improve the disease trajectory in PH patients is not completely explored (10).

*Lumens et al* developed a computer simulation of severe PAH and showed improvements in cardiac pump function with simulated RV free wall pacing (152). *Hardziyenka et al* performed a study that included 14 patients with CTEPH who had diastolic inter-ventricular delay as assessed by tissue Doppler echocardiography. Temporary sequential RA-RV pacing at the RV apex at the optimal atrioventricular interval resulted in an increase in LV outflow tract velocity time integral, a reduction in diastolic inter-ventricular delay, reduced RV end-systolic area, increased LV end-diastolic area, and significant improvements in RV global and longitudinal contractility and LV longitudinal contractility (151). It is not yet known whether similar improvements would be seen in other forms of PH, or whether acutely improved haemodynamics and LA-LV mechanics would be maintained and translate to improved clinical outcomes in the long term.

## 4.5 Conclusion

This study demonstrates that the left atrial function is impaired in patients with idiopathic pulmonary arterial hypertension compared to healthy volunteers. Among the strain indices conduit function was the most affected. Conduit function is the passage of blood to the LV during early diastole and is dependent on atrial compliance but is also affected by early LV relaxation. Parallel interaction from a prolonged RV contraction causing impaired early LV relaxation is the likely dominant mechanism in the absence of intrinsic left heart disease in this patient population. The lack of early LV filling is to a degree compensated by LA booster pump function which is augmented in IPAH patients compared to healthy volunteers. Further research is needed to explore the impact of pre-existing medical therapy and mechanical resynchronisation therapy on LV - LA mechanics. It is not yet known whether similar improvements would be seen in other forms of pulmonary hypertension, or whether acutely improved haemodynamics would be maintained and translate to improved clinical outcomes in the long term.

## 4.6 Limitations

There are several limitations to our study. This was a single centre retrospective observational study. There were patients who were diagnosed with IPAH who were not included in the study if they did not undergo CMR imaging. This may exclude patients with more severe disease who probably did not manage MR due to severe breathlessness (breath holding difficulties) and may also exclude patients with mild disease who may not be diagnosed till they show significant symptoms. CMR feature tracking can be affected by through plane motion artefacts and also is limited by pixel size (175, 193). Previous feature tracking strain studies have demonstrated significant variability of strain values, mainly due to the lack of standardization in signal acquisition and image processing(177). We also didn't study inter-observer reproducibility of left atrial indices.

**Chapter 5 Non-invasive measurement of myocardial damage in pulmonary hypertension using Native T1 mapping from CMR: a novel segmentation technique and association with haemodynamic variables.**

## 5.1 Introduction

The differences in LV strain and the presence of LV intra-ventricular dyssynchrony in IPAH patients compared to healthy volunteers were discussed in Chapter 3. This was despite the conventional measure of LV function i.e. LVEF being preserved. Furthermore, IPAH patients with more severe disease demonstrated worse LV strain and LV dyssynchrony when compared to patients with less severe disease. Interestingly, LV mechanics were associated with known markers of disease severity and predicted survival in patients with IPAH and these LV variables were probably superior to known RV CMR variables in terms of their ability to reflect disease severity and predict survival.

Many CMR measures have shown to be strongly predictive of mortality and survival thus offering potential for monitoring and determining response to treatment in PH. Stroke volume, RVEF and RVEDVI are recognised as the key MR prognostic measures in PAH patients (91, 94). In a multicentre study prospectively using CMR before and during PAH disease specific treatment, *Peacock et al* demonstrated the importance of including both left sided and right sided variables when determining cardiac function (99). *Swift et al* demonstrated that CMR measurements reflecting RV structure and stiffness of the proximal pulmonary vasculature to be independent predictors of outcome in PAH (97).

The advantage of CMR is the ability to achieve high resolution 3D imaging of the heart without using radiation. Recently, there have been significant focus on non-invasive myocardial tissue characterisation. Longitudinal relaxation time (T1) and transverse relaxation time (T2) are central properties of tissue which is determined by its molecular make up. T1 relaxation time is defined as the time when longitudinal proton magnetization recovers 63% of its equilibrium value (169). Late gadolinium enhancement has been the gold standard for determination of myocardial fibrosis. This is based on the difference in distribution of contrast between normal and fibrotic myocardium. The areas of fibrosis demonstrated a shorter T1 time than adjacent normal tissue. Conventionally this method is performed using inversion recovery gradient-echo sequences 10-15 minutes after gadolinium injection. Retention of contrast within the extracellular space results in shortening of the inversion time (T1) and hyper enhancement relative to normal myocardium. The main limiting factor when using LGE is that fibrotic process is

often a diffuse process thus lacking the normal non-fibrotic myocardium for reference. To ameliorate this issue, T1 mapping has been developed to quantify diffuse, non-ischemic myocardial fibrosis, as it does not rely on contrasting signal intensity.

*Blyth et al* used contrast enhanced CMR imaging to determine the presence of LGE in PH. They hypothesised that myocardial abnormalities may exist in patients with PH, that they could be identified by contrast enhanced CMR imaging and that the severity of the contrast enhancement would relate to the severity of PH. LGE was present in almost all patients with PH and the extent of contrast enhancement was associated with RV volumes, RV function as well as mPAP derived at right heart catheterisation. The authors also found LGE to be associated with bowing of the interventricular septum and concluded that this may provide a novel marker for occult septal abnormalities directly relating to the haemodynamic stress experienced by these patients (133). *McCann et al* found similar results with the extent of LGE related to RV function and RV stroke volume. In two other patients who had post mortem histological analysis of the RV insertion regions, myocardial fibrosis was present suggesting this may be the causal mechanism, however there was also evidence of interstitial space expansion and a small increase in fat which may have contributed to late gadolinium enhancement. In a study by *Freed et al*, patients with RV insertion point LGE had larger RV volume index, lower RVEF and higher mPAP and LGE was a predictor for adverse outcomes ( $p=0.026$ ) in this population (134). In a study by *Shehata et al*, LGE at RV insertion points were observed in almost all patients with PH and LGE was associated with pulmonary haemodynamics, reduced RV function and reduced eccentricity index (127). Reduced longitudinal strain of the basal anterior septal insertion point was independently associated with LGE although the same was not observed for the posterior insertion point. The authors suggested that the two insertion regions may behave differently as they are part of anatomically and functionally distinct regions i.e. RV outflow and inflow tracts.

There have been numerous T1 based techniques for quantification of fibrosis. The modified Look Locker inversion recovery (MOLLI) technique was designed to overcome the limitations of motion and prolonged acquisition time (136). Specifics included an ability to acquire data within one breath-hold at a designated time

within the cardiac cycle and the capability of merging images from multiple Look Locker experiments at different consecutive inversion times into one data set. MOLLI sequencing employs a balanced steady-state free precession (SSFP) readout to achieve a higher signal to noise ratio with a narrow image acquisition period of less than 200 ms in end-diastole to minimize motion artefact. In a later study *Messroghli et al* demonstrated high reproducibility of this technique (137). *Piechnik et al* shortened MOLLI sequence (ShMOLLI) that generated immediate, high-resolution myocardial T1-maps in a short breath-hold with high precision. Other prototype vendor specific sequences have been developed including a modified Look-Locker FIESTA technique using saturation-recovery imaging, saturation-recovery single shot acquisition (SASHA), and saturation pulse prepared heart-rate-independent inversion recovery, which consists of a combination of saturation and inversion pulses (131).

Typically, a series of short axis images are acquired pre contrast and approximately 12 minutes' post gadolinium contrast with between 6 and 12 consecutively longer inversion times depending on the protocol. Image acquisition is usually performed with ECG gating with breath holding at end-inspiration. Offline, standard basal, mid-ventricular and/or apical slices are then selected and can be further divided into conventional myocardial segments (or discrete regions of interest) and blood-pool for analysis if desired. A curve fitting technique is employed to reconstruct the consecutively acquired images into one data set from which a T1 map of voxels is generated.

The signal intensity of each voxel directly represents the T1 relaxation time of the corresponding myocardial tissue. An exponential recovery curve of signal intensities at the different inversion times is then created for each designated region of interest (slice or segment) to determine the myocardial T1 relaxation time. These can be averaged to extrapolate T1 as an index of diffuse fibrosis, where shorter T1 time and higher signal intensity correspond to increased gadolinium contrast accumulation within the extra cellular matrix. Standardization of myocardial T1 values to non-myocardial tissue (blood) assists in minimizing the dynamic features of gadolinium contrast. The ratio of myocardial to blood post-contrast T1 values is expressed as the partition coefficient. By preceding post-contrast T1 mapping with pre-contrast T1 mapping,

myocardial extra-cellular volume (ECV) can similarly be derived (131, 169). This pseudo-equilibrium technique employs the reciprocals of myocardial and blood T1 values pre-contrast and post-contrast and then adjusts for haematocrit to correct for the blood contrast volume of distribution. This ECV is expressed as a percentage of the total myocardial extracellular space. Gadolinium equilibrium between blood and myocardium must be achieved prior to image acquisition to enable accurate estimation of ECV.

Native T1 mapping has the potential to identify both focal and diffuse myocardial fibrosis without the need for contrast administration and reflects myocardial disease involving the myocyte and interstitium.

In a study by *Sprujit et al*, myocardium in IPAH, connective tissue disease associated PH and CTEPH patients were characterised using native T1 mapping. Native T1 values were determined using regions of interest in the RV and LV free wall, RV insertion points and the IVS. In PH patients, native T1-values of the interventricular insertion regions were significantly higher than the native T1-values of the RV free wall, LV free wall and IVS and related to disease severity (138). *Saunders et al* also used regions of interest in the IVS, LV free wall and RV insertion points during T1 mapping assessment. Elevated myocardial native T1 was found to a similar extent in PH patient subgroups and was independently associated with IVS angle. The authors did not find an additive value of native T1 mapping in the diagnostic and prognostic evaluation of PH patients(139). In a study by *Reiter et al*, 58 patients with suspected PH were studied with right heart catheterisation and CMR imaging (132). LV global, segmental and ventricular insertion point (VIP) T1 times were evaluated manually and corrected for blood T1. The American Heart Association (AHA) LV segmentation technique was used to segment the LV myocardium including RV insertion points. Septal, lateral and global VIP T1 times were significantly higher in PH than in non-PH subjects. LV eccentricity strongly correlated with VIP T1 time, which in turn was strongly associated with T1 times in the entire LV myocardium. Although identification of raised native T1 times has been used to identify myocardial histological changes, success has been limited due to

1. The need for visual assessment of the insertion points (*Sprujit et al*) or,

2. The existing AHA segmentation of the LV fails to isolate the regions of RV insertion for analysis (*Reiter et al*)

The aims of our study were twofold: firstly, to avoid the use of contrast agent and, secondly to develop a novel method of myocardial segmentation during T1 mapping, which isolated the regions of RV insertion points without requiring visual assessment. We hypothesised that the regional T1 values would identify myocardial abnormalities which relate to markers of disease severity and prognosis. Because this technique is non-invasive, we would then be able to use it in longitudinal studies. A validation cohort was also studied where ECV fraction following Gadolinium was used to dichotomise the T1 changes to cellular and interstitial changes. We hoped that this would provide insight into the pathophysiological processes underlying RV failure in PH.

## 5.2 Methods

### 5.2.1 Patient recruitment

We identified 130 treatment-naïve patients referred to the Scottish Pulmonary Vascular Unit between December 2014 and December 2016. As mentioned in the methods chapter, during the diagnostic admission patients underwent multidisciplinary evaluation based on right heart catheterisation, echocardiography, pulmonary function testing and CT scan of thorax. All patients underwent invasive haemodynamic measurements and CMR within 72 hours, gave informed consent to undergo these procedures and the study was reviewed by the local ethics reviewed committee.

Five patients were excluded from the study due to previous myocardial infarction (which will have an impact on segmental T1 values) and four were excluded as a result of poor image quality of the cine images or/and the T1 maps. Of the remainder (121), 20 without PH (defined as mPAP < 25 mm Hg during right heart catheterisation) were used as controls and were included to provide reference values for T1 mapping. A second group (the Validation cohort) of 7 patients with known PAH on established treatment underwent CMR imaging with gadolinium contrast administration for the validation phase of the study. These subjects did not undergo right heart catheterisation. The study design is summarised in Figure 5-1.

The Subjects in the treatment naïve cohort were further categorised into WHO groups of PH. Idiopathic pulmonary arterial hypertension (IPAH), connective tissue disease, congenital heart disease (all group 1), left sided heart disease (group 2), hypoxic lung disease (group 3), chronic thromboembolic disease (group 4) and miscellaneous causes (group 5).

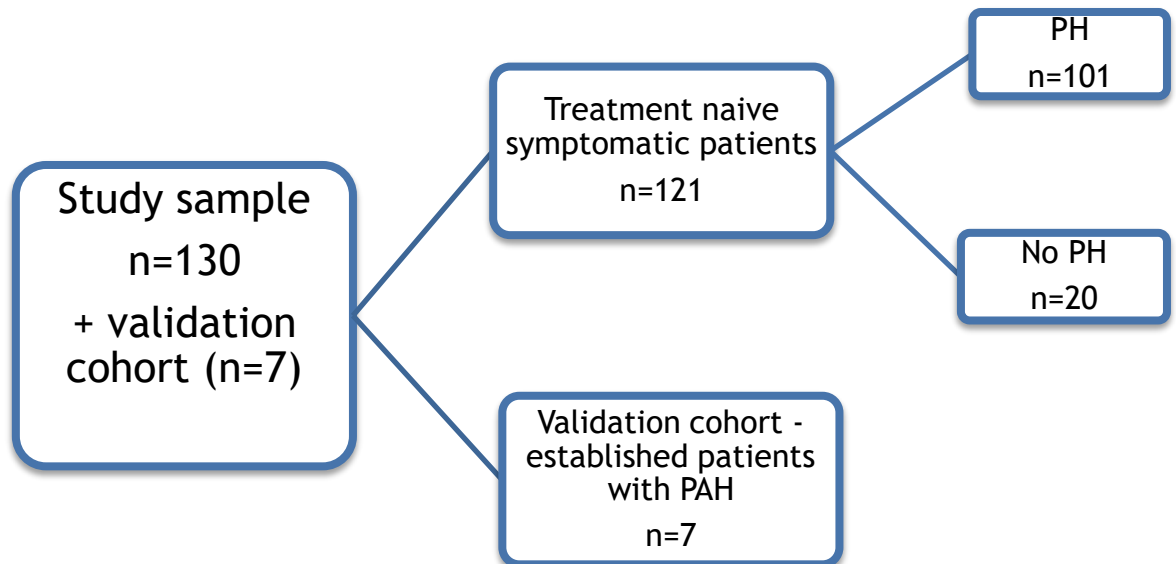


**Figure 5-1 The study design.**

We identified 130 treatment-naïve patients referred to the Scottish Pulmonary Vascular Unit between December 2014 and December 2016. All patients underwent invasive haemodynamic measurements and CMR within 72 hours. Five patients were excluded from the study due to previous myocardial infarction and four were excluded as a result of poor image quality of the cine images or/and the T1 maps. Of the remainder (121), 20 without pulmonary hypertension (defined as mPAP < 25 mm Hg during right heart catheterisation) were used as controls and were included to provide reference values for T1 mapping. A second group (the Validation cohort) of 7 patients with known PAH on established treatment underwent CMR imaging with gadolinium contrast administration for the validation phase of the study. These subjects did not undergo right heart catheterisation.

### 5.2.2 CMR imaging

CMR imaging was performed in the supine position on a 1.5T MRI scanner (Avanto, Siemens, Erlangen, Germany). T1 maps were acquired using a MOLLI (Modified Look-Locker Inversion Recovery) sequence on a mid-ventricular short axis plane with a trigger delay to coincide with systole.

As mentioned above, previous studies involving patients with PH has used the traditional AHA segmentation or visual analysis. However, this existing AHA segmentation of the LV fails to isolate the RV insertion regions for analysis. Figure 5-1-A demonstrates the traditional AHA segmentation in a patient with PAH. The RV insertion regions with raised native T1 falls between segments making it difficult to identify, quantify and also to monitor longitudinal myocardial changes. Thus, a novel segmentation which isolate these regions is required specifically for the assessment of PAH patients.

The LV was segmented using a novel modified AHA segmentation carefully excluding blood pool, papillary muscles and trabeculae. S6 was drawn with the inferior RV insertion point at its centre and S4 and S6 were defined as RV insertion regions (Figure 5-2-B).

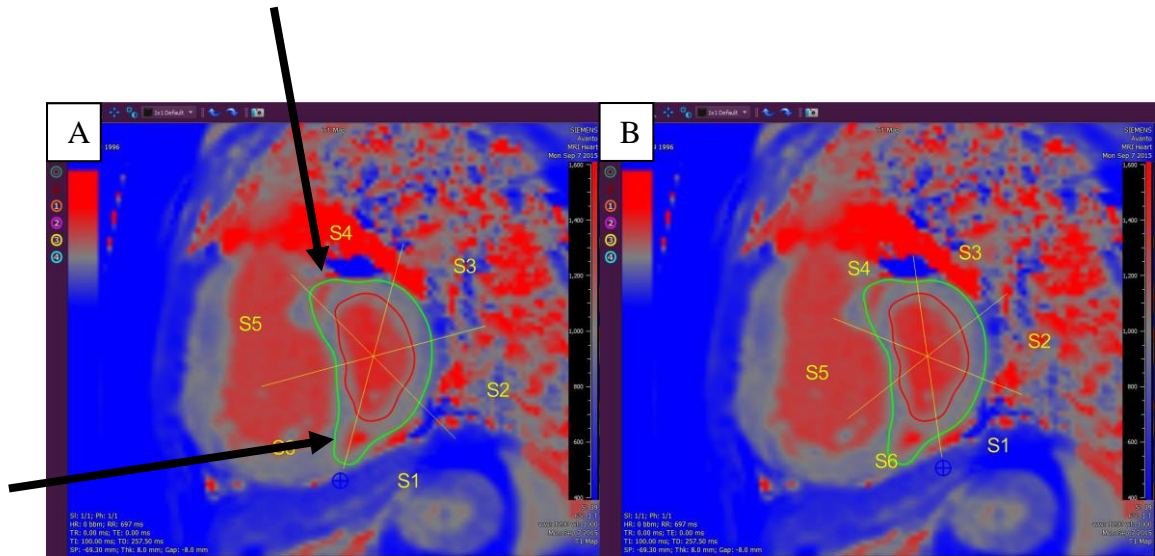


**Figure 5-2 CMR mid ventricular T1 map of a patient with pulmonary arterial hypertension**

The figure demonstrates raised native T1 at RV insertion points (arrows). The image A) uses traditional AHA segmentation. The attachment of the RV wall to the LV (RV insertion points) is used to identify and separate the septum from the LV anterior and inferior free walls during the traditional AHA segmentation. Image B) demonstrates the novel segmentation proposed which encompasses the two insertion points into segments S4 and S6. T1 maps were generated from the individual motion corrected T1 relaxation images. The LV was segmented using our modified AHA technique carefully excluding blood pool, papillary muscles and trabeculae. Segment 6 was drawn with the inferior RV insertion point at its centre. Segment 4 and Segment 6 were defined as anterior and inferior RV insertion segments respectively. Segments 1, 2 and 3 represented the LV lateral wall.

In the validation cohort, subjects underwent native and post contrast T1 mapping. Extracellular volume fraction (ECV) values were calculated from T1 maps acquired pre and post contrast calibrated by blood haematocrit. ECV value was calculated as  $ECV = (1 - \text{hematocrit}) \left( \frac{1}{T1_{\text{myocardium post contrast}}} - \frac{1}{T1_{\text{myocardium pre contrast}}} \right) \left( \frac{1}{T1_{\text{blood post contrast}}} - \frac{1}{T1_{\text{blood pre contrast}}} \right)$ .

### **5.2.3 Right heart catheterisation**

Right heart catheterisation was performed during free breathing in the supine position with a 7 F quadruple lumen, flow directed balloon tipped Swan - Ganz catheter using the internal jugular approach. The method and the measurements taken during right heart catheterisation is described in detail in the Methods section 2.5.

### **5.2.4 CMR imaging analysis**

All CMR images were analysed by the author using the Medis suite analysis software (Medis medical imaging systems, Leiden, Netherlands). A second observer (D.B) analysed twenty T1 mapping scans for inter-rater agreement. Individual scans were coded by number and analysed in batches by the author who was blinded to the identity and haemodynamic results of any given subject at the time of analysis. RV and LV volumes were determined by manual planimetry of selected short axis images, as described previously (166, 167). Particular methodological points of note included the deliberate inclusion of trabeculations and papillary muscles in all analyses, as discussed by previous authors (167). RV and LV volumes, RVEF and LVEF, and RV and LV mass were determined as previously described in the Methods section. RV mass was determined as RV free wall mass, the IVS was considered part of the LV. Ventricular Mass index (VMI) was determined as  $RV \text{ Mass} / LV \text{ Mass}$ . For correlation analyses, RV and LV volumes were indexed to BSA.

### **5.2.5 T1 mapping analysis**

T1 maps were generated from the individual motion corrected T1 relaxation images using Qmap (Medis medical imaging systems, Leiden, Netherlands). The LV was segmented using our modified AHA technique carefully excluding blood pool,

papillary muscles and trabeculae. Segment 6 was drawn with the inferior RV insertion point at its centre. Segment 4 and Segment 6 were defined as anterior and inferior RV insertion segments respectively and in combination formed the RV insertion region. Segments 1, 2 and 3 represented the LV lateral wall (Figure 2). Definition of regions with the new myocardial segmentation using a modified AHA model is summarised in table 5.1.

**Table 5.1 Definition of regions with the new myocardial segmentation using a modified AHA model.**

Segments	Definition
4 and 6	Right ventricular insertion region (anterior and inferior segment respectively)
1, 2 and 3	LV lateral wall
5	Septal segment

### 5.2.6 Statistical analysis

All T1 values are given milliseconds. Continuous variables are summarised as median and interquartile range due to the small sample size in some groups. Categorical variables are summarised as n (%). Pearson or Spearman correlations are used to assess association between continuous variables. Normality of T1 values was assessed using a Kolmogorov-Smirnov test. Inter-rater variability of determination of T1 times was calculated from paired measurements of the RV insertion regions using an interclass correlation coefficient with a two-way mixed model for absolute agreement. Kruskal-Wallis tests were used to compare Insertion region T1 values between the WHO groups and patients with no PH. PH and non PH patient groups were compared using Mann-Whitney U tests and Fisher's exact tests, where appropriate. Multivariable linear regression models were used to determine whether any of haemodynamics, ventricular function, mass, or volume finding was independently associated with variations of T1 times. Statistical analysis was performed using SPSS (IBM SPSS Statistics) and Graphpad Prism (Graphpad Software inc). A p-value of greater than 0.05 indicated a lack of statistical significance.

### 5.3 Results

Demographics of the study population are given in table 5.2. There was no significant difference between the PH and the non-PH group in terms of gender, age, BSA, systemic blood pressure or heart rate.

**Table 5.2 Demographics of the study population.**

	All	PH	No PH	PH vs no PH
n	121	101	20	
Male gender	59 (49%)	54 (54%)	5 (25%)	0.0269
Age (years)	61(53,70.5)	61(54,70)	64.5(47.8,75)	0.5971
BSA (m <sup>2</sup> )	1.9(1.8,2.1)	1.9(1.8,2.1)	1.8(1.6,2)	0.2409
Systolic BP	129(113,147)	128(111,147)	133(120,152)	0.4542
Heart rate	73(64,90.5)	73(64,91)	77(64,89)	0.8853
TRPG(mmHg)	60(47,76)	64(54,80)	32(25,44)	<0.0001
TAPSE (cm)	1.7 (1.4,1.9)	1.7(1.3,2)	1.8(1.7,2)	0.1106
LVEF	65.1(54.9,71.2)	64.2(54.4,71)	65.6(57.8,74.3)	0.6241
RVEF	42.9(31.3,53.5)	38.9(28.7,48.6)	53.9(49.5,62.4)	<0.0001

There was no significant difference between the PH and the non PH group in terms of gender, age, BSA, systemic blood pressure or heart rate. Results are shown as median (Interquartile range). P values are from Mann-Whitney U tests for continuous variables or Fisher's tests for categorical variables. A p-value of greater than 0.05 indicated a lack of statistical significance. BSA – Body surface area, TRPG – tricuspid regurgitant pressure gradient, TAPSE – tricuspid annular systolic plane excursion, LVEF – LV ejection fraction, RVEF – RV ejection fraction

### **5.3.1 Treatment naive patient cohort - haemodynamics, ventricular volumes, mass and function**

Haemodynamics during right heart catheterisation and ventricular volumes, mass and function by CMR were evaluated in all subjects (Table 5.3). The PH group demonstrated higher pulmonary artery pressures, PVR, and RV chamber dilatation, hypertrophy and functional impairment as expected. However, the two groups did not differ in terms of cardiac output (and cardiac index) and left sided CMR variables.

**Table 5.3 Haemodynamics during right heart catheterisation and biventricular volumes, mass and function determined by CMR for PH and for patients without PH.**

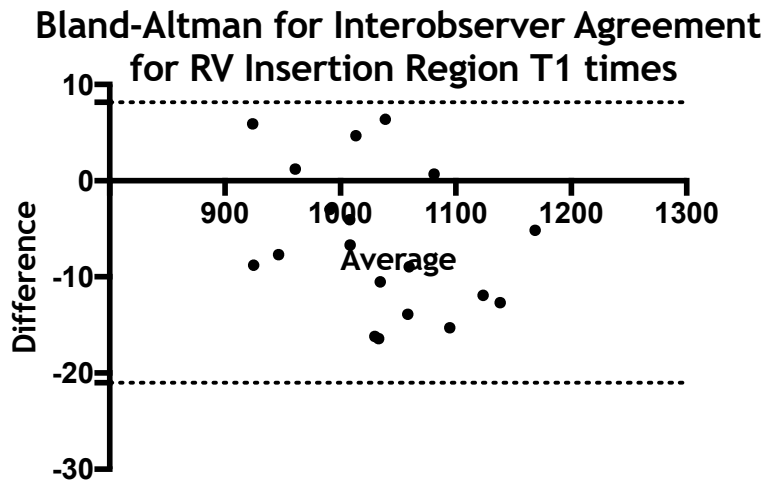
	PH	No PH	PH vs no PH
n	(n=101)	(n=20)	
RAP	7(3,10)	4(2.8,8)	0.1047
mPAP	44(37,52)	18(16,21)	<0.0001
PAWP	8(5,10)	9(6,14)	0.4862
Cardiac output	4.1(3.2,5.3)	4.2(3.6,5.5)	0.8039
PVR	8.7(5.6,12.8)	2.5(1.5,3.4)	<0.0001
Cardiac Index	2.2(1.7,2.7)	2.3(1.9,2.8)	0.5873
SVO2	65.3(57.7,71.8)	73.5(68.4,75.8)	<0.01
LVEDVI	57.5(49,77.7)	63.9(53.7,72.6)	0.3764
LVESVI	21.7(14.9,28.1)	22.6(14.4,29)	0.7590
LVEF	64.2(54.4,71)	65.5(57.8,74.3)	0.6241
LV mass index	49.9(40.5,57.5)	41.5(35.8,46.3)	<0.01
RVEDVI	106(87.8,127.1)	77.6(67.7,105.9)	<0.001
RVESVI	67.3(45.1,90.5)	34.7(27.5,49.2)	<0.0001
RV ejection fraction	38.8(28.7,48.6)	53.9(49.5,62.4)	<0.0001
RV mass Index	28.1(22.9,35.1)	16.8(14.4,23.8)	<0.0001
VMI	0.5(0.3,0.6)	0.3(0.2,0.3)	<0.0001

Haemodynamics during right heart catheterisation and ventricular volumes, mass and function by CMR were evaluated in all subjects. The PH group demonstrated higher pulmonary artery pressures, PVR and RV CMR variables as expected. However, the two groups did not differ in terms of cardiac output (and cardiac index) and left sided CMR variables. Results are shown as median (interquartile range). PH and non PH patient groups were compared using Mann-Whitney U tests. A p-value of greater than 0.05 indicated a lack of statistical significance. RAP – Right atrial pressure, mPAP – mean pulmonary artery pressure, PAWP – Pulmonary artery wedge pressure, PVR – Pulmonary vascular resistance, SvO2 – mixed venous saturations, LVEDVI – LV end-diastolic volume index, LVESVI – LV end-systolic volume index, RVEDVI – RV end-diastolic volume index, RVESVI – RV end-systolic volume index, VMI – ventricular mass index

### **5.3.2 T1 analysis Inter-rater variability**

There was excellent agreement between the two observers GJ and DB for RV insertion region T1 values (Interclass correlation 0.995; 95%CI 0.992 to 0.999) and for global myocardial T1 values (Interclass correlation 0.991; 95%CI 0.975 to 0.996) using the novel AHA segmentation proposed earlier in this chapter. The Bland - Altman plots for the RV insertion region T1 values as well global myocardial T1 values are shown in Figure 5-3.

A



B

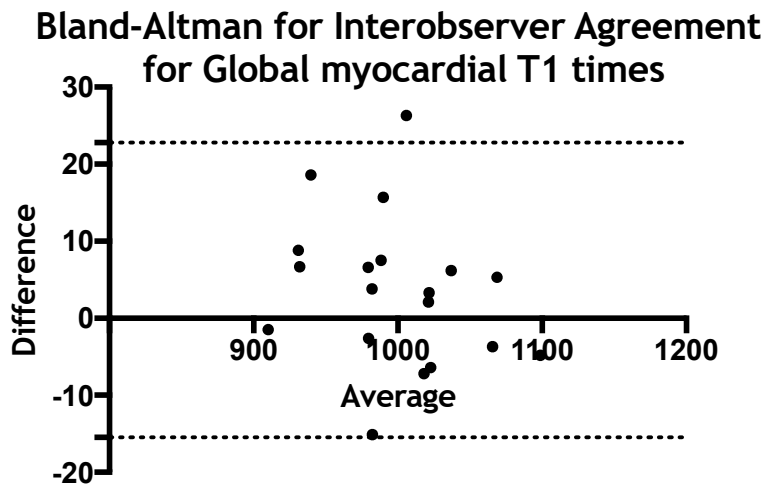


**Figure 5-3 Bland Altman plots for interobserver agreement for A) RV insertion region T1 times and B) global myocardial T1 values using the novel segmentation proposed in the thesis.**

There was excellent agreement between the two observers for RV insertion region T1 values (Interclass correlation 0.995; 95%CI 0.992 to 0.999) and for global myocardial T1 values (Interclass correlation 0.991; 95%CI 0.975 to 0.996) using the novel AHA segmentation proposed earlier in this chapter. Inter-rater variability of determination of T1 times was calculated from paired measurements of the RV insertion regions using an interclass correlation coefficient with a two-way mixed model for absolute agreement.

### **5.3.3 Relationship between global T1 values, regions and segments**

The anterior insertion segment T1 values were strongly associated with global ( $r=0.855$ ), inferior insertion segment ( $r=0.732$ ) and septal segment ( $r=0.740$ ) T1 values. The Inferior insertion segment was strongly associated with global ( $r=0.890$ ) and septal segment ( $r=0.822$ ). Anterior and inferior insertion segments showed moderate associations with lateral region values ( $r=0.628$  and  $r=0.621$  respectively). The Insertion Region T1 values correlated very strongly with global T1 values ( $r=0.935$ ) (Figure 5-4).

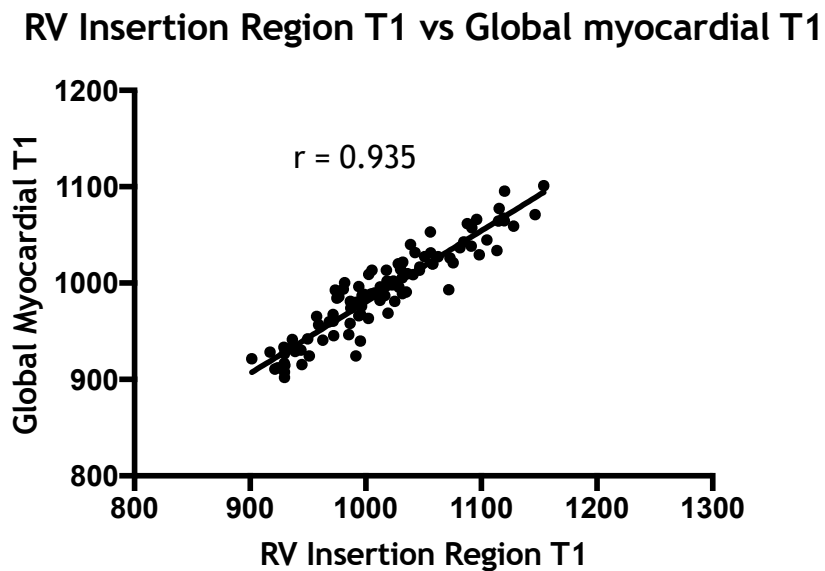
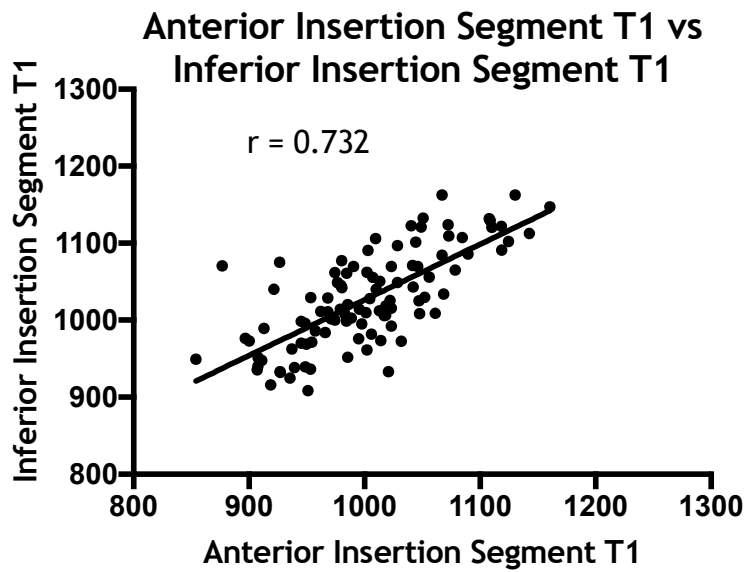


**Figure 5-4 The association between a) anterior insertion segment and inferior insertion segment, b) RV insertion region and global myocardial T1 values of the LV.**

The anterior insertion segment T1 values were strongly associated inferior insertion segment ( $r=0.732$ ) T1 values. The Insertion Region T1 values correlated very strongly with global T1 values ( $r=0.935$ ). The Insertion region consists of both anterior and inferior insertion segments. Pearson correlations were used to assess association between continuous variables. Normality of insertion region T1 values was assessed using a Kolmogorov-Smirnov test. A p-value of greater than 0.05 indicated a lack of statistical significance.

### 5.3.4 Global, regional and segmental T1 times

The global T1 times were higher in the PH population compared to non PH controls (990.5 vs 960.3,  $p=0.0022$ ). There was no significant difference between LV lateral wall regional T1 times (972.7 vs 958.3,  $p=0.344$ ) between the PH and non PH groups. The Insertion region T1 values was higher in PH compared to non PH (1012 vs 962.9,  $p<0.0001$ ). Anterior Insertion segment (1002 vs 948.2,  $p<0.0001$ ), inferior insertion segment (1020 vs 970.2,  $p<0.0001$ ) and septal segment T1 values (995.2 vs 962,  $p=0.0008$ ) were higher in PH compared to No PH (Table 5.4, Figure 5-5. and Figure 5-6).

**Table 5.4 Global, regional and segmental T1 values between PH and non PH patients**

	PH	No PH	PH vs no PH
n	(n=101)	(n=20)	
Global myocardial	991 (960,1021)	960 (931,986)	0.0022
RV Insertion Region [(S4 + S6)/2]	1012 (974, 1054)	963 (940,983)	<0.0001
LV Lateral Wall [(S1+S2+S3)/3]	972 (940, 995)	958 (924,994)	0.3444
Anterior Insertion Segment (S4)	1002 (954,1045)	948 (928,971)	<0.0001
Inferior Insertion Segment (S6)	995 (956,1024)	962 (934,980)	0.0008
Septal Segment (S5)	1020 (979,1021)	970 (946,998)	<0.0001

Anterior Insertion segment (1002 vs 948.2,  $p < 0.0001$ ), inferior insertion segment (1020 vs 970.2,  $p < 0.0001$ ) and septal segment T1 values (995.2 vs 962,  $p = 0.0008$ ) were higher in PH compared to No PH. There was no significant difference between LV lateral wall regional T1 times (972.7 vs 958.3,  $p = 0.344$ ) between the PH and non PH groups. The LV was segmented using our modified AHA technique carefully excluding blood pool, papillary muscles and trabeculae. The inferior insertion segment was drawn with the inferior RV insertion point at its centre. Anterior and Inferior insertion segments were combined to define the RV insertion region. The septal region completed the interventricular septum. Lateral region was defined to contain the LV lateral wall. The PH and no PH group for each region or segment is compared by Mann Whitney U test. \*\*\*\* represents  $p < 0.0001$  and \*\*\* represents  $p < 0.001$ .

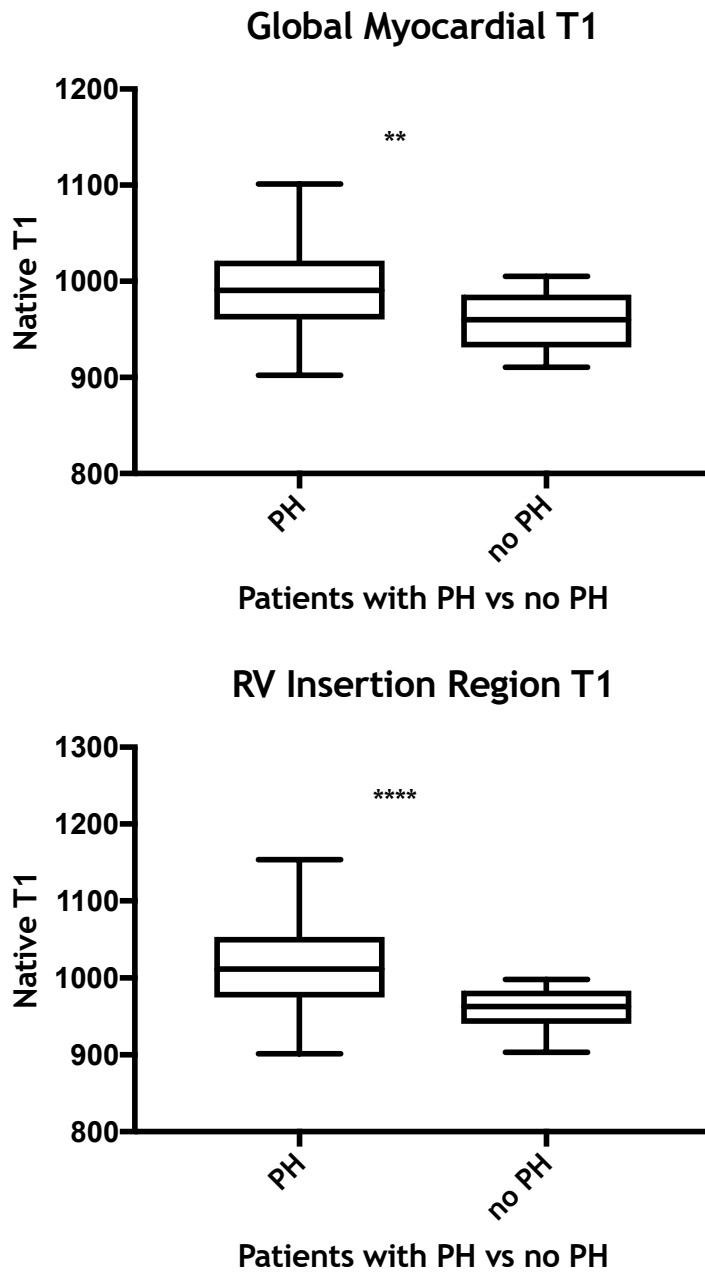


**Figure 5-5 Boxplots demonstrating a) Global myocardial T1 values between PH and no PH patients b) Insertion region T1 values between PH and non PH groups.**

The global T1 times were higher in the PH population compared to non PH controls (990.5 vs 960.3,  $p=0.0022$ ). The Insertion region T1 values was higher in PH compared to non PH (1012 vs 962.9,  $p<0.0001$ ). The LV was segmented using our modified AHA technique carefully excluding blood pool, papillary muscles and trabeculae. The inferior insertion segment was drawn with the inferior RV insertion point at its centre. Anterior and Inferior insertion segments were combined to define the RV insertion region. The two groups were compared by a Mann Whitney U test. A p-value of greater than 0.05 indicated a lack of statistical significance. \*\*\*\* represents  $p < 0.0001$  and \*\* represent  $p<0.01$ .

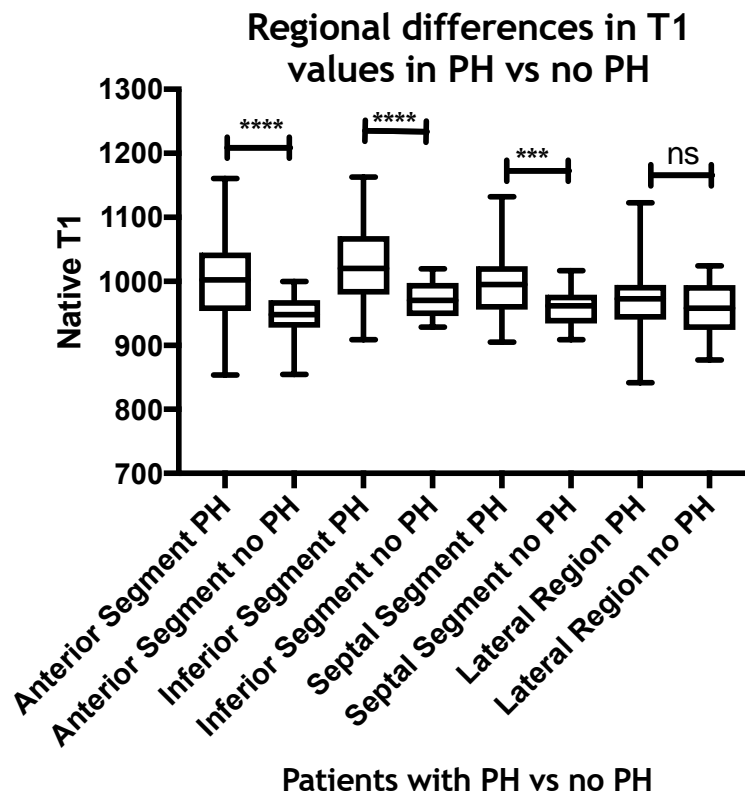


**Figure 5-6** Boxplots of T1 values between PH and no PH groups grouped according to regional and segmental values.

Anterior Insertion segment (1002 vs 948.2,  $p < 0.0001$ ), inferior insertion segment (1020 vs 970.2,  $p < 0.0001$ ) and septal segment T1 values (995.2 vs 962,  $p = 0.0008$ ) were higher in PH compared to No PH. There was no significant difference between LV lateral wall regional T1 times (972.7 vs 958.3,  $p = 0.344$ ) between the PH and non PH groups. The LV was segmented using our modified AHA technique carefully excluding blood pool, papillary muscles and trabeculae. The inferior insertion segment was drawn with the inferior RV insertion point at its centre. Anterior and Inferior insertion segments were combined to define the RV insertion region. The septal region completed the interventricular septum. Lateral region was defined to contain the LV lateral wall. The PH and no PH group for each region or segment is compared by Mann Whitney U test. \*\*\*\* represents  $p < 0.0001$  and \*\*\* represents  $p < 0.001$ .

### 5.3.5 WHO groups of PH

The patients were classified according to the WHO group of PH (1- PAH, 2 - PH due to left heart disease, 3 - PH due to hypoxic lung disease, 4- CTEPH, and no pulmonary hypertension). There were no patients with group 5 disease in the study population. There were significant differences between the groups in global T1 times ( $p = 0.0214$ ), however on post hoc analysis the only significant difference was found between group 1 and no PH groups ( $p=0.018$ ). Insertion region T1 times were different between the groups ( $p<0.0001$ ), and significant differences were observed in group 1 vs no PH ( $p<0.0001$ ) and Group 3 vs no PH ( $p=0.0361$ ). However, there were no differences between groups in LV lateral regional T1 times (Figure 5-7).

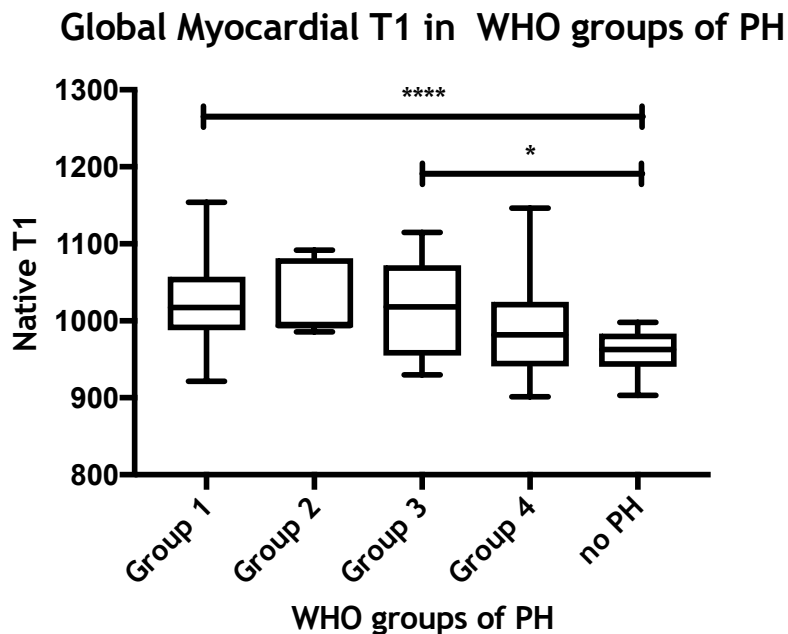
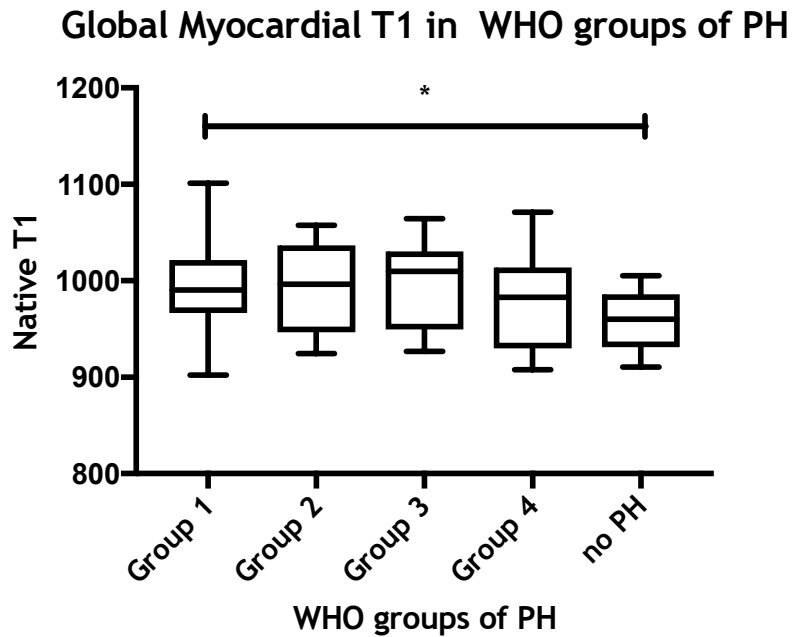


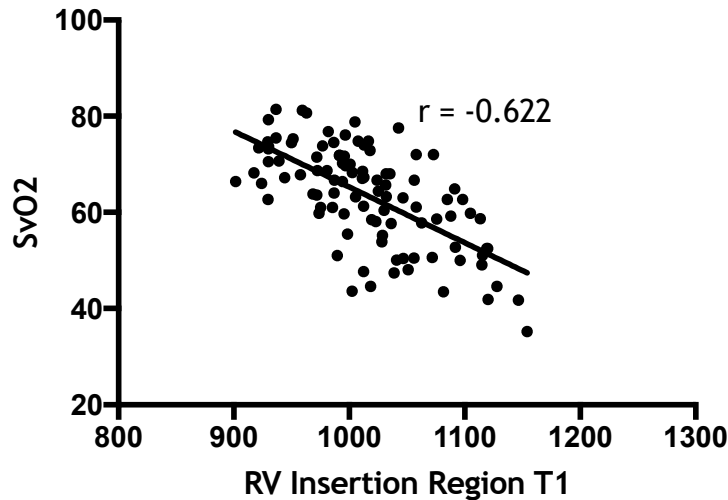
**Figure 5-7** Boxplots of global myocardial T1 values and insertion region T1 values between different WHO groups of pulmonary hypertension and symptomatic patients with no PH.

There were significant differences between the groups in global T1 times ( $p = 0.0214$ ), however on post hoc analysis the only significant difference was found between group 1 and no PH groups ( $p=0.018$ ). Insertion region T1 times were different between the groups ( $p<0.0001$ ), and significant differences were observed in group 1 vs no PH ( $p<0.0001$ ) and Group 3 vs no PH ( $p=0.0361$ ). Kruskal-Wallis tests were used to compare Insertion region T1 values between the WHO groups and patients with no pulmonary hypertension and post hoc analysis was done using a Dunns multiple comparison test. A p-value of greater than 0.05 indicated a lack of statistical significance. \*\*\*\* represents  $p < 0.0001$  and \* represents  $p<0.05$ .

### **5.3.6 Haemodynamics at right heart catheterisation and CMR findings**

Insertion region T1 values demonstrated moderate correlation with mixed venous saturations obtained at right heart catheterisation ( $r=-0.622$ ), pulmonary vascular resistance ( $r=0.530$ ) and right atrial pressure ( $r= 0.483$ ). The relationship with invasive pressure measurements (sPAP, dPAP, mPAP) was weaker. There were no significant correlations between insertion region T1 times and LV volume, mass or function measurements by CMR. However, insertion region T1 times correlated significantly with RVESVI ( $r = 0.693$ ), RVEDVI ( $r =0.632$ ,  $p<0.0001$ ), RV mass index ( $r=0.619$ ) and RVEF ( $r=-0.599$ ) measured by CMR (Figure 5-8) (table 5.5 and table 5.6).

### RV Insertion Region T1 vs Mixed Venous Saturations



### RV Insertion Region T1 vs RV End-systolic Volume Index

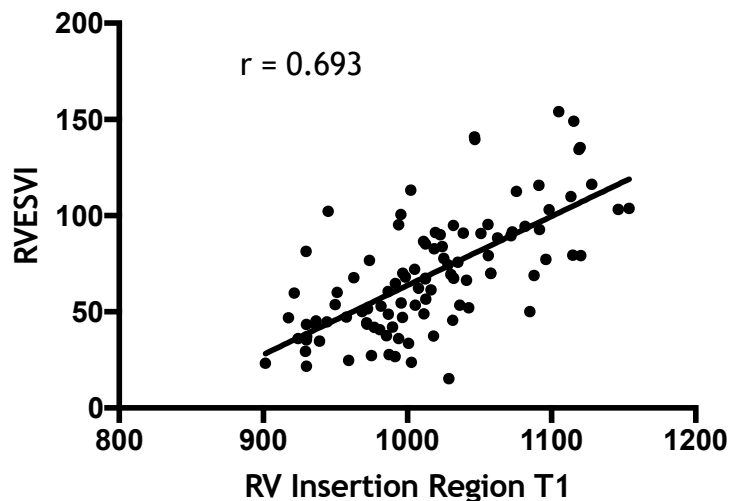


**Figure 5-8 Associations between a) right ventricular end systolic volume index measured by CMR and b) mixed venous saturations obtained during right heart catheterisation and RV insertion region T1 values.**

RV insertion region T1 values demonstrated moderate correlation with mixed venous saturations obtained at right heart catheterisation ( $r = -0.622$ ). The relationship with invasive pressure measurements (sPAP, dPAP, mPAP) was weaker. RV insertion region T1 times correlated significantly with RVESVI ( $r = 0.693$ ) measured by CMR. Pearson or Spearman correlations were used to assess association between continuous variables as appropriate. Normality of insertion region T1 values was assessed using a Kolmogorov-Smirnov test. A p-value of greater than 0.05 indicated a lack of statistical significance.

**Table 5.5 Correlation between RV insertion region and global myocardial T1 values and haemodynamics during right heart catheterisation.**

	RA	mPAP	CO	PVR	Cardiac Index	SvO2
RV insertion Region T1	.483****	.392****	-.524****	.530****	-.515****	-.622****
Global T1	.456****	.351***	-.432****	.439****	-.427****	-.591****

Pearson or Spearman correlations were used to assess association between continuous variables as appropriate. Normality of insertion region T1 values was assessed using a Kolmogorov-Smirnov test. \*\*\*\* represents  $p < 0.0001$  and \*\*\* represents  $p < 0.001$ . RA – right atrial pressure, mPAP – mean pulmonary artery pressure, CO – cardiac output, PVR – pulmonary vascular resistance, SvO2 – mixed venous saturations.

**Table 5.6 Correlation between RV insertion region and global myocardial T1 values and RV CMR variables.**

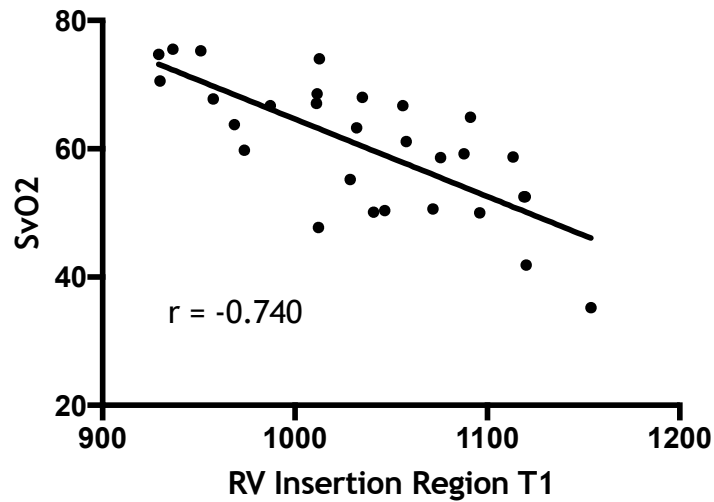
	RVEDVI	RVESVI	RVEF	RV Mass Index	VMI
RV insertion Region T1	.619****	.693****	-.599****	.619****	.495****
Global T1	.535****	.578****	-.497****	.571****	.435****

Pearson or Spearman correlations were used to assess association between continuous variables as appropriate. Normality of insertion region T1 values was assessed using a Kolmogorov-Smirnov test. \*\*\*\* represents  $p < 0.0001$ . RVEDVI – right ventricular end-diastolic volume index, RVESVI – right ventricular end systolic volume index, VMI – ventricular mass index

### **5.3.7 Subgroup analysis of IPAH**

In patients with IPAH, the association of Insertion region T1 times with markers of disease severity including cardiac Index, RV volumes and function were more apparent. RV insertion region T1 changes were not associated with pulmonary artery pressure in this population (Figure 5-8) (Table 5.7).

### RV Insertion Region T1 vs Mixed Venous Saturations



### RV Insertion Region T1 vs RV End-systolic Volume Index

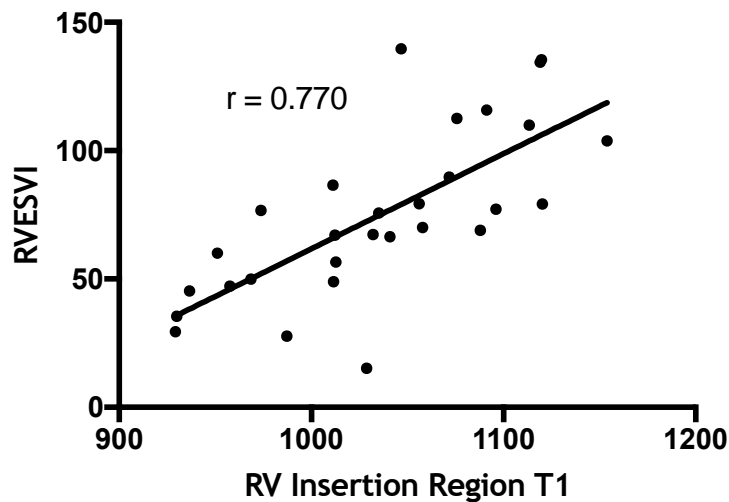


**Figure 5-9 Correlation between a) RV insertion region T1 values and mixed venous saturations at right heart catheterisation and b) RV insertion region T1 values and RV end systolic volume index by CMR in IPAH patients.**

In patients with IPAH, the association of Insertion region T1 times with markers of disease severity including cardiac Index, right ventricular volumes and function were more apparent. RV insertion region T1 values were not associated with pulmonary artery pressure in this population. Spearman correlations were used to assess association between continuous variables as appropriate

**Table 5.7 Association between Insertion region T1 times, haemodynamics during right heart catheterisation and CMR variables in IPAH patients.**

	RA	mPAP	PVR	CI	SvO2	RVESVI	RV Mass Index
RV insertion Region T1	.654****	.189	.569***	-.704****	-.734****	.770****	-.621****

In patients with IPAH, the association of RV insertion region T1 times with markers of disease severity including cardiac Index, RV volumes and function were more apparent. RV insertion region T1 values were not associated with pulmonary artery pressure in this population. Spearman correlations were used to assess association between continuous variables as appropriate. \*\*\*\* represents  $p < 0.0001$  and \*\*\* represents  $p < 0.001$ . RA – right atrial pressure, mPAP – mean pulmonary artery pressure, PVR – pulmonary vascular resistance, CI – cardiac index, SvO2 – mixed venous saturations, RVESVI – right ventricular end-systolic volume index

### 5.3.8 Multivariable linear regression

A multivariable linear regression model was used to assess the association between RV volume and insertion region T1 times, independently of haemodynamics during right heart catheterisation. A model containing RA pressure, pulmonary vascular resistance and RVESVI gave an adjusted R-squared value of 0.554 determining insertion region T1 values. All were significant predictors of Insertion region T1 values (Table 5.8).

**Table 5.8 Multivariable linear regression analysis showing associations between haemodynamics during right heart catheterisation, RV structure and insertion region T1 times.**

Variable	Regression coefficient	95% CI	P-value
RAP	.207	.537 to 3.940	0.010
PVR	.233	0.915 to 4.472	0.003
RVESVI	.407	.595 to 1.2	<0.001

A multivariable linear regression model was used to assess the association between RV volume and insertion region T1 times, independently of haemodynamics during right heart catheterisation. A model containing RA pressure, pulmonary vascular resistance and RVESVI gave an adjusted R-squared value of 0.554 determining insertion region T1 values. All were significant predictors of Insertion region T1 values. RAP - right atrial pressure, PVR – pulmonary vascular resistance, RVESVI – right ventricular end-systolic volume index.

### 5.3.9 Validation cohort

In the validation cohort of patients with established PAH T1 values were measured pre and post Gadolinium enhancement as a measure of ECV fraction. ECV values were significantly higher in the RV Insertion region compared to lateral region ( $36.97 \pm 4.4$  vs  $28.2 \pm 5.1$ ,  $p < 0.05$ , 95%CI -14.8 to -2.7) (Figure 5-9). ECV values demonstrated very good correlation with native T1 values ( $r=0.71$ ).

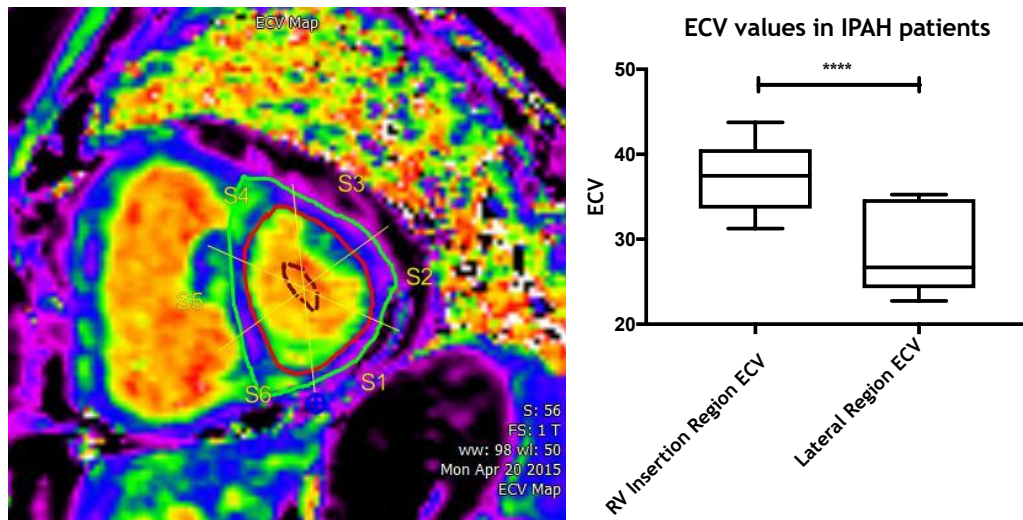


**Figure 5-10 a) ECV map demonstrating raised ECV values in the RV insertion regions, b) boxplot of the ECV values in the RV insertion regions in patients with established PAH.**

In the validation cohort of patients with established PAH using Gadolinium enhancement a) ECV map demonstrating raised ECV values in the RV insertion regions, b) boxplot of the ECV values in the RV insertion regions demonstrating significantly higher values compared to the LV lateral region. In the validation cohort, subjects underwent native and post contrast T1 mapping. Extracellular volume fraction (ECV) values were calculated from T1 maps acquired pre and post contrast calibrated by blood haematocrit. ECV value was calculated as  $ECV = (1 - \text{hematocrit}) \left( \frac{1}{T1 \text{ myocardium post contrast}} - \frac{1}{T1 \text{ myocardium pre contrast}} \right) \left( \frac{1}{T1 \text{ blood post contrast}} - \frac{1}{T1 \text{ blood pre contrast}} \right)$ . ECV values were significantly higher in the RV Insertion region compared to lateral region ( $36.97 \pm 4.4$  vs  $28.2 \pm 5.1$ ,  $p < 0.05$ , 95%CI -14.8 to -2.7). The two groups were compared by a Mann Whitney U test. \*\*\*\*represents  $p < 0.0001$ . (Author's own image)

## 5.4 Discussion

This is the first study using a novel myocardial segmentation to identify T1 changes from CMR in PH. We believe there are a number of reasons to use this novel segmentation rather than the pre-existing AHA segmentation in the focused assessment of patients with PH. Firstly, the pre-existing segmentation technique fails to isolate the RV insertion points /regions which are the most susceptible to deformation in PH. Secondly, the visual assessment of the insertion regions fails to identify subtle myocardial changes because it requires manual contouring of a region of interest. Finally, myocardial changes may have a prognostic significance in PH, and a methodology that is reproducible and not reliant on visual assessment is paramount for this use. Thus, we introduced a novel segmentation of the myocardium that is feasible, reproducible and, because it does not rely on the use of potentially harmful contrast, can be used in longitudinal assessment of this population.

In our study, global native T1 times were significantly higher in patients with PH compared to symptomatic patients without PH. However, LV lateral wall regional T1 values were not raised in our PH population compared to patients with no PH in contrast to *Reiter et al* (132). It is important to note that Reiter et al used a healthy volunteer cohort as their control population.

We did not identify significant differences between RV insertion region T1 times in different groups of pulmonary hypertension, however, the trend demonstrated highest native T1 changes in group 1 followed by group 3 disease, with lower native T1 times in the insertion regions in patients with CTEPH. We believe that PH independent of its cause, result in changes in RV insertion regions.

We showed that native T1 changes at the RV insertion regions are associated with invasive measurements of disease severity including right atrial pressure, PVR and mixed venous saturations. However, the relationship with pulmonary artery pressure measurements was weak. In the subgroup of patients with IPAH these relationships were more apparent with a lack of association with pulmonary artery pressure. The RV insertion region T1 times were significantly associated with changes in RV volume, mass and function measured by CMR. Raised native T1 was

an independent predictor of an increased right ventricular systolic index, suggesting reduced myocardial contractility resulted by changes in myocardial architecture, although the order of the two events isn't clear. We suggest the most likely mechanism to be of progressive RV dilatation and reduced RV contractility, shifting the interventricular septum towards the LV, which in turn results in increased stress at the interventricular regions; this leads to changes in myocardial architecture leading to myocardial fibre disarray and fibrosis.

We showed that in a subgroup of patients with IPAH, native T1 changes are strongly associated with markers of disease severity, including cardiac Index, PVR, mixed venous saturations, RV volumes and function but not with mPAP. These findings are consistent with previous literature of LGE and its association with disease severity in PH.

Extracellular volume fraction is a marker of myocardial tissue remodelling. Apart from amyloid, an increased ECV is most likely due to excessive collagen deposition and is a more robust measure of myocardial fibrosis. In the validation cohort of patients with established PAH, we identified raised ECV values in the RV insertion regions which were consistent with native T1 changes we identified in our treatment-naïve study population.

## 5.5 Conclusion

We conclude that,

1. Raised T1 times in RV insertion regions were associated with RV volume, mass and function by cardiac MR as well as markers of disease severity during right heart catheterisation,
2. Native T1 mapping (which does not use contrast) is an alternative to late gadolinium enhancement in assessment of severity of damage to the heart in pulmonary hypertension. Native T1 mapping allows myocardial tissue characterisation without the need for a reference area or contrast administration and hence can be repeated without concern, for example in the long term evaluation of treatment.

The main problem with previous attempts to use T1 mapping in PH patients is that they used visual regions of interest which do not allow precise repetition. We therefore further conclude that this novel myocardial segmentation described in our study will identify myocardial histological changes in patients with pulmonary hypertension. This will provide an opportunity to use myocardial histological characterisation in longitudinal studies in patients with PH and to identify treatment related changes in the myocardial tissue architecture in this disease population.

## **5.6 Limitations**

We applied a non-contrast CMR protocol in our treatment-naïve study population, thus we were not able to determine LGE of the insertion regions. Post contrast T1 and ECV values as well as LGE in this patient group, would have provided further insight into pathophysiology behind CMR changes in the RV insertion points. However, in our validation cohort of patients where T1 mapping was used post Gadolinium, we identified similar ECV changes to native T1 changes seen in our study population thus suggesting the native T1 changes are likely due to myocardial fibrosis rather than an alternate pathology.

We used a patient population with no pulmonary hypertension, albeit with symptoms requiring admission and right heart catheterisation as our control group. Although this may be viewed as a study limitation, we PH rather than healthy volunteers will be an ideal to way optimise and use T1 mapping techniques during clinical use.

**Chapter 6 Longitudinal cardiac  
changes by CMR in a Sugen-  
hypoxia small animal model of  
pulmonary arterial  
hypertension**

## 6.1 Introduction

Small animal (rodent) models are increasingly used to identify pathophysiology as well as therapies for PAH with the intention of translating the findings to humans. Accurate monitoring of disease in rodents with emphasis on ventricular function and with the ability to monitor the disease state without killing the animal is needed. The careful categorisation to distinguish PAH from other groups of PH (especially PH due to left heart disease) is often overlooked in rodent studies. Various small animal models to recapitulate human PH have been produced. Rats have the advantage that they display a more profound pulmonary vascular response to angiogenic stimuli, although mice have the advantage of being genetically modifiable.

Various rodent models to recapitulate human PAH have been produced. Taraseviciene-Stewart et al described the Sugen-hypoxia (SuHx) rat model in 2001 (156). Based on the fact that VEGF is an important maintenance and differentiating factor for vascular endothelial cells, they designed an experiment to inhibit VEGF signalling in rats exposed to chronic hypoxia and normoxia. They showed that a selective VEGF Receptor-2 (VEGFR-2) inhibitor, SU5416 (Sugen) to cause mild PH and pulmonary vascular remodelling in rats exposed to normoxia. However, in rats exposed to chronic hypoxia, Sugen caused severe PH associated with pulmonary arterial endothelial cell proliferation. The VEGFR-2 blockade caused endothelial cell apoptosis, which under chronic hypoxic conditions triggered luminal oblitative endothelial cell proliferation.

Subsequently in 2010, Abe et al showed that SuHx rats demonstrated evidence of severe pulmonary arteriopathy including concentric neo-intimal and complex plexiform-like lesions which closely resemble plexiform lesions seen in humans (157). Subsequently, other groups have attempted to characterize hemodynamics in a SuHx model beyond right heart catheterization alone. Vitali et al evaluated longitudinal changes in a SuHx mouse model of PH. In this study, echocardiographic and invasive measurements were performed after 3 weeks of hypoxia and after 10 weeks of recovery in normoxia. Ten weeks in recovery after hypoxic exposure, RV systolic pressure had decreased, but remained elevated

compared to normoxic controls. However, RV hypertrophy had resolved. They observed very few angio-obliterative lesions at the 10 week follow up (158). De Raaf et al used telemetry to characterise haemodynamic response in SuHx rats and associated these with serial histology. There was severe PH observed in response to SuHx but the RV systolic pressure decreased upon return to normoxia (however remained elevated compared to controls). There was progressive vascular remodelling characterised by progressive intima obstruction (159). Jones et al demonstrated a good correlation between M-mode and Doppler Echo vs. right heart catheterisation in the monocrotaline rat model (161). In a study by Urboniene et al assessing validation of high resolution echocardiography and cardiac MR vs high fidelity catheterisation in experimental PH monocrotaline rat model, non-invasive measures of RV free wall thickness/mass correlated well with post-mortem measurements (160).

Our group has a proven track record in using CMR imaging to evaluate RV function in humans with PAH (99, 104, 133). The same non-invasive and repeatable measurements would be of great advantage for the study of rodent models to allow a detailed understanding of bi-ventricular structural and functional changes that occur during disease progression, to enhance efficacy in translational medicine. We investigated whether CMR is feasible in a SuHx rat model of PH. Subsequently we investigated the structural and functional changes associated with the model during disease progression. Finally, we discussed the suitability of the SuHx model for translational studies of the mechanisms of RV dysfunction in PAH.

## 6.2 Method

### 6.2.1 Ethics

All experimental procedures were carried out in accordance with the United Kingdom Animal Procedures Act (1986) and with the US NIH publication No. 85-23, revised 1996, and ethical approval was also granted by the University of Glasgow Ethics Committee. Rodents were housed in a 12-hour light dark cycle with access to food and water ad libitum.

### 6.2.2 Study design

Male Sprague Dawley rats (three weeks) (n=32) were divided into two groups (n=16 in each group). Group 1) *Sugen-hypoxia* - a single dose of subcutaneous Sugen-5416 (Sigma, UK) suspended in vehicle (20mg/kg), before being placed in a hypobaric chamber (atmospheric pressure 550 mbar) for 2 weeks and then placed in normal room pressure (1013 mbar) for 3 weeks whilst PH developed. Group 2) *Normoxia* maintained at normal room pressure for 5 weeks. In each group (n=16) half the animals entered the CMR arm of the study (n=8) while the other half underwent right heart catheterization for hemodynamic assessment (n=8). Animals were assessed at five weeks and eight weeks from the beginning of the study. The study design is summarized in Figure 6-1.

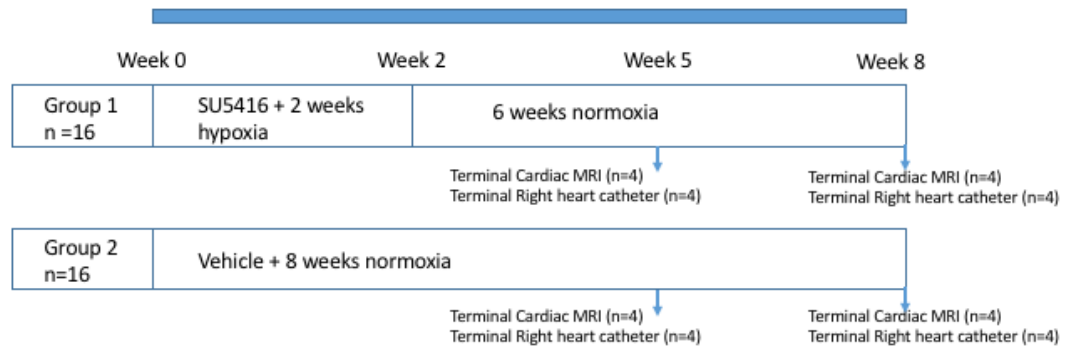


### Figure 6-1 Study design

Male Sprague Dawley rats (n=32) were divided into two groups (n=16 in each group). Group 1) Sugden hypoxia (SuHx) - a single dose of Sugden-5416, before being placed in a hypobaric chamber for two weeks and then placed in normal room pressure for three weeks whilst PH developed, animals receive control chow throughout. Group 2) normoxic maintained at normal room pressure for 5 weeks. In each group half the animals entered the cardiac MRI arm of the study (n=8) while the other half underwent right heart catheterization for hemodynamic assessment (n=8). Animals were assessed at 5 weeks and 8 weeks from the beginning of the study with right heart catheterization, CMR and gross anatomy at autopsy.

### 6.2.3 *In vivo* hemodynamic measurements

Animals were anaesthetically induced with 3% (v/v) isoflurane and then maintained at 2% (v/v) isoflurane supplemented with a constant flow of 5% (v/v) oxygen. Hemodynamic measurements were taken using an ultra-miniature Polyimide Nylon catheter capable of measuring ventricular pressure continuously (AD instruments spr-869NR, Millar). The catheter was used as per the manufacturer's instructions with the PowerLab 35 Series data acquisition system with LabChart Pro and the pressure volume (PV) Loop analysis module. For right heart pressure analysis, the catheter was inserted into the jugular vein and guided into the RV to measure RVSP.

### **6.2.4 RV hypertrophy and tissue harvest**

RV hypertrophy and tissue harvest was performed as described in the Methods section 2.11

### **6.2.5 Gross anatomy postpartum**

Gross anatomy postpartum was performed as described in the Methods section 2.12.

### **6.2.6 Pulmonary vascular remodelling**

Pulmonary vascular remodelling assessment was performed as described in the methods section 2.13.

### **6.2.7 CMR imaging**

CMR imaging was performed in a Bruker Biospec 7-T/30-cm (Bruker Biospin, Ettlingen, Germany) system with a gradient coil insert (400 mT/m). Using a 72mm transmit birdcage resonator and 4 channel phased array rat cardiac receiver coil. Anaesthesia was induced with gas flow at 2-3 l/min, and the isoflurane delivered via a vaporizer (Vetamac, Rossville, IN) at 3-4%. The exhaust was connected to the Omnicon F/Air device (AM Bickford). After induction, animals were maintained at 2% (v/v) isoflurane supplemented with a constant flow of 5% (v/v) oxygen. An external water jacket was used to maintain a core temperature of 37°C. During all procedures, body temperature, ECG, and respiration were monitored (Echo: Indus Instruments, Houston, TX; MRI: SA Instruments, Stony Brook, NY; Cath: Powerlab, Ad instruments, Colorado Springs, CO). Long and short axis scout images were acquired so that short axis images could be planned using a segmented, cardiac - triggered FLASH sequence. The images were acquired with a slice thickness of 1.5mm ensuring the entire biventricular length is covered. The CMR parameters were as follows. Slice thickness-1.50mm, field of View-30.00mm x 30.00mm, image matrix-192 x 192 pixels, image resolution-156µm x 156µm, Flip angle-15 degrees, Echo time-2.50ms, Rep. time-7.02ms, number of frames-25, number of averages-6, software version-Paravision 5.1.

### 6.2.8 CMR analysis

Scans were coded by number and analysed in batches by the author who was blinded to the identity and hemodynamic results at the time of analysis. A second observer (A.U) analysed 5 scans for inter-rater agreement analysis. Trabeculations and papillary muscles were considered as part of the blood pool. The epicardial and endocardial borders were manually outlined in end-diastolic and end-systolic frames using Qmass (Medis medical imaging systems, Leiden, Netherlands). Stroke volume was determined from LVEDV- LVESV. Ejection fraction  $[(SV/EDV)*100\%]$  was also determined. RV and LV masses were determined by manual planimetry at diastole. Ventricular mass index was defined as the ratio between RV to LV mass, with the IVS considered part of the LV. LV eccentricity index (LVEI) was defined as the ratio between maximum anterior-posterior to septal lateral diameters of the LV and was measured at both systole and diastole. All ventricular volumes and mass measurements were indexed to body surface area (171).

### 6.2.9 Statistical analysis

Ventricular volumes and mass are given as  $\mu\text{lcm}^{-2}$  and  $\text{mgcm}^{-2}$  respectively indexed for body surface area. Statistical analysis was performed using SPSS (IBM, SPSS Statistics, USA) and Graphpad Prism (Graphpad, USA). A significance level of 0.05 was employed for statistical tests. An analysis of variance test was used to compare RV and LV mass, volumes and function between normoxic animals and different stages of SuHx. If there was statistical significance a Tukey test was used for post hoc analysis. To compare different methods of ventricular mass index measurement (CMR vs autopsy) a spearman correlation was used. Inter-rater variability for determination of LV and RV function were calculated from paired measurements of the LVEF and RVEF of two readers as intra-class correlation coefficient with a two-way mixed model for absolute agreement. Results are shown as mean +/- SD unless otherwise stated.

## 6.3 Results

### 6.3.1 Right heart catheterisation and RV hypertrophy

Compared to normoxic rats ( $23.87 \pm 4.1$  mmHg) RVSP was significantly elevated in SuHx rats at both five and eight weeks ( $40.95 \pm 15.5$  mmHg  $p=0.03$ ,  $48.89 \pm 9.6$  mmHg  $p=0.002$  respectively). There were no significant differences in RVSP between SuHx rats at five and eight weeks. Similarly, relative RV mass measured at autopsy by  $RV / (LV + \text{septum})$  was significantly elevated at five week ( $0.36 \pm 0.1$   $p=0.021$ ) and eight week ( $0.4 \pm 0.04$   $p=0.004$ ) SuHx compared to controls ( $0.25 \pm 0.04$ ). Immunohistochemical analysis of  $\alpha$ -smooth muscle actin staining in the smooth muscle layer of small pulmonary arteries of the lungs demonstrated vascular thickening and remodelling at both 5 and 8 weeks of SuHx. Although there was statistically significant difference between the percentage of remodelled vessels between normoxia and SuHx groups ( $57.4\% \pm 7.3$  vs  $77.6\% \pm 10.3$   $p=0.02$ ,  $57.4\% \pm 7.3$  vs  $78.5\% \pm 9.4$   $p=0.02$ ), there was no significant difference observed between SuHx rats at five and eight weeks. (Figure 6-2)

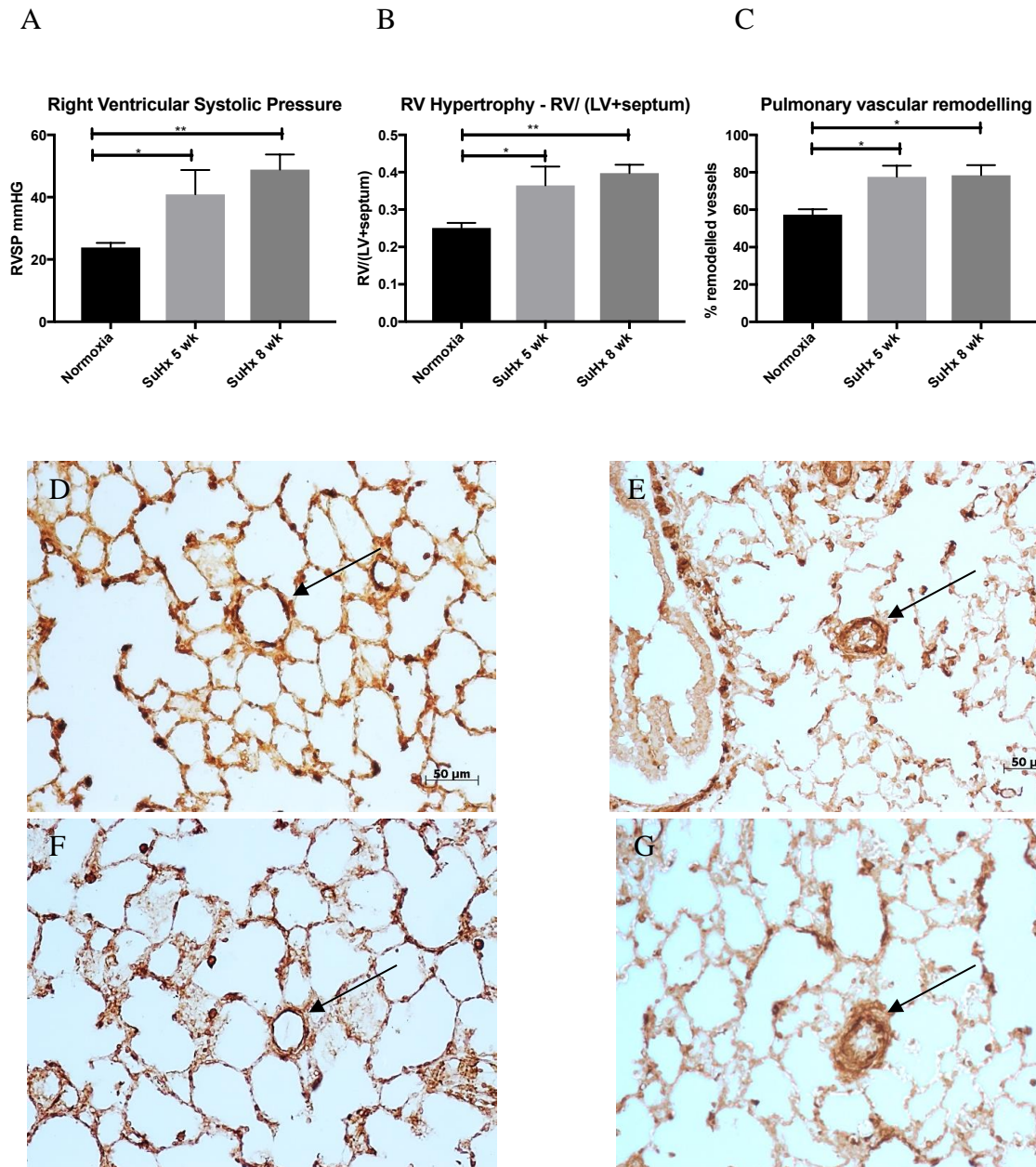


**Figure 6-2 Right ventricular systolic pressure measured by right heart catheterization (A), RV/(LV + septum) by gross weight (B), the percentage of remodelled vessels in a lung section (C) and immunohistochemical analysis of  $\alpha$ -smooth muscle actin ( $\alpha$ -SMA) staining in the smooth muscle layer of small pulmonary arteries of the lungs (D - G).**

For right heart pressure analysis, the catheter was inserted into the jugular vein and guided into the RV to measure RV systolic pressure (RVSP). Animals were culled, the heart was isolated, atria were removed and RV/(LV + septum) were measured to assess RV hypertrophy. Although there are significant differences between the normoxic group (n=8) and Sugen hypoxic groups at 5 (n=4) and 8 weeks (n=4), there were no significant differences in RVSP nor RV/(LV + septum) at autopsy between Sugen hypoxia 5 and 8 weeks. Vascular thickening was determined by smooth muscle actin antibody (ab5694, Abcam, Cambridge, UK) staining, thickening was characterized by an increase in the vessel wall diameter of more than 50% of the arterial wall or complete occlusion. The number of remodelled vessels over the total number of vessels present in a lung section was determined. Results are shown as mean  $\pm$  SEM. ANOVA test was used to compare the three groups, and if there was statistical significance a Tukey HSD test was used for post hoc analysis. \* represents  $p < 0.05$  and \*\* represents  $p < 0.01$ . For immunohistochemical analysis of  $\alpha$ -smooth muscle actin ( $\alpha$ -SMA) staining in the smooth muscle layer of small pulmonary arteries of the lung sections were viewed at  $\times 200$ . D and F demonstrate normoxic animals at 5 and 8 weeks while E and G demonstrate vascular thickening and remodelling of the pulmonary vasculature (black arrows) in Sugen hypoxic rats at 5 and 8 weeks respectively.

### **6.3.2 CMR**

A representative long axis image (A) and a short axis cine stack (B-F) are shown in Figure 6-3. The LV and the RV demonstrated good spatial and temporal resolution allowing manual planimetry. All of the images in normoxic or SuHx animals were suitable for analysis. Initial scout images were acquired to identify the cardiac chambers.

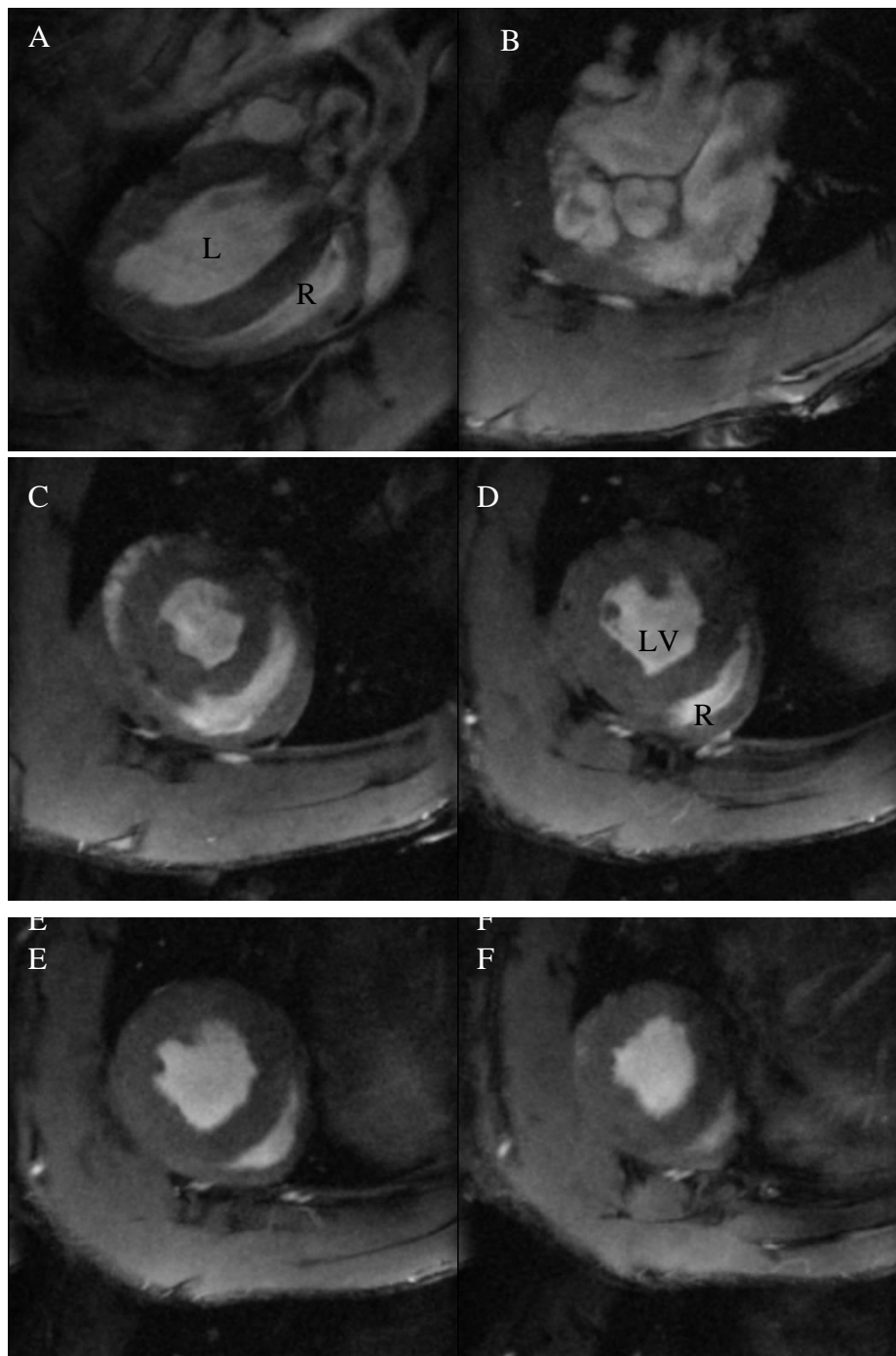


**Figure 6-3 Cardiac MRI short axis image taken from a long axis (A) and a short axis cine stack (B – F) of a normoxic Sprague Dawley rat.**

CMR imaging was performed in a Bruker 7T (Bruker, Biospin, Germany) system. Anaesthesia was induced by placing the rat in an anaesthesia induction chamber with gas flow at 2–3 l/min, and the isoflurane was delivered via a vaporizer (Vetamac, Rossville, IN) at 3–4%. After induction, animals were then maintained at 2% (v/v) isoflurane supplemented with a constant flow of 5% (v/v) oxygen. An external water jacket was used to maintain a core temperature of 37°C. During all procedures, body temperature, ECG, and respiration were monitored using a rodent monitoring system (Echo: Indus Instruments, Houston, TX; MRI: SA Instruments, Stony Brook, NY; Cath: Powerlab, Ad instruments, Colorado Springs, CO). Long axis and short axis scout images were acquired so that a true short axis images could be planned using a segmented, cardiac – triggered FLASH sequence. The short axis images were acquired with a slice thickness of 1.5 mm ensuring the entire biventricular length is covered.

### 6.3.3 Inter-rater variability

There was excellent agreement between the two observers (ICC 0.97, 95%CI 0.74 to 1.0) for LVEF as well as for RVEF (ICC 0.96, 95%CI 0.64 to 1.0).

### 6.3.4 Right ventricle

RVESVI was significantly increased in SuHx rats at 8 weeks ( $0.28 \pm 0.04$   $p=0.003$ ) compared to normoxic rats ( $0.18 \pm 0.03$ ). There were no significant differences between normoxia and SuHx at five weeks. Compared to normoxic rats ( $0.17 \pm 0.03$ ), RV mass index was increased in the SuHx rats at five weeks ( $0.28 \pm 0.04$   $p=0.002$ ) and eight weeks ( $0.27 \pm 0.04$   $p=0.002$ ). RV demonstrated progressive dilatation (increasing RVEDVI) at eight weeks of SuHx compared to normoxic rats ( $0.75 \pm 0.13$  vs  $0.56 \pm 0.1$   $p=0.022$ ). In RVEF, there were no significant differences between normoxic rats and 5 and 8 week SuHx rats however demonstrating trends towards impairment (RVEF =  $68.3 \pm 5.1\%$ ,  $69.4 \pm 6.9\%$  and  $62.6 \pm 6.1\%$  respectively). SVI was preserved in the SuHx model at five and eight weeks compared to normoxia ( $0.44 \pm 0.1$  vs  $0.5 \pm 0.04$  vs  $0.49 \pm 0.1$ ). VMI after five weeks ( $0.34 \pm 0.06$   $p=0.003$ ) and eight weeks of SuHx ( $0.34 \pm 0.06$   $p = 0.002$ ) were significantly higher than normoxic rats ( $0.21 \pm 0.04$ ). (Figure 6-4)

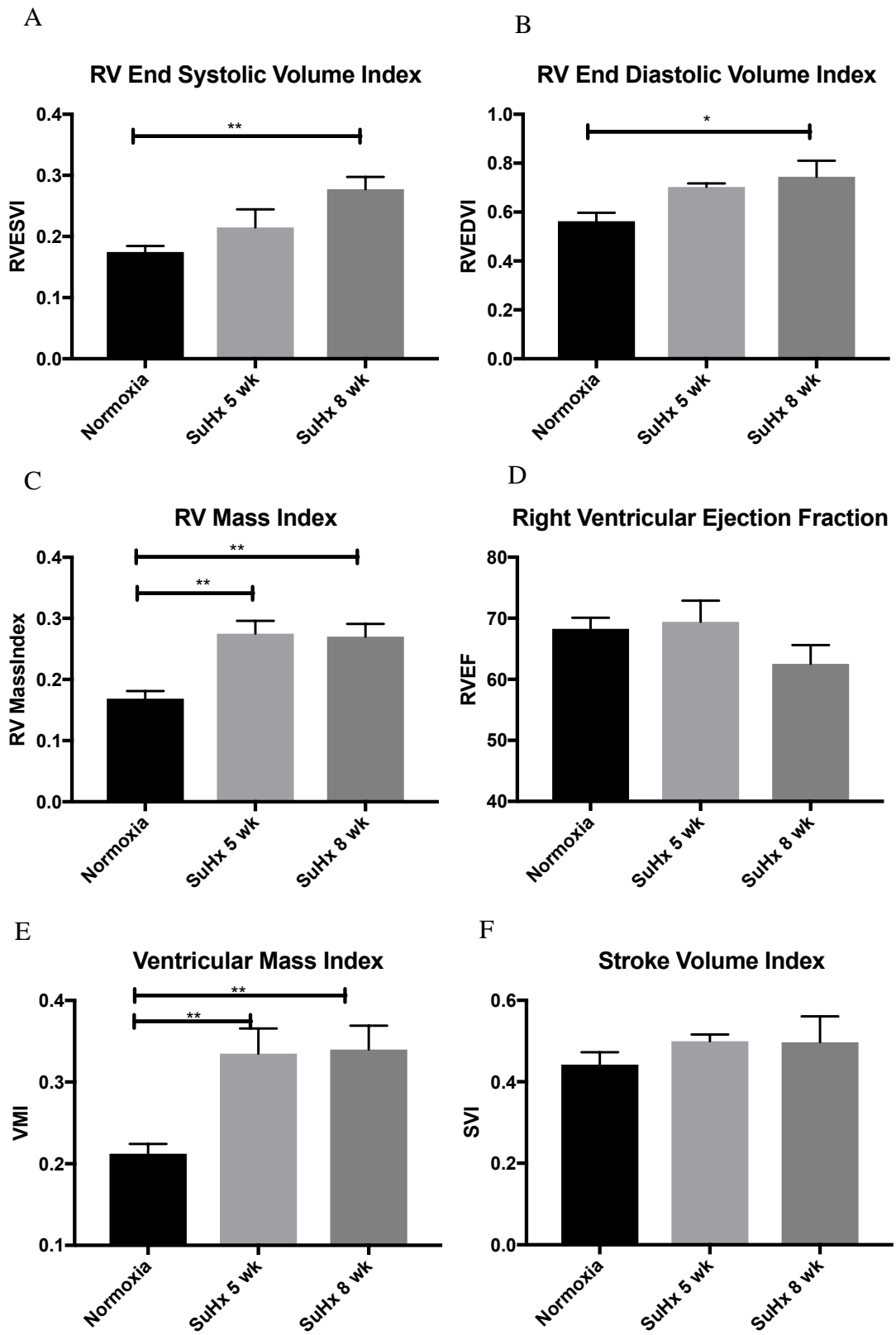


**Figure 6-4 RV end systolic volume index (RVESVI) (A), RV end diastolic volume index (RVEDVI) (B), RV mass index (C), RV ejection fraction (RVEF) (D), Ventricular mass index (VMI) (E) and Stroke volume index (SVI) (F).**

Graphs show comparison in normoxia (n=8), 5 week Sugen hypoxia (n=4) and 8 week Sugen hypoxia (n=4). RV end diastolic and end systolic volumes and RV mass were determined by manual planimetry and indexed to body surface area. RVEF was determined by  $[(RVEDV - RVESV)/RVEDV] \times 100\%$ . A demonstrates progressive increase in RV end systolic volume index during the course of sugen hypoxia, while B demonstrates RV dilatation at eight weeks. RV mass index (C) was significantly increased in 5 week and 8 week Sugen hypoxia compared to normoxic rats. RVEF (D) was preserved however trending towards deterioration at eight weeks. Ventricular mass index (VMI) was calculated as the ratio between RV mass to LV mass. Interventricular septum was considered as part of the LV. VMI maybe an alternative to  $RV/(LV + \text{septum})$  measured at autopsy as discussed. Results demonstrated increased VMI at 5 weeks and 8 weeks of Sugen hypoxia compared to normoxic rats (E). There were no significant differences in stroke volume index (SVI) between normoxia, 5 week Sugen hypoxia and 8 week Sugen hypoxia (F). Results are shown as mean  $\pm$  SEM. The groups were compared by ANOVA and if there was statistical significance a Tukey HSD test was used for post hoc analysis. \* represents  $p < 0.05$  and \*\* represents  $p < 0.01$ .

### 6.3.5 Left ventricle

No differences were observed between the normoxic and SuHx groups (normoxia, 5 and 8 weeks respectively) in terms of LVEDVI ( $0.73 \pm 0.08$  vs  $0.74 \pm 0.06$  vs  $0.75 \pm 0.16$ ), LVESVI ( $0.29 \pm 0.05$  vs  $0.24 \pm 0.04$  vs  $0.25 \pm 0.03$ ), LV mass index ( $0.79 \pm 0.07$  vs  $0.82 \pm 0.09$  vs  $0.8 \pm 0.15$ ) or LVEF ( $60.3 \pm 7.03$  vs  $67.8 \pm 3.16$  vs  $66.5 \pm 3.12$ ). (Figure 6-5)

### 6.3.6 LV eccentricity index (LVEI)

LVEI measured at systole was significantly higher in SuHx rats at five weeks ( $1.2 \pm 0.07$   $p=0.006$ ) and in SuHx rats at eight weeks ( $1.22 \pm 0.14$   $p=0.004$ ) compared to normoxic rats ( $0.98 \pm 0.08$ ). There were no differences between LVEI at diastole between normoxia and SuHx at 5 or 8 weeks ( $1.06 \pm 0.05$  vs  $1.14 \pm 0.04$  vs  $1.1 \pm 0.06$ ). (Figure 6-5)

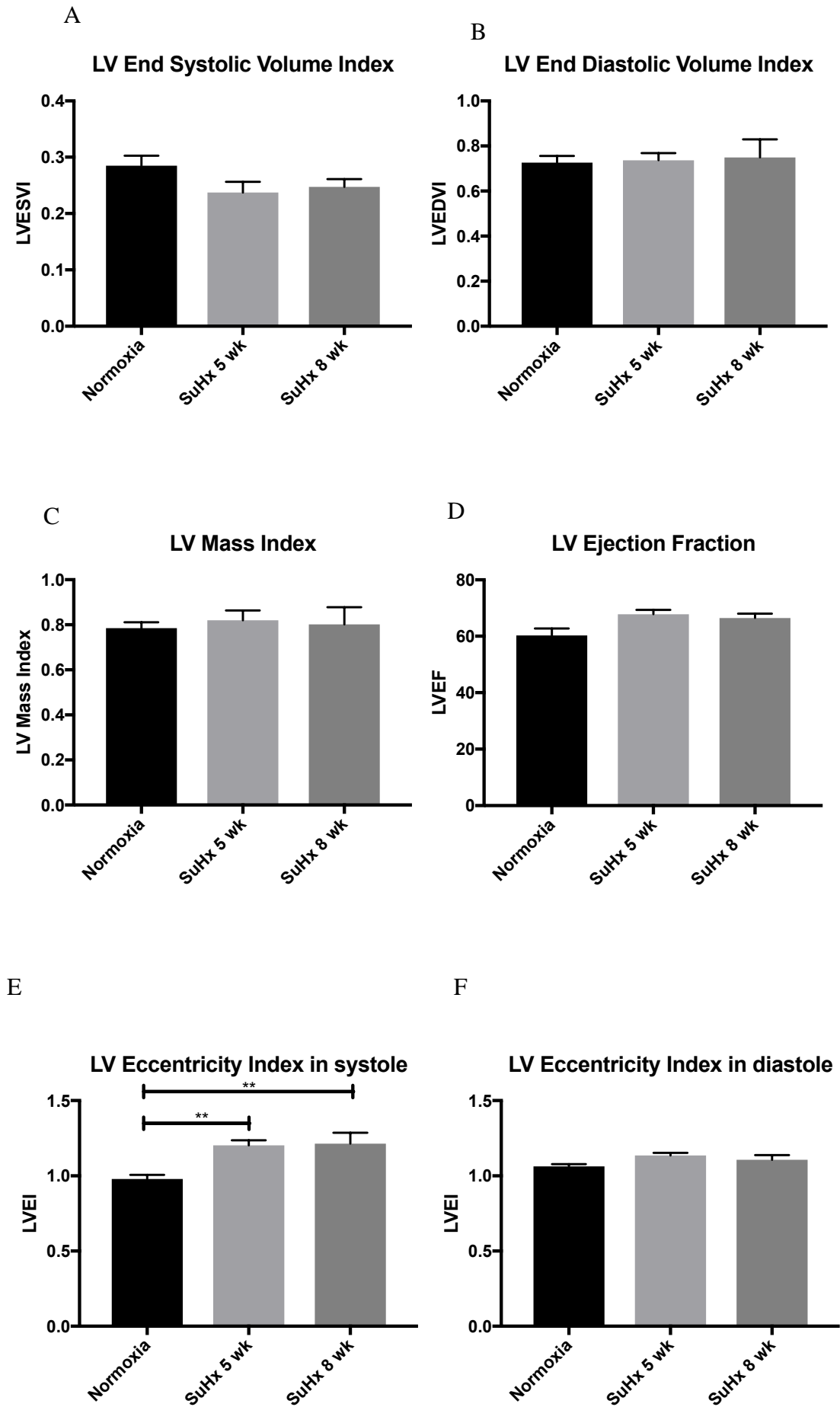


**Figure 6-5** LV end systolic volume index (LVESVI) (A), LV end diastolic volume index (LVEDVI) (B), LV mass index (C), LV ejection fraction (LVEF) (D), LV eccentricity index (LVEI) in systole (E) and LV eccentricity index in diastole (F)

Graphs are shown in normoxia (n=8), Sugen hypoxia at 5 weeks (n=4) and Sugen hypoxia at 8 weeks (n=4). LV end diastolic and end systolic volumes and LV mass were determined by manual planimetry and indexed to body surface area. LVEF was determined by  $[(LVEDV - LVESV)/LVEDV] \times 100\%$ . There were no significant differences between the normoxic group and different stages of sugen hypoxia in LVESVI, LVEDVI, LV mass index and LVEF. Left ventricular eccentricity index (LVEI) was defined as the ratio of the anterior-inferior and septal-posterolateral cavity dimensions at the mid-ventricular level and was measured at both systole (E) and diastole (F). Although there were no significant differences between the three groups in the LVEI in diastole, LVEI was higher in both sugen hypoxic groups compared to normoxia in systole. Previous human studies had demonstrated LVEI in systole to correlate with pulmonary hypertension. The groups were compared by ANOVA and if there was statistical significance a Tukey HSD test was used for post hoc analysis. Results are shown as mean  $\pm$  SEM. \*\* represents  $p < 0.05$ .

### **6.3.7 Autopsy vs CMR in the measurement of RV hypertrophy**

CMR images taken from a normoxic and SuHx animal and light microscopy images of the same animals at autopsy were compared. Although both techniques could visually demonstrate ventricular size and wall thickness (hypertrophy), CMR demonstrated functional aspects of RV contraction including septal flattening and paradoxical septal motion during systole in SuHx animals. Figure 6-6 demonstrates short axis CMR images (A, B and C) and light microscopy images (D and E) of short axis sections of the same rat hearts at autopsy. B and C demonstrates a SuHx animal at the same short axis at diastole (B) and systole (C). The SuHx animal demonstrated a significantly dilated and hypertrophied RV with paradoxical septal motion at systole. There was very good correlation between VMI measured by CMR vs autopsy (Spearman  $r = 0.8328$  95% CI 0.5633 to 0.9422  $p < 0.0001$ ). However, CMR images demonstrate functional aspects of RV contraction including septal flattening and paradoxical septal motion during systole due to RV pressure overload.

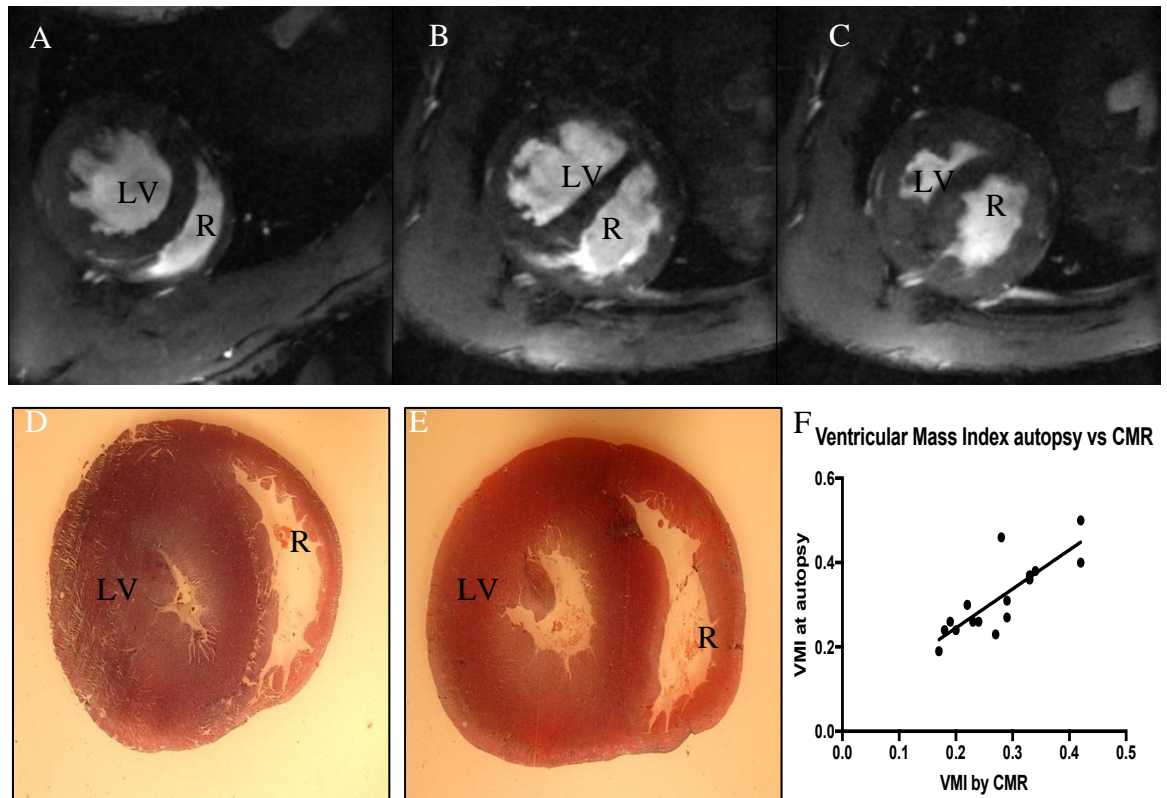


**Figure 6-6 Cardiac MR images (A – C) and light microscopy images (D and E) of short axis sections of rat hearts.**

A and D demonstrate a normoxic rat. B, C and E demonstrate a Sugen hypoxic rat. B and C demonstrates the same animal short axis at diastole (B) and systole (C). F demonstrates the correlation between RV hypertrophy assessed by weighing RV and LV+S at autopsy and by ventricular mass index by CMR in normoxic rats and sugen hypoxic rats. There was very good correlation between VMI measured by CMR vs autopsy (Spearman  $r = 0.8328$ ). However, CMR images demonstrate functional aspects of RV contraction including septal flattening and paradoxical septal motion during systole (C) due to RV pressure overload.

## 6.4 Discussion

To best of our knowledge, this is the first study demonstrating longitudinal biventricular mass, volume and function in a PH animal model using CMR. Previous studies had used echocardiography to examine biventricular function and structure in small animal models of PAH (158). Previous CMR studies used phase contrast imaging but did not explore LV and RV volume and functional variables known to be prognostic in PH, nor look at longitudinal changes (160).

Our study demonstrated the feasibility of CMR in a small animal model of PAH with good spatial and temporal resolution and excellent inter-observer reproducibility. The future advantage of CMR over cardiac catheterization and autopsy is the ability to perform imaging serially on the same animal to look at disease progression and response to treatment without killing the animal.

The main cause of morbidity and mortality in patients with PAH is RV failure. It had been assumed that the cause of RV dysfunction was alterations to the pulmonary vasculature and therefore treatment focus had been centred on improving pulmonary haemodynamics, with the assumption that improvement in RV would follow. However, it is now evident that cardiac response to a given level of pulmonary hemodynamic overload is variable but important in the subsequent prognosis of these patients (95). Although traditionally right heart catheterization and post mortem studies have been used, there is a need for non-invasive tests of RV function in animal models of PAH. In addition, we need to have a better understanding of the longitudinal changes in ventricular function in animal models of PAH. Although the RV is the obvious focus of attention, LV dysfunction can occur through cardiac interaction as I have discussed in previous chapters thus simultaneous evaluation of the LV is important. Echocardiography is widely available and can be used to estimate RVSP, however imaging of the RV with its complex geometry is difficult.

### 6.4.1 The SuHx small animal model – PH

Plexiform lesions in the pulmonary vasculature are known to be the hallmark of PAH and attempts have been made to establish an animal model that closely mimic human disease. The major limitation of other animal models of PH such as chronic hypoxia and the monocrotaline rat model is that they do not develop occlusive neointimal and plexiform lesions that are seen in human disease. The SuHx model has been shown to cause severe PH with the development of plexiform lesions. We used a SuHx model consisting of an injection of Sugen, 2 weeks of hypobaric hypoxia and 3 weeks of normoxia. *Dean et al* explored the effects of Metformin on the development of PH via Aromatase inhibition, a similar SuHx model was used (Sugen + 2 weeks of hypobaric hypoxia and 3 weeks of normoxia)(202). The study demonstrated similar haemodynamics and RV hypertrophy compared to our study population after 8 weeks. In a longitudinal study looking at effects of exercise in a small animal model of PH, SuHx rats (sugen + 3 weeks normobaric hypoxia + normobaric normoxia), underwent echocardiography and RV/ (LV + septum) assessment. Sedentary PH and exercised PH animals had relatively similar RV/ (LV+ septum) ( $0.47 \pm 0.03$  and  $0.47 \pm 0.05$ ) ratio as to our study (203). In a study by *Long et al*, investigating the effects of BMP ligands targeting the BMP2 signalling pathway, using a sugen hypoxia rat model, similar RVSP was observed at 8 weeks from sugen injection, however demonstrating higher RV/ (LV + septum). *Abe et al* investigated the longitudinal hemodynamic and histological changes in the model. At 13 to 14 weeks after Sugen, the rats had very high RVSP ( $96 \pm 11$  vs 21) and severe RV hypertrophy (0.76 at five weeks, 0.74 at 8 weeks and 0.74 at 13-14 weeks)(157). In another study by *Al-Husseini et al* looking at the effects of diethylcarbamazine (DEC) on PH, SuHx rats (sugen + 3 weeks hypobaric hypoxia + 2 weeks normoxia) demonstrated RVSP of around 60 mmHg (204). Our study demonstrated persistent PH as measured by RVSP during right heart catheterisation in the SuHx model. The varying degrees of RVSP and RV hypertrophy in these studies, is likely related to the duration of exposure to hypoxia, however, could also be related to the animal strain, gender and age at exposure.

### 6.4.2 The SuHx small animal model – RV function

In humans with PAH, progressive narrowing of the pulmonary vasculature causes increased load to the RV. The RV adaptation results in increasing wall thickness (hypertrophy) and contractility (coupling). Ventriculo-arterial coupling preserves stroke volume and ventricular efficiency. The RV then dilates, increasing wall stress and oxygen consumption per gram resulting in uncoupling and reduced stroke volume (149). In our study, RV hypertrophy was followed by subsequent dilatation. However, stroke volume and RVEF were relatively preserved. This was despite the presence of persistently elevated RVSP. We believe this study represents the natural history of RV hypertrophy and failure, demonstrating compensated RV hypertrophy (adaptive remodelling) before progression into maladaptive remodelling with further RV dilatation and RV failure, with reduction of RV output.

### 6.4.3 Adaptive vs maladaptive remodelling

*Wang et al* hypothesized that a SuHx mouse model may capture the transition from adaptive to maladaptive RV remodelling including impairment in RV function by studying pressure volume measurements in vivo. The results suggested that RV remodelling may begin to shift from adaptive to maladaptive with increasing duration of SuHx exposure. However, for the duration of SuHx exposure used in their study, no drop in cardiac output was observed (205). Similarly, *Sutendra et al* studied the natural history of RV failure from a compensated RV hypertrophy to decompensated RV hypertrophy in a monocrotaline rat model of PH by serially assessing clinical variables (weight loss, mortality, ascites) (206). We believe that our study demonstrates a period of adaptive remodelling of the RV with compensated hypertrophy with minimal RV dilatation at later stages of the study. By lengthening the exposure to SuHx we may be able to identify the transition from adaptive to maladaptive remodelling and identify decompensated right heart failure in this model. Most patients present to clinical assessment when there are signs of more severe RV dysfunction and in contrast pre-clinical SuHx model demonstrate adaptive remodelling at least early in its disease progression. This is of importance in the design of pre-clinical studies as intervention with experimental therapeutics is likely to occur at this early adaptive stage of disease

progression where RV function/stroke volume seem to be preserved despite the presence of PAH.

#### **6.4.4 Small animal model - LV function**

In PAH, impaired LV performance is explained by series interaction of low RV cardiac output and direct ventricular interaction due to inter-ventricular dyssynchrony and paradoxical septal motion (130, 187). Previous human studies have demonstrated that patients with progressive illness demonstrated LV volume changes compared to stable patients. Previous echocardiography studies have also demonstrated impaired LV strain and torsion in PAH patients (130). We observed preserved LV systolic function with preserved LV mass and volume variables in this small animal model of PAH. Although PAH animals demonstrated paradoxical septal motion of the septum in our study, preserved RV output probably explains the preserved LV function. Further studies are required to study LV mechanics in detail in small animal models of PAH.

### **6.5 Conclusion**

CMR is feasible in a small animal model of PAH and could be used in pre-clinical animal studies to explore bi-ventricular structural and functional changes during the course of illness. It is likely that the SuHx model demonstrates adaptive remodelling to persistently elevated pulmonary pressures which is demonstrable by preserved RV function and stroke volume with hypertrophy of the RV. Further longitudinal studies are required to assess this model in detail, especially focusing on longitudinal RV response. We observed preserved LV systolic function with preserved LV mass and volume variables in this small animal model of PAH. Although PAH animals demonstrated paradoxical septal motion of the septum in our study, preserved RV output probably explains the preserved LV function. The search for better animal models of PH continues because our understanding of the pathobiology of disease and the development of new therapeutic strategies depends on robust animal models, but at present no single model has all the features of human disease.

## 6.6 Limitations

The study assessed rats at 5 and 8 weeks from Sugen exposure, while assessment later may have demonstrated worsened haemodynamics and RV variables mimicking disease presentation in humans. The rats were anaesthetized with Isoflurane, previous studies using halogenated anaesthetics have been shown to impair RV-PA coupling, however these effects were seen both in hypoxia and hyperoxia (207). Future studies with late gadolinium enhancement data will provide further insights into myocardial remodelling in PAH.

# Chapter 7 **General Discussion and Conclusions**

Treatment of pulmonary arterial hypertension has significantly advanced over the recent years. A various combination of drugs as well as surgical and interventional procedures has improved morbidity and survival in patients with PH (10). The hemodynamic diagnosis of PH requires direct measurement of the pulmonary artery pressure by right heart catheterisation. However, right heart catheterisation is an invasive test and does carry a small risk of morbidity and mortality. Diagnostic algorithms have been devised that combines clinical history and examination, cardio- respiratory assessment by non-imaging techniques and subsequently imaging techniques in patients suspected of having PH (7). The aim of these investigations is to establish a probable diagnosis of PH and also to identify the likely underlying aetiology. The initial non-invasive tests provide information regarding disease severity, prognosis and can also be used to assess response to disease modifying treatment. Advancing imaging techniques may also help us to understand mechanisms responsible for the pathophysiology of PH in both the pulmonary circulation and the RV.

As pulmonary hypertension is a disease of the pulmonary vasculature and as the mortality is associated with RV failure, RV has been the widely studied chamber in PH. Although a disease of the pulmonary circulation and the RV, there is now evidence demonstrating LV abnormalities in PH (16, 17). The left atrial volume has been used in identifying patients with HFpEF (18), however whether the left atrial function provides any incremental or addition information regarding cardiac function in patients with PAH is unknown. Pulmonary arterial hypertension is a rare disease and small animal models are increasingly used to identify pathophysiology and therapies for PH with the intention of translating these findings to the human disease (19). So far studies involving small animals have focused on cardiac catheterisation and less frequently echocardiography to monitor disease. Accurate monitoring of disease in rodents with emphasis on ventricular function and with the ability to monitor the disease state without killing the animal is needed.

The overall aim of the thesis was to determine if CMR could be used to address current issues in the assessment of patients with PAH.

## **7.1 Left ventricular strain and intra-ventricular dyssynchrony by CMR in idiopathic pulmonary arterial hypertension**

Traditionally measures of RV volumes and function and LV volumes (especially LV end-diastolic volume) have been variables monitored during follow up of patients with PAH (99). Myocardial strain which is a measure of myocardial deformation and measures of ventricular synchrony both by echocardiography and by CMR have shown to provide incremental prognostic information in various cardiac diseases (181-183).

Although the impact of the RV on LV function is minimal under normal conditions, this does change when it comes to a pressure loaded RV (149). There are both parallel and series interactions of the RV on the LV. In PH, the direct effect of the paradoxical motion and the bowing of the IVS impairs early diastolic filling of the LV. This is due to the prolonged isovolumetric contraction of the RV. The main mechanism appears to be increased RV wall tension; RV contraction continues while the LV is already in its diastolic phase. LV filling is also affected by the low RV cardiac output. There is also the anatomical consideration of RV dilatation with a geometrically restricted pericardial sac. Thus, measures of ventricular interaction and interdependency are extremely useful to assess disease severity as this not only contains information regarding stroke volume but also increasing ventricular wall tension. As mentioned in the introduction, several large studies in the past have shown the prognostic value of LV volume variables in PAH patients.

Chapter 3 explored LV mechanics including longitudinal, circumferential and radial myocardial deformation and LV intra-ventricular synchrony in patients with IPAH to assess the LV mechanics beyond LV volume and function measured by LVEF. CMR-FT was used in this study to assess LV strain and intra-ventricular synchrony with the advantage being that there is no requirement for additional image acquisition or time consuming protocols. In this study patients with IPAH had significant differences in LV strain and demonstrated intra-ventricular dyssynchrony of the LV compared to healthy volunteers. This was despite the conventional measures of LV function i.e., LVEF being normal. Furthermore, IPAH patients with more severe disease demonstrated worse LV strain and LV

dyssynchrony when compared to patients with less severe disease. Interestingly some of these LV markers of myocardial deformation were superior to known RV CMR variables in terms of their ability to reflect disease severity and predict survival. The study concluded that LV strain measurements do provide incremental and additional prognostic information in IPAH probably as they reflect both RV cardiac output and RV wall tension/ septal bowing. The proposed mechanism of impairment of LV mechanics is shown in Figure 7-1.

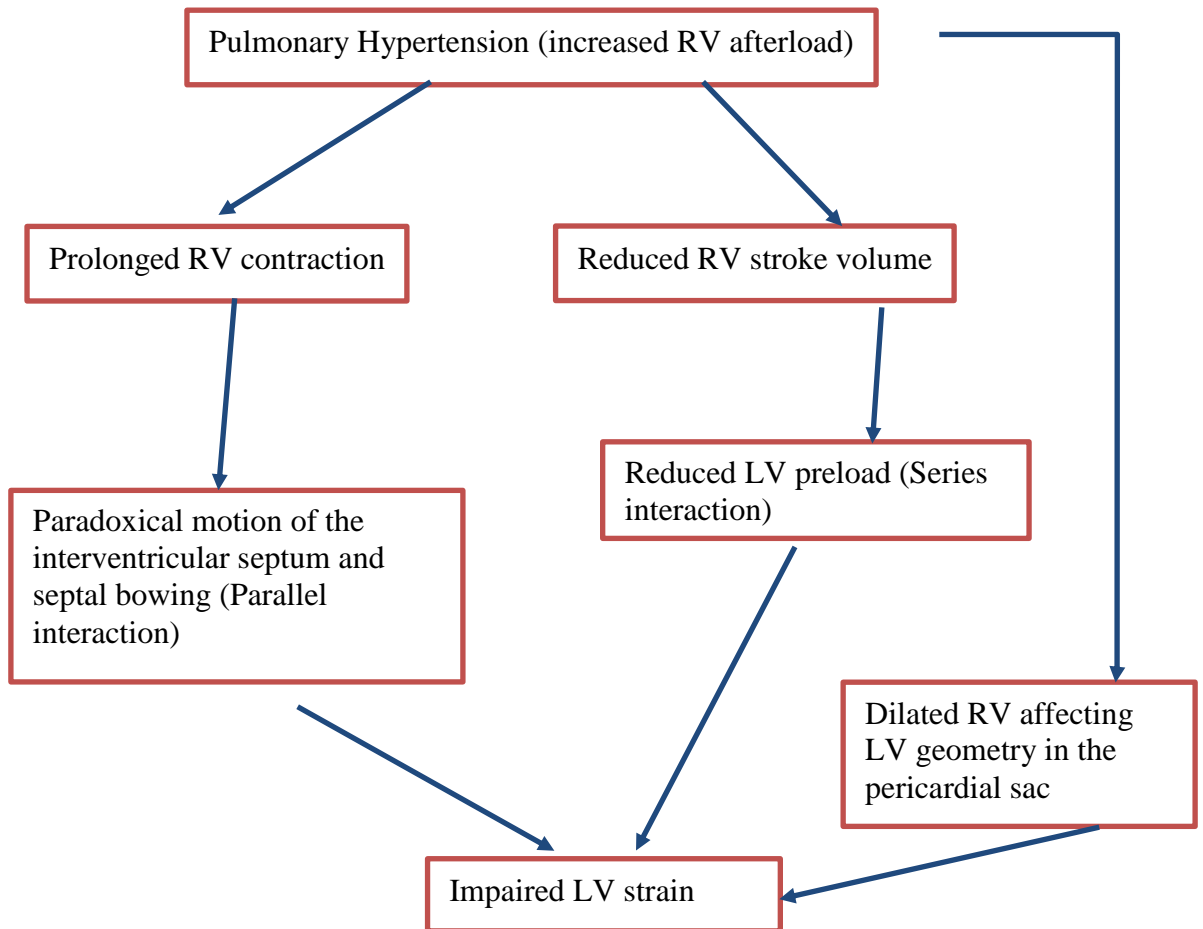


**Figure 7-1 The proposed mechanism of impaired LV mechanics in pulmonary arterial hypertension**

There are both parallel and series interactions of the RV on the LV. In PAH, the direct effect of the paradoxical motion and the bowing of the interventricular septum impairs early diastolic filling of the LV. This is due to the prolonged isovolumetric contraction of the RV. The main mechanism appears to be increased RV wall tension; RV contraction continues while the LV is already in its diastolic phase. LV filling is also affected by the low RV cardiac output. There is also the anatomical consideration of RV dilatation within a geometrically restricted pericardial sac.

## 7.2 Left atrial strain by CMR in idiopathic pulmonary arterial hypertension

Left atrial assessment in PH has been limited to measuring the volume or area of the left atrium. This is to distinguish PAH from HFpEF (18). There is increasing evidence showing LA function assessment providing stronger evidence determining cardiovascular outcomes in patients with left sided heart diseases (195, 197). Although PAH is partly defined by normal LV filling pressures, LV function/performance can be affected as discussed in detail in Chapter 3. Considering the significant interplay that exist between LV and LA, studying LA function will provide further insight into left heart dysfunction in PAH.

Chapter 4 explored LA function assessment in patients with IPAH using CMR-FT. This study demonstrated impaired LA strain indices in patients with IPAH compared to healthy volunteers. The most significantly affected LA index is LA conduit function. LA conduit function is related to atrial compliance, however significantly affected by early LV relaxation / LV compliance. Considering atrial compliance is unlikely to be affected in the absence of intrinsic left heart disease, impaired LA conduit function is likely related to impaired LV relaxation. Early LV relaxation is affected by paradoxical septal motion of the RV during systole and prolonged RV contraction.

LA conduit function, representing passive movement of blood during early diastole, demonstrated significant association with known markers of disease severity, however, LA reservoir function (related to LV preload) did not. LA conduit function was also the index that was significantly affected in the severe disease population compared to mild / intermediate disease. The lack of early LV filling is to a degree compensated by LA booster pump function which is augmented in IPAH patients compared to healthy volunteers. Whether this initial compensatory mechanism subsequently fails and progress into global LA impairment is to be explored. The study concluded that future research is needed to explore the impact of pre-existing medical therapy and mechanical interventions on LV - LA mechanics. Figure 7-2 shows the proposed mechanism of impaired LA mechanics in PAH.

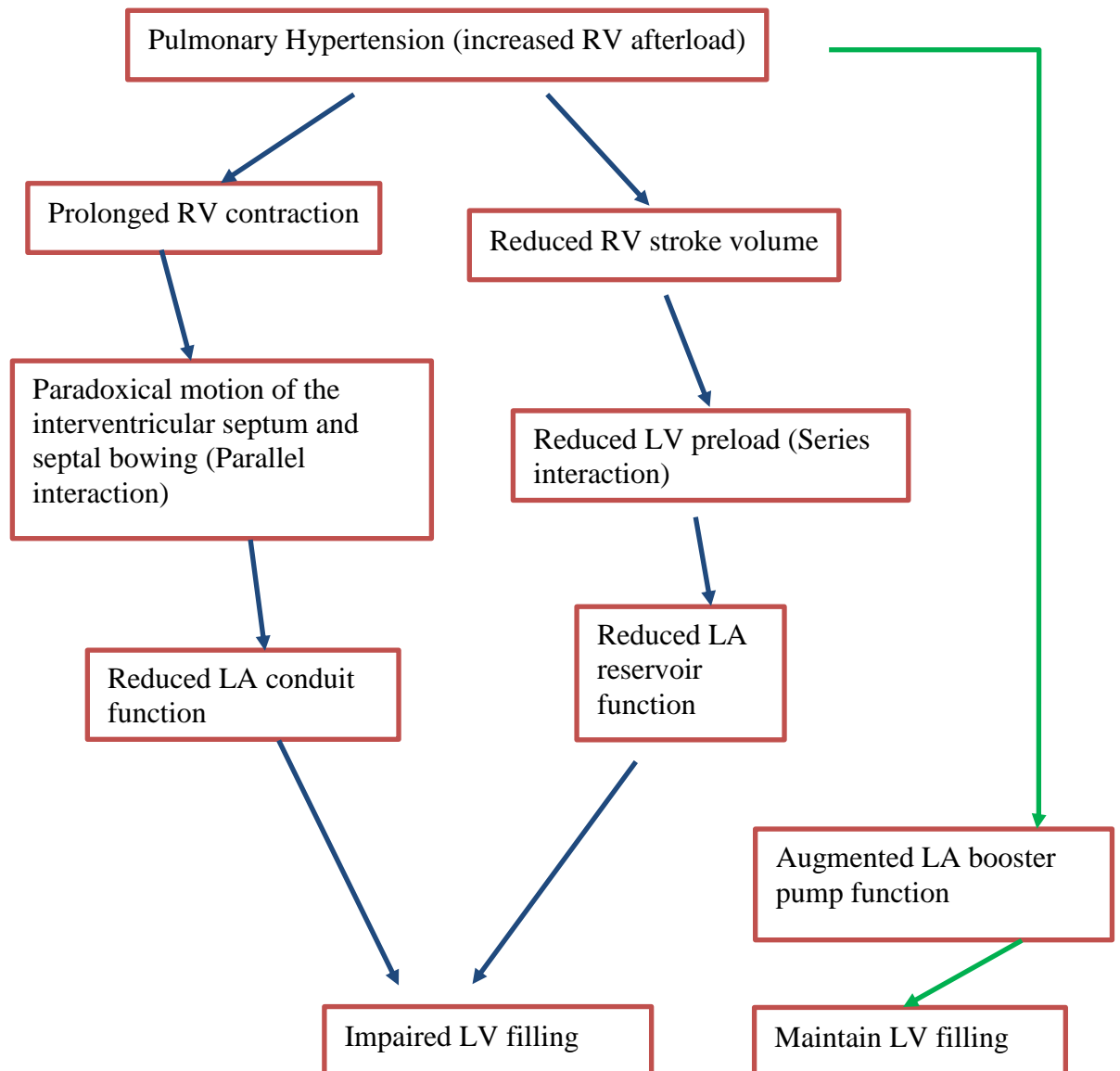


**Figure 7-2 The proposed mechanism of impaired LA mechanics in pulmonary arterial hypertension**

This study demonstrates that the most significantly affected LA index is LA conduit function. LA conduit function is related to atrial compliance, however significantly affected by early LV relaxation / LV compliance. Considering atrial compliance is unlikely to be affected in the absence of intrinsic left heart disease, impaired LA conduit function is likely related to LV relaxation. Early LV relaxation is affected by paradoxical septal motion of the RV during systole and prolonged RV contraction. LA conduit function, representing passive movement of blood during early diastole, demonstrated significant association with known markers of disease severity, however, LA reservoir function (related to LV preload) did not. LA conduit function was also the index that was significantly affected in the severe disease population compared to mild disease. The lack of early LV filling is to a degree compensated by LA booster pump function which is augmented in IPAH patients compared to healthy volunteers although did not reach a statistical significance

### **7.3 Non-invasive measurement of myocardial damage in pulmonary hypertension by CMR**

Recently there has been significant focus on non-invasive myocardial tissue characterisation by CMR. LGE has been the gold standard in determining myocardial fibrosis. Although identification of native T1 times has been used to identify myocardial changes in PH, this has been limited to the need for visual assessment of RV insertion regions as well as due to the failure of the pre-existing AHA segmentation in isolating these for analysis (132, 138).

In Chapter 5, a novel myocardial segmentation to identify T1 changes in PH was introduced. There are a number of reasons to use this novel segmentation rather than the pre-existing AHA segmentation in the focused assessment of patients with PH. Firstly, the pre-existing segmentation fails to isolate the RV insertion points /regions which are the most susceptible to deformation in PH. Secondly, the visual assessment of the insertion regions fails to identify subtle myocardial changes because it requires manual contouring of a region of interest. Finally, myocardial changes may have a prognostic significance in PH, and a methodology that allows longitudinal assessment is required.

In this study, RV insertion region native T1 times were significantly higher in patients with PH compared to symptomatic patients without PH. The study showed that native T1 changes at the RV insertion regions are associated with invasive measurements of disease severity including right atrial pressure, PVR and mixed venous saturations. Raised native T1 was an independent predictor of an increased right ventricular systolic index, suggesting reduced myocardial contractility resulted by changes in myocardial architecture, although the order of the two events isn't clear. It is suggested that the most likely mechanism to be of progressive RV dilatation and reduced RV contractility, shifting the interventricular septum towards the LV, which in turn results in increased stress at the interventricular regions; this leads to changes in myocardial architecture leading to myocardial fibre disarray and fibrosis.

In a small group of patient who had ECV mapping, the findings were consistent with native T1 mapping. This suggest that the RV insertion region changes seen in

native T1 mapping are likely due to myocardial fibrosis. The study concluded that native T1 mapping with the novel myocardial segmentation allows myocardial tissue characterisation and can be used in the longitudinal assessment of PH patients.

The proposed mechanism of native T1 changes at the RV insertion regions in PAH patients is shown in Figure 7-3.

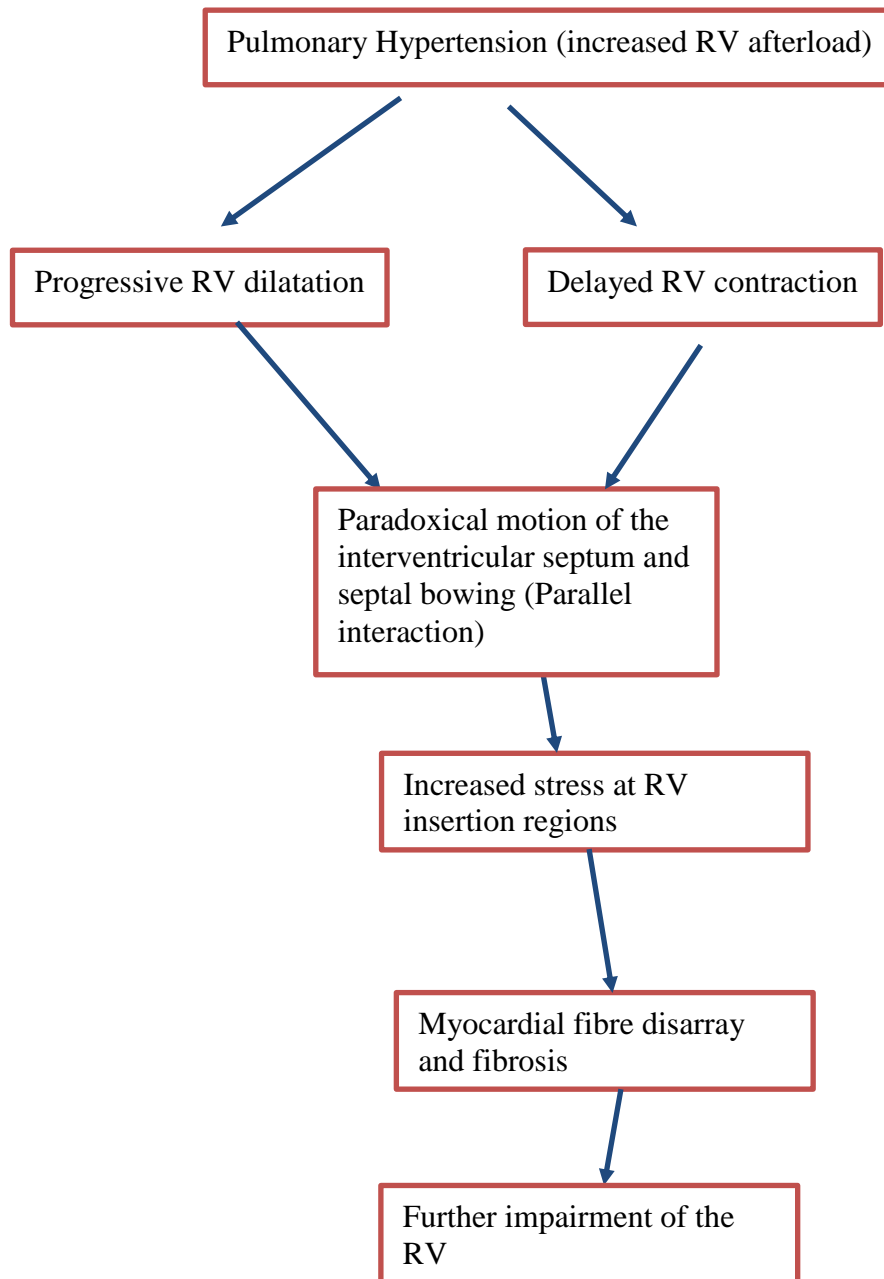


**Figure 7-3 The proposed mechanism of native T1 changes at the RV insertion regions in pulmonary arterial hypertension**

Raised native T1 was an independent predictor of an increased right ventricular systolic index, suggesting reduced myocardial contractility resulted by changes in myocardial architecture, although the order of the two events isn't clear. It is suggested that the most likely mechanism to be of progressive RV dilatation and reduced RV contractility, shifting the interventricular septum towards the LV, which in turn results in increased stress at the interventricular regions; this leads to changes in myocardial architecture leading to myocardial fibre disarray and fibrosis.

## **7.4 Longitudinal cardiac changes by CMR in a sugen-hypoxia small animal model of pulmonary arterial hypertension.**

Finally, we studied the feasibility of CMR in a small animal model of PAH and explored whether this could be used in pre-clinical animal studies to explore bi-ventricular structural and functional changes during the course of illness. We also investigated the suitability of the Sugeng-hypoxia model for translations studies of the mechanism of RV dysfunction and ventricular interdependence in PAH. Based on the findings, it is likely that the Sugeng-hypoxia model demonstrates adaptive remodelling to persistently elevated pulmonary pressures which is demonstrated by preserved RV function and stroke volume with hypertrophy of the RV. The search for better animal models of PH continues because our understanding of the pathobiology of disease and the development of new therapeutic strategies depends on robust animal models, but at present no single model has all the features of human disease.

## **7.5 Future Directions**

Further research is needed to explore the impact of pre-existing medical therapy and mechanical interventions on LV - LA mechanics in patients with PAH. This is of importance as unloading the RV and improving LV preload might induce LV failure. Thus, the impact of pharmaceutical as well as mechanical interventions in PAH patients on the LV mechanics need to be explored in detail in a future study. Both the left heart studies discussed in this thesis were retrospective studies conducted in a heterogeneous population of patients. A multicentre study is required in a carefully selected patient group to confirm the findings in this thesis but also more importantly to identify changes in the LV strain variables with disease progression and treatment.

Non-invasive myocardial tissue characterisation is a unique advantage of CMR over other imaging modalities. Future studies should focus on exploring myocardial mechanics contributing to tissue changes that was seen at RV insertion regions. Although not explored in the study, feature tracking CMR could be used to assess whether LV / RV strain is associated with these changes in the RV insertion regions. Also of interest in a future study would be to identify longitudinal changes that

occur in the RV insertion regions with disease targeted pharmaceutical therapy as well as mechanical interventions.

The advantage of CMR in translational research is the ability to accurately monitor disease in rodents with emphasis on ventricular function and with the ability to monitor the disease state without killing the animal. After peer-reviewed publication of the small animal CMR study, colleagues at the SPVU have since embarked on a study involving small animal CMR and assessing response to disease targeted therapy (170). The study is exploring Macitentan treatment and its impact on the dysfunctional right ventricle in a sugen-hypoxia rat model of pulmonary hypertension using longitudinal repeated CMR in the same animal. It would also be of interest to study LV mechanics (LV strain and dyssynchrony) in animal models of PH to understand the degree of ventricular interaction compared to humans with PH.

## **7.6 Limitations**

I have discussed the limitations of individual studies at the end of each chapter. It is also important to note that it was not possible to perform sex differences analysis in any of the studies performed both in humans and small animals. Considering the importance of the topic, future studies on the subject is warranted.

## **7.7 Final comment**

Non-invasive imaging provides information regarding disease severity, prognosis and can also be used to assess response to disease modifying treatment in PH. Advancing imaging techniques may also help us to understand mechanisms responsible for the pathophysiology of PH in both the pulmonary circulation and the RV. However, focus in this thesis was on measures of ventricular interaction and interdependency that are extremely useful to assess disease severity and prognosis in PH. The search for better animal models of PH continues because our understanding of the pathobiology of disease and the development of new therapeutic strategies depends on robust animal models.



1. Badesch DB, Champion HC, Sanchez MA, Hoeper MM, Loyd JE, Manes A, et al. Diagnosis and assessment of pulmonary arterial hypertension. *Journal of the American College of Cardiology*. 2009;54(1 Suppl):S55-66.
2. Hoeper MM, Humbert M. The new haemodynamic definition of pulmonary hypertension: evidence prevails, finally! *Eur Respir J*. 2019;53(3).
3. Simonneau G, Montani D, Celermajer DS, Denton CP, Gatzoulis MA, Krowka M, et al. Haemodynamic definitions and updated clinical classification of pulmonary hypertension. *Eur Respir J*. 2019;53(1).
4. Dresdale DT, Schultz M, Michtom RJ. Primary pulmonary hypertension. I. Clinical and hemodynamic study. *Am J Med*. 1951;11(6):686-705.
5. Barst RJ. Pulmonary hypertension: past, present and future. *Ann Thorac Med*. 2008;3(1):1-4.
6. Hatano S ST, World Health Organization. . Primary pulmonary hypertension: report on a WHO meeting, Geneva, 15-17 October 1973. World Health Organization; 1975.
7. Hoeper MM, Bogaard HJ, Condliffe R, Frantz R, Khanna D, Kurzyna M, et al. Definitions and diagnosis of pulmonary hypertension. *Journal of the American College of Cardiology*. 2013;62(25 Suppl):D42-50.
8. Kovacs G, Berghold A, Scheidl S, Olschewski H. Pulmonary arterial pressure during rest and exercise in healthy subjects: a systematic review. *Eur Respir J*. 2009;34(4):888-94.
9. Kiely DG, Doyle O, Drage E, Jenner H, Salvatelli V, Daniels FA, et al. Utilising artificial intelligence to determine patients at risk of a rare disease: idiopathic pulmonary arterial hypertension. *Pulm Circ*. 2019;9(4):2045894019890549.
10. Gaine S, McLaughlin V. Pulmonary arterial hypertension: tailoring treatment to risk in the current era. *Eur Respir Rev*. 2017;26(146).
11. Jenkins D, Madani M, Fadel E, D'Armini AM, Mayer E. Pulmonary endarterectomy in the management of chronic thromboembolic pulmonary hypertension. *Eur Respir Rev*. 2017;26(143).
12. Ghofrani HA, D'Armini AM, Grimminger F, Hoeper MM, Jansa P, Kim NH, et al. Riociguat for the treatment of chronic thromboembolic pulmonary hypertension. *N Engl J Med*. 2013;369(4):319-29.
13. Lang I, Meyer BC, Ogo T, Matsubara H, Kurzyna M, Ghofrani HA, et al. Balloon pulmonary angioplasty in chronic thromboembolic pulmonary hypertension. *Eur Respir Rev*. 2017;26(143).
14. Hoeper MM, Lee SH, Voswinckel R, Palazzini M, Jais X, Marinelli A, et al. Complications of right heart catheterization procedures in patients with pulmonary hypertension in experienced centers. *Journal of the American College of Cardiology*. 2006;48(12):2546-52.
15. Crowe T, Jayasekera G, Peacock AJ. Non-invasive imaging of global and regional cardiac function in pulmonary hypertension. *Pulm Circ*. 2018;8(1):2045893217742000.
16. Gan C, Lankhaar JW, Marcus JT, Westerhof N, Marques KM, Bronzwaer JG, et al. Impaired left ventricular filling due to right-to-left ventricular interaction in patients with pulmonary arterial hypertension. *Am J Physiol Heart Circ Physiol*. 2006;290(4):H1528-33.
17. Manders E, Bogaard HJ, Handoko ML, van de Veerdonk MC, Keogh A, Westerhof N, et al. Contractile dysfunction of left ventricular cardiomyocytes

in patients with pulmonary arterial hypertension. *Journal of the American College of Cardiology*. 2014;64(1):28-37.

18. Crawley SF, Johnson MK, Dargie HJ, Peacock AJ. LA volume by CMR distinguishes idiopathic from pulmonary hypertension due to HFpEF. *JACC Cardiovasc Imaging*. 2013;6(10):1120-1.
19. Maarman G, Lecour S, Butrous G, Thienemann F, Sliwa K. A comprehensive review: the evolution of animal models in pulmonary hypertension research; are we there yet? *Pulm Circ*. 2013;3(4):739-56.
20. Zenker G, Forche G, Harnoncourt K. Two-dimensional echocardiography using a subcostal approach in patients with COPD. *Chest*. 1985;88(5):722-5.
21. Danchin N, Cornette A, Henriquez A, Godenir JP, Ethevenot G, Polu JM, et al. Two-dimensional echocardiographic assessment of the right ventricle in patients with chronic obstructive lung disease. *Chest*. 1987;92(2):229-33.
22. Shimada R, Takeshita A, Nakamura M. Noninvasive assessment of right ventricular systolic pressure in atrial septal defect: analysis of the end-systolic configuration of the ventricular septum by two-dimensional echocardiography. *The American journal of cardiology*. 1984;53(8):1117-23.
23. Ryan T, Petrovic O, Dillon JC, Feigenbaum H, Conley MJ, Armstrong WF. An echocardiographic index for separation of right ventricular volume and pressure overload. *Journal of the American College of Cardiology*. 1985;5(4):918-27.
24. Jayasekera GPA. *Advanced Imaging in Pulmonary Hypertension. Pulmonary Hypertension: Basic science to clinical medicine*. 2015.
25. Nakao S, Come PC, McKay RG, Ransil BJ. Effects of positional changes on inferior vena caval size and dynamics and correlations with right-sided cardiac pressure. *The American journal of cardiology*. 1987;59(1):125-32.
26. Kircher BJ, Himelman RB, Schiller NB. Noninvasive estimation of right atrial pressure from the inspiratory collapse of the inferior vena cava. *The American journal of cardiology*. 1990;66(4):493-6.
27. Aessopos A, Farmakis D, Taktikou H, Loukopoulos D. Doppler-determined peak systolic tricuspid pressure gradient in persons with normal pulmonary function and tricuspid regurgitation. *Journal of the American Society of Echocardiography : official publication of the American Society of Echocardiography*. 2000;13(7):645-9.
28. McQuillan BM, Picard MH, Leavitt M, Weyman AE. Clinical correlates and reference intervals for pulmonary artery systolic pressure among echocardiographically normal subjects. *Circulation*. 2001;104(23):2797-802.
29. Syyed R, Reeves JT, Welsh D, Raeside D, Johnson MK, Peacock AJ. The relationship between the components of pulmonary artery pressure remains constant under all conditions in both health and disease. *Chest*. 2008;133(3):633-9.
30. Galie N, Humbert M, Vachiery JL, Gibbs S, Lang I, Torbicki A, et al. 2015 ESC/ERS Guidelines for the diagnosis and treatment of pulmonary hypertension: The Joint Task Force for the Diagnosis and Treatment of Pulmonary Hypertension of the European Society of Cardiology (ESC) and the European Respiratory Society (ERS): Endorsed by: Association for European Paediatric and Congenital Cardiology (AEPC), International Society for Heart and Lung Transplantation (ISHLT). *Eur Respir J*. 2015;46(4):903-75.
31. Kitabatake A, Inoue M, Asao M, Masuyama T, Tanouchi J, Morita T, et al. Noninvasive evaluation of pulmonary hypertension by a pulsed Doppler technique. *Circulation*. 1983;68(2):302-9.

32. Isobe M, Yazaki Y, Takaku F, Koizumi K, Hara K, Tsuneyoshi H, et al. Prediction of pulmonary arterial pressure in adults by pulsed Doppler echocardiography. *The American journal of cardiology*. 1986;57(4):316-21.
33. Matsuda M, Sekiguchi T, Sugishita Y, Kuwako K, Iida K, Ito I. Reliability of non-invasive estimates of pulmonary hypertension by pulsed Doppler echocardiography. *British heart journal*. 1986;56(2):158-64.
34. Gardin JM, Davidson DM, Rohan MK, Butman S, Knoll M, Garcia R, et al. Relationship between age, body size, gender, and blood pressure and Doppler flow measurements in the aorta and pulmonary artery. *American heart journal*. 1987;113(1):101-9.
35. Torbicki A, Kurzyna M, Ciurzynski M, Pruszczyk P, Pacho R, Kuch-Wocial A, et al. Proximal pulmonary emboli modify right ventricular ejection pattern. *Eur Respir J*. 1999;13(3):616-21.
36. Raymond RJ, Hinderliter AL, Willis PW, Ralph D, Caldwell EJ, Williams W, et al. Echocardiographic predictors of adverse outcomes in primary pulmonary hypertension. *Journal of the American College of Cardiology*. 2002;39(7):1214-9.
37. Tei C, Dujardin KS, Hodge DO, Bailey KR, McGoon MD, Tajik AJ, et al. Doppler echocardiographic index for assessment of global right ventricular function. *Journal of the American Society of Echocardiography : official publication of the American Society of Echocardiography*. 1996;9(6):838-47.
38. Cheung MM, Smallhorn JF, Redington AN, Vogel M. The effects of changes in loading conditions and modulation of inotropic state on the myocardial performance index: comparison with conductance catheter measurements. *European heart journal*. 2004;25(24):2238-42.
39. Kaul S, Tei C, Hopkins JM, Shah PM. Assessment of right ventricular function using two-dimensional echocardiography. *American heart journal*. 1984;107(3):526-31.
40. Karatasakis GT, Karagounis LA, Kalyvas PA, Manginas A, Athanassopoulos GD, Aggelakas SA, et al. Prognostic significance of echocardiographically estimated right ventricular shortening in advanced heart failure. *The American journal of cardiology*. 1998;82(3):329-34.
41. Forfia PR, Fisher MR, Mathai SC, Houston-Harris T, Hemnes AR, Borlaug BA, et al. Tricuspid annular displacement predicts survival in pulmonary hypertension. *American journal of respiratory and critical care medicine*. 2006;174(9):1034-41.
42. Ghio S, Klersy C, Magrini G, D'Armini AM, Scelsi L, Raineri C, et al. Prognostic relevance of the echocardiographic assessment of right ventricular function in patients with idiopathic pulmonary arterial hypertension. *International journal of cardiology*. 2010;140(3):272-8.
43. Augustine DX, Coates-Bradshaw LD, Willis J, Harkness A, Ring L, Grapsa J, et al. Echocardiographic assessment of pulmonary hypertension: a guideline protocol from the British Society of Echocardiography. *Echo Res Pract*. 2018;5(3):G11-G24.
44. Grapsa J, O'Regan DP, Pavlopoulos H, Durighel G, Dawson D, Nihoyannopoulos P. Right ventricular remodelling in pulmonary arterial hypertension with three-dimensional echocardiography: comparison with cardiac magnetic resonance imaging. *European journal of echocardiography : the journal of the Working Group on Echocardiography of the European Society of Cardiology*. 2010;11(1):64-73.
45. Bhave NM, Patel AR, Weinert L, Yamat M, Freed BH, Mor-Avi V, et al. Three-dimensional modeling of the right ventricle from two-dimensional

- transthoracic echocardiographic images: utility of knowledge-based reconstruction in pulmonary arterial hypertension. *Journal of the American Society of Echocardiography : official publication of the American Society of Echocardiography*. 2013;26(8):860-7.
46. Ascha M, Renapurkar RD, Tonelli AR. A review of imaging modalities in pulmonary hypertension. *Ann Thorac Med*. 2017;12(2):61-73.
  47. Chang CH. The normal roentgenographic measurement of the right descending pulmonary artery in 1,085 cases and its clinical application. II. Clinical application of the measurement of the right descending pulmonary artery in the radiological diagnosis of pulmonary hypertensions from various causes. *Nagoya journal of medical science*. 1965;28(1):67-80.
  48. Kanemoto N, Furuya H, Etoh T, Sasamoto H, Matsuyama S. Chest roentgenograms in primary pulmonary hypertension. *Chest*. 1979;76(1):45-9.
  49. Lupi HE, Horwitz S, Tejada VM, Dumont C, Galland F. [Indications and radiological measurements in the evaluation of pulmonary artery hypertension]. *Archivos del Instituto de Cardiologia de Mexico*. 1975;45(1):34-42.
  50. Aaron RS, Escher DW, Schwedel JB, Young D. The roentgenologic diagnosis of pulmonary hypertension in mitral stenosis. *American heart journal*. 1957;53(2):163-70.
  51. Arnould P, Pernot C, Simon A. [Pulmonary arterial hypertension & pneumonectomy; significance of preoperative occlusion of the pulmonary artery]. *Revue medicale de Nancy*. 1958;83:895-907.
  52. Chang CH. Roentgenographic correlation in pulmonary venous hypertension. Prediction of pulmonary venous pressure from plain chest films. *Nihon Igaku Hoshasen Gakkai zasshi Nippon acta radiologica*. 1968;28(9):1222-31.
  53. Woodruff WW, 3rd, Hoeck BE, Chitwood WR, Jr., Lyerly HK, Sabiston DC, Jr., Chen JT. Radiographic findings in pulmonary hypertension from unresolved embolism. *AJR American journal of roentgenology*. 1985;144(4):681-6.
  54. Tilkian AG, Schroeder JS, Robin ED. Chronic thromboembolic occlusion of main pulmonary artery or primary branches. Case report and review of the literature. *Am J Med*. 1976;60(4):563-70.
  55. Moser KM, Spragg RG, Utley J, Daily PO. Chronic thrombotic obstruction of major pulmonary arteries. Results of thromboendarterectomy in 15 patients. *Annals of internal medicine*. 1983;99(3):299-304.
  56. Benotti JR, Ockene IS, Alpert JS, Dalen JE. The clinical profile of unresolved pulmonary embolism. *Chest*. 1983;84(6):669-78.
  57. Tunariu N, Gibbs SJ, Win Z, Gin-Sing W, Graham A, Gishen P, et al. Ventilation-perfusion scintigraphy is more sensitive than multidetector CTPA in detecting chronic thromboembolic pulmonary disease as a treatable cause of pulmonary hypertension. *J Nucl Med*. 2007;48(5):680-4.
  58. Gopalan D, Delcroix M, Held M. Diagnosis of chronic thromboembolic pulmonary hypertension. *Eur Respir Rev*. 2017;26(143).
  59. Worsley DF, Palevsky HI, Alavi A. Ventilation-perfusion lung scanning in the evaluation of pulmonary hypertension. *J Nucl Med*. 1994;35(5):793-6.
  60. Dion J, Terrier B, Jais X, Mehdaoui A, Sattler C, Amar D, et al. Atypical vasculitis mimicking chronic thromboembolic pulmonary hypertension. *Am J Med*. 2015;128(10):e47-9.
  61. Bowman AW, Albers BK, Jain MK. Acquired Whole-lung Mismatched Perfusion Defects on Pulmonary Ventilation/Perfusion Scintigraphy. *Indian J Nucl Med*. 2018;33(4):312-6.

62. Moguillansky NI, Verma N, Shah P, Knapik J, Mohammed TL. Pulmonary artery sarcoma: Case report and review of the literature. *Respir Med Case Rep.* 2019;27:100857.
63. Bailey CL, Channick RN, Auger WR, Fedullo PF, Kerr KM, Yung GL, et al. "High probability" perfusion lung scans in pulmonary venoocclusive disease. *American journal of respiratory and critical care medicine.* 2000;162(5):1974-8.
64. Pitton MB, Kemmerich G, Herber S, Schweden F, Mayer E, Thelen M. [Chronic thromboembolic pulmonary hypertension: diagnostic impact of Multislice-CT and selective Pulmonary-DSA]. *Rofo.* 2002;174(4):474-9.
65. Soler X, Kerr KM, Marsh JJ, Renner JW, Hoh CK, Test VJ, et al. Pilot study comparing SPECT perfusion scintigraphy with CT pulmonary angiography in chronic thromboembolic pulmonary hypertension. *Respirology.* 2012;17(1):180-4.
66. Kiely DG, Levin D, Hassoun P, Ivy DD, Jone PN, Bwika J, et al. EXPRESS: Statement on imaging and pulmonary hypertension from the Pulmonary Vascular Research Institute (PVRI). *Pulm Circ.* 2019;2045894019841990.
67. Kuriyama K, Gamsu G, Stern RG, Cann CE, Herfkens RJ, Brundage BH. CT-determined pulmonary artery diameters in predicting pulmonary hypertension. *Invest Radiol.* 1984;19(1):16-22.
68. Ng CS, Wells AU, Padley SP. A CT sign of chronic pulmonary arterial hypertension: the ratio of main pulmonary artery to aortic diameter. *J Thorac Imaging.* 1999;14(4):270-8.
69. Mahammedi A, Oshmyansky A, Hassoun PM, Thiemann DR, Siegelman SS. Pulmonary artery measurements in pulmonary hypertension: the role of computed tomography. *J Thorac Imaging.* 2013;28(2):96-103.
70. Truong QA, Massaro JM, Rogers IS, Mahabadi AA, Kriegel MF, Fox CS, et al. Reference values for normal pulmonary artery dimensions by noncontrast cardiac computed tomography: the Framingham Heart Study. *Circ Cardiovasc Imaging.* 2012;5(1):147-54.
71. Tan RT, Kuzo R, Goodman LR, Siegel R, Haasler GB, Presberg KW. Utility of CT scan evaluation for predicting pulmonary hypertension in patients with parenchymal lung disease. *Medical College of Wisconsin Lung Transplant Group. Chest.* 1998;113(5):1250-6.
72. Perloff JK, Hart EM, Greaves SM, Miner PD, Child JS. Proximal pulmonary arterial and intrapulmonary radiologic features of Eisenmenger syndrome and primary pulmonary hypertension. *The American journal of cardiology.* 2003;92(2):182-7.
73. Shimizu H, Tanabe N, Terada J, Masuda M, Sakao S, Kasahara Y, et al. Dilatation of bronchial arteries correlates with extent of central disease in patients with chronic thromboembolic pulmonary hypertension. *Circulation journal : official journal of the Japanese Circulation Society.* 2008;72(7):1136-41.
74. Hoey ET, Gopalan D, Agrawal SK, Screatton NJ. Cardiac causes of pulmonary arterial hypertension: assessment with multidetector CT. *European radiology.* 2009;19(11):2557-68.
75. Rajaram S, Swift AJ, Condliffe R, Johns C, Elliot CA, Hill C, et al. CT features of pulmonary arterial hypertension and its major subtypes: a systematic CT evaluation of 292 patients from the ASPIRE Registry. *Thorax.* 2015;70(4):382-7.
76. Swift AJ, Dwivedi K, Johns C, Garg P, Chin M, Currie BJ, et al. Diagnostic accuracy of CT pulmonary angiography in suspected pulmonary hypertension. *European radiology.* 2020.

77. Groves AM, Win T, Charman SC, Wisbey C, Pepke-Zaba J, Coulden RA. Semi-quantitative assessment of tricuspid regurgitation on contrast-enhanced multidetector CT. *Clinical radiology*. 2004;59(8):715-9.
78. Yeh BM, Kurzman P, Foster E, Qayyum A, Joe B, Coakley F. Clinical relevance of retrograde inferior vena cava or hepatic vein opacification during contrast-enhanced CT. *AJR American journal of roentgenology*. 2004;183(5):1227-32.
79. Hinderliter AL, Willis PWT, Long W, Clarke WR, Ralph D, Caldwell EJ, et al. Frequency and prognostic significance of pericardial effusion in primary pulmonary hypertension. PPH Study Group. *Primary pulmonary hypertension. The American journal of cardiology*. 1999;84(4):481-4, A10.
80. Sherrick AD, Swensen SJ, Hartman TE. Mosaic pattern of lung attenuation on CT scans: frequency among patients with pulmonary artery hypertension of different causes. *AJR American journal of roentgenology*. 1997;169(1):79-82.
81. Arakawa H, Stern EJ, Nakamoto T, Fujioka M, Kaneko N, Harasawa H. Chronic pulmonary thromboembolism. Air trapping on computed tomography and correlation with pulmonary function tests. *Journal of computer assisted tomography*. 2003;27(5):735-42.
82. Remy-Jardin M, Remy J, Louveigny S, Artaud D, Deschildre F, Duhamel A. Airway changes in chronic pulmonary embolism: CT findings in 33 patients. *Radiology*. 1997;203(2):355-60.
83. Nishiyama KH, Saboo SS, Tanabe Y, Jasinowodolinski D, Landay MJ, Kay FU. Chronic pulmonary embolism: diagnosis. *Cardiovasc Diagn Ther*. 2018;8(3):253-71.
84. Willeminck MJ, van Es HW, Koobs L, Morshuis WJ, Snijder RJ, van Heesewijk JP. CT evaluation of chronic thromboembolic pulmonary hypertension. *Clinical radiology*. 2012;67(3):277-85.
85. Bergin CJ, Sirlin C, Deutsch R, Fedullo P, Hauschildt J, Huynh T, et al. Predictors of patient response to pulmonary thromboendarterectomy. *AJR American journal of roentgenology*. 2000;174(2):509-15.
86. Swensen SJ, Tashjian JH, Myers JL, Engeler CE, Patz EF, Edwards WD, et al. Pulmonary venoocclusive disease: CT findings in eight patients. *AJR American journal of roentgenology*. 1996;167(4):937-40.
87. Resten A, Maitre S, Humbert M, Rabiller A, Sitbon O, Capron F, et al. Pulmonary hypertension: CT of the chest in pulmonary venoocclusive disease. *AJR American journal of roentgenology*. 2004;183(1):65-70.
88. Grothues F, Moon JC, Bellenger NG, Smith GS, Klein HU, Pennell DJ. Interstudy reproducibility of right ventricular volumes, function, and mass with cardiovascular magnetic resonance. *American heart journal*. 2004;147(2):218-23.
89. Semelka RC, Tomei E, Wagner S, Mayo J, Caputo G, O'Sullivan M, et al. Interstudy reproducibility of dimensional and functional measurements between cine magnetic resonance studies in the morphologically abnormal left ventricle. *American heart journal*. 1990;119(6):1367-73.
90. Beerbaum P, Korperich H, Barth P, Esdorn H, Gieseke J, Meyer H. Noninvasive quantification of left-to-right shunt in pediatric patients: phase-contrast cine magnetic resonance imaging compared with invasive oximetry. *Circulation*. 2001;103(20):2476-82.
91. van Wolferen SA, Marcus JT, Boonstra A, Marques KM, Bronzwaer JG, Spreeuwenberg MD, et al. Prognostic value of right ventricular mass,

- volume, and function in idiopathic pulmonary arterial hypertension. *European heart journal*. 2007;28(10):1250-7.
92. Vonk-Noordegraaf A, van Wolferen SA, Marcus JT, Boonstra A, Postmus PE, Peeters JW, et al. Noninvasive assessment and monitoring of the pulmonary circulation. *Eur Respir J*. 2005;25(4):758-66.
  93. Campo A, Mathai SC, Le Pavec J, Zaiman AL, Hummers LK, Boyce D, et al. Hemodynamic predictors of survival in scleroderma-related pulmonary arterial hypertension. *American journal of respiratory and critical care medicine*. 2010;182(2):252-60.
  94. van Wolferen SA, van de Veerdonk MC, Mauritz GJ, Jacobs W, Marcus JT, Marques KM, et al. Clinically significant change in stroke volume in pulmonary hypertension. *Chest*. 2011;139(5):1003-9.
  95. van de Veerdonk MC, Kind T, Marcus JT, Mauritz GJ, Heymans MW, Bogaard HJ, et al. Progressive right ventricular dysfunction in patients with pulmonary arterial hypertension responding to therapy. *Journal of the American College of Cardiology*. 2011;58(24):2511-9.
  96. Yamada Y, Okuda S, Kataoka M, Tanimoto A, Tamura Y, Abe T, et al. Prognostic value of cardiac magnetic resonance imaging for idiopathic pulmonary arterial hypertension before initiating intravenous prostacyclin therapy. *Circulation journal : official journal of the Japanese Circulation Society*. 2012;76(7):1737-43.
  97. Swift AJ, Capener D, Johns C, Hamilton N, Rothman A, Elliot C, et al. Magnetic Resonance Imaging in the Prognostic Evaluation of Patients with Pulmonary Arterial Hypertension. *American journal of respiratory and critical care medicine*. 2017.
  98. Mauritz GJ, Kind T, Marcus JT, Bogaard HJ, van de Veerdonk M, Postmus PE, et al. Progressive changes in right ventricular geometric shortening and long-term survival in pulmonary arterial hypertension. *Chest*. 2012;141(4):935-43.
  99. Peacock AJ, Crawley S, McLure L, Blyth K, Vizza CD, Poscia R, et al. Changes in right ventricular function measured by cardiac magnetic resonance imaging in patients receiving pulmonary arterial hypertension-targeted therapy: the EURO-MR study. *Circ Cardiovasc Imaging*. 2014;7(1):107-14.
  100. Sanz J, Kuschnir P, Rius T, Salguero R, Sulica R, Einstein AJ, et al. Pulmonary arterial hypertension: noninvasive detection with phase-contrast MR imaging. *Radiology*. 2007;243(1):70-9.
  101. Mousseaux E, Tasu JP, Jolivet O, Simonneau G, Bittoun J, Gaux JC. Pulmonary arterial resistance: noninvasive measurement with indexes of pulmonary flow estimated at velocity-encoded MR imaging--preliminary experience. *Radiology*. 1999;212(3):896-902.
  102. Helderma F, Mauritz GJ, Andringa KE, Vonk-Noordegraaf A, Marcus JT. Early onset of retrograde flow in the main pulmonary artery is a characteristic of pulmonary arterial hypertension. *J Magn Reson Imaging*. 2011;33(6):1362-8.
  103. Sanz J, Kariisa M, Dellegrottaglie S, Prat-Gonzalez S, Garcia MJ, Fuster V, et al. Evaluation of pulmonary artery stiffness in pulmonary hypertension with cardiac magnetic resonance. *JACC Cardiovasc Imaging*. 2009;2(3):286-95.
  104. Brewis MJ, Bellofiore A, Vanderpool RR, Chesler NC, Johnson MK, Naeije R, et al. Imaging right ventricular function to predict outcome in pulmonary arterial hypertension. *International journal of cardiology*. 2016;218:206-11.

105. Guazzi M, Naeije R, Arena R, Corrà U, Ghio S, Forfia P, et al. Echocardiography of Right Ventriculoarterial Coupling Combined With Cardiopulmonary Exercise Testing to Predict Outcome in Heart Failure. *Chest*. 2015;148(1):226-34.
106. Swift AJ, Rajaram S, Hurdman J, Hill C, Davies C, Sproson TW, et al. Noninvasive estimation of PA pressure, flow, and resistance with CMR imaging: derivation and prospective validation study from the ASPIRE registry. *JACC Cardiovasc Imaging*. 2013;6(10):1036-47.
107. Roeleveld RJ, Marcus JT, Boonstra A, Postmus PE, Marques KM, Bronzwaer JG, et al. A comparison of noninvasive MRI-based methods of estimating pulmonary artery pressure in pulmonary hypertension. *J Magn Reson Imaging*. 2005;22(1):67-72.
108. Simpson RM, Keegan J, Firmin DN. MR assessment of regional myocardial mechanics. *J Magn Reson Imaging*. 2013;37(3):576-99.
109. Reisner SA, Lysyansky P, Agmon Y, Mutlak D, Lessick J, Friedman Z. Global longitudinal strain: a novel index of left ventricular systolic function. *Journal of the American Society of Echocardiography : official publication of the American Society of Echocardiography*. 2004;17(6):630-3.
110. Leitman M, Lysyansky P, Sidenko S, Shir V, Peleg E, Binenbaum M, et al. Two-dimensional strain—a novel software for real-time quantitative echocardiographic assessment of myocardial function. *Journal of the American Society of Echocardiography : official publication of the American Society of Echocardiography*. 2004;17(10):1021-9.
111. Helle-Valle T, Crosby J, Edvardsen T, Lyseggen E, Amundsen BH, Smith HJ, et al. New noninvasive method for assessment of left ventricular rotation: speckle tracking echocardiography. *Circulation*. 2005;112(20):3149-56.
112. Amundsen BH, Helle-Valle T, Edvardsen T, Torp H, Crosby J, Lyseggen E, et al. Noninvasive myocardial strain measurement by speckle tracking echocardiography: validation against sonomicrometry and tagged magnetic resonance imaging. *Journal of the American College of Cardiology*. 2006;47(4):789-93.
113. Rajdev S, Nanda NC, Patel V, Singh A, Mehmood F, Vengala S, et al. Tissue Doppler assessment of longitudinal right and left ventricular strain and strain rate in pulmonary artery hypertension. *Echocardiography*. 2006;23(10):872-9.
114. Borges AC, Knebel F, Eddicks S, Panda A, Schattke S, Witt C, et al. Right ventricular function assessed by two-dimensional strain and tissue Doppler echocardiography in patients with pulmonary arterial hypertension and effect of vasodilator therapy. *The American journal of cardiology*. 2006;98(4):530-4.
115. Filusch A, Mereles D, Gruenig E, Buss S, Katus HA, Meyer FJ. Strain and strain rate echocardiography for evaluation of right ventricular dysfunction in patients with idiopathic pulmonary arterial hypertension. *Clin Res Cardiol*. 2010;99(8):491-8.
116. Lang RM, Badano LP, Mor-Avi V, Afilalo J, Armstrong A, Ernande L, et al. Recommendations for cardiac chamber quantification by echocardiography in adults: an update from the American Society of Echocardiography and the European Association of Cardiovascular Imaging. *Eur Heart J Cardiovasc Imaging*. 2015;16(3):233-70.
117. Sachdev A, Villarraga HR, Frantz RP, McGoon MD, Hsiao JF, Maalouf JF, et al. Right ventricular strain for prediction of survival in patients with pulmonary arterial hypertension. *Chest*. 2011;139(6):1299-309.

118. Haeck ML, Scherptong RW, Marsan NA, Holman ER, Schalij MJ, Bax JJ, et al. Prognostic value of right ventricular longitudinal peak systolic strain in patients with pulmonary hypertension. *Circ Cardiovasc Imaging*. 2012;5(5):628-36.
119. Rajagopal S, Forsha DE, Risum N, Hornik CP, Poms AD, Fortin TA, et al. Comprehensive assessment of right ventricular function in patients with pulmonary hypertension with global longitudinal peak systolic strain derived from multiple right ventricular views. *Journal of the American Society of Echocardiography : official publication of the American Society of Echocardiography*. 2014;27(6):657-65.e3.
120. Park JH, Kusunose K, Kwon DH, Park MM, Erzurum SC, Thomas JD, et al. Relationship between Right Ventricular Longitudinal Strain, Invasive Hemodynamics, and Functional Assessment in Pulmonary Arterial Hypertension. *Korean Circ J*. 2015;45(5):398-407.
121. Park JH, Park MM, Farha S, Sharp J, Lundgrin E, Comhair S, et al. Impaired Global Right Ventricular Longitudinal Strain Predicts Long-Term Adverse Outcomes in Patients with Pulmonary Arterial Hypertension. *J Cardiovasc Ultrasound*. 2015;23(2):91-9.
122. Li Y, Wang Y, Ye X, Kong L, Zhu W, Lu X. Clinical study of right ventricular longitudinal strain for assessing right ventricular dysfunction and hemodynamics in pulmonary hypertension. *Medicine*. 2016;95(50):e5668.
123. Vitarelli A, Mangieri E, Terzano C, Gaudio C, Salsano F, Rosato E, et al. Three-dimensional echocardiography and 2D-3D speckle-tracking imaging in chronic pulmonary hypertension: diagnostic accuracy in detecting hemodynamic signs of right ventricular (RV) failure. *J Am Heart Assoc*. 2015;4(3):e001584.
124. Haeck ML, Hoke U, Marsan NA, Holman ER, Wolterbeek R, Bax JJ, et al. Impact of right ventricular dyssynchrony on left ventricular performance in patients with pulmonary hypertension. *The international journal of cardiovascular imaging*. 2014;30(4):713-20.
125. Badagliacca R, Poscia R, Pezzuto B, Papa S, Gambardella C, Francone M, et al. Right ventricular dyssynchrony in idiopathic pulmonary arterial hypertension: determinants and impact on pump function. *The Journal of heart and lung transplantation : the official publication of the International Society for Heart Transplantation*. 2015;34(3):381-9.
126. Badagliacca R, Reali M, Poscia R, Pezzuto B, Papa S, Mezzapesa M, et al. Right Intraventricular Dyssynchrony in Idiopathic, Heritable, and Anorexigen-Induced Pulmonary Arterial Hypertension: Clinical Impact and Reversibility. *JACC Cardiovasc Imaging*. 2015;8(6):642-52.
127. Shehata ML, Basha TA, Tantawy WH, Lima JA, Vogel-Claussen J, Bluemke DA, et al. Real-time single-heartbeat fast strain-encoded imaging of right ventricular regional function: normal versus chronic pulmonary hypertension. *Magn Reson Med*. 2010;64(1):98-106.
128. Scatteia A, Baritussio A, Bucciarelli-Ducci C. Strain imaging using cardiac magnetic resonance. *Heart Fail Rev*. 2017;22(4):465-76.
129. de Siqueira ME, Pozo E, Fernandes VR, Sengupta PP, Modesto K, Gupta SS, et al. Characterization and clinical significance of right ventricular mechanics in pulmonary hypertension evaluated with cardiovascular magnetic resonance feature tracking. *J Cardiovasc Magn Reson*. 2016;18(1):39.
130. Puwanant S, Park M, Popovic ZB, Tang WH, Farha S, George D, et al. Ventricular geometry, strain, and rotational mechanics in pulmonary hypertension. *Circulation*. 2010;121(2):259-66.

131. Jellis CL, Kwon DH. Myocardial T1 mapping: modalities and clinical applications. *Cardiovasc Diagn Ther*. 2014;4(2):126-37.
132. Reiter U, Reiter G, Kovacs G, Adelsmayr G, Greiser A, Olschewski H, et al. Native myocardial T1 mapping in pulmonary hypertension: correlations with cardiac function and hemodynamics. *European radiology*. 2017;27(1):157-66.
133. Blyth KG, Groenning BA, Martin TN, Foster JE, Mark PB, Dargie HJ, et al. Contrast enhanced-cardiovascular magnetic resonance imaging in patients with pulmonary hypertension. *European heart journal*. 2005;26(19):1993-9.
134. Freed BH, Gomberg-Maitland M, Chandra S, Mor-Avi V, Rich S, Archer SL, et al. Late gadolinium enhancement cardiovascular magnetic resonance predicts clinical worsening in patients with pulmonary hypertension. *J Cardiovasc Magn Reson*. 2012;14:11.
135. Swift AJ, Rajaram S, Capener D, Elliot C, Condliffe R, Wild JM, et al. LGE patterns in pulmonary hypertension do not impact overall mortality. *JACC Cardiovasc Imaging*. 2014;7(12):1209-17.
136. Messroghli DR, Radjenovic A, Kozerke S, Higgins DM, Sivananthan MU, Ridgway JP. Modified Look-Locker inversion recovery (MOLLI) for high-resolution T1 mapping of the heart. *Magn Reson Med*. 2004;52(1):141-6.
137. Messroghli DR, Plein S, Higgins DM, Walters K, Jones TR, Ridgway JP, et al. Human myocardium: single-breath-hold MR T1 mapping with high spatial resolution--reproducibility study. *Radiology*. 2006;238(3):1004-12.
138. Spruijt OA, Vissers L, Bogaard HJ, Hofman MB, Vonk-Noordegraaf A, Marcus JT. Increased native T1-values at the interventricular insertion regions in precapillary pulmonary hypertension. *The international journal of cardiovascular imaging*. 2016;32(3):451-9.
139. Saunders LC, Johns CS, Stewart NJ, Oram CJE, Capener DA, Puntmann VO, et al. Diagnostic and prognostic significance of cardiovascular magnetic resonance native myocardial T1 mapping in patients with pulmonary hypertension. *J Cardiovasc Magn Reson*. 2018;20(1):78.
140. Garcia-Alvarez A, Garcia-Lunar I, Pereda D, Fernandez-Jimenez R, Sanchez-Gonzalez J, Mirelis JG, et al. Association of myocardial T1-mapping CMR with hemodynamics and RV performance in pulmonary hypertension. *JACC Cardiovasc Imaging*. 2015;8(1):76-82.
141. Homsí R, Luetkens JA, Skowasch D, Pizarro C, Sprinkart AM, Gieseke J, et al. Left Ventricular Myocardial Fibrosis, Atrophy, and Impaired Contractility in Patients With Pulmonary Arterial Hypertension and a Preserved Left Ventricular Function: A Cardiac Magnetic Resonance Study. *J Thorac Imaging*. 2017;32(1):36-42.
142. Skrok J, Shehata ML, Mathai S, Girgis RE, Zaiman A, Mudd JO, et al. Pulmonary arterial hypertension: MR imaging-derived first-pass bolus kinetic parameters are biomarkers for pulmonary hemodynamics, cardiac function, and ventricular remodeling. *Radiology*. 2012;263(3):678-87.
143. Vogel-Claussen J, Skrok J, Shehata ML, Singh S, Sibley CT, Boyce DM, et al. Right and left ventricular myocardial perfusion reserves correlate with right ventricular function and pulmonary hemodynamics in patients with pulmonary arterial hypertension. *Radiology*. 2011;258(1):119-27.
144. Hagan G, Southwood M, Treacy C, Ross RM, Soon E, Coulson J, et al. (18)FDG PET imaging can quantify increased cellular metabolism in pulmonary arterial hypertension: A proof-of-principle study. *Pulm Circ*. 2011;1(4):448-55.

145. Can MM, Kaymaz C, Tanboga IH, Tokgoz HC, Canpolat N, Turkyilmaz E, et al. Increased right ventricular glucose metabolism in patients with pulmonary arterial hypertension. *Clin Nucl Med.* 2011;36(9):743-8.
146. Wang L, Zhang Y, Yan C, He J, Xiong C, Zhao S, et al. Evaluation of right ventricular volume and ejection fraction by gated (18)F-FDG PET in patients with pulmonary hypertension: comparison with cardiac MRI and CT. *J Nucl Cardiol.* 2013;20(2):242-52.
147. Bokhari S, Raina A, Rosenweig EB, Schulze PC, Bokhari J, Einstein AJ, et al. PET imaging may provide a novel biomarker and understanding of right ventricular dysfunction in patients with idiopathic pulmonary arterial hypertension. *Circ Cardiovasc Imaging.* 2011;4(6):641-7.
148. Delicce AV, Makaryus AN. Physiology, Frank Starling Law. *StatPearls.* Treasure Island (FL)2020.
149. Vonk Noordegraaf A, Westerhof BE, Westerhof N. The Relationship Between the Right Ventricle and its Load in Pulmonary Hypertension. *Journal of the American College of Cardiology.* 2017;69(2):236-43.
150. Mauritz GJ, Marcus JT, Westerhof N, Postmus PE, Vonk-Noordegraaf A. Prolonged right ventricular post-systolic isovolumic period in pulmonary arterial hypertension is not a reflection of diastolic dysfunction. *Heart.* 2011;97(6):473-8.
151. Hardziyenka M, Surie S, de Groot JR, de Bruin-Bon HA, Knops RE, Remmelink M, et al. Right ventricular pacing improves haemodynamics in right ventricular failure from pressure overload: an open observational proof-of-principle study in patients with chronic thromboembolic pulmonary hypertension. *Europace.* 2011;13(12):1753-9.
152. Lumens J, Arts T, Broers B, Boomars KA, van Paassen P, Prinzen FW, et al. Right ventricular free wall pacing improves cardiac pump function in severe pulmonary arterial hypertension: a computer simulation analysis. *Am J Physiol Heart Circ Physiol.* 2009;297(6):H2196-205.
153. Hoit BD. Left atrial size and function: role in prognosis. *Journal of the American College of Cardiology.* 2014;63(6):493-505.
154. Kowallick JT, Kutty S, Edelmann F, Chiribiri A, Villa A, Steinmetz M, et al. Quantification of left atrial strain and strain rate using Cardiovascular Magnetic Resonance myocardial feature tracking: a feasibility study. *J Cardiovasc Magn Reson.* 2014;16:60.
155. Murata M, Iwanaga S, Tamura Y, Kondo M, Kouyama K, Murata M, et al. A real-time three-dimensional echocardiographic quantitative analysis of left atrial function in left ventricular diastolic dysfunction. *The American journal of cardiology.* 2008;102(8):1097-102.
156. Taraseviciene-Stewart L, Kasahara Y, Alger L, Hirth P, Mc Mahon G, Waltenberger J, et al. Inhibition of the VEGF receptor 2 combined with chronic hypoxia causes cell death-dependent pulmonary endothelial cell proliferation and severe pulmonary hypertension. *FASEB J.* 2001;15(2):427-38.
157. Abe K, Toba M, Alzoubi A, Ito M, Fagan KA, Cool CD, et al. Formation of plexiform lesions in experimental severe pulmonary arterial hypertension. *Circulation.* 2010;121(25):2747-54.
158. Vitali SH, Hansmann G, Rose C, Fernandez-Gonzalez A, Scheid A, Mitsialis SA, et al. The Sugen 5416/hypoxia mouse model of pulmonary hypertension revisited: long-term follow-up. *Pulm Circ.* 2014;4(4):619-29.
159. de Raaf MA, Schalij I, Gomez-Arroyo J, Rol N, Happe C, de Man FS, et al. SuHx rat model: partly reversible pulmonary hypertension and progressive intima obstruction. *Eur Respir J.* 2014;44(1):160-8.

160. Urboniene D, Haber I, Fang YH, Thenappan T, Archer SL. Validation of high-resolution echocardiography and magnetic resonance imaging vs. high-fidelity catheterization in experimental pulmonary hypertension. *Am J Physiol Lung Cell Mol Physiol*. 2010;299(3):L401-12.
161. Jones JE, Mendes L, Rudd MA, Russo G, Loscalzo J, Zhang YY. Serial noninvasive assessment of progressive pulmonary hypertension in a rat model. *Am J Physiol Heart Circ Physiol*. 2002;283(1):H364-71.
162. SPVU. Scottish Pulmonary Vascular Unit - website.
163. Scotland NRo. Population estimates by administrative area, Scotland, mid-2018
- .
164. National Audit of Pulmonary Hypertension 2019 [Available from: [https://files.digital.nhs.uk/BA/4EF20E/NAPH\\_10AR\\_Main\\_Report.pdf](https://files.digital.nhs.uk/BA/4EF20E/NAPH_10AR_Main_Report.pdf)].
165. Barst RJ, McGoon M, Torbicki A, Sitbon O, Krowka MJ, Olschewski H, et al. Diagnosis and differential assessment of pulmonary arterial hypertension. *Journal of the American College of Cardiology*. 2004;43(12 Suppl S):40S-7S.
166. Lorenz CH, Walker ES, Morgan VL, Klein SS, Graham TP, Jr. Normal human right and left ventricular mass, systolic function, and gender differences by cine magnetic resonance imaging. *J Cardiovasc Magn Reson*. 1999;1(1):7-21.
167. Sievers B, Kirchberg S, Bakan A, Franken U, Trappe HJ. Impact of papillary muscles in ventricular volume and ejection fraction assessment by cardiovascular magnetic resonance. *J Cardiovasc Magn Reson*. 2004;6(1):9-16.
168. Kowallick JT, Morton G, Lamata P, Jogiya R, Kutty S, Hasenfuss G, et al. Quantitative assessment of left ventricular mechanical dyssynchrony using cine cardiovascular magnetic resonance imaging: Inter-study reproducibility. *JRSM Cardiovasc Dis*. 2017;6:2048004017710142.
169. Kellman P, Hansen MS. T1-mapping in the heart: accuracy and precision. *J Cardiovasc Magn Reson*. 2014;16:2.
170. Jayasekera G. Understanding longitudinal biventricular structural and functional changes in a pulmonary hypertension Sugen-hypoxia rat model by cardiac magnetic resonance imaging. *Pulmonary Circulation*. 2020.
171. Gouma E, Simos Y, Verginadis I, Lykoudis E, Evangelou A, Karkabounas S. A simple procedure for estimation of total body surface area and determination of a new value of Meeh's constant in rats. *Lab Anim*. 2012;46(1):40-5.
172. Petersen SE, Aung N, Sanghvi MM, Zemrak F, Fung K, Paiva JM, et al. Reference ranges for cardiac structure and function using cardiovascular magnetic resonance (CMR) in Caucasians from the UK Biobank population cohort. *J Cardiovasc Magn Reson*. 2017;19(1):18.
173. Ghio S, Constantin C, Klersy C, Serio A, Fontana A, Campana C, et al. Interventricular and intraventricular dyssynchrony are common in heart failure patients, regardless of QRS duration. *European heart journal*. 2004;25(7):571-8.
174. Zerhouni EA, Parish DM, Rogers WJ, Yang A, Shapiro EP. Human heart: tagging with MR imaging--a method for noninvasive assessment of myocardial motion. *Radiology*. 1988;169(1):59-63.
175. Pedrizzetti G, Claus P, Kilner PJ, Nagel E. Principles of cardiovascular magnetic resonance feature tracking and echocardiographic speckle tracking for informed clinical use. *J Cardiovasc Magn Reson*. 2016;18(1):51.

176. Schuster A, Hor KN, Kowallick JT, Beerbaum P, Kutty S. Cardiovascular Magnetic Resonance Myocardial Feature Tracking: Concepts and Clinical Applications. *Circ Cardiovasc Imaging*. 2016;9(4):e004077.
177. Schuster A, Stahnke VC, Unterberg-Buchwald C, Kowallick JT, Lamata P, Steinmetz M, et al. Cardiovascular magnetic resonance feature-tracking assessment of myocardial mechanics: Intervendor agreement and considerations regarding reproducibility. *Clinical radiology*. 2015;70(9):989-98.
178. Moody WE, Taylor RJ, Edwards NC, Chue CD, Umar F, Taylor TJ, et al. Comparison of magnetic resonance feature tracking for systolic and diastolic strain and strain rate calculation with spatial modulation of magnetization imaging analysis. *J Magn Reson Imaging*. 2015;41(4):1000-12.
179. Hor KN, Gottliebson WM, Carson C, Wash E, Cnota J, Fleck R, et al. Comparison of magnetic resonance feature tracking for strain calculation with harmonic phase imaging analysis. *JACC Cardiovasc Imaging*. 2010;3(2):144-51.
180. Schuster A, Paul M, Bettencourt N, Morton G, Chiribiri A, Ishida M, et al. Cardiovascular magnetic resonance myocardial feature tracking for quantitative viability assessment in ischemic cardiomyopathy. *International journal of cardiology*. 2013;166(2):413-20.
181. Schneeweis C, Qiu J, Schnackenburg B, Berger A, Kelle S, Fleck E, et al. Value of additional strain analysis with feature tracking in dobutamine stress cardiovascular magnetic resonance for detecting coronary artery disease. *J Cardiovasc Magn Reson*. 2014;16:72.
182. Buss SJ, Breuninger K, Lehrke S, Voss A, Galuschky C, Lossnitzer D, et al. Assessment of myocardial deformation with cardiac magnetic resonance strain imaging improves risk stratification in patients with dilated cardiomyopathy. *Eur Heart J Cardiovasc Imaging*. 2015;16(3):307-15.
183. Heermann P, Hedderich DM, Paul M, Schulke C, Kroeger JR, Baessler B, et al. Biventricular myocardial strain analysis in patients with arrhythmogenic right ventricular cardiomyopathy (ARVC) using cardiovascular magnetic resonance feature tracking. *J Cardiovasc Magn Reson*. 2014;16:75.
184. Cho GY, Song JK, Park WJ, Han SW, Choi SH, Doo YC, et al. Mechanical dyssynchrony assessed by tissue Doppler imaging is a powerful predictor of mortality in congestive heart failure with normal QRS duration. *Journal of the American College of Cardiology*. 2005;46(12):2237-43.
185. Tanaka H, Nesser HJ, Buck T, Oyenuga O, Janosi RA, Winter S, et al. Dyssynchrony by speckle-tracking echocardiography and response to cardiac resynchronization therapy: results of the Speckle Tracking and Resynchronization (STAR) study. *European heart journal*. 2010;31(14):1690-700.
186. Hardegree EL, Sachdev A, Fenstad ER, Villarraga HR, Frantz RP, McGoon MD, et al. Impaired left ventricular mechanics in pulmonary arterial hypertension: identification of a cohort at high risk. *Circ Heart Fail*. 2013;6(4):748-55.
187. Marcus JT, Gan CT, Zwanenburg JJ, Boonstra A, Allaart CP, Gotte MJ, et al. Interventricular mechanical asynchrony in pulmonary arterial hypertension: left-to-right delay in peak shortening is related to right ventricular overload and left ventricular underfilling. *Journal of the American College of Cardiology*. 2008;51(7):750-7.
188. Gan CT, McCann GP, Marcus JT, van Wolferen SA, Twisk JW, Boonstra A, et al. NT-proBNP reflects right ventricular structure and function in pulmonary hypertension. *Eur Respir J*. 2006;28(6):1190-4.
189. Hung CL, Verma A, Uno H, Shin SH, Bourgoun M, Hassanein AH, et al. Longitudinal and circumferential strain rate, left ventricular remodeling, and

- prognosis after myocardial infarction. *Journal of the American College of Cardiology*. 2010;56(22):1812-22.
190. Baessler B, Schaarschmidt F, Dick A, Michels G, Maintz D, Bunck AC. Diagnostic implications of magnetic resonance feature tracking derived myocardial strain parameters in acute myocarditis. *Eur J Radiol*. 2016;85(1):218-27.
191. Taylor RJ, Umar F, Lin EL, Ahmed A, Moody WE, Mazur W, et al. Mechanical effects of left ventricular midwall fibrosis in non-ischemic cardiomyopathy. *J Cardiovasc Magn Reson*. 2016;18:1.
192. Gupta S, Torres F, Bollineni S, Mohanka M, Kaza V. Left Ventricular Dysfunction After Lung Transplantation for Pulmonary Arterial Hypertension. *Transplant Proc*. 2015;47(9):2732-6.
193. Morais P, Marchi A, Bogaert JA, Dresselaers T, Heyde B, D'Hooge J, et al. Cardiovascular magnetic resonance myocardial feature tracking using a non-rigid, elastic image registration algorithm: assessment of variability in a real-life clinical setting. *J Cardiovasc Magn Reson*. 2017;19(1):24.
194. Hoit BD. Assessment of Left Atrial Function by Echocardiography: Novel Insights. *Curr Cardiol Rep*. 2018;20(10):96.
195. Mondillo S, Cameli M, Caputo ML, Lisi M, Palmerini E, Padeletti M, et al. Early detection of left atrial strain abnormalities by speckle-tracking in hypertensive and diabetic patients with normal left atrial size. *Journal of the American Society of Echocardiography : official publication of the American Society of Echocardiography*. 2011;24(8):898-908.
196. Kojima T, Kawasaki M, Tanaka R, Ono K, Hirose T, Iwama M, et al. Left atrial global and regional function in patients with paroxysmal atrial fibrillation has already been impaired before enlargement of left atrium: velocity vector imaging echocardiography study. *Eur Heart J Cardiovasc Imaging*. 2012;13(3):227-34.
197. Gupta S, Matulevicius SA, Ayers CR, Berry JD, Patel PC, Markham DW, et al. Left atrial structure and function and clinical outcomes in the general population. *European heart journal*. 2013;34(4):278-85.
198. Hedberg P, Selmerud J, Leppert J, Henriksen E. Long-term prognostic impact of left atrial volumes and emptying fraction in a community-based cohort. *Heart*. 2017;103(9):687-93.
199. Kobayashi Y, Wheeler M, Finocchiaro G, Ariyama M, Kobayashi Y, Perez MV, et al. Left atrial function and phenotypes in asymmetric hypertrophic cardiomyopathy. *Echocardiography*. 2017;34(6):843-50.
200. Liu YT, Li RJ, Fang F, Zhang Q, Yan BP, Lam YY, et al. Left atrial function assessed by tissue doppler imaging as a new predictor of cardiac events after non-ST-elevation acute coronary syndrome. *Echocardiography*. 2012;29(7):785-92.
201. Stojnic BB, Brecker SJ, Xiao HB, Helmy SM, Mbaissouroum M, Gibson DG. Left ventricular filling characteristics in pulmonary hypertension: a new mode of ventricular interaction. *British heart journal*. 1992;68(1):16-20.
202. Dean A, Nilsen M, Loughlin L, Salt IP, MacLean MR. Metformin Reverses Development of Pulmonary Hypertension via Aromatase Inhibition. *Hypertension*. 2016;68(2):446-54.
203. Hargett LA, Hartman LJ, Scruggs AK, McLendon JM, Haven AK, Bauer NN. Severe pulmonary arterial hypertensive rats are tolerant to mild exercise. *Pulm Circ*. 2015;5(2):349-55.

204. Al-Husseini A, Wijesinghe DS, Farkas L, Kraskauskas D, Drake JI, Van Tassel B, et al. Increased eicosanoid levels in the Sugen/chronic hypoxia model of severe pulmonary hypertension. *PLoS One*. 2015;10(3):e0120157.
205. Wang Z, Schreier DA, Hacker TA, Chesler NC. Progressive right ventricular functional and structural changes in a mouse model of pulmonary arterial hypertension. *Physiol Rep*. 2013;1(7):e00184.
206. Sutendra G, Dromparis P, Paulin R, Zervopoulos S, Haromy A, Nagendran J, et al. A metabolic remodeling in right ventricular hypertrophy is associated with decreased angiogenesis and a transition from a compensated to a decompensated state in pulmonary hypertension. *J Mol Med (Berl)*. 2013;91(11):1315-27.
207. Kerbaul F, Rondelet B, Motte S, Fesler P, Hubloue I, Ewalenko P, et al. Isoflurane and desflurane impair right ventricular-pulmonary arterial coupling in dogs. *Anesthesiology*. 2004;101(6):1357-62.

**Appendix 1 LV Strain variables and association with known markers of disease severity.**

	RVEF	RVEDVI	RVESVI	TAPSE	NTPBNP	RAP	mPAP	CO	CI	PVR	SVI	SvO2
Err <sub>LV</sub>	0.66****	-0.43***	-0.59****	0.51****	-0.40**	-0.05	-0.15	0.54****	0.47****	-0.51****	0.44***	0.43***
Ecc <sub>LV</sub>	-0.43	0.45	0.49	-0.40	0.16	-0.04	0.18	-0.31	-0.25	0.37	-0.26	-0.28
Ell <sub>LV</sub>	-0.49****	0.45***	0.51****	-0.61****	0.24	0.19	0.27*	-0.37**	-0.42***	0.45****	-0.42***	-0.46****
Radial dyssynchrony	-0.44***	0.39***	0.46***	-0.33**	0.40**	0.15	0.07	-0.33**	-0.32**	0.28*	-0.24*	-0.35**
Circ. dyssynchrony	-0.07	0.25*	0.20	-0.37**	0.14	0.10	0.02	-0.12	-0.12	0.14	-0.02	-0.20
Long. dyssynchrony	-0.01	0.22	0.16	-0.30*	0.27*	0.07	-0.06	-0.24*	-0.25*	0.15	0.03	-0.27*
Radial strain rate	0.5****	-0.38**	-0.47****	0.47***	-0.36**	-0.03	-0.10	0.46****	0.40***	-0.41***	0.31**	0.38**
Circ. strain rate	-0.30*	0.41***	0.41***	-0.39**	0.12	-0.07	0.21	-0.28*	-0.23	0.36**	-0.17	-0.24*
Long. strain rate	-0.32**	0.31**	0.34**	-0.45****	0.02	0.01	0.20	-0.24*	-0.31**	0.31**	-0.24*	-0.30*

Err<sub>LV</sub> was significantly associated with known markers of disease severity including RVEF (r=0.66), RVESVI (r=-0.59), PVR (r=0.51) and SVI (r=0.44). The association of longitudinal and circumferential strain with markers of disease severity was significant, however with a weaker strength. Among the LV dyssynchrony indices, radial dyssynchrony demonstrated the strongest association with known markers of disease severity (r values RVEF =-0.44, RVESVI=0.46 respectively). Spearman correlations are used to assess association between continuous variables. \*, \*\*, \*\*\* and \*\*\*\* indicates p <0.05, <0.01, <0.001 and <0.0001 respectively. Ecc<sub>LV</sub> – LV circumferential strain, Ell<sub>LV</sub> – LV longitudinal strain, Err<sub>LV</sub> – LV radial strain, RVEF- RV ejection fraction, RVEDVI - RV end-diastolic volume index, RVESVI – RV end Systolic Volume, TAPSE – tricuspid annular systolic plane excursion, NTPBNP- N Terminal Brain Natriuretic Peptide RAP – right atrial pressure, mPAP – mean pulmonary artery pressure, CO – cardiac output, CI – cardiac index, PVR- pulmonary vascular resistance, SVI- stroke volume index, SvO2- mixed venous saturations

**Appendix 2 RV strain variables and association with known markers of disease severity**

	RVEF	RVEDVI	RVESVI	TAPSE	NTPBNP	RAP	mPAP	CO	CI	PVR	SVI	SvO2
<b>Free wall strain</b>	-0.62****	0.37**	0.56****	-0.68****	0.38**	0.21	0.08	-0.56****	0.62****	0.51****	-0.62****	-0.55****
<b>Septum strain</b>	-0.53****	0.32**	0.46****	-0.38**	0.22	0.14	0.02	-0.37**	-0.40***	0.38**	-0.45****	-0.48****
<b>Average strain</b>	-0.70****	0.44***	0.63****	-0.64****	0.41***	0.22	0.08	-0.59****	-0.60****	0.57****	-0.63****	-0.59****
<b>Free wall strain rate</b>	-0.55****	0.43***	0.56****	-0.57****	0.36**	0.15	0.10	-0.59****	-0.63****	0.55****	-0.46****	-0.51****
<b>Septum strain rate</b>	-0.10	0.13	0.13	-0.16	0.13	-0.13	-0.13	-0.20	-0.22	0.13	-0.09	-0.22
<b>Average strain rate</b>	-0.55****	0.38**	0.52****	-0.54****	0.34**	0.09	0.02	-0.49****	-0.57****	0.44***	-0.46****	-0.48****

RV average strain (average of septal and free wall strain) demonstrated strong association with RVEF ( $r=-0.7$ ), RVESVI ( $r=0.63$ ) and SVI ( $r=-0.63$ ). Spearman correlations are used to assess association between continuous variables. \*, \*\*, \*\*\* and \*\*\*\* indicates  $p < 0.05$ ,  $< 0.01$ ,  $< 0.001$  and  $< 0.0001$  respectively. RVEF- RV ejection fraction, RVEDVI - RV end-diastolic volume index, RVESVI – RV end-systolic volume index, TAPSE – tricuspid annular systolic plane excursion, NTPBNP- N Terminal Brain Natriuretic Peptide, mPAP – mean Pulmonary Artery Pressure, RAP – Right atrial pressure, CO – cardiac output, CI – cardiac index, PVR- pulmonary vascular resistance, SVI- stroke volume index, SvO2- mixed Venous Saturation

